Ana Catarina Bernardino Baptista
Mestre em Biotecnologia

Development of Bio-Batteries based on Electrospun Membranes

Dissertação para obtenção do Grau de Doutor em

Ciência e Engenharia de Materiais

Orientador:	Doutora Isabel Maria das Mercês Ferreira, Professora Associada, Faculdade de Ciências e Tecnologia da Universidade Nova de Lisboa
Co-orientador:	Doutor João Paulo Miranda Ribeiro Borges, Professor Auxiliar, Faculdade de Ciências e Tecnologia da Universidade Nova de Lisboa

Júri:

Presidente:	Prof. Doutor Rodrigo Ferrão de Paiva Martins
Arguentes:	Prof. Doutor Senentxu Lanceros-Mendez
	Prof. Doutor João Lemos Pinto
Vogais:	Prof. Doutora Maria Helena Mendes Gil
	Prof. Doutora Maria Teresa Varanda Cidade
	Prof. Doutor José Inácio Ferrão de Paiva Martins
	Prof. Doutor Rodrigo Ferrão de Paiva Martins

FACULDADE DE CIÊNCIAS E TECNOLOGIA
UNIVERSIDADE NOVA DE LISBOA

Dezembro 2014

Ana Catarina Bernardino Baptista

Mestre em Biotecnologia

Development of Bio-Batteries based on Electrospun Membranes

Dissertação para obtenção do Grau de Doutor em

Ciência e Engenharia de Materiais

Orientador:	Doutora Isabel Maria das Mercês Ferreira, Professora Associada, Faculdade de Ciências e Tecnologia da Universidade Nova de Lisboa
Co-orientador:	Doutor João Paulo Miranda Ribeiro Borges, Professor Auxiliar, Faculdade de Ciências e Tecnologia da Universidade Nova de Lisboa

Júri:

Presidente:	Prof. Doutor Rodrigo Ferrão de Paiva Martins
Arguentes:	Prof. Doutor Senentxu Lanceros-Mendez
	Prof. Doutor João Lemos Pinto
Vogais:	Prof. Doutora Maria Helena Mendes Gil
	Prof. Doutora Maria Teresa Varanda Cidade
	Prof. Doutor José Inácio Ferrão de Paiva Martins
	Prof. Doutor Rodrigo Ferrão de Paiva Martins

Dezembro 2014

– This page is intentionally blank –

Development of Bio-Batteries based on Electrospun Membranes

– This page is intentionally blank –

É certo que sempre ouvi dizer
Que do querer ao fazer
Vai um enorme esticão
Mas haverá quem possa negar
Que querer é poder
E o nunca é uma invenção

Nuno Figueiredo e Jorge Benvinda

– This page is intentionally blank –

Acknowledgements

Because a scientific work is made of lessons, exchanging experiences and collaborations, there were a great number of people who helped me making this journey possible.
Foremost, I would like to express my gratitude to my supervisors: Prof. Dr. Isabel Ferreira and Prof. Dr. João Paulo Borges. I would like to thank you both for your scientific support; for letting me grow as a scientist; for your daily motivation; and particularly for being part of this journey. It was a pleasure to work and learn with you!
To Prof. Dr. José Inácio Martins from Faculdade de Engenharia da Universidade do Porto. I am particularly grateful for his large expertise and knowledge in electrochemical characterization and for all his support during this research.
To Prof. Dr. Elvira Fortunato and Prof. Dr. Rodrigo Martins for the opportunity to work in such excellent research facilities such as the CENIMAT and CEMOP centers.
I also want to express my sincere gratitude to those that direct or indirectly have collaborated with me and provided crucial contributions for this work. I am particularly grateful to Msc. Alexandre Botas, MSc. Ana Aires, MSc. Ana Manjua, MSc. Beatriz Roma, BSc. Teresa Nicolau, BSc. Joana Nobre and Bsc. Inês Ropio. A special acknowledgment goes to MSc. Joana Neto, a good colleague and friend that always motivated me for this research and contaminated me with her positive energy. Thank you for your efforts and collaboration!
To Prof. Dr. Joaquim Leitão, Prof. Dr. Jorge Soares and Dr. Bruno Falcão from the Physics Department of Universidade de Aveiro for the photoluminescence measurements and their scientific contribution in this field.
To Prof. Dr. Jorge Silva and Prof. Dr. Célia Henriques, from the Physiscs Department of FCT/UNL, for all their support and expertise in the cytotoxic assays.
To Professor Isabel Sá-Nogueira and MSC. Mário Ferreira from the Microbial Genetics Lab, Centro de Recursos Microbiológicos (CREM), FCT-UNL for their support with the antibacterial assays.
I would also like to thanks to MSc. Ana Almeida for collaborating in the antibacterial assays. Thank you for your help and friendship during these years.
To Dr. Daniela Gomes for the beautiful SEM images presented in this thesis. I have really appreciated all your efforts in the SEM sessions.
My acknowledgments go also to my colleagues from the Materials for Electronics, Opto-

electronics and Nanotechnologies Group and the Soft and Biofunctional Materials Group that helped me during these years. I am particularly grateful to Dr. Joana Vaz Pinto and Dr. Rita Branquinho for all the discussions about electrochemistry; to Dr. Sumita Goswami for sharing her knowledge about polianiline synthesis; to MSc. Lídia Santos, MSc. Diana Gaspar, MSc. Raquel Barros, Msc. Sónia Pereira, MSc. Alexandra Gonçalves, MSc. Alexandra Rodrigues, MSc. Marisa Ferreira and BSc. Filipe Silvestre for all the help provided; to Dr. João Canejo, Dr. Susete Fernandes, Dr. Coro Echeverria and MSc. Paula Soares for their motivation and promptness to support me along this research.

To MSc. Adriana Nogueira, MSc. Ana Pedrosa, MSc. Carlos João, MSc. Rafael Santos, Dr. Iwona Bernarcka, Ing. Jonas Deuermeier, Dr. Sergej Filonovich, Dr. Vitor Figueiredo, and Dr. Joana Loureiro, thank you for all the fun and unforgettable moments that we have shared during the past years. Thank you also to Sara Oliveira and to Sónia Seixas from DCM secretariat for all the administrative support given throughout the course of this thesis.

In addition, I am extremely grateful for the financial support provided by Fundação para a Ciência e a Tecnologia (FCT-MCTES) under the grant SFRH/BD/69306/2010 which allowed this research to be accomplished.

Finally, thank you to my beloved family for all your unconditional love and support. A special thanks to my dear João Fernandes for all his love, friendship, patience and understanding.

Abstract

A new class of energy supply systems is emerging with the ability to be flexible and conform to complex surfaces such as those of the human body. Considering that harvesting energy directly from the environment is probably the most effective and promising approach for powering long-term biomedical devices, the present thesis aims at the development of a cellulose-based bio-battery made of electrospun fibers which can be activated in the presence of biological fluids

The concept of bio-battery here proposed takes advantage of the high surface area of electrospun membranes using them not only as a separator but also as part of the electrode composition.

The cellulose acetate (CA) electrospun membranes were successfully produced by electrospinning forming a highly porous matrix composed of sub-micrometric fibers with an average diameter of 243 $\pm$ 58 nm. Due to their large surface area, flexibility and biocompatibility, CA electrospun fibers are seen as favorable templates for the development of conductive polymer composites.

Considering the good electrical conductivity of polymers such as Polypyrrole (PPy) and Polyaniline (PANI), the *in situ* chemical polymerization of pyrrole and aniline monomers was performed over the surface of CA fibers. Highly conductive CA/PPy and CA/PANI composite fibers were produced with interesting electrical conductivities, 10^{-2} and 10^{-1} $S.cm^{-1}$, respectively. These composite materials allow the preservation of the main properties of the electrospun membrane making them appealing electrodes of the bio-batteries.

The electrochemical characterization of bio-batteries was performed under simulated physiological conditions. For the three different bio-batteries structures tested – PPy/CA/PANI, PPy/CA/Au mesh and PANI/CA/Au mesh – power densities of 1.7 $mW.g^{-1}$, 8.0 $mW.g^{-1}$ and 1.4 $mW.g^{-1}$ were respectively obtained.

The bio-batteries developed are therefore promising for powering a wide variety of ultralow-power consumption biomedical devices, such as pacemakers, insulin pumps or other devices to monitor bodily functions.

Keywords: bio-bateries, electrospinning, cellulose, polypyrrole, polyaniline and medical devices

– This page is intentionally blank –

Resumo

Uma nova categoria de sistemas de fornecimento de energia elétrica flexíveis surge com a capacidade de se adaptar a superfícies curvilíneas e complexas, como as presentes no corpo humano. Considerando que a produção de energia a partir do meio envolvente é provavelmente a forma mais eficaz e promissora de alimentar dispositivos médicos de longa duração, a presente tese ambiciona o desenvolvimento de uma bio-bateria de base celulósica composta por fibras produzidas por electrofiação sendo esta activada na presença de fluidos biológicos.

O conceito de bio-bateria aqui proposto tira partido da elevada área superficial característica das membranas fibrosas, utilizando-as não só como separador mas também como parte integrante dos eléctrodos.

As fibras de acetato de celulose (CA) foram produzidas por electrofiação formando uma matriz extremamente porosa, composta por fibras submicrométricas com um diâmetro médio de 243 ± 58 nm. Devido à sua elevada área superficial, flexibilidade e biocompatibilidade, as fibras de CA tornam-se um suporte vantajoso para o desenvolvimento de materiais condutores compósitos.

Considerando as boas características eléctricas que polímeros como o Polipirrol (PPy) e a Polianilina (PANI) apresentam, foi realizada a polimerização química *in situ* dos monómeros de pirrol e anilina à superfície das fibras de CA. Os materiais compósitos resultantes permitiram a preservação das principais características da membrana tornando-os vantajosos como eléctrodos para as bio-baterias.

A caracterização electroquímica das bio-baterias foi realizada utilizando uma solução que simula os fluidos fisiológicos. Diferentes bio-baterias foram testadas – PPy/CA/PANI, PPy/CA/Au and PANI/CA/Au – obtendo-se uma potência máxima de 1.7 $mW.g^{-1}$, 8.0 $mW.g^{-1}$ and 1.4 $mW.g^{-1}$, respectivamente.

As bio-baterias desenvolvidas revelaram-se promissoras para a alimentação de dispositivos médicos de baixo consumo como pacemakers, bombas de insulina ou outros dispositivos que poderão permitir a monotorização de funções biológicas.

Palavras-chave: bio-baterias, electrofiação, celulose, polipirrol e dispositivos médicos

– This page is intentionally blank –

Scientific contributions

The main contributions of this PhD thesis were published in peer-reviewed journals, as book chapters and presented in several international conferences.
The list of publications supporting this thesis is the following:

I. A. C. Baptista, J. I. Martins, E. Fortunato, R. Martins, J. P. Borges, and I. Ferreira. Thin and flexible bio-batteries made of electrospun cellulose-based membranes. *Biosensensors and Bioelectronics*, 26(5):2742–5, 2011

II. Ana Baptista, Isabel Ferreira, and João Paulo Borges. *Cellulose-based bioelectronic devices*, Chapter 4. Cellulose - Medical, Pharmaceutical and Electronic Applications book edited by Theo van de Ven and Louis Godbout, InTech, 2013

III. Ana Baptista, Isabel Ferreira, and João Paulo Borges. *Cellulose-based composite systems for biomedical applications*, Chapter 3. Biomass based Biocomposites book edited by Vijay Kumar Thakur and A.S. Singha, Smithers Rapra Technology, U.K., 2013

IV. Ana Baptista, Paula Soares, Isabel Ferreira, and João Paulo Borges. *Nanofibers and nanoparticles in biomedical applications*, Chapter 4. Bioengineered Nanomaterials book edited by Atul Tiwari and Ashutosh Tiwari, CRC Press (Taylor & Francis Group), USA, 2013

V. A. C. Baptista, Isabel Ferreira, and João Paulo Borges. Electrospun fibers in composite materials for medical applications. *Journal of Composites and Biodegradable Polymers*, 1:56–65, 2013

VI. A. C. Baptista, A. M. Botas, A. P. C. Almeida, A. T. Nicolau, B. P. Falcão, M. J. Soares, J. P. Leitão, R. Martins, J. P. Borges, and I. Ferreira. Down conversion photoluminescence on PVP/Ag-nanoparticles electrospun composite fibers. *Optical Materials* (*in press*). DOI: 10.1016/j.optmat.2014.11.015

VII. J. P. Neto, **A. C. Baptista**, J. I. Martins, E. Fortunato, R. Martins, J. P. Borges, and I. Ferreira. Fabrication and characterization of PCL microfibers for sustainable bio-power sources. *(submitted)*

VIII. A. C. Baptista, J. P. Neto, J. I. Martins, R. Martins, J. P. Borges, and I. Ferreira. Electrochemical performances of electrospun cellulose acetate membranes for biodevice applications. *(in preparation)*

IX A. C. Baptista, B. Romba, J. P. Nobre, J. Silva, C. Henriques, J. I. Martins, J. P. Borges, and I. Ferreira. Highly conductive cellulose acetate electrospun fibers functionalized with polypyrrole. *(in preparation)*

Other publications

- A. F. R. Pimenta, **A. C. Baptista**, T. Carvalho, P. Brogueira, N. M. T. Loureno, C. A. M. Afonso, S. Barreiros, P. Vidinha, and J. P. Borges. Electrospinning of ion jelly fibers. *Materrials Letters*, 83:161–164, 2012

- I. Ferreira, **A. C. Baptista**, J. P. Leitão, J. Soares, E. Fortunato, R. Martins, and J. P. Borges. Strongly photosensitive and fluorescent F8T2 electrospun fibers. *Macromolecular Materials and Engineering*, 298(2):174–180, 2013

Conference contributions

Oral presentations

- **A.C. Baptista**, J.I. Martins, E. Fortunato, R. Martins, J.P. Borges and I. Ferreira. Cellulose-based bio-batteries. *1st International Conference on Natural Fibers*, 9-11 June 2013, Guimarães, Portugal

- **A.C. Baptista**, J.P. Neto, J.I. Martins, E. Fortunato, R. Martins, J.P. Borges and I. Ferreira. Electrochemical devices based on biocompatible electrospun membranes. *9th International Conference on Nanosciences & Nanotechnologies*, 3-6 July 2012, Thessaloniki, Greece

- J.P. Borges, **A.C. Baptista**, R. Santos, I. Ferreira, P. Vidinha and S. Barreiros. Functional bio-inspired materials and devices based on electrospun fibres. *Electrospinning: Principles possibilities and Practice 2012*, 21-22 March 2012, Institute of Physics, London, UK

- **A.C. Baptista**, J.P. Neto, J.I. Martins, E. Fortunato, R. Martins, J.P. Borges and I. Ferreira. Flexible and lightweight bioelectrochemical devices based on electrospun membranes. *EMRS-Fall Meeting 2011*, 19-23 September 2011, Warsaw, Poland

Poster presentations

- Ferreira, **A.C. Baptista**, J. Leito, J. Soares, E. Fortunato, R. Martins and J. P. Borges. Highly photosensitivity and fluorescent F8T2 electrospun fibers. *9th International Conference on Nanosciences & Nanotechnologies*, 3-6 July 2012, Thessaloniki, Greece

- **A.C. Baptista**, J.P. Neto, J.I. Martins, E. Fortunato, R. Martins, J.P. Borges and I. Ferreira. Polymeric electrospun membranes for bioelectrochemical devices. *Hybrid Materials 2011*, 6-10 March 2011, Strasbourg, France

– This page is intentionally blank –

Contents

List of Figures

List of Tables

Abbreviations

AFM	Atomic Force Microscope
An	Aniline
BET	Brunauer Emmett-Teller
BMSCs	Bone Marrow Stromal Cells
CA	Cellulose Acetate
CE	Counter Electrode
Cipro	Ciprofloxacin Hydrochloride
CNTs	Carbon Nanotubes
CV	Cyclic Voltammetry
Dex	Dexamethasone
DMAc	Dimethylacetamide
DS	Dextran Sulfate
ECPs	Electrically Conductive Polymers
ECM	Extracellular Membrane
EC	Ethyl cellulose
EGF	Epidermal Growth Factor
ES	Electrospinning
FITC-dextran	Fuorescein Isothiocyanate-dextran
FTIR	Fourier Transform Infrared Mpectroscopy
F8T2	Poly[(9,9-dioctylfluorenyl-2,7-diyl)-co-bithiophene
GOx	Glucose Oxidase
HA	Hydroxyapatite
HPC	Hydroxypropylcellulose
ILs	Ionic Liquids
IMDs	Implantable Medical Devices
LASER	Light Amplification by the Stimulated Emission of Radiation
MEH	Mechanical Energy Harvester
MEMS	Microelectromechanical Systems
Mon	Monomers
MTJ	Musclestendon Junction
MWNTs	Multiwalled Nanotubes

NPs	Nanoparticles
PAA	Poly(acrylic acid)
PANI	Polyaniline
PC12	Pheochromocytoma 12
PCL	Polycaprolactone
PDGF	Platelet-Derived Growth Factor-bb
PEDOT:PSS	Poly(3,4-ethylenedioxythiophene):Poly(styrenesulfonate)
PEG	Poly(ethylene glycol)
PEI	Poly(ethyleneimine)
PELCL	Poly(ethyleneglycol)-b-poly(L-lactide-co-caprolactone
PELGA	Poly(ethylene glycol)-b-poly(L-lactide-coglycolide)
PL	Photoluminescence
PLA	Polylactic acid
PLGA	Poly(lactic-co-glycolic acid)
PLLA	Poly-L-lactide
PMMA	Poly(methyl methacrylate)
PPy	Polypyrrole
PPVs	Poly(p-phenylene vinylenes
PThs	Polythiophenes
PVK	Poly(9-vinylcarbazole)
PVP	Polyvinylpyrrolidone
Py	Pyrrole
PZT	Piezoelectric lead Zirconate Titanate
P3HT	Poly(3-hexylthiophene-2,5-diyl)
Ox	Oxidant
RE	Reference Electrode
RGG	Rhodamine 6G
rhEGF	recombinant human Epidermal Growth Factor
RTIL	Room Temperature Ionic Liquid
SBF	Simulated body fluid
SEM	Scanning Electron Microscope
SEM-FIB	Focused Ion Beam Scanning Electron Microscope
SDF-1	Stromal Cell Derived Factor-1
SWG	Single Wire Generator
TEG	Thermoelectrics Generators
TEM	Transmission Electron Microscopy
THF	Tetrahydrofuran
TS	Tensile Strength
US	Unites States

UV	Ultra Violet radiation
VECs	Vascular Endothelial Cells
VEGFs	Vascular Endothelial Growth Factors
VSMCs	Vascular Smooth Muscle Cells
WE	Working Electrode

Symbols

A	Area
$D_{average}$	Average Diameter
E	Young Modulus
E_a	Activation Energy
I	Current
Isc	Short-Circuit Current
k_B	Boltzmann Constant
L	Length
T	Temperature
t_{pol}	Time of Ppolimerization
V	Voltage
Voc	Open-circuit Voltage
W_t	Weight
σ	Electrical Conductivity

Chapter 1

Motivation

This chapter introduces implantable medical devices and the growing need for the development of flexible power sources that can supply them. Market data is presented which supports the claim that such power sources are in increasing demand both from an industrial and scientific point of views. This thesis's objectives are subsequently presented as a result of the innovative insight forecasted for the development of functionalized materials that can lead to the creation of such electrical power sources. The chapter ends with an outline of the thesis.

1.1 Introduction

Among the many diseases that may seriously impair health, some of them can only be treated by means of medications or self-recovery mechanisms of the human body. For that reason, there is a growing number of medical devices being implanted in patients to treat diseases such as Parkinson's disease, arrhythmia, diabetes, among others. Such products are generally called Implantable Medical Devices (IMDs).

Demographic factors such as changes in standard of living, the pronounced incidence of chronic degenerative diseases and the population aging are the foremost factors that influence the rising development of IMDs. Figure 1.1 shows the IMDs demand growth in the United States (US). According to this estimation, orthopedic implants remains the largest implantable device segment in the market, reflecting the evolution of degenerative

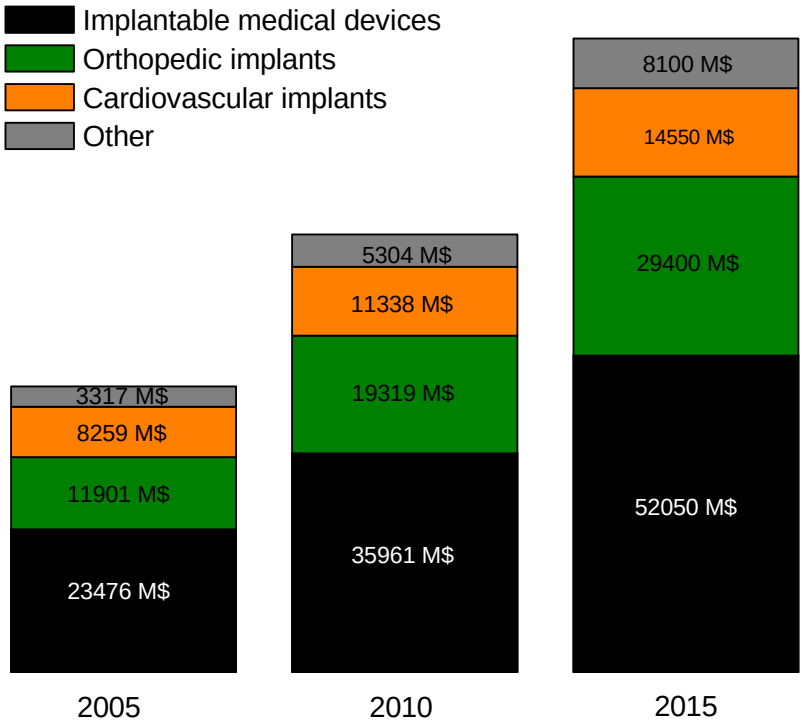

Figure 1.1: Implantable medical devices demand growth in United States (market value in million dollars, M$), forecasted by The Freedonia Group Inc in 2010. Adapted from [1].

musculoskeletal disorders and lifestyle changes that place people at risk during sports and often result in injuries. Hypertension is highly prevalent in the US and when uncontrolled it may result in the occurrence of complications such as a stroke, heart failure and others. For that reason, cardiovascular implants are expected to expand its market value and they have the potential to reduce the overall treatment cost for heart disease and contribute significantly to improved quality of life.

With the increasing number of people using IMDs, the mismatch between the patients' longevity and service life of IMDs come into focus, especially in the devices which need batteries to provide power. The IMDs that need electrical power are designated as active devices while those that do not need are denominated as passive ones.

As illustrated in Figure 1.2, there are numerous active devices implanted in patients covering various assistances through the whole human body. Some of them work in the inner body to help or replace the function of certain organs.

Long-term powering and recharging of an IMD in a highly safe and efficient way is, therefore, extremely important. Several conventional batteries, such as lithium cells, nuclear

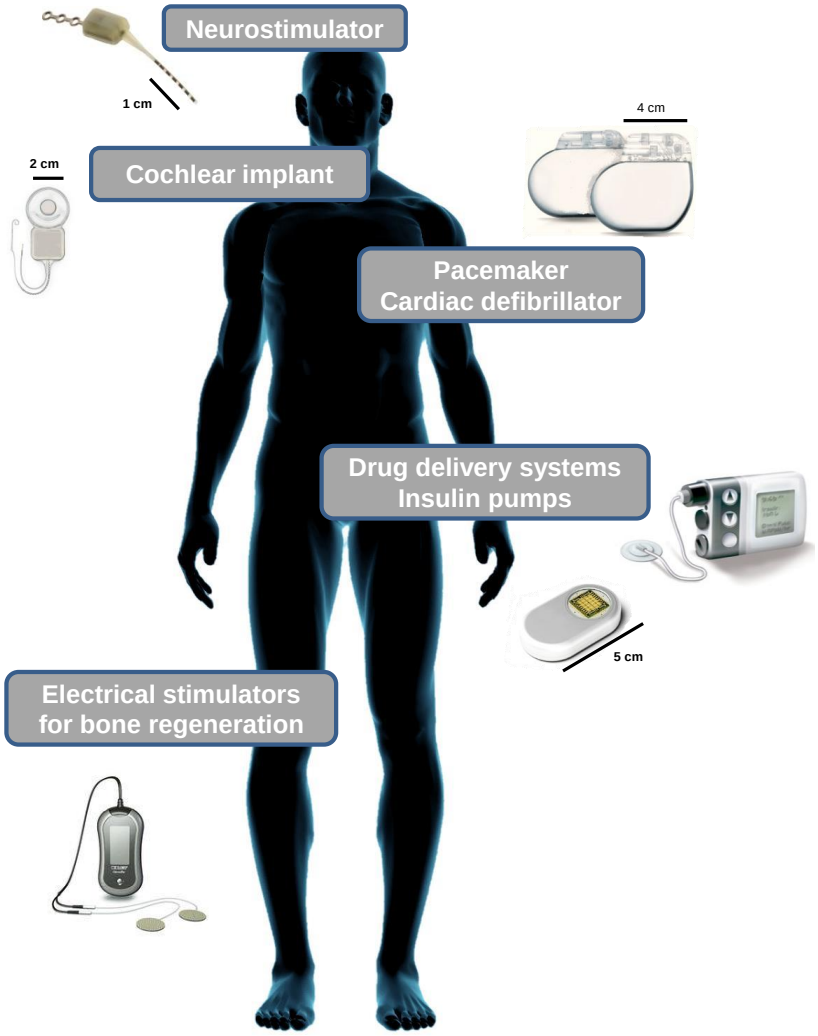

Figure 1.2: An overview of the most common active IMDs that can be found in the human body.

cells and bio-fuel cells have been used to power IMDs. Even if some medical batteries may have long lifetime, the battery will eventually require replacement or recharging. For short term applications, the conventional battery may thus provide a sufficient device lifespan but, for long term applications, alternative power sources may be preferable to replace these batteries, especially if the substitution or recharge procedure is invasive.

For instance, implanted biomedical devices such as cardiac pacemakers and insulin pumps have a limited life, ranging from less than a year to perhaps 10 years. Currently, replacing the battery requires its surgical removal, typically along with the entire device that it services. This procedure brings health risks to the patient and added costs. Additionally,

it is also remarkable the growing number of new devices that intends to be implanted in highly restricted spaces in the human body such as artificial retinas and cochlea. Due to space restrictions, the power sources for such devices must be highly compact and easy to adapt to the human body's curvilinear surfaces. Considering the replacement cost and risk inherent to conventional implanted batteries along with the growing need for power sources miniaturization, it is therefore essential to develop new concepts of electrical power sources for implantable medical batteries.

1.2 Background

Biomedical technology usually requires portable and wearable implantable devices that can interface with biological systems. Their continued scaling and integration have enabled dramatic reductions in energy consumption. Table 1.1 summarizes the power requirements of the most common implantable medical devices. Implanted devices such as pacemakers, hearing aids or cochlear processors are relatively mature applications with power consumption levels ranging from a few microwatts to a few milliwatts. Nevertheless, their batteries' lifetime is limited and the replacement of the entire IMD and/or only its battery is required, often risking the health and well-being of the patient.

Table 1.1: Power requirements of common implantable medical devices. Adapted from [2].

Device	**Power**	**Battery lifetime**	**Ref**
Pacemaker and cardioverter-defibrillator	< 10 μW	10 years	[3]
Hearing aid	100-2000 μW	1 week	[4], [5]
Analog cochlear	200 μW	1 week	[6], [7]
Neural recording	1-10 mW	n.a.	[8], [9]
Retinal stimulator	250 μW	n.a.	[10], [11]

The history of the implantable cardiac pacemaker is traced back to its inception in 1951 and can be followed through its development and trials in 1958, to its successful implantation in 10 patients in 1960 and its subsequent commercialization [12]. Since then, the

usage of implanted pacemakers has been increasing. Figure 1.3 shows the evolution of pacemaker size and weight from 1960 to 2013. As observed, there is a demand to make these medical devices smaller, lighter and more reliable.

Currently, there has been a strong interest in ultrathin and stretchable energy devices to meet the various design requirements of modern electronic devices. Figure 1.4 shows the great increase of papers related to bio-batteries for medical applications and reveals the tremendous interest for this field of research. Additionally, it is also remarkable the recent interest for stretchable and bendable batteries as a result of the rapid growth of flexible electronics.

In this context, this work aims to fulfill the needs previously described as well as to contribute for the development of flexible electronics for medical devices. Considering the evolution of IMDs, the development of an inexpensive and flexible energy supply system is proposed to overcome some of the drawbacks of the existing batteries.

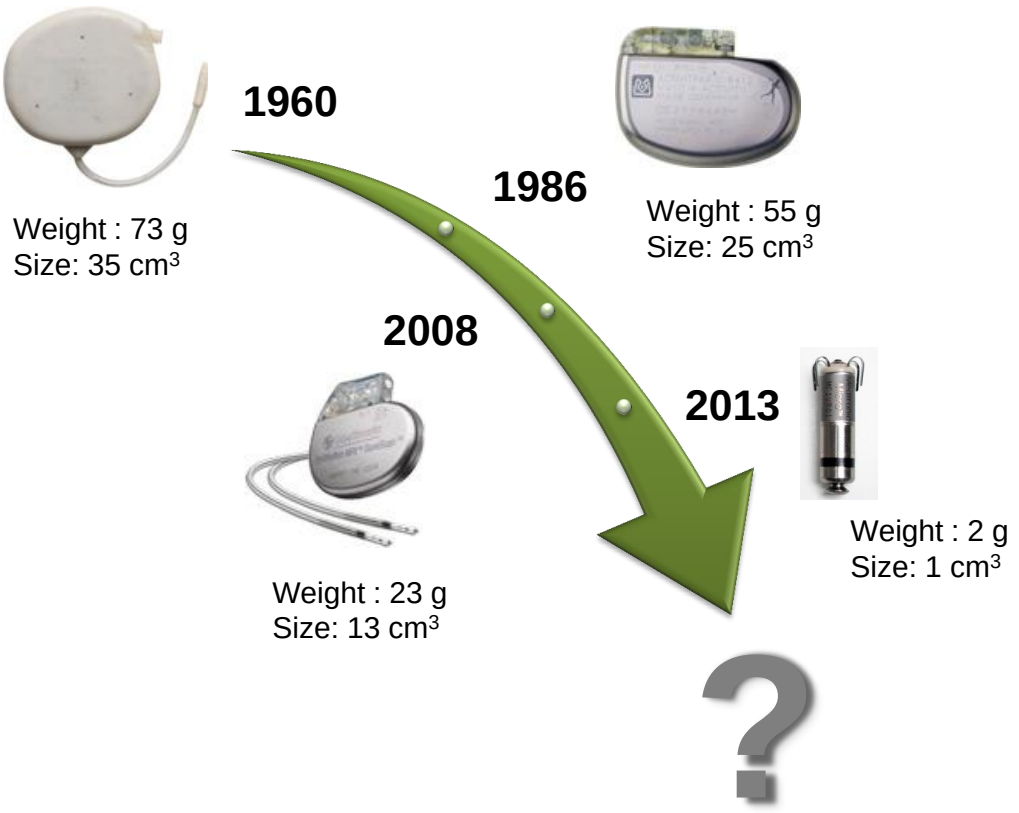

Figure 1.3: Size evolution of pacemakers from 1960 to 2013. Adapted from [13], [14].

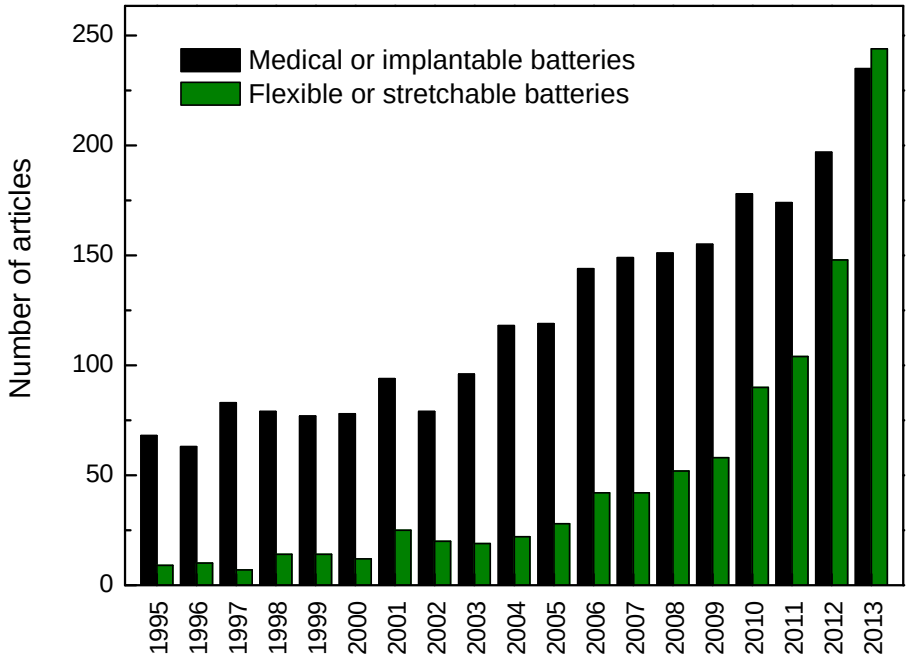

Figure 1.4: Number of scientific articles using the keywords "Medical or implantable batteries" and "Flexible or stretchable batteries" published on the ISI Web of Knowledge.

1.3 Innovative insight

The scientific research presented in this thesis foresees the use of electrospun fibers in the development of functionalized materials opening a new path for the creation of novel, lightweight and flexible nanostructures. Polymer-based electronics represents a different and even more challenging technology, with unique properties and with the ability to be flexible and conform to complex surfaces. The bio-battery – or biocompatible battery – here proposed is mainly composed of an ultrathin electrospun polymeric membrane. The polymeric matrix is simultaneously a separator membrane and the support for the electrodes. The electrodes can be formed directly on the electrospun fibers by functionalizing them in order to achieve the desirable electrical conductivity.

Considering that harvesting energy directly from the environment is probably the most effective and promising approach for powering long-term biomedical devices, the bio-batteries can take advantage of the ionic content present in physiological fluids – such as blood and sweat – to generate electrical energy. When fully developed, they should

be able to power a variety of ultralow-power consumption biomedical devices, such as pacemakers, artificial retinas, insulin pumps, cochlear implants, vagus nerve stimulators, and other future devices that will monitor bodily functions.

1.4 Objectives

Based on this innovative insight, the main objective of the current work is to develop, produce and validate the bio-battery concept proposed. Figure 1.5 summarizes that this bio-battery concept relies on the production of a ultrathin cellulose-based electrospun membrane with electrical properties enhanced through fiber functionalization which is capable of harvesting energy directly from the environment to generate the electrical power that biomedical devices require in the long term.

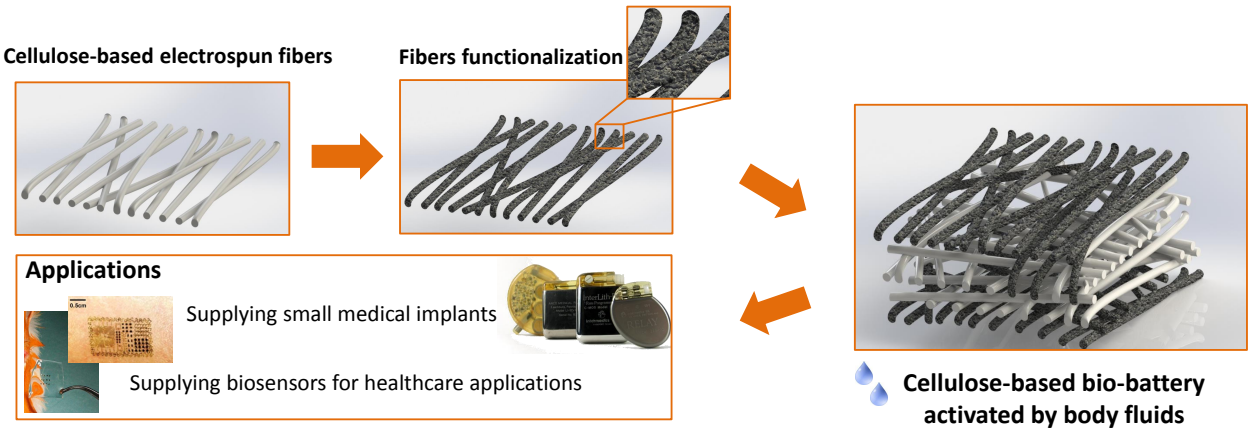

Figure 1.5: Illustration of the bio-battery concept proposed in this thesis.

The major advantage of the bio-battery concept shown in Figure 1.5 relatively to the state-of-the-art is the flexibility associated to low quantity of material needed and thus low production cost. Previous research and initial demonstrators showed that the bio-battery concept here proposed, when in contact with sweated skin, could reach potentials in the range of 0.3 V and currents around 100 μA [15]. This thesis envisions that, when fully optimized, these bio-batteries are able to supply a variety of ultralow-power consumption biomedical devices. To reach the scientific and technical know-how needed to provide these bio-batteries, the research was split into three main tasks:

1. **Production and characterization of cellulose-based electrospun membranes**. The first task involves the study and optimization of the electrospinning process and the morphological characterization of the membranes produced.

2. **Development of functional fibers**. The second task involves the use of conductive polymers to enhance the electrical properties of the electrospun fibers.

3. **Bio-batteries electrochemical characterization and concept validation**. The final task consists in the construction of bio-batteries and the investigation of its electrochemical behaviour and biocompatibility.

1.5 Thesis outline

The following section is an outline of the remaining chapters of this thesis:

Chapter 1: Motivation. This chapter presents the objectives and motivation of this PhD thesis.

Chapter 2: Literature review. A literature review about the power sources found in modern electronics is given, highlighting the ultralow-power sources in the medical field.

Chapter 3: Production and characterization of cellulose-based electrospun fibers. This chapter gives a brief overview about cellulose-based materials and describes the production of nanofibers through the electrospinning technique. The experimental details and the results achieved during this work are presented and discussed.

Chapter 4: Development of cellulose-based conductive fibers for bio-batteries. The advantages of using electrically conductive polymer-based materials in medical applications are summarized in this chapter. A detailed methodology to obtain electrically conductive composite fibers is given and the main results are presented and discussed. Different bio-batteries structures are evaluated and electrochemically characterized.

Chapter 5: Exploring functional electrospun fibers for other applications. This chapter explores the functionalization of electrospun fibers envisaging applications in organic optoelectronics. Preliminary results are presented and discussed.

Chapter 6: Conclusions and perspectives. This final chapter presents the main conclusions of this work and provides new perspectives for future research.

Chapter 2

Literature review

This chapter provides the fundamental scientific background regarding the use of nanofibers in medicine with particular emphasis in tissue regeneration, drug delivery and biosensors. A brief overview about the most innovative and challenging work performed in the field of energy harvesting system envisaging medical purposes is also provided.

2.1 Electrospun fibers in medicine

Advances in nanotechnology have given the possibility of tailoring the materials' structure at the nanometer scale. Nanofibers are nanostructures that have at least one dimension in the nanometer scale. Being a two-dimensional nanomaterial, nanofibers normally have their diameters between tens and hundreds of nanometers. Due to that their low diameter size and high specific surface area are attractive physical characteristics for a wide range of applications. It also exhibit new or enhanced size-dependent properties when compared with larger structures of the same material.

Several methods such as drawing, phase-separation, template, self-assembly and electrospinning have been used to fabricate nanofibers. The drawing process makes a single fiber at each time using a sharp tip. For instance, the tip of an atomic force microscope (AFM) can be used to pull a fiber from a droplet of a viscoelastic solution by applying a voltage [16]. This process is possible only with viscoelastic materials that undergo strong deformations while being cohesive enough to support the stresses developed during the

drawing.

The phase separation method consists in mixing the polymer and the solvent before gelation. After phase separation, the solvent is removed by drying and then a porous nanofibrous structure is created [17]. However, the whole process takes relatively long time. For the template synthesis, a nanoporous membrane is used as a template to make nanofibers with controlled shape and diameter [18]. This method allows the use of electrically conductive polymers, metals, carbon-based materials and semiconductors as raw materials.

An additional process is the self-assembly in which individual pre-existing components organize themselves into desired patterns and functions [19]. The intermolecular forces are the main mechanism responsible for the assembling of molecule units that determine the shape of nanofibers. Similarly to the phase separation process, self-assembly is a time-consuming process for the production of continuous polymer nanofibers. The usefulness of these methods is thus restricted by limited number of material combinations, high costs and low production rates. In contrast, electrospinning is perhaps the simplest process for producing nanofibers with relatively high productivity. Electrospinning is a broadly used technology that uses an electrical field to create a charged jet of a polymer solution [20]. In a conventional setup, a polymer solution passes through a capillary and a high voltage is applied such that the particles within the solution are charged creating a repulsive force. At a critical voltage, the repulsive force overcomes the surface tension of the solution and a jet erupts from the tip of the capillary towards a grounded collector. There are a wide range of polymers and precursors that can be electrospun such as polylactic acid (PLA) [21], polyurethanes [22], silk fibroin [23], collagen [24], cellulose and its derivatives [25], [26], composites [27], and ceramics [28]. The electrospinning is therefore a versatile and inexpensive way to produce nanofibers with controllable sizes and properties.

The electrospinning also enables the production highly porous 3D structures having large surface to volume ratios with suitable physical and chemical properties for a wide variety of applications, such as sensors [29], antibacterial surfaces [30], scaffolds [31], photocatalysis [32] and solar energy applications [33] (Figure 2.1). Moreover, in electrospinning it is

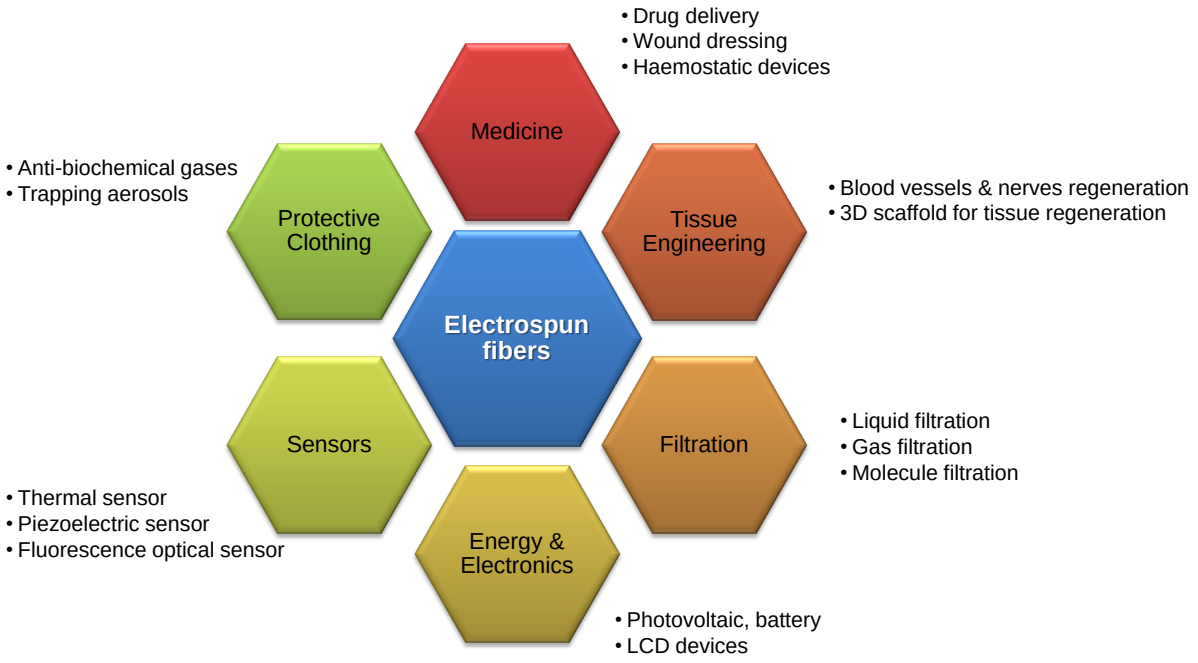

Figure 2.1: Field of application of the electrospun fibers [34].

possible to combine different materials with singular morphological structures making it a powerful tool to design functional materials especially for biomedical applications, such as in tissue engineering, drug delivery and biosensors.

2.1.1 Tissues Engineering

Tissue engineering has emerged as an interdisciplinary field that applies the engineering and life science principles to develop biological substitutes for restoring, maintaining or improving the function of human tissues. One of the main challenges in this field is the design and engineering of scaffolds or polymeric matrices that mimic the structure and biological functions of the extracellular membrane (ECM).

A functional scaffold must combine a high degree of porosity and an appropriate pore size distribution and interconnectivity with the structural integrity preventing the collapse of scaffolds pores during neo-tissue formation. Furthermore, the scaffold should be nontoxic, biocompatible and interact with the cells to promote adhesion, proliferation, migration and differentiated cell functions. Many studies can be found in literature where scaffolds made of electrospun nanofibers have been used for mimicking tissues such as blood vessels,

bones and muscles.

- **Blood Vessels**

Tissue engineering of blood vessels is mostly focused on the development of vascular grafts with small diameter (inner diameter < 5 mm). The long-term unblocking of small-diameter vascular grafts is still a challenging issue because of easy restenosis caused by thrombosis and bursting pressure. For that reason, tissue engineering offers an alternative approach to address the need for small-diameter vascular grafts through the design of non-thrombogenic interface.

Electrospinning provides the construction of vascular scaffolds due to the simplicity of shaping tubular constructs using rotation and translational motion. Vaz [27] and colleagues have been using a sequential multi-layering electrospinning with a rotating mandrel-type collector to produce scaffolds that mimic morphologically and mechanically the architecture of a blood vessel (Figure 2.2). It is well known that in the media layer of the native blood vessels, the smooth muscle cells (SMCs) and collagen fibrils have a marked circumferential orientation to provide the mechanical strength necessary to withstand high circulatory pressures. Additionally, the intima layer of the native blood vessels consists in endothelial cells coating the vessels' internal surface. Between those two layers exists an internal elastic lamina mainly composed of elastin, which confers elastic properties to the blood vessels. Therefore, a bi-layered tubular scaffold composed by oriented and stiff PLA fibers in the outside and random and elastic polycaprolactone (PCL) fibers in the inside was proposed [27]. The fabricated scaffold showed a desirable level of malleability (elastic up to 10% strain) and proved to be capable of promoting cell growth and proliferation making it suitable for blood vessel tissue engineering.

The electrospinning of collagen and elastin has also become possible [36]. These two biopolymers are the main structural components of the vascular ECM. Collagen is responsible for the structural integrity and tensile strength of tissues and elastin gives them elasticity. Electrospinning of pure collagen or elastin has shown some limitations due to the poor mechanical properties of the produced fibers. Incorporation of biodegradable synthetic polymers into the structure will impart the scaffolds' strength, which will si-

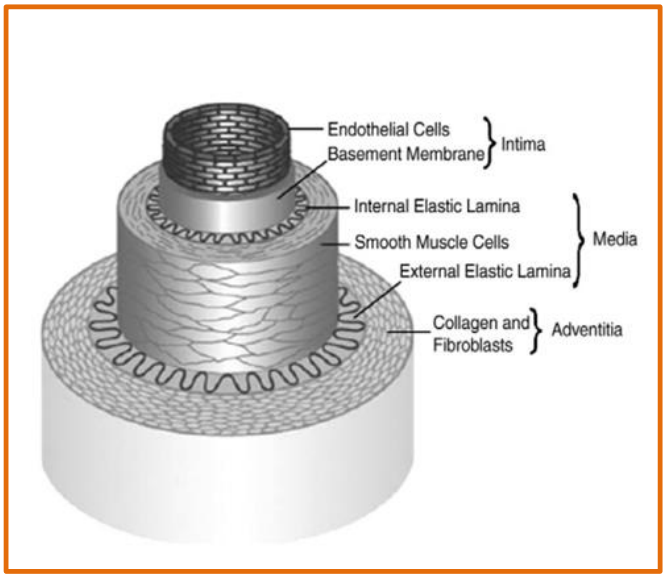

Figure 2.2: Representative illustration of the arterial wall composed by intima, media and adventitia primary layers [35].

multaneously maintain a high level of bioactivity due to the presence of the biopolymer (collagen or elastin). Lee [37] has reported the fabrication of a composite vascular scaffolding system by electrospinning PCL and collagen (type I) blends. These composite scaffolds were designed to provide sufficient biomechanical properties and configured to accommodate vascular endothelial and smooth muscle cells to be used in vascular tissue engineering applications. Polycaprolactone is an aliphatic polyester that degrades slowly and possesses high tensile and elongation properties for vascular grafts. The resulting composite scaffold showed good biocompatibility and support for cell growth and proliferation *in vitro*.

During tissue repair, growth factors induce specific biological responses including cell proliferation and migration, matrix synthesis, angiogenesis and release of growth factors. For an appropriate regeneration of small-diameter blood vessels, the proliferation of vascular endothelial cells (VECs) is desirable on the lumen of the graft in the first 7 to 10 days, followed by the growth of vascular smooth muscle cells (VSMCs) on the outer layer, which makes the tissue regeneration more stable without thrombosis or burst.

Vascular endothelial growth factors (VEGFs) can stimulate endothelialization and it can also inhibit excessive proliferation of VSMCs [38]. Conversely, platelet-derived growth

factor has high ability to stimulate VSMCs proliferation [39]. To overcome this problem, different release devices must be designed to control the rapid delivery of VEGF and prolonged release of platelet-derived growth factor-bb (PDGF). For that purpose, two modied coaxial electrospinning techniques were developed by Zhang [40] to encapsulate VEGFs and PDGF, respectively, in order to regulate proliferation of VECs and VSMCs. The double-layered membranes were prepared via coaxial electrospinning of chitosan hydrogel/poly(ethyleneglycol)-b-poly(L-lactide-co-caprolactone) (PELCL) loaded with VEGF in the inner layer and methoxy poly(ethylene glycol)-b-poly(L-lactide-co-glycolide) (PELGA) emulsion/PELCL loaded with PDGF in the outer layer. PELGA was added to PELCL by emulsion/coaxial electrospinning to slow down the initial release rate of PDGF and accelerate it in the later release period. These authors have found that dual-release of VEGF and PDGF could effectively accelerate VEC proliferation in the first 6 days and slowly moderate VSMC proliferation in the initial 3 days while generating rapid proliferation after day 6. In summary, dual-delivery of VEGF and PDGF using the modified electrospun membranes may facilitate revascularization and can bring great benefits for blood vessel regeneration.

- **Bones**

Electrospun nanofiber meshes have been studied intensively in bone tissue engineering due to their ability to support cell growth and differentiation into osteogenic phenotypes. A key cellular phenotype is the osteoblast, which is the cell type that lays down the ECM of bone tissue and thus the target cell type for recruitment and differentiation in bone reconstruction.

Synthetic polymers and their copolymers, natural polymers, composites of natural and synthetic polymers, inorganic materials, such as bioactive glass and hydroxyapatite (HA), and composites of inorganic materials with synthetic and natural polymers have been used to produce appropriate nanofiber scaffolds for osseous tissue engineering. A scaffold that maintains stability and promotes cell growth and proliferation but gradually degrades along with the construction of new tissues is required. Ultimately, it should be completely replaced by the new tissue. Prabhakaran [41] have studied the electrospinning fabrication

of poly-L-lactide (PLLA), PLLA/HA and PLLA/collagen/HA substrates and its applicability as scaffolds for bone tissue regeneration. Poly-L-lactide is a biodegradable polymer with controlled degradation characteristics that can be used in tissue engineering and drug delivery therapies. Hydroxyapatite is a bioceramic frequently found in biomedical implant applications due to its biodegradability, bioactivity and osteoconductive properties. As a bioceramic, HA cannot be easily shaped in the bone defect sites due to its natural rigidity. However, synthetic biodegradable polymers can improve significantly the mechanical properties of HA. The *in vitro* assays demonstrated that when HA is introduced in the polymer matrix (PLLA/HA scaffolds) cell proliferation is observed and enhanced comparing to PLLA scaffolds.

Furthermore, the presence of collagen has accelerated the cell attachment and proliferation on PLLA/collagen/HA scaffolds. Osteoblasts were found to adhere and grow actively on PLLA/collagen/HA nanofibers with mineral deposition 57% higher than in the PLLA/HA nanofibers. The study concluded that the synergistic effect of the presence of an ECM protein, collagen and HA in a biocomposite scaffold holds great potential for adhesion, proliferation and mineralization of osteoblasts.

In order to develop a bioactive membrane for guided bone regeneration, Wei Ji [42] has proposed the functionalization of an electrospun membrane with a chemotactic factor.

Guided bone regeneration is typically used as a strategy to heal bone defects in the craniomaxillofacial region. For that purpose, the creation and preservation of an isolated space using a membrane as a barrier to avoid the invasion of fast growing epithelial and other soft tissues into the osseous defect is required. This allows osteogenic cell populations originating from the parent bone to inhabit the osseous defect [43]. These membranes need to be flexible to adapt to a bone defect, preserve the space for bone formation and to attach to soft tissues. On the other hand, biodegradability is also a requirement since it avoids surgery in order to remove the membrane. Among the multiple types of progenitor cells located in the bone marrow, bone marrow stromal cells (BMSCs) are considered the most powerful ones during bone regeneration due to its multi-lineage differentiation capacity [44]. In addition, cytokines and chemokines are important factors in mobiliza-

tion control, trafficking and homing of stem/progenitor cells [45]. Thus, it is essential to increase their local concentration at the target site to induce BMSCs recruitment.
Wei Ji [42] described the preparation of an electrospun membrane of PCL blended with B-type gelatin functionalized with stromal cell derived factor-1 (SDF-1) by physical adsorption. Among various cytokines or chemokines, SDF-1 is particularly important in BMSCs homing and localization within the bone marrow. These authors found that PCL/gelatin electrospun membranes clearly acted as a SDF-1 carrier providing a diffusion-controlled release profile. The bioactive membrane also induced *in vitro* BMSCs recruitment, demonstrating a great potential for guided bone regeneration.

- **Muscles**

Skeletal muscle tissue is composed of bundles of highly oriented and densely packed muscle fibers each with multinucleated cells derived from myoblasts. The fibers are densely packed together in ECM to constitute an organized muscle tissue that generates longitudinal contraction. For muscle tissue reconstruction, scaffolds should allow cellular organization mimicking native individual fiber formation with unidirectional orientation. Electrospun scaffolds should thus have appropriate material characteristics for skeletal muscles: biocompatibility to allow cell adhesion and growth, degradability over time and elasticity to accommodate contractile function.
Similar to what has been done for blood vessels regeneration, Choi [46] studied the feasibility of using PCL/collagen based nanofibers as a scaffold system for implantable engineered muscles. They investigated how the orientation of electrospun PCL/collagen nanofibers influences morphology, adhesion, proliferation, differentiation and organization of human skeletal muscle cells. They concluded that unidirectional oriented nanofibers can signicantly induce the alignment of muscle cell and myotube formation compared to randomly oriented nanofibers. Aligned nanofiber scaffolds may provide implantable functional muscle tissues for patients with large muscle defects.
It has been reported so far the development of single tissue types. However, there is an increasing demand for complex composite tissue engineering, such as tissue interfaces, possessing coordinated functions [47]. Ladd [48] has proposed the engineering of muscles-

tendon junction (MTJ) tissues. One challenge in engineering MTJs is the design of a continuous scaffold suitable for both tissue types. Muscle-tendon junctions require a high quality interface to allow force transfer from muscle to tendon. These authors proposed the fabrication of a dual scaffold which exhibits local mechanical property differences mimicking the trends seen in native MTJs. Co-electrospinning was used to create three distinct scaffold regions: a PCL/collagen region (one end side), a PLLA/collagen region (opposite end side) and an overlap region (center). Both polymers were blended with collagen since it improves cell attachment. The mechanical properties of the three regions were evaluated: the PLLA/collagen side of the scaffold was the stiffest one showing the lowest strain (similar to the tendon); the PCL/collagen side was the most compliant displaying the highest strain (analogous to the muscle); and the middle region possesses an intermediate stiffness and strain levels (similar to the junction). The structure had distinct mechanical properties and demonstrated to be an attractive solution for MTJ tissue engineering.

2.1.2 Drug delivery

Controlled release is an efficient process for delivering drugs in medical therapy. In a controlled release system, the active substance is loaded into a carrier or device and then released at a predictable rate. Exciting developments have been recently made in this field. Due to the high surface area to volume ratio, electrospun nanofibers provide a useful pathway for drug delivery and the release profile can be finely controlled by modulation of nanofiber morphology, porosity and composition [49]. The simplicity of the electrospinning process can also provide the ability to conveniently incorporate therapeutic compounds into the electrospun fibers. The drug can be loaded to the electrospun fibers by several methods such as coating, embedding, and encapsulating by coaxial and emulsion electrospinning.

Using the coating method, drug molecules can be adsorbed or cross-linked to the surface of electrospun fibers via a physical or chemical method. Choi [50] has reported the chemically conjugation of a recombinant human epidermal growth factor (rhEGF) with the

surface of electrospun nanobers for *in vivo* wound healing treatment of diabetic ulcers. Current treatments for diabetic foot ulcers include the administration of disinfectants followed by application of epidermal growth factor (EGF)-containing gels around the lesions. This work involved the electrospinning of biocompatible nanofibers with functional amine groups on the surface (PCL and PCL/poly(ethylene glycol, PEG, block copolymer). Upon immersion in an aqueous solution, the exposed functional amino groups on the surface of the nanofibers were chemically conjugated to rhEGF by activating the carboxylic groups of the protein. Human primary keratinocytes were cultivated on EGF-conjugated nanofibers in order to investigate the effect of EGF nanofibers on the differentiation of keratinocytes. Therefore, wound healing effects of the EGF nanofibers were successfully confirmed in diabetic animals with dorsal wounds.

Another possibility to produce drug-loaded fibers is to electrospun a polymer solution that also contains the therapeutic compound. It is required in this process that the drug solution and polymer solution must be either miscible liquids or that solid drug particles can be well dispersed into the polymer solution. Peng [51] has investigated the use of poly(ethylene glycol)/poly(D,L-Lactide copolymer electrospun fibers as a drug delivery system. This copolymer is known to have a good biocompatibility *in vivo* and improved degradation rate. Paracetamol (acetaminophen, N-(4-hydroxy-phenyl) acetamide) was chosen as the model drug since it is widely used as analgesic and antipyretic drug. The drug was mixed with the copolymer solution and electrospun to form the fiber mats. *In vitro* matrix degradation profiles of these fibers were characterized by measuring their weight loss, the molecular weight decrease and their morphology change. It was observed from these studies that scaffolds with smaller fiber diameter have a higher contact area between polymer and water which, consequently, accelerates the matrix breakdown. In addition, *in vitro* drug release assays have demonstrated that the release behavior mainly depends on polymer matrix degradation and drug diffusion. In conclusion, the drug release rate can be controlled by polymer degradation which can be tuned by adjusting the electrospun fiber diameter and its porosity.

Since the loading of bioactive drugs into electrospun fibers via embedding method is still

a challenge, the electrospun of core-shell and hollow structured fibers come as a solution for the preparation of drug delivery systems for larger molecules.

The emulsion electrospinning is an attractive approach to encapsulate a drug into a fiber. This process is quite similar to conventional electrospinning except that the solution is replaced with a water-in-oil emulsion [52]. Kai Wei [53] proposed a fluorescein isothiocyanate-dextran (FITC-dextran)/poly(lactic-co-glycolic acid) (PLGA) fibrous composite scaffold. Used as a model drug, FITC-dextran was previously dissolved in an aqueous solution and then was emulsified with the PLGA oil phase to prepare the emulsion to be electrospun. Morphological characterization showed that the inner component FITC-dextran was properly wrapped in the center of PLGA. Moreover, the core-shell structure helped the sustained release of the model drug from the fiber. A burst release profile of 60% was obtained for the first 2 weeks after which the scaffold exhibited a sustained release profile of approximately 1% cumulative release per day for 4 weeks long. The developed scaffold exhibited a release profile that might be useful for site-specific drug-release systems.

2.1.3 Biosensors

The integration of biomolecules with electronic elements to form multifunctional devices has been recently the subject of intense scientific research. The need of new sensors exhibiting a high selectivity and a total reliability in connection with smart systems and actuators for real time diagnostic and monitoring of diseases has driven wonderful developments in sensors and particularly in biosensors. Biosensors can be regarded as complementary tools to classical analytical methods due to their inherent simplicity, relative low cost, rapid response and proneness to miniaturization, thereby allowing continuous monitoring. They can integrate portable and implantable devices and be used in biological and biomedical systems. However, the development of biocompatible, nontoxic and lightweight power sources devices is still challenging. It would enable the production of various functional devices mechanically flexible and self-sustained, allowing their integration into a wide range of innovative products such as in implantable medical devices.

Enzymes are well-known biological sensing materials used in the development of biosensors due to their specificity. The immobilization of the enzyme is a critical step in the design of the sensor, since it is essential that the biological element exhibits maximum activity in its immobilized environment. Tang [54] proposed the modification of Pt electrodes with electrospun titanium dioxide (TiO_2) nanofibers for electrochemical detection. TiO_2 nanofibers were prepared by electrospinning and deposited onto Pt electrodes surface. The surface of the modified electrodes was later coated with glucose oxidase (GOx). As a result, the amperometric response of the prepared enzyme electrodes indicated a higher sensitivity to glucose than those without the nanofibers. The enzyme showed good affinity to TiO_2 nanofibers due to its relevant biocompatibility and higher surface area. They concluded to be essential the modification of Pt electrodes with an optimal density of nanofibers to obtain the maximum improvement of glucose bioelectrocatalytic properties.

Recently, novel free probe type nanoscale biosensor based on a single mesoporous Zinc Oxide (ZnO)/Chitosan hybrid nanostructure has been proposed by Zhao [55]. A single mesoporous ZnO nanofiber prepared by electrospinning with subsequent annealing process was placed on the surface of the substrate electrode (SiO_2 /Au). The GOx enzymes were successfully immobilized in the ZnO nanofibers by electrostatic adsorption interaction and chitosan was further applied onto the electrode surface to prevent possible enzyme leakage. Thus, the prepared biosensor exhibited excellent sensitivity and fast response. The characteristic structure of mesoporous ZnO with pores and protuberances is favorable for enzymes loading and contributes to enhance the electrical communication efficiency. The free probe construction indicates that the single ZnO/Chitosan hybrid nanostructure has the potential to be further developed as a nanoprobe for trace detection in microcell and microbial monomer in *in-vivo* research.

The immobilization of biological compounds is regarded as an essential step for biosensors since it affects the sensitivity, selectivity and long-term stability of the device. Therefore, electrospun nanofibers appear as ideal support for the immobilization of biomolecules.

2.2 Energy harvesting systems for modern medicine

Batteries developed for implantable medical devices can have different functional requirements depending of the application envisaged. Still, it is fundamental that medical batteries must operate for long periods to minimize surgical frequency, be safe during installation and use, have predictable performance and be highly reliable. Additionally, the medical batteries must have high volumetric energy to enable the design of small devices that minimize discomfort for the patient [56].

Medical devices such as cochlear implants, spinal-cord stimulators, glucose sensors and cardiac rhythm management devices are currently powered by Li-ion cells. Besides having a limited lifetime, these batteries typically require packaging to avoid safety concerns which create certain limitations for their use in flexible and lightweight implantable devices.

For non-implantable medical devices, batteries can be recharged or replaced easily, but for the comfort and patient well-being it should be as infrequently as possible. To supply energy to implanted devices, harvesting ambient energy in which the source of energy exists inherently as part of the system is the most suitable energy gathering approach.

Emerging strategies to replace batteries demonstrate uncommon methods to extract power from chemical, mechanical and thermal processes in the human body. Recent investigations were carried out to convert the body heat into electricity by using miniaturized thermoelectric generators (TEG). In 2007, Yang Yang has performed theoretical studies to evaluate the real energy generation capability of a commercial TEG module simulating the temperature differences between the body core and the skin surface [57]. Later, the same author reported the development of a prototype composed by two implanted TEG modules and a specified boosted circuit. During *in vivo* testing such device combination has demonstrated to be capable of supporting a clock circuit whose power consumption is much higher than an ordinary cardiac pacemaker [58].

Last year, S. J. Kim [59] proposed the conversion of body heat into electrical energy by using a thin and flexible thermoelectric power generator printed on a transparent fabric. This approach consists on the printing of n-type (Bi_2Te_3) and p-type (Sb_2Te_3) thermo-

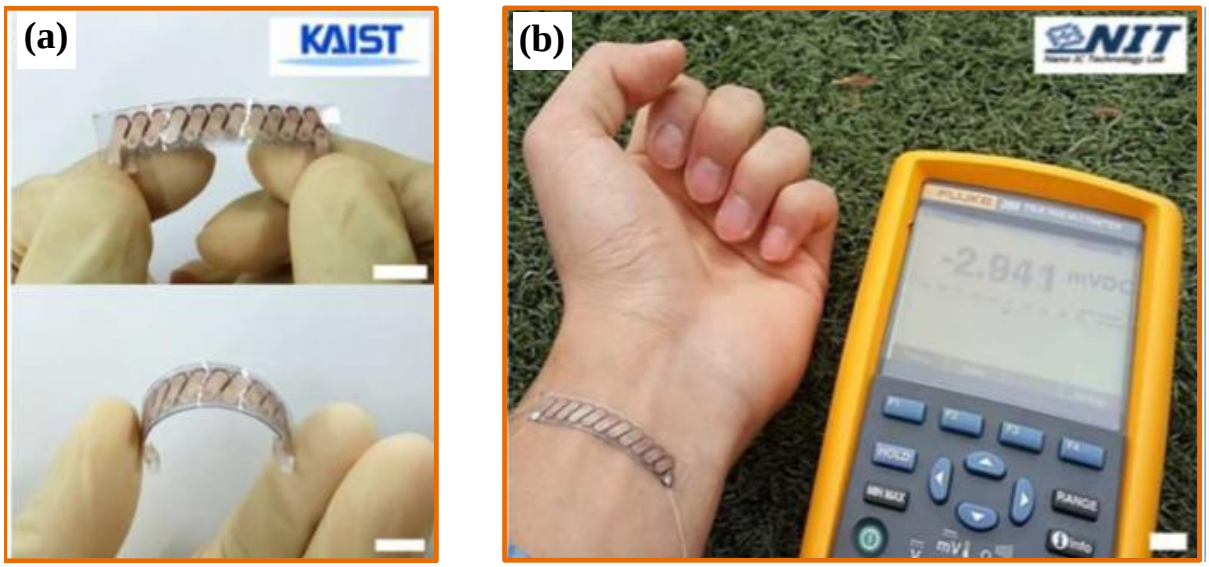

Figure 2.3: Flexible thermoelectric generator for harvesting thermal energy from human skin: (a) Photograph of the prototype and (b) demonstration of electricity generation measured on human skin at air temperature of 15°C. Scale bar, 1cm [59].

electric materials on a glass fabric-based textile by using a screen printing technique. A prototype comprising 11 couples of Bi_2Te_3 and Sb_2Te_3 thin films was fabricated on a glass fabric and applied to human skin as a body heat energy harvester (Figure 2.3 (a)). The thermoelectric module demonstrated to be capable to generate an open-circuit voltage (Voc) of 2.9 mV and an output power of 3 μW when associated with an external load at air temperature of 15°C (Figure 2.3 (b)). The power density showed to be promising to activate sub-microwatt or microwatt wearable devices such as temperature sensors [59].

Harvesting energy from human body can also be possible by converting hydraulic energy from blood flow, heart beats and blood vessels contraction. In 2009, Rusen Yang [60] described the development of a single wire generator (SWG) for harvesting energy from small-scale dynamic muscle movement. For that purpose, the two ends of a zinc oxide piezoelectric nanowire were fixed on the top of a flexible polyimide film. The concept was validated by attaching the SWG to the joint position of the finger. With repeated bending, the finger movement deforms the ZnO nanowire producing a piezoelectric potential within the wire which drives the flow of external electrons and produces electric power output (Figure 2.4) [60]. For such demonstration, the single nanowire device displayed

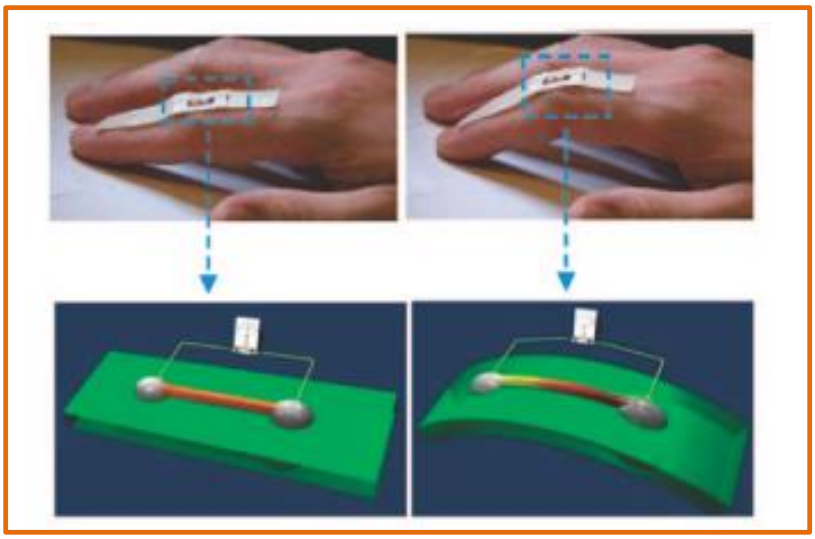

Figure 2.4: Energy harvesting from an oscillating human index finger using a single wire generator [60].

a voltage output up to 25 mV, and a current output higher than 150 pA. The series connection of four nanogenerators were also tested in a live hamster converting the body motions, such as running movement, into an output voltage greater than 0.1 V.

The research group of Dr. John Roger [61] has recently proposed an innovative integrated system that enables high-efficiency mechanical-to-electrical energy conversion from natural contractile and relaxation motions of the heart, lung and diaphragm. The fabrication of a piezoelectric lead zirconate titanate (PZT) mechanical energy harvester (MEH) has been described and validated using animal models. The main structure consists in a layer of PZT sandwiched between a bottom electrode of Pt and a top electrode of Au, as illustrated in Figure 2.5 (a). An MEH module is composed by 12 groups of 10 units of the proposed structure connected in series (Figure 2.5 (b)). Finally, devices were encapsulated with biocompatible materials to avoid contact with body fluids and tissue, minimizing the risks of failure or immune response. A co-integrated collection of such energy-harvesting elements with rectifiers and microbatteries provided an entire flexible system, able to be integrated with the beating heart and showed efficiencies of ≈2%.

The *in vivo* tests involved the anchoring of the devices to pericardial sites of bovine and ovine hearts. Figure 2.5 (b) shows a PZT MEH on the left and right ventricles of the

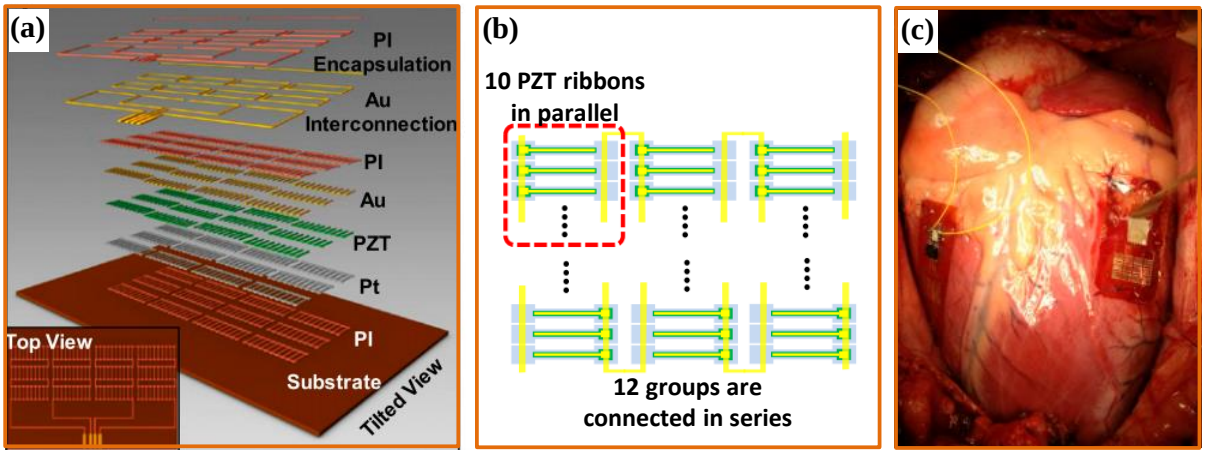

Figure 2.5: Flexible mechanical energy harvester based on thin ribbons of PZT: (a) Schematic illustration with a top view, (b) Schematic illustration of PZT ribbons grouped and connected in series and (c) Photograph of a PTZ MEH system on the left and right ventricles of the bovine heart [61].

bovine heart. It was observed that PZT MEH maintained conformal contact with the heart during the entire cycle of cardiac motion from contraction to relaxation. The orientation of the device showed to be an important factor since bending in the longitudinal direction relative to the orientation of the PZT ribbons provided the highest efficiency. Additionally, the size of the heart, the beat rate and the force of contraction has significantly affected the voltage output of the device [61].

2.3 Cellulose-based batteries

Recently, cellulose paper has been (re)discovered as a smart material that can be used in electronics [62]. Cellulose-based energy storage devices have significant inherent advantages in comparison with many currently employed batteries and supercapacitors regarding environmental friendliness, flexibility, cost and versatility. The development of cellulose-based flexible energy storage devices is particularly interesting due to the simple procedures for manufacturing these cellulosic composites which are, consequently, relatively inexpensive. Various types of devices, such as thin film transistors [63], active matrix displays, sensors, capacitors [64] and batteries [65] have been fabricated on paper substrate [66].

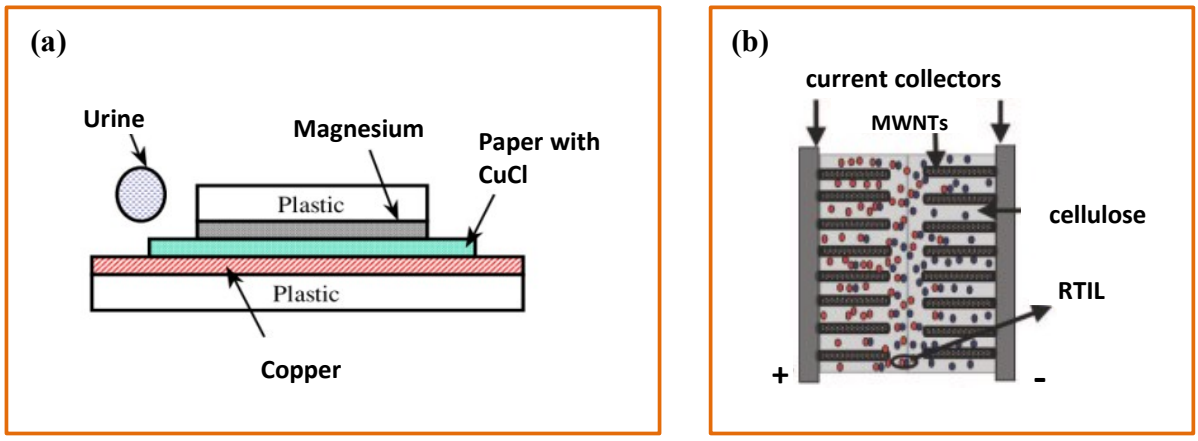

Figure 2.6: Schematic illustration of (a) the urine-activated paper battery [67] and (b) structure of the supercapacitor [68].

The earliest urine-activated paper battery was developed by Ki Bang Lee in 2005 [67]. This device consists of a copper chloride (CuCl)-doped filter paper between a copper layer and a magnesium one working as the cathode and the anode, respectively (Figure 2.6 (a)). The whole assembly is sandwiched between two plastic layers followed by a lamination process at 120°C. When a droplet of human urine is added to the battery, the urine soaks through the paper between the Mg and Cu layers working as an electrolyte. Urine is mainly composed of water-based solution of metabolic wastes such as urea and uric acid, dissolved salts such as sodium chloride and organic materials. The chemical composition of urine is widely used as a way of testing various diseases and also as an indicator of a general state of health. The activated-paper battery displayed a maximum voltage of 1.47 V and a maximum power of 1.5 mW for a 1 kΩ load resistor. Thus, the described work has demonstrated the viability of a urine-activated paper battery for biological application devices including home based health test kits [67].

In 2007, Victor Pushparaj [68] proposed a new methodology for the fabrication of a supercapacitor based on flexible CNTs-cellulose-room temperature ionic liquid (RTIL) nanocomposite sheets. They suggested the use of unmodified plant cellulose dissolved in a RTIL followed by their immersion in multiwalled nanotubes (MWNTs). After solidification on dry ice, the nanocomposite is immersed in ethanol to completely extract the excess of RTIL. Figure 2.6 (b) shows the nanocomposites paper structure in which

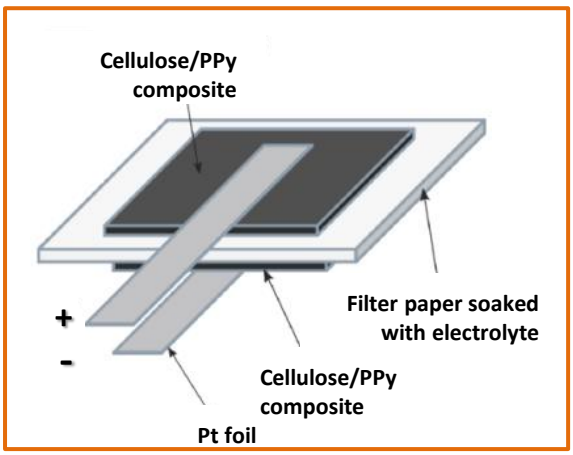

Figure 2.7: Schematic illustration of the composite all-polymer paper-based battery cell [69].

MWNTs acts as the working electrode and the cellulose surrounding individual MWNTs and RTIL acts as the self-sustaining electrolyte. The paper displayed an operating voltage of 2.3 V, approximately, and a specific capacitance of 22 $F.g^{-1}$. Besides using RTIL as electrolyte, the authors also proposed the use of body fluids as a suitable electrolyte for possible application in body implants.

Later, a research group in Uppsala University [69] developed an all-polymer paper-based battery. They reported the fabrication of a nanostructured polymeric electrode composed by cellulose fibers of algae origin individually coated with Polypyrrole (PPy). In order to evaluate the composite material for energy storage, a battery was assembled with the oxidized (p-doped) and reduced (undoped) forms of PPy as electrodes separated by a filter paper soaked with sodium chloride as electrolyte (Figure 2.7). The battery proposed exhibited charge capacities between 25 and 33 $mAh.g^{-1}$ per weight of the composite material. Finally, the long-term cycling properties were evaluated over 100 subsequent charge-discharge cycles resulting in a capacity loss of only 6%.

In the same year, Liangbing Hu [64] and his colleagues have demonstrated the application of commercial paper on energy storage devices by coating it with a solution of CNTs (Figure 2.8 (a)). Since paper absorbs solvents easily and binds with CNTs strongly, the fabrication of conductive paper is quite simpler when compared with other substrates, such as glass or plastics. The strong adhesion of CNTs to paper is attributed to Van

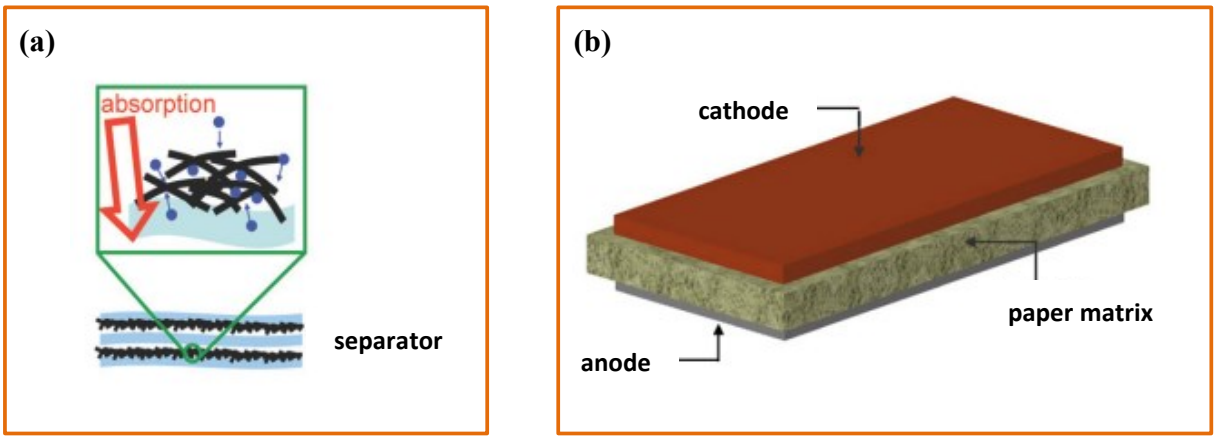

Figure 2.8: Schematic illustration of paper-based energy storage devices: (a) supercapacitor based on CNT conductive paper [64] and (b) paper battery [70].

der Walls forces explaining the high stability of the CNTs film against damage, such as scratching and peeling off. The high conductivity and the large surface area of conductive paper are valuable characteristics for supercapacitors applications as active electrodes and current collectors. The specific capacitance of the all-paper supercapacitor proposed was 200 $F.g^{-1}$ in sulfuric acid electrolyte and showed a good cycle life with only 3% of capacitance losses [64].

A paper-battery has been recently reported by Isabel Ferreira and co-workers [70]. This research team proposed the use of a commercial sheet of paper as a permeable membrane with thin film metal layers of copper (cathode) and aluminium (anode) deposited in each side (Figure 2.8 (b)). A single battery cell displayed a Voc of 0.6 V, approximately and a current density that varies from 0.194 $\mu A.cm^{-2}$ to 6.94 $\mu A.cm^{-2}$ for a relative humidity in the range of 50 - 65%. They successfully demonstrated that a 3 V paper battery, composed by a series integration of 8 cell units, is able to open and close the gate of a field effect paper transistor [70].

In 2011, and aligned with the present thesis, Ana Baptista and co-authors [15] have reported a new concept of a flexible and lightweight cellulose-based battery, so called bio-battery, activated by biological fluids. By depositing metallic thin films electrodes onto both sides of an ultrathin monolithic structure of a cellulose acetate electrospun membrane, the original flexibility and surface area of the membrane was preserved and a

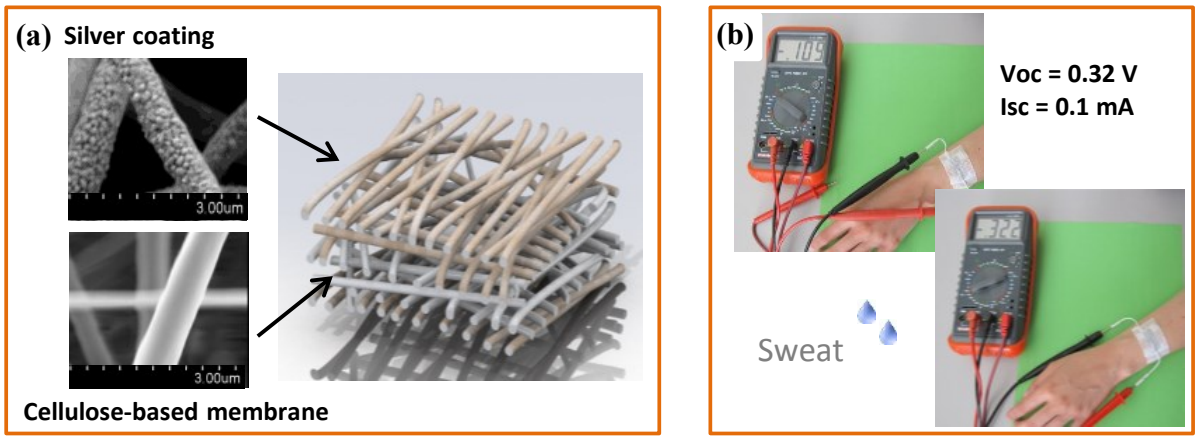

Figure 2.9: Cellulose-based bio-battery made of electrospun fibers (a) schematic illustration and (b) Validation of the concept in sweated skin [15].

highly flexible and foldable electrochemical device was achieved, as illustrated in Figure 2.9 (a). Considering that harvesting energy directly from the environment is probably the most effective and promising approach for powering long-term biomedical devices, the bio-battery proposed took advantage of the ionic content of physiological fluids to generate electric energy to supply low power consumption biomedical systems, such as implantable devices and biosensors.

The concept was validated by placing the bio-battery (with a dimension of 1 cm x 2 cm and a thickness of 53 μm, approximately) in contact with sweated skin using aluminium and silver thin films layers as the anode and the cathode, respectively. A Voc of 0.32 V and a short-circuit current (Isc) of 0.1 mA were directly measured with a multimeter, as showed in Figure 2.9 (b). Higher voltage values can be achieved throughout the integration of several cells in series, which can be performed by proper interconnection of external contacts. For such device, a power density of 3.38 μW.cm^{-2} was determined during the electrochemical characterization under simulated body fluids. This device provides energy in the context of a metal-air battery, where the cathode reaction is mainly due to the oxygen reduction on the silver electrode along with the reversible reactions of the cellulose-based material and the anodic reaction is attributed to aluminium oxidation [15].

Two years later, using a similar concept to what was previously described, Sha Li and

co-authors [71] have proposed the development of a cellulose-based composite for zinc bio-batteries activated by simulated body fluids. Composites materials of PPy/CNTs were chemically synthetized and deposited on cellulose filter paper as the cathode. Here, the cellulose membrane also works, simultaneously, as the substrate and the separator of the bio-battery. For batteries characterization, a zinc foil was used as the anode material and protein free simulated body fluid as the electrolyte. The battery mechanism proposed is also similar to that of a typical metal-air battery. The composite cathode is used as the catalyst for the oxygen reduction process along with the reversible redox process of PPy, while zinc is the unlimited sacrificial electrode. Such battery was able to discharges up to 24.5 hours at a current density of 60 μA.cm^{-2} under simulated physiological conditions.

2.4 Research opportunities

The scientific progress in biomedical technology has enabled a decrease in the electrical requirements of miniaturized devices. To meet the new design requirements and necessities of the next generation of implantable devices, looking for ultrathin and stretchable power sources able to obtain electrical energy from the human body is now a societal demand and a great scientific challenge.

The present thesis arises from the synergy of three relevant scientific fields – medicine, electronics and nanotechnology – and is motivated by a modern and growing topic of investigation envisaging the development of thin and flexible cellulose-based bio-batteries made of electrospun fibers. Figure 2.10 illustrates how the current thesis is positioned at the research interface between medicine, electronics and nanotechnology. The bio-battery proposed and development in this thesis shall be able to power implantable medical devices taking advantage of the ionic content of the biological fluids to generate energy.

As described throughout the course of this chapter, the use of electrospun fibers in the medical field is not a novel subject although their application in energy conversion systems for medical devices is, so far, an innovative and a promising approach. Polymer-based electronics represents an inspiring technology with unique properties and with the ability to be flexible and conform to complex surfaces. Additionally, the increasing environmental

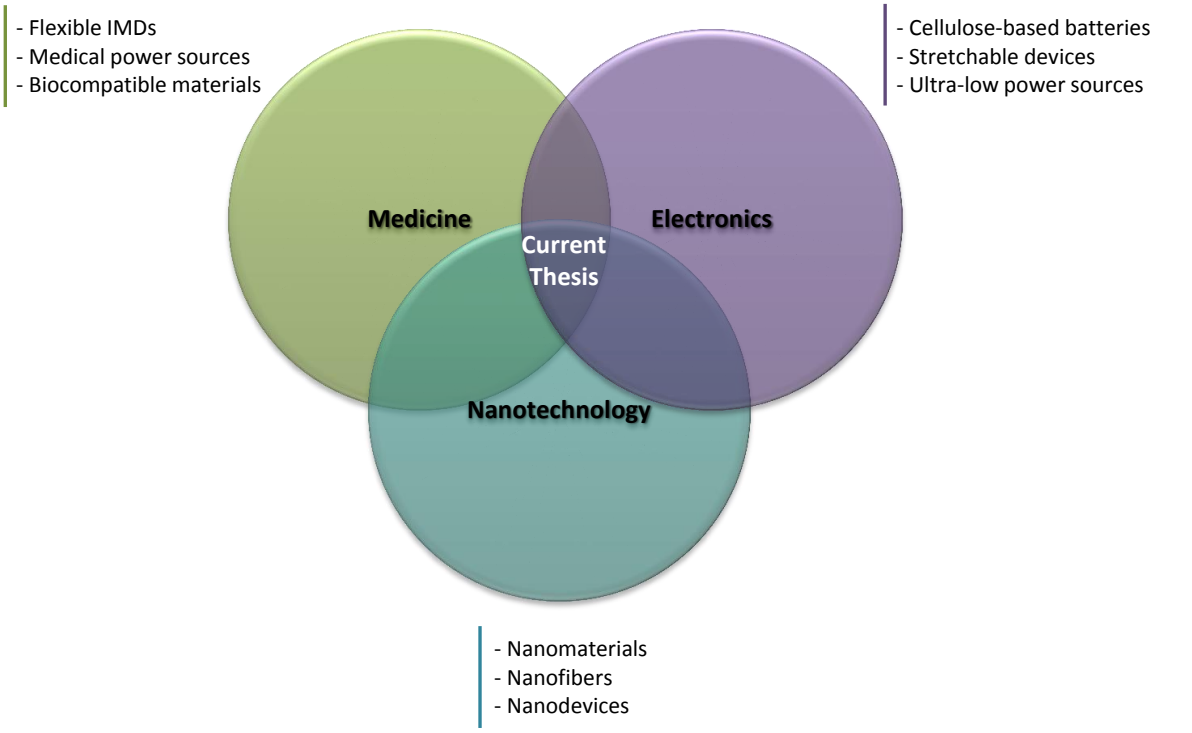

Figure 2.10: Illustration of the synergy between the three relevant scientific fields influencing the current dissertation.

consciousness and ecological concerns have renewed the interest of using natural-based materials in electronics. Therefore, the use of cellulose-based feedstock appears as a promising alternative route to develop "green" polymer devices that can be economically attractive.

Reports on cellulose-based batteries have been recently found in literature. Still, this work demonstrated pioneer achievements regarding the development of cellulose-based bio-batteries made of electrospun fibers for medical applications. Innovative strategies to prepare biocompatible and flexible electrodes are considered in this thesis regarding the use of functional electrospun fibers as a valuable alternative to the materials currently found in medical batteries.

Finally, the potential to eliminate batteries or, at least, the need to replace them frequently represents the major motivation of the present thesis work. The original concept of bio-battery here proposed envisages powering a wide variety of ultralow-power consumption biomedical devices, such as pacemakers, insulin pumps, cochlear implants, nerve stimula-

tors and other devices to monitor body functions. The subsequent chapters will present the scientific progresses achieved throughout the course of this doctoral research to meet the previous goals.

Chapter 3

Production and characterization of cellulose-based electrospun fibers

The bio-batteries proposed in this thesis are mainly composed of cellulose-based electrospun membranes. These membranes have a high surface area making them appealing to work both as the separator and as part of the electrodes composition of the bio-battery. This chapter provides a brief overview about cellulose-based materials and describes the production of nanofibers through the electrospinning technique. All the experimental setup used for the production and characterization of the electrospun matrix are indicated and the main results achieved during this task are presented and discussed.

3.1 Background

Products made from renewable and sustainable resources, non-petroleum based, and with low environmental safety risk are being increasingly explored by consumers, industry and governments. Half of the biomass produced by photosynthetic organisms such as plants, algae, and some bacteria is made up of cellulose, which is one of the most abundant polymers on the planet. Natural cellulose-based materials, such as wood and cotton, have been used by our society as engineering materials for thousands of years.

3.1.1 Cellulose

Cellulose exhibits excellent characteristics, which include hydrophilicity, chirality, biodegradability, capacity for broad chemical modication, and ability to form semicrystalline fiber morphologies, which has been encouraging interdisciplinary research on cellulose-based materials [72]. Cellulose plays a significant role in the structural support of wood, plants, and composites because of its good mechanical properties. Wood remains the most important raw material source of cellulose. The structure of wood is highly complex due to the presence of lignin, a three-dimensional polymer network that binds to carbohydrates (hemicellulose and cellulose) to form a tight and compact structure. The compact structure of wood biomass is particularly challenging because in its native state is insoluble in conventional solvents. Traditionally, cellulose is extracted from wood through the Kraft pulping process [73] which involves toxic chemicals and intensive processing conditions. Recently, research studies focused on a "greener" process that uses Ionic Liquids (ILs) for wood dissolution [74]. A wide variety of plant materials have been studied for the extraction of cellulose including cotton, potato tubers, sugar beet pulp, soybean stock, and banana rachis [75], [76]. Furthermore, cellulose microfibrils can be produced by several species of algae, such as green, gray, red, and yellow-green. Among the algae species, differences in cellulose microfibrils structures can be obtained due to the different biosynthesis process [77]. The cellulose obtained from algal species contains porous or spongy like structure, which is substantially different from the higher plant cellulose. Cellulose microfibrils can also be segregated by bacteria under special culturing conditions. Bacteria can produce a thick gel composed of cellulose microfibrils and water (97% of water content). The major advantage found in bacterial cellulose is the possibility to modify microfibrils structure by changing the culture conditions [78].

The solubility of cellulose depends on many factors especially on its structure, molecular weight and source. Polysaccharides are well-known to manifest a strong tendency to aggregate or to incomplete solubilization due to the formation of hydrogen bonds. The hydrogen bonding patterns in cellulose are considered as one of the most relevant factors on its physical and chemical properties. The solubility, crystalinity and hydroxyl reactiv-

ity can be directly affected by intra- and intermolecular bond formation (Figure 3.1) [79].

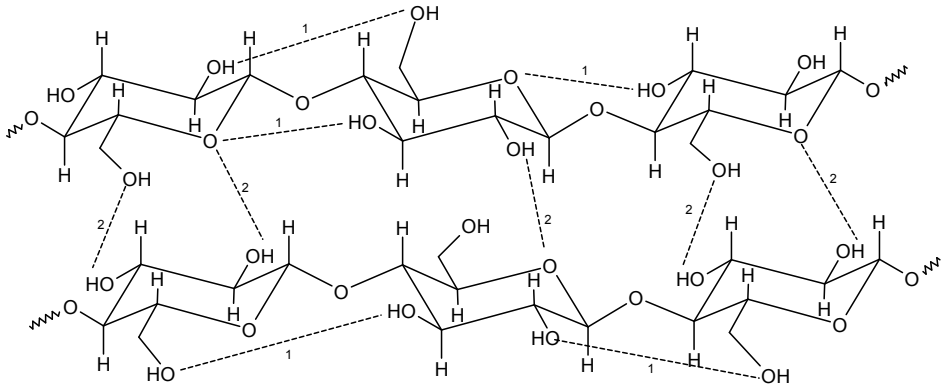

Figure 3.1: The structure and intra- (1) and interchain (2) hydrogen bonding pattern in cellulose [72].

Moreover, cellulose can be chemically modified to yield cellulose derivatives. The cellulose derivatives were designed and fine-tuned to obtain certain desired properties and the chemical functionalization of cellulose is done by changing the inherent hydrogen bond network and by introducing different substituents (Figure 3.2). The properties of cellulose derivatives are mainly determined by the group of substituents and the degree of substitution. These substituents can prevent spontaneous formation of hydrogen bonding or even create new interactions between the cellulose chains.

With this insight, recent progress has been made in cellulose chemical modification achieving new routes that are now available for the production of functional and sustainable cellulose-based materials [80]. The chemical modification of cellulose surface is a classical approach to transform the polar hydroxyl groups sitting at the surface of cellulose into moieties able to enhance interactions with the matrix. Indeed, the high density of free hydroxyl groups in cellulose makes it a helpful solid substrate that can undergo functionalization to come into novel advanced applications. Owing to cellulose chain rigidity, some cellulose derivatives can form thermotropic or lyotropic mesophases (in suitable solvents). Among cellulose ethers, hydroxypropylcellulose (HPC) have encouraged the scientific community due to its cholesteric liquid crystalline organization at high concentration [81]. These liquid crystalline phases, with an internal periodic modulation of the refractive

index, exhibit many remarkable optical properties as a result of their photonic band structure, which have applications such as polarized light sources, information displays, and storage devices [25]. These phases may also mimic the structural organization of type I collagen and are good analogues of the extracellular matrix, with a structure close to that of biological tissues. These materials can be used either in tissue repair or as models for the culture of cells in 3D, the study of their migration and signaling activities, in a manner close to physiological conditions [82].

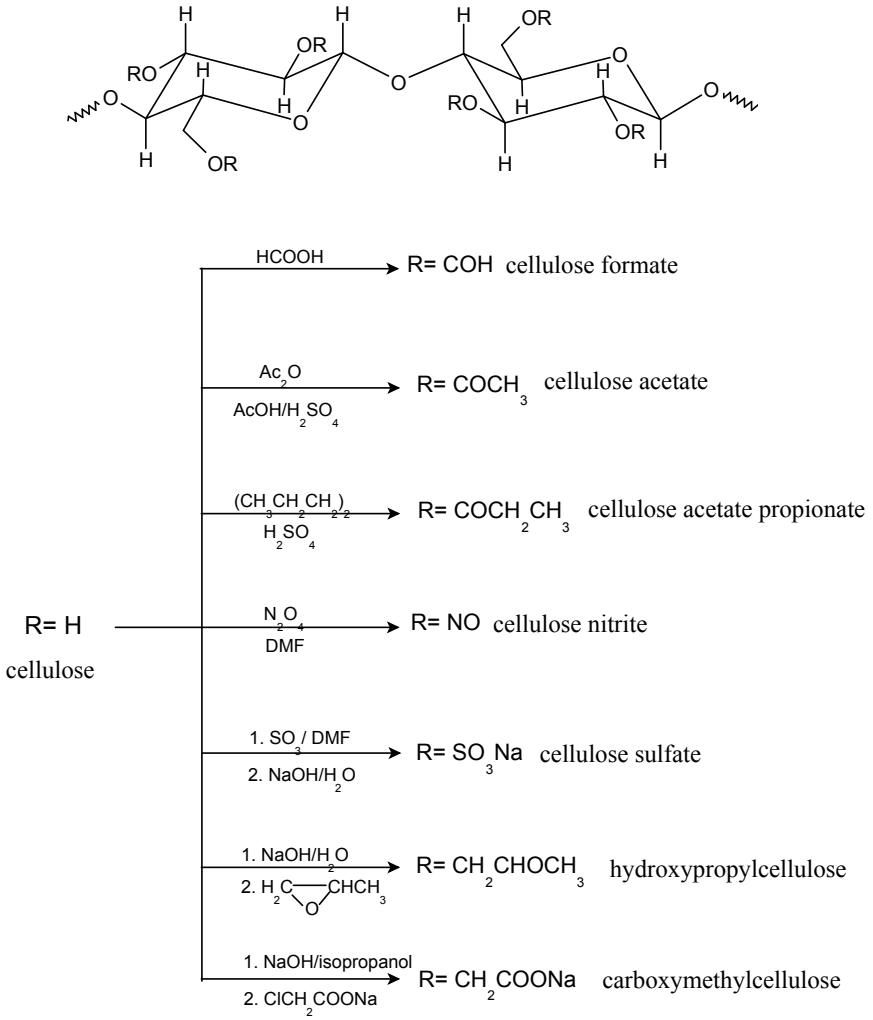

Figure 3.2: The most relevant cellulose derivatives and their synthesis pathways [72].

3.1.2 Electrospinning of cellulose derivatives

Recently, the electrospinning technique has attracted attention for the preparation of functional materials. Electrospinning is a broadly used technology for fiber formation which utilizes electrical forces to produce polymer fibers with diameters ranging from 2 nm to several micrometers using polymer solutions of both natural and synthetic polymers. In a conventional setup (Figure 3.3), a polymer solution passes through a capillary and a high voltage is applied such that the particles within the solution are charged creating a repulsive force. At a critical voltage, the repulsive force overcomes the surface tension of the solution and a jet erupts from the tip of the capillary towards a grounded collector. The morphology of electrospun fibers depends upon process parameters such as: the solution properties (viscosity, conductivity, and surface tension); the processing conditions (the flow rate of the solution through the syringe, the voltage applied to the needle, and the distance between the needle and the collector); and the environmental conditions (temperature and humidity) [83, 84]. Each of the above parameters, separately or combined can control the fiber diameter, its uniformity and shape and consequently electrospun fibers with a wide variety of cross-sectional shapes such as cylindrical, ribbons or helices can be obtained [25].

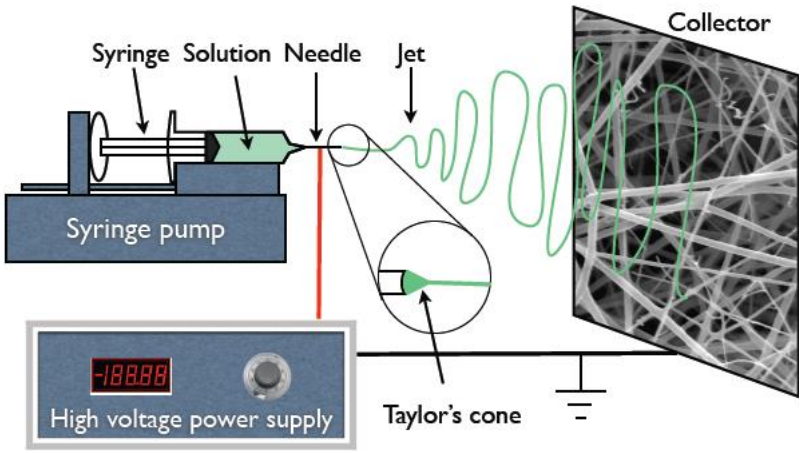

Figure 3.3: Schematic electrospinning apparatus.

Electrospun nanofibers offer several advantages such as an extremely high surface-to-volume ratio and tunable porosity. Because of these advantages, electrospun nanomate-

rials have unique properties applicable to a wide range of fields, including the fabrication of nanomaterials for use in energy conversion devices.

The electrospinning of cellulose and derivatives has been actively studied and well reported in literature [25], [15]. Due to their extraordinary properties, such as porosity and large specific surface area, electrospun polysaccharide fibers have been used in biomedical applications such as tissue engineering [85], drug delivery [86], antimicrobial medical implants [87] and biosensors [88, 89].

For all these reasons, the use of electrospun fibers in the development of functional materials opens a new path for the creation of novel, lightweight and flexible nanostructures that are promising for energy harvesting applications. The following sections describe the optimization of the electrospinning process for the production of a cellulose-based matrix that composes the bio-battery here proposed.

3.2 Methodology

3.2.1 Electrospinning process

In order to evaluate the optimal conditions to produce beaded free cellulose acetate fibers, the influence of polymer concentration and process conditions on the membranes' morphology were evaluated by caring out an extensive study under controlled environmental conditions.

Table 3.1 describes the parameters that were studied: CA concentration (from 5% to 14% wt); the applied voltage (15 and 20 kV); the distance between the needle tip and the collector (10 and 15 cm); and the flow rate of the polymer solution through the syringe (0.1, 0.2 and 0.4 $ml.h^{-1}$).

For that purpose, CA (Mn 61,000 with 40% acetyl groups, purchase from Sigma Aldrich) solutions were prepared in a mixed-solvent system of acetone-dimethylacetamide (DMAc) with a solvent ratio of 2:1 (wt:wt). To produce the fibers, the polymeric solution was loaded into a 5ml syringe (B.Braun). Then a syringe pump (100 series from Kd. Scientific) was used to squeeze out the polymer solution at a controllable speed through a needle

Table 3.1: Combination of the parameters studied for the ES process: polymer concentration, applied voltage, distance between the needle and the collector, and the flow rate.

%CA (wt)	**ES Parameters**							**Sample No**
	Voltage (kV)		**Distance (cm)**		**Flow rate (ml.h^{-1})**			
	15	20	10	15	0.1	0.2	0.4	
5	x		x		x			1
	x		x			x		2
	x		x				x	3
		x	x		x			4
		x	x			x		5
		x	x				x	6
	x			x	x			7
	x			x		x		8
	x			x			x	9
		x		x	x			10
		x		x		x		11
		x		x			x	12
8	x		x		x			13
	x		x			x		14
	x		x				x	15
		x	x		x			16
		x	x			x		17
		x	x				x	18
	x			x	x			19
	x			x		x		20
	x			x			x	21
		x		x	x			22
		x		x		x		23
		x		x			x	24
10	x		x		x			25
	x		x			x		26
	x		x				x	27
		x	x		x			28
		x	x			x		29
		x	x				x	30

Continued on next page

Table 3.1: Continued.

%CA (wt)	ES Parameters							Sample No
	Voltage (kV)		Distance (cm)		Flow rate (ml.h^{-1})			
	15	20	10	15	0.1	0.2	0.4	
10	x			x	x			31
	x			x		x		32
	x			x			x	33
		x		x	x			34
		x		x		x		35
		x		x			x	36
12	x		x		x			37
	x		x			x		38
	x		x				x	39
		x	x		x			40
		x	x			x		41
		x	x				x	42
	x			x	x			43
	x			x		x		44
	x			x			x	45
		x		x	x			46
		x		x		x		47
		x		x			x	48
14	x		x		x			49
	x		x			x		50
	x		x				x	51
		x	x		x			52
		x	x			x		53
		x	x				x	54
	x			x	x			55
	x			x		x		56
	x			x			x	57
		x		x	x			58
		x		x		x		59
		x		x			x	60

while a high voltage was applied (using a Glassman High Voltage Power Supply) between the needle and a grounded collector. The needle used in this study had an internal diameter of 21G (0.61 mm, from ITEC, Iberiana Technical). The environmental conditions were kept constant at a relative humidity between 40% and 42.5% and temperature between

22°Cand 24°C. All the membranes were electrospun for 20 min and collected on an Al foil (static collector). The ES experimental setup is presented in Figure 3.4.

After defining the best conditions for the ES process (Sample No. 47), CA electrospun membranes were produced during 3 consecutive hours under controlled environmental conditions. The membrane thickness was around 56 ± 24 μm.

Figure 3.4: Photograph of the ES experimental setup used in this work.

3.2.2 Morphological characterization

The surface morphology of the electrospun composites was evaluated using a Focused Ion Beam Scanning Electron Microscope (SEM-FIB) from Zeiss (model Auriga). Double-sided conductive carbon tape was used to attach the samples to the samples' support. The samples were sputtered with gold to avoid charging.

Fiber diameters were measured from SEM images using an image processing software (ImageJ, NIST). It was ensured that fibers were not counted twice and those lying outside the focal plane were not used in the statistical analysis.

3.2.3 Mechanical characterization

Mechanical characterization of the electrospun membranes was carried out using a commercial mechanical testing system (Rheometric Scientific, Minimat Firmware 3.1) shown in Figure 3.5. Ten samples were collected from the nonwoven membrane of CA (12%wt) to obtain mean values for tensile strength (TS), Young's modulus (E) and strain. The applied deformation rate was 1 $mm.min^{-1}$ and the temperature was kept constant at 25°C.

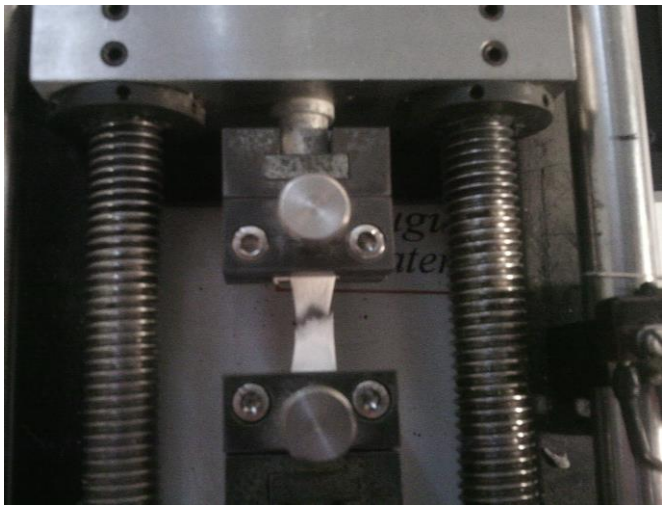

Figure 3.5: Photograph of the mechanical testing system.

3.2.4 Electrochemical characterization

The electrochemical characteristics of the CA electrospun membranes were evaluated by cyclic voltammetry (CV) and carried out using a potentiostat (Reference 600TM - Gamry Instruments). The CV measurements were performed in an electrochemical cell constructed with a piece of membrane (1 cm^2) impregnated with a physiological solution sandwiched between two symmetrical gold electrodes. Due to the low thickness (<0.1mm) of membranes, all measurements were carried out in a cell with two-electrode configuration (Figure 3.6). Two-electrode systems have been widely used in electrochemical industries and academic fields involving solid-state electrochemistry for the characterization of new materials and design of electrochemical devices such as supercapacitors [90] and batteries

[91], [92].

The reference electrode (RE) and the counter electrode (CE) are merged into one electrode in a two-electrode system and the potential of the working electrode (WE) versus the RE (also as the CE) is controlled and measured. The potential is scanned in both directions between -1 and 1 V with different scan rates, at room temperature and under atmospheric conditions. Since the body fluids are mainly composed of water and ionic species such as Na^+, Cl^- and K^+, a physiological solution of 0.9% (wt/v) NaCl and a Simulated Body Fluid (SBF) solution were used (Table 3.2). SBF is a typical buffer solution often used in bioactivity assays since it has a concentration of inorganic ions similar to those found in human fluids.

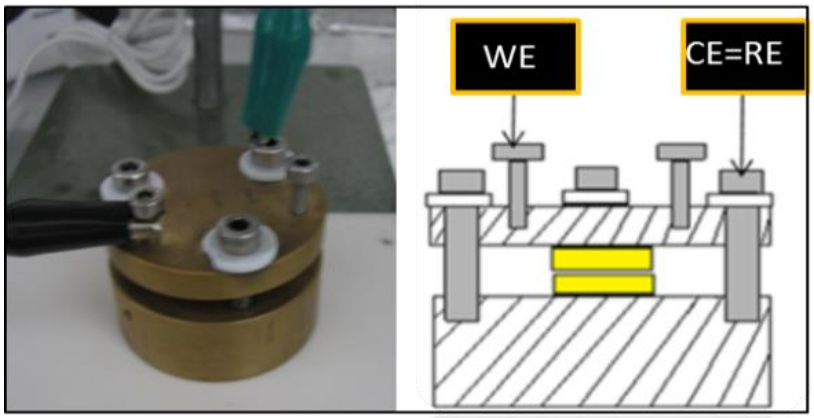

Figure 3.6: Electrochemical cell used for the CV measurements. All measurements were carried out in a cell with two-electrode configuration. The reference electrode (RE) and the counter electrode (CE) are merged to be one electrode in a two-electrode system and the potential of the working electrode (WE) versus the RE (also as the CE) is controlled and measured.

3.2.5 Production of other electrospun membranes

In order to compare cellulose fibers with other biocompatible fibers, PCL fibers were produced. For that, a Polycaprolactone (PCL) solution, 13% wt (Mw 70 000-90 000,

Table 3.2: Ionic content of the human blood plasma, human sweat, simulated body fluid solution and NaCl solution used in this work.

Ion	**Blood plasma (mM) [93]**	**Human sweat[a] (mM) [94]**	**SBF (mM) [95]**	**NaCl (mM)**
Na^+	142	84-98	142	155
K^+	4	5-6	6.5	-
Ca^{2+}	2.5	n.a.[b]	2.5	-
Mg^{2+}	1.5	n.a.	1.5	-
Cl^-	103	70-77	148	155

[a] Sweat concentrations after 2 h of intense exercise
[b] Not available

from Sigma-Aldrich), in 75/25 (v/v) of methylene chloride and dimethylformamide, was loaded into a 1 ml syringe. The solution flow rate was controlled by a syringe pump at 0.8 $ml.h^{-1}$. A voltage of 15 kV was applied between the needle and a grounded collector at 15 cm of distance. The produced PCL membrane has a thickness of about 281 ± 54 μm.

Ethyl cellulose (EC), from Sigma Aldrich, was dissolved in Tetrahydrofuran (THF)/DMAc according to volume ratio of 20/60 in a concentration of 15% (wt/v). The solution was loaded into a 1 ml syringe and the solution flow rate was controlled by a syringe pump at 0.4 $ml.h^{-1}$. A voltage of 15 kV was applied between the needle and a grounded collector at 10 cm of distance. The produced EC membrane has a thickness of 62 ± 24 μm, approximately.

3.2.6 Production of cellulose acetate films

To evaluate the surface area influence on the electrochemical behaviour, CA nonporous films were produced by film casting process. A cellulose acetate solution, 12% (wt) in acetone/DMAc (2:1) was casted and sheared by moving a casting knife at a controlled shear rate (5 $mm.s^{-1}$). The final thickness of the film was approximately 85 ± 32 μm.

3.3 Results and discussion

This section presents and discusses the production and characterization of the cellulosic membrane that composes the bio-battery. A cellulose acetate membrane was produced using the electrospinning technique. The optimization of the electrospinning process was carried out in order to produce beaded free fibers. Finally, the electrospun membranes obtained were morphologically, mechanically and electrochemically characterized.

3.3.1 Morphological characterization

In the electrospinning process, a number of parameters can influence the morphology of the obtained fibers. These parameters can be categorized into three main types:

1. **Solution properties** – e.g. concentration, viscosity, surface tension and conductivity of the polymer solution.

2. **Processing conditions** – e.g. the flow rate of the solution through the syringe, the voltage applied to the needle, and the distance between the needle and the collector.

3. **Environmental conditions** – e.g. temperature and relative humidity in the spinning chamber.

Studies found in literature report the effect that solvent systems can have on the morphological appearance and/or on size of electrospun cellulose acetate membranes [96, 97]. They have concluded that the use of a acetone-DMAc mixed-solvent system can improve the electro-spinnability of the solution making possible the production of smooth and beaded free cellulose acetate fibers. For that reason, a 2:1 (wt:wt) acetone-DMAc was used in this work to prepare the spinnable solutions of CA.

In order to evaluate the influence of polymer concentration and process conditions on membranes morphology, an extensive study was carried out in controlled environmental conditions (see Table 3.1). The most relevant samples are listed in Table 3.3 with the indication of their corresponding average fiber diameter and main morphology. Detailed

information about the fiber diameter distribution of the evaluated samples can be found in Appendix A.

Table 3.3: Summary of the morphology of the produced samples with the indication of their fiber average diameter. The corresponding polymer concentration and ES condition are indicated for each sample.

Sample No.	**CA (%wt)**	**ES parameters**	**D_{av} (nm)**	**Morphology**
11	5	20 kV/15 cm/0.2ml.h^{-1}	n.m.[a]	Beads
23	8	20 kV/15 cm/0.2ml.h^{-1}	96 ±23	Fibers and beads
35	10	20 kV/15 cm/0.2ml.h^{-1}	130 ± 55	Fibers
38	12	15 kV/10 cm/0.2ml.h^{-1}	340 ± 92	Fibers
41	12	20 kV/10 cm/0.2ml.h^{-1}	265 ± 118	Fibers
44	12	15 kV/15 cm/0.2ml.h^{-1}	243 ± 99	Fibers
46	12	20 kV/15 cm/0.1ml.h^{-1}	268 ± 90	Fibers
47	12	20 kV/15 cm/0.2ml.h^{-1}	243 ± 58	Fibers
48	12	20 kV/15 cm/0.4ml.h^{-1}	257 ± 76	Fibers
59	14	20 kV/15 cm/0.2ml.h^{-1}	487 ± 199	Fibers

[a] Not measured.

- **Influence of the polymer concentration**

In this study, the polymer concentration (and thus viscosity) revealed to be the most determinant parameter affecting the fiber diameter.

Figure 3.7 shows a selection of SEM images in order to illustrate the effect of the concentration of CA solutions on the morphological appearance of the obtained as-pun materials. It is clear that at low viscosities small fibers with beads are produced, and with the increasing viscosity fibers become thicker while the beads are scarcer leading finally to smooth fiber morphology. The most likely explanation for such observation is the greater increase in the viscoelastic force as a result of the large increase in the degree of chain entanglements (due to the increase of solution concentration/viscosity) in comparison with the Coulombic force.

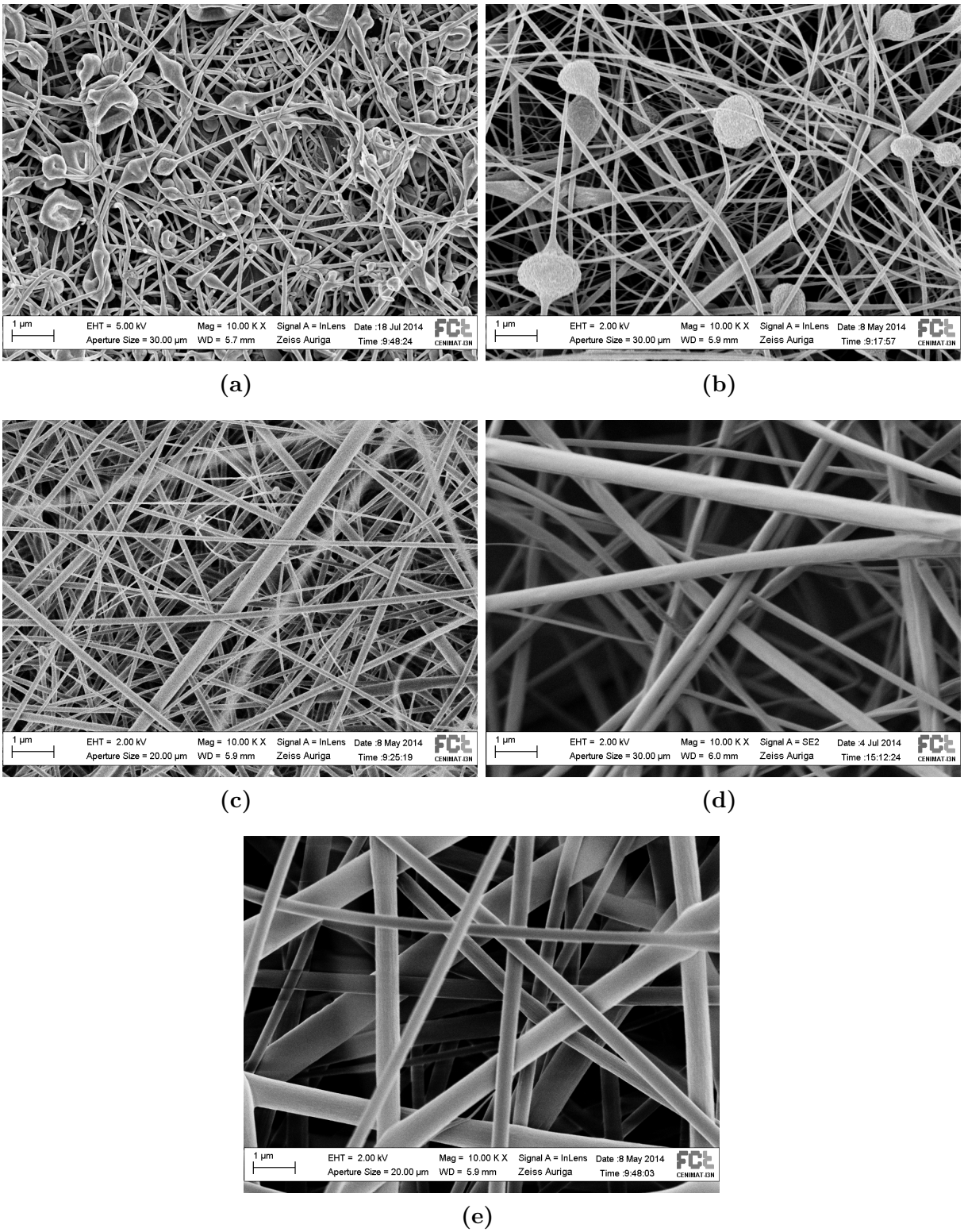

Figure 3.7: SEM images of electrospun membranes produced at 20 kV, 15 cm and 0.2 ml.h^{-1} a) CA 5% wt, b) CA 8% wt, c) CA 10% wt, d) CA 12% wt and e) CA 14% wt.

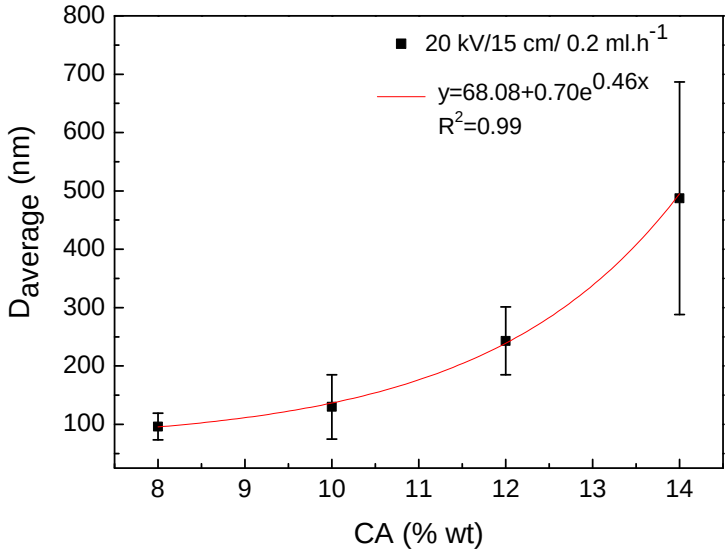

Figure 3.8: Exponential dependence of the average fiber diameter ($D_{average}$) with the polymer concentration.

According to Figure 3.8, an exponential relationship can be found between the average fiber diameter and the polymer concentration, which is in agreement with other authors observations [98, 99].

As long as a polymer can be electrospun into nanofibers, the ideal membrane would be defect-free and with controllable fiber diameter. Additionally, since the surface area of a fiber depends linearly of the diameter and the volume depends of the square of the diameter, the specific surface area is inversely dependent of the diameter. So, membranes with a higher specific surface area can be obtained with thinner fibers. For that reason, defect-free electrospun membranes composed by thinner fibers with controllable diameters are the target of this study.

Regarding the histograms shown in Figure 3.9 (a)-(c), it is possible to assume that the electrospun membrane produced from 12% wt CA solution is the desirable one since it has a narrow and controlled fiber diameter distribution.

- **Influence of the ES parameters**

Besides the influence of different polymer concentrations, it was also investigated some process conditions such as the influence of the applied voltage, the distance between the needle tip and the collector plate and the flow rate of the polymer solution through the

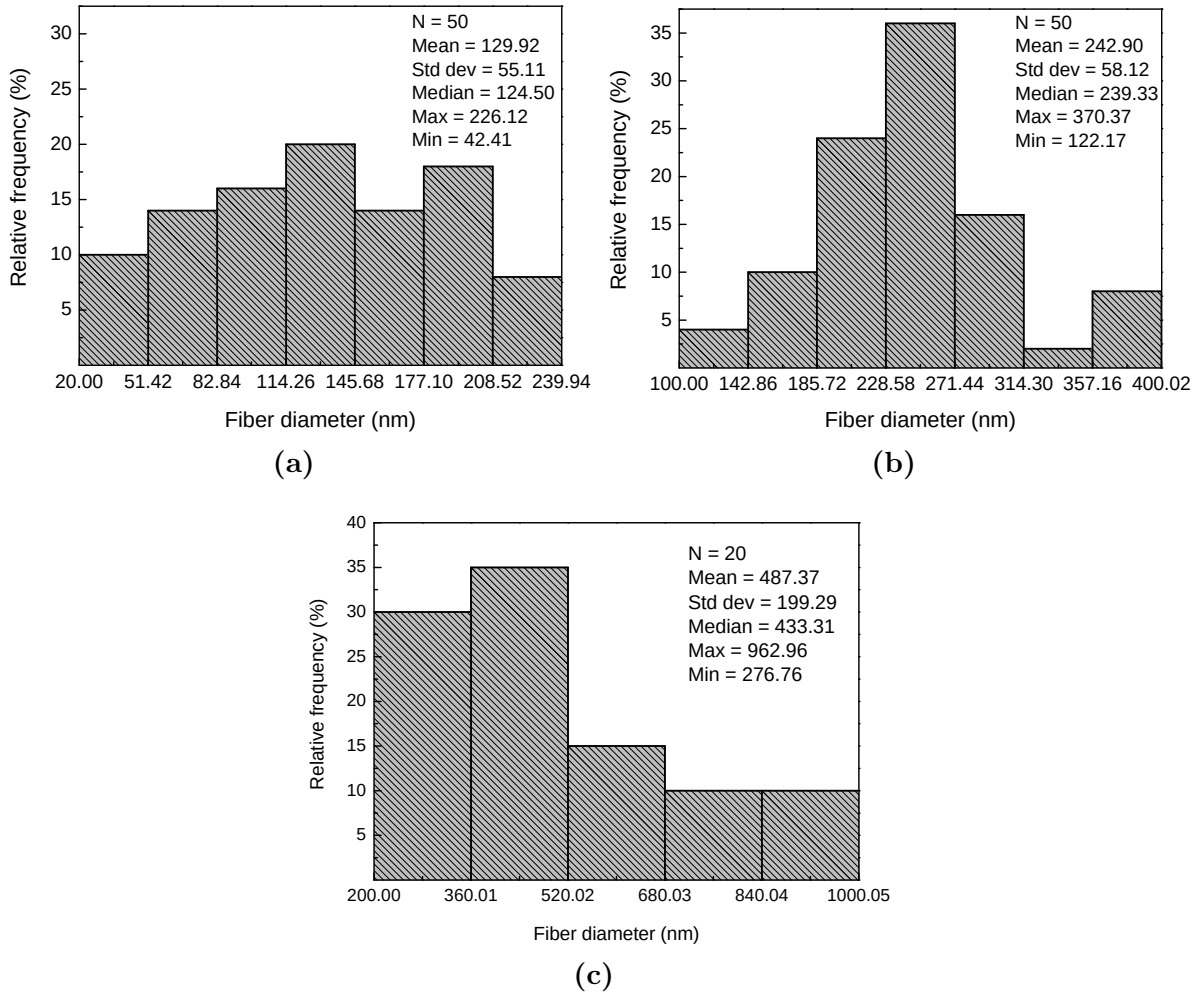

Figure 3.9: Fiber diameter distribution of CA solutions: (a) 10% wt (Sample No. 35), (b) 12% wt (Sample No. 47) and (c) 14% wt (Sample No. 59). All the membranes were produced under the same ES conditions: 20kV, 15 cm and 0.2 ml.h^{-1}.

syringe.

In the electrospinning process, the applied voltage has a critical role since it initiates the jetting and causes instabilities, which stretch the jet. As observed in Figure 3.10 (a), it is possible to identify two distinct behaviors. When the distance between the needle and the collector is 10 cm, the average fiber diameter is slightly affected by the applied voltage. The decrease of fiber's diameter due to the higher voltage is a consequence of the higher electrostatic forces on the jet, which favor the formation of thinner fibers. On the other hand, for higher distances (15 cm) fiber diameters tend to be thinner since larger distance may enhance the evaporation of solvent regardless of reduced electric field. However, the influence of the applied voltage on the fiber diameter is not statistically significant.

Typically, a higher feeding rate for the solution always leads to the formation of thicker fibers [100]. The flow rates chosen for this study did not had a significant influence on the fiber diameter, as it can be seen in Figure 3.10 (b).

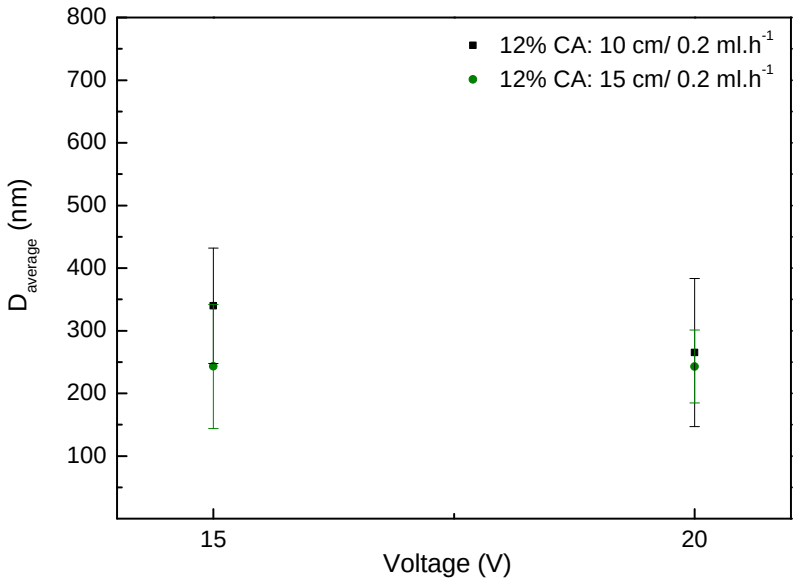

(a)

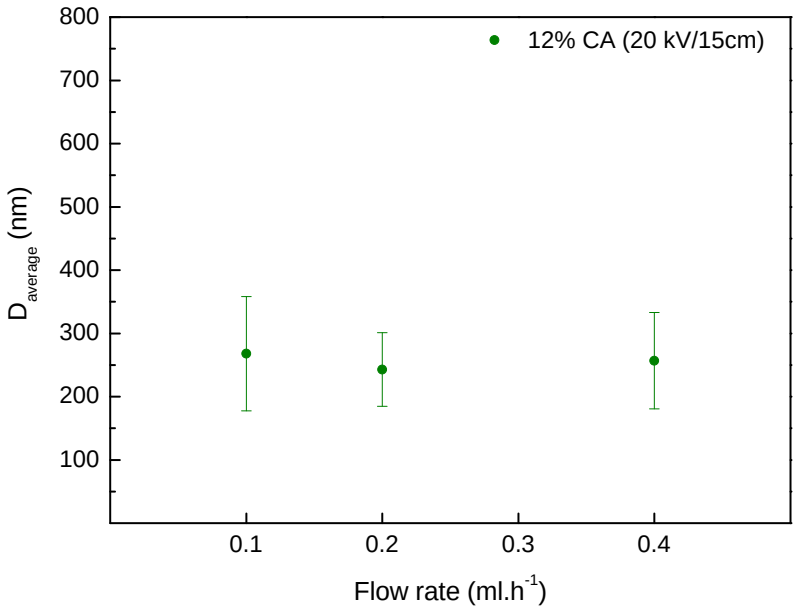

(b)

Figure 3.10: Dependence of the average fiber diameter ($D_{average}$) with (a) the applied voltage (15 and 20 kV) and the distance between the needle and the collector (10 and 15 cm); and (b) with the flow rate of the polymer solution through the syringe (0.1, 0.2 and 0.4 $ml.h^{-1}$).

In summary, this study allowed to define the better conditions to obtain smooth fibers with a narrow and controlled fiber diameter distribution. For that reason, the sample No. 47 (12% CA at 20kV, 15 cm and 0.2ml.h^{-1}) was selected as the ideal membrane, showing a controlled average fiber diameter of 243 ± 58 nm .

3.3.2 Mechanical characterization

Generally, the mechanical properties of nonwoven fibers are poorer when compared to textile fibers and films made from the same polymer. This can be explained since polymer molecules are not fully aligned during the stretching caused by electrospinning and also due to the reduced interaction between polymer molecules in nanofibers [101].
An example of a typical stress-strain curve obtained for CA electrospun membranes is shown in Figure 3.11.

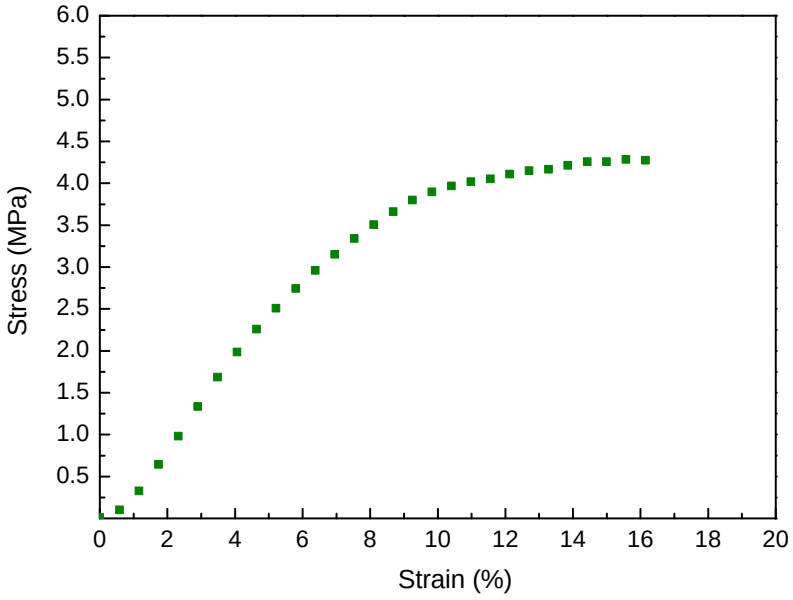

Figure 3.11: Typical stress-strain curve obtained for the nonwoven CA membrane in uniaxial strain.

Table 3.4 indicates the average values of Young's modulus, TS and strain obtained for the CA electrospun membrane comparing them with the ones found for human skin.
The CA nonwoven membrane is composed of nanofibers that are loosely packed together without any chemical crosslinking point among fibers. Consequently, its tensile strength

Table 3.4: Comparison of the mechanical properties of the CA nonwoven membrane with those of human skin.

Sample	**Young's modulus (MPa)**	**TS (MPa)**	**Strain (%)**
CA nonwoven membrane	42.1±13.8	3.7±1.0	14.3±5.0
Human skin[a] [102] [103]	15-150	1-20	30-70

[a] mechanical properties of soft tissues depend strongly on the topography, risk factors, age, species, physical and chemical environmental factors such as temperature, osmotic pressure, pH, traction direction and on the strain rate.

is relatively low.

Many authors consider that the tensile strength of a nonwoven mat is quite similar to that of a natural skin [84]. Moreover, the tensile stress-strain behavior of skin, an organ consisting mainly of connective tissues, can be representative of the mechanical behavior of many others (collagenous) soft connective tissues. The important characteristics of soft tissues are heterogeneity, anisotropy and the mobility of the fibers. Depending on the resistance to crack propagation and degree of initial orientation of the fibers, the tensile response of soft tissue is nonlinear stiffening and tensile strength depends on the strain rate.

For that reason, it can be assumed that the produced electrospun membrane have a mechanical behavior similar to soft materials which is a valuable characteristic for biomedical applications, such as the one here proposed.

3.3.3 Electrochemical characterization

The electrochemical behaviour of the electrospun membranes was determined by cyclic voltammetry. The cyclic voltammograms of a CA pristine membrane compared with the one of a membrane after adding distilled water (less than 0.1ml) are depicted in Figure 3.12.

The dry pristine membranes show an invariable electrochemical behavior and very low current densities, around 20 nA cm^{-2}. After adding distilled water , the current density increases to 5 $\mu A.cm^{-2}$ and a typical diffusion behavior is observed. Since the body fluids

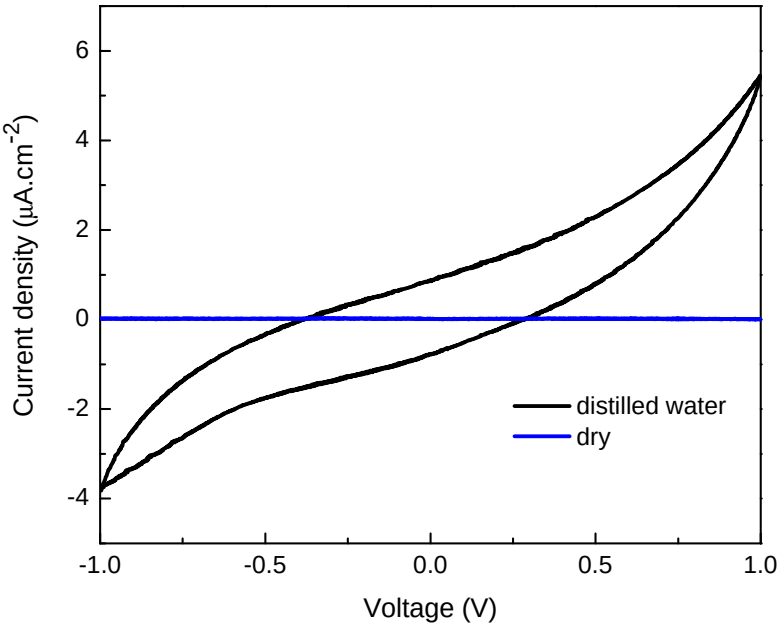

Figure 3.12: Cyclic voltammogram of an CA electrospun membrane in a dry form and after distilled water addition. All measurements were performed with a 47.6 μm membrane thickness at a voltage scan rate of 40 mV/s.

are mainly composed of water and ionic species such as Na^+, Cl^- and K^+, simulating body fluids solutions were used, such as SBF and NaCl (0.9% wt/v).

Adding the saline solutions, a similar electrochemical behavior was obtained (Figure 3.13). In both cases, the current density increases up to 100 $\mu A.cm^{-2}$, and the voltammogram shows two distinct peaks around $\pm$ 0.15 V, suggesting an adsorption/desorption phenomena and/or the occurrence of redox reactions. Due to its easier preparation and maintenance, the NaCl solution was selected to continue the electrochemical studies.

The enhancement of the current density can be explained by ions diffusion through the membrane or by redox reactions at the hydroxyl groups of the polymer structure, represented in Figure 3.14. In both cases an enhancement of the current should be expected when the membrane thickness increases due to the increase of the surface area and amount of the available hydroxyl groups. As the electrospun nonwoven membranes are produced layer-by-layer, it means that its surface area is enhanced as the thickness increases. For that reason, the electrochemical behavior of CA membranes with different thicknesses (between 26 μm and 134 μm) was evaluated.

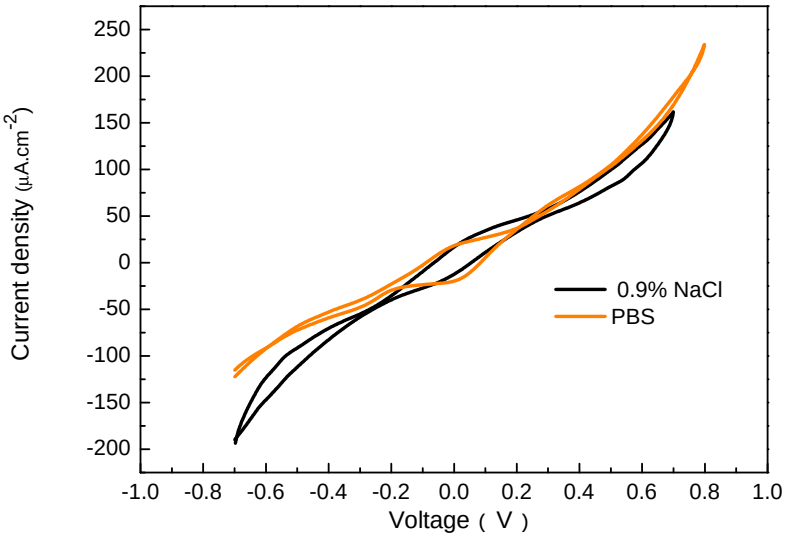

Figure 3.13: Cyclic voltammogram of an CA electrospun membrane after SBF and NaCl (0.9% wt/v) addition. All measurements were performed with a 47.6 μm membrane thickness at a voltage scan rate of 40 mV/s.

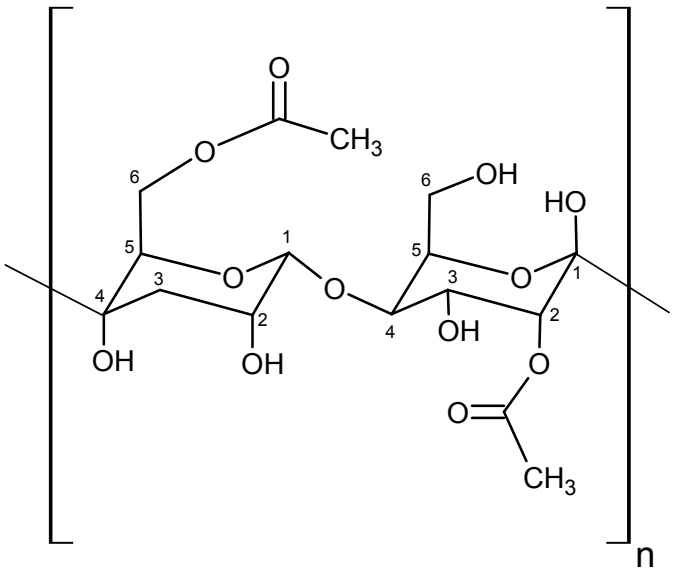

Figure 3.14: Structure of the repeating unit of a CA molecule with 33% of acetil groups.

As expected, the current densities increase with the increase of membranes thickness (Figure 3.15). The empirical dependence between the current densities and the membrane thickness obtained for the cathodic ($|j_c|$) and anodic ($|j_a|$) peaks can be described by linear

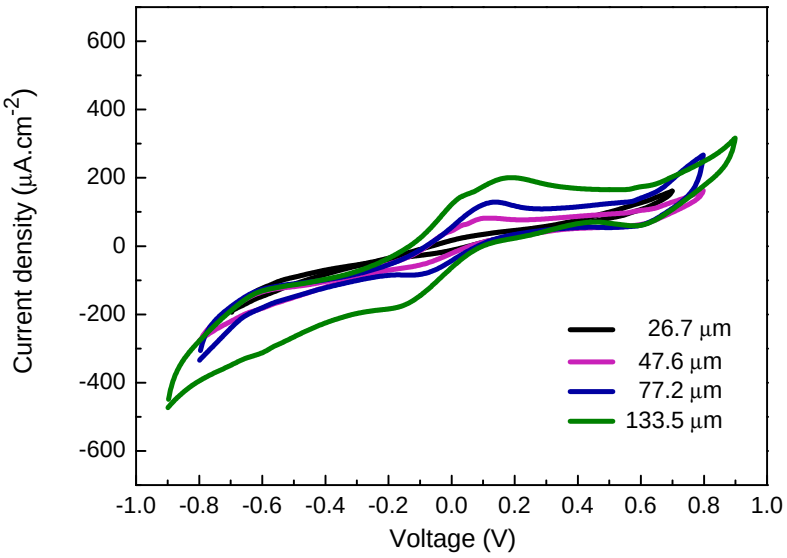

Figure 3.15: Cyclic voltammogram of CA electrospun membranes with different thicknesses (26.7, 47.6, 77.2 and 133.5 μm) after NaCl (0.9% wt/v) addition. All measurements were carried out at a voltage scan rate of 40 mV/s.

dependences on thickness (shown in Figure 3.16):

$$|j_a|(\mu A.cm^{-2}) = 1.52 \times thickness(\mu m) + 1.67 \quad with \quad R^2 = 0.95 \tag{3.1}$$

$$|j_c|(\mu A.cm^{-2}) = 1.48 \times thickness(\mu m) - 24.55 \quad with \quad R^2 = 0.96 \tag{3.2}$$

The transport of protons through the cellulose backbone is also strongly dependent on the relationship between the level of hydration and structure of the polymer [104, 92]. The intra- and inter-molecular hydrogen bonds established with the hydroxyl and acetyl groups in hydrated membrane, may contribute to enhance ionic conductivity. The protons can diffuse by vehicular mechanism in the form of protonated molecules (H_3O^+), as well as by Grotthuss mechanism [105] where the protons are transferred between molecules through hydrogen bonding (cleavage/forming). The presence of Na^+ ions inside the 3D/porous polymeric structure contribute to increase the ionic conductivity, due to a single charge transfer mechanism (Na^+) based on ion-polymer interactions mediated by the polymer chain motions (segmental motion) [105]. However, the origin of the observed symmetric

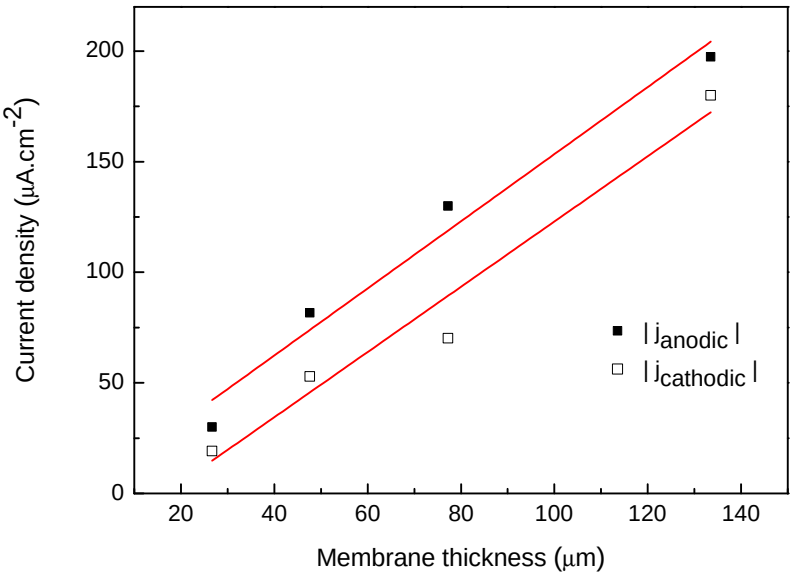

Figure 3.16: Linear dependence of the current densities with the membrane thickness.

peaks is not yet well understood. They could be due to adsorption/desorption phenomena or redox reactions occurrence, or even due to both phenomena.

Additionally, it was also carried out electrochemical measurements on a CA nonporous film in the presence of NaCl (single drop and after swelling during 24h). These results confirm a diffusion-like process with very low current density in both test conditions (Figure 3.17). Thus, we can anticipate that the observed peaks in the electrospun matrix are related with the high surface area of the electrospun membranes and consequently with the increase of the available active sites of the polymer.

Possible oxidation of gold electrodes was also taken into account. The gold electrodes were immersed into two different NaCl solutions (0.9% (wt/v) and 5% (wt/v)) and the electrochemical characterization was performed. The peaks observed in Figure 3.18 can be related with the formation of an auric chloride film in the surface of the gold electrode, which can be confirmed by the formation of a dark film over the electrode surface. However, those peaks do not correspond to that found on the voltammograms of CA membrane.

The adsorption/desorption phenomena was also evaluated. The adsorption phenomenon consists of an electrostatic interaction between ions and the electrode surface. A progressive accumulation of species or ions on the surface of the electrode can be detected by

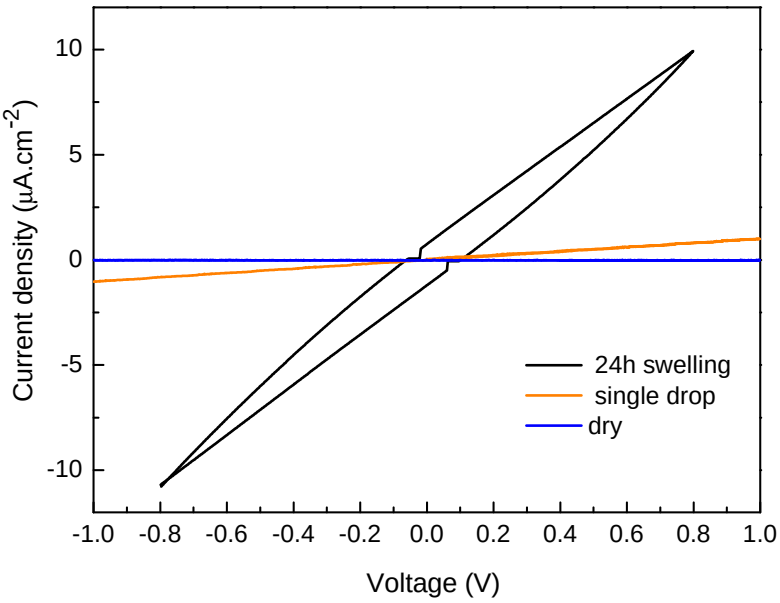

Figure 3.17: Cyclic voltammogram of a CA nonporous film, with a thickness of 75 μm, in a dry form, after NaCl (0.9% wt/v) addition, and after a swelling period of 24h in the same saline solution. All measurements were carried out at a voltage scan rate of 40 mV/s.

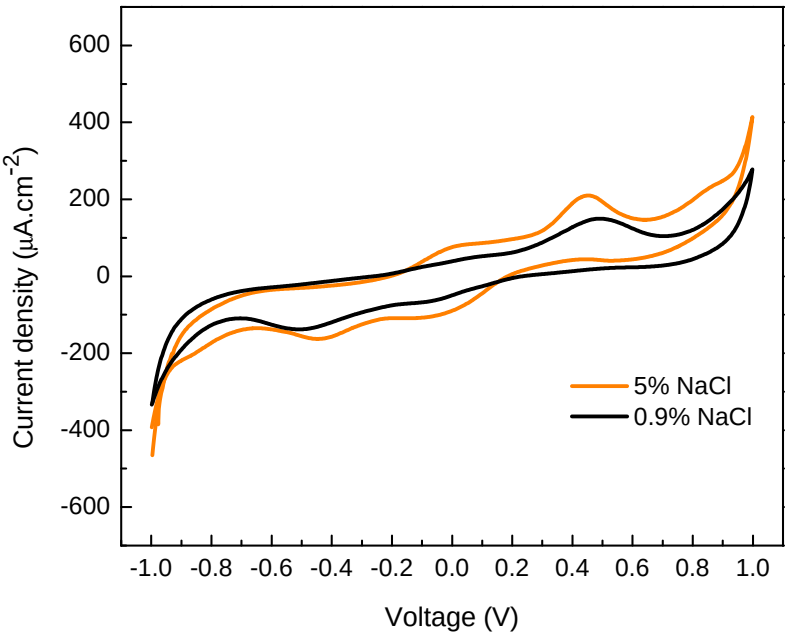

Figure 3.18: Electrochemical behavior of gold electrodes immersed in two different NaCl solutions (0.9% and 5% wt/v). All the measurements were carried out at a voltage scan rate of 40 mV/s.

cyclic voltammetry. An indication of the presence of this phenomenon is the detection of a gradual increase of the peaks current (both anodic and cathodic one) with the increase of the number of cycles. In this way, continuous cycles were performed on CA electro-

spun membranes using two solutions: 0.9% (wt/v) NaCl and 0.9% (wt/v) $NaHCO_3$. For the first one, a stable electrochemical behavior was detected suggesting the absence of adsorption/desorption (Figure 3.19).

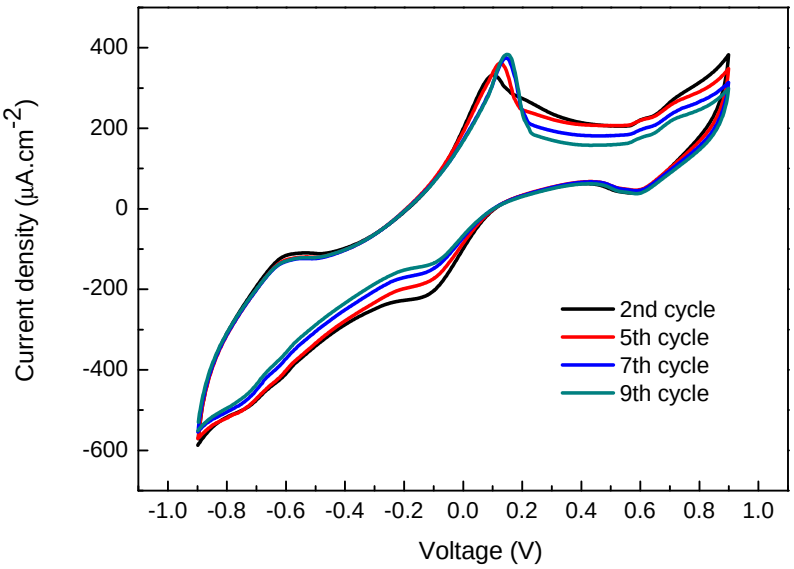

Figure 3.19: Cyclic voltammogram of a CA electrospun membrane during 9 consecutive cycles in the presence of NaCl solution (0.9% wt/v). The membrane has a thickness of 133.5 μm and the measurement was carried out at a voltage scan rate of 80 mV/s.

On the other hand, in the presence of $NaHCO_3$ the current density values observed in Figure 3.20 indicate the existence of a diffusional behavior associated with an adsorption/desorption phenomena.

Moreover, a similar electrochemical study was carried for PCL and EC electrospun membranes. Considering their chemical structures (Figure 3.21) it is expected a similar electrochemical behavior due to the presence of OH groups. The redox peaks observed in Figure 3.22 are quite similar to those found for CA matrix. The difference on current density values can be related with the difference in membrane thickness.

After all the previous considerations, it was possible to draw a conclusion about the detected reactions. From the electrochemical studies performed, it is clearly deduced that the observed reactions are not related with electrode interface phenomena, otherwise no influence on the membrane thickness would be detected; even the hypothesis of an adsorption/desorption phenomena was not corroborated by the results obtained.

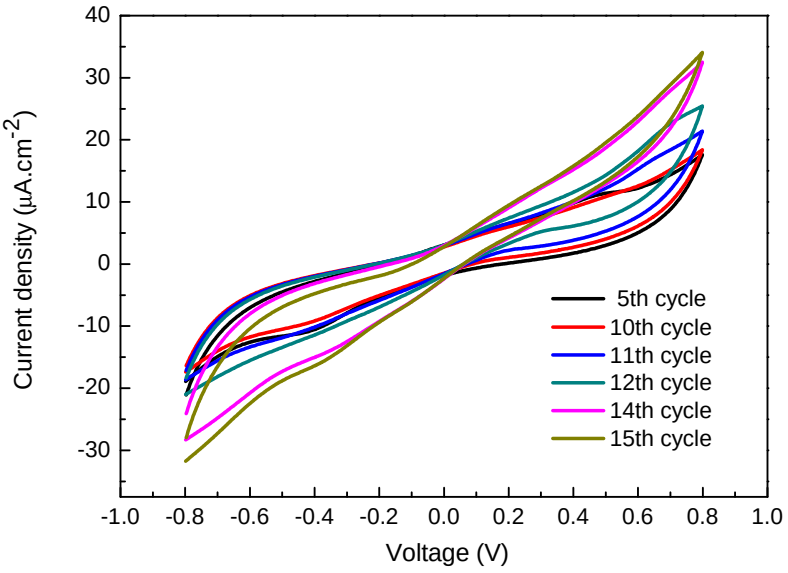

Figure 3.20: Cyclic voltammogram of a CA electrospun membrane during 15 consecutive cycles in the presence of $NaHCO_3$ solution (0.9% wt/v). The membrane has a thickness of 133.5 μm and the measurement was carried out at a voltage scan rate of 80 mV/s.

From this point of view, the electrochemical reactions detected for the CA membrane are related with the high surface area of the electrospun matrix and, consequently, with the increase of the available active sites of the polymer. Since the CA used is not completely acetylated (40% of acetyl groups), three reactive hydroxyl groups at the C-2, C-3 and C-6 atoms position can be easily identified. Thus, it is suggested that the electrochemical reactions are preferentially associated with the free hydroxyl groups allocated at position C-6 (primary alcohol OH group).

The proposed reaction can be described as follows:

$$RCH_2 - OH \rightleftharpoons R - CH = O + 2H^+ + 2e^- \tag{3.3}$$

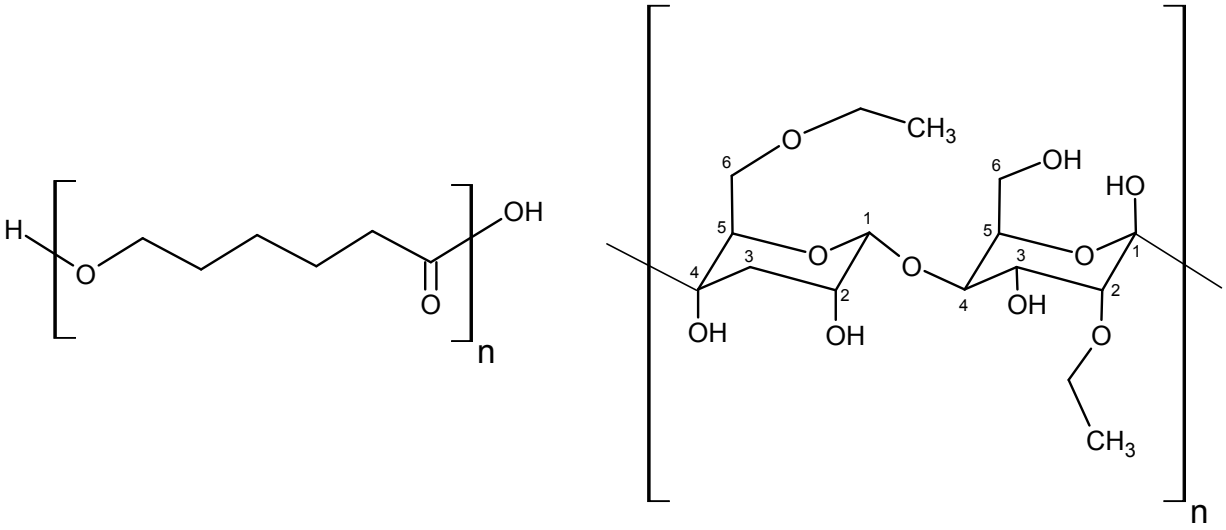

Figure 3.21: PCL and EC molecular structures.

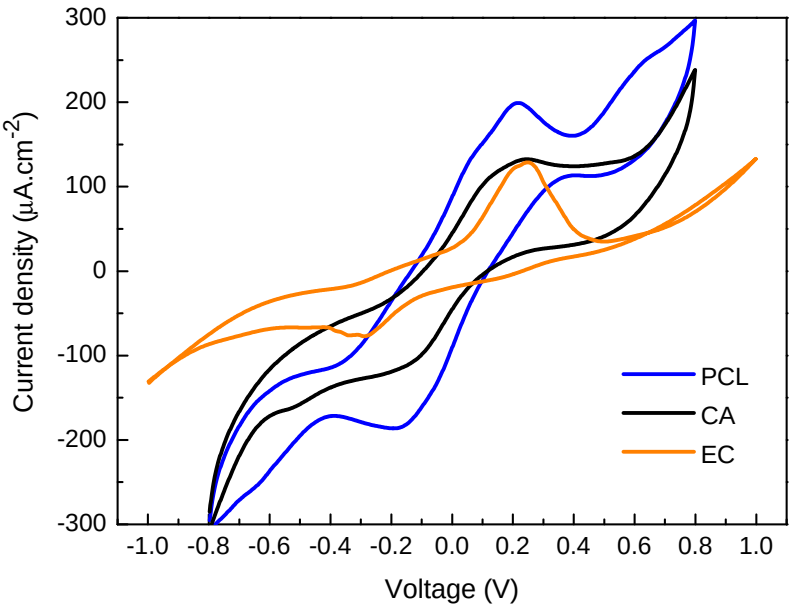

Figure 3.22: Cyclic voltammogram of PCL, CA and EC electrospun membranes in the presence of NaCl solution (0.9% wt/v). All the measurements were carried out at a voltage scan rate of 40 mV/s.

3.4 Summary

The current chapter provided an extensive overview about the use of cellulose-based feedstock in the development of environment-friendly and economically attractive functional materials.

The bio-battery envisage in this PhD thesis is mainly composed of cellulose acetate fibers produced through the electrospinning technique. During the electrospinning, a number of process parameters can influence the morphology of the obtained fibers. For that reason, the effects of polymer concentration and process conditions on membrane morphology was evaluated to produce defect-free fibers with controlled diameters. Smooth fibers with a $D_{average}$ of 243 ± 58 nm were obtained using a solution of CA 12% (wt) in acetone/ DMAc (2:1) for the following ES conditions: 20 kV, 15 cm and 0.2 $ml.h^{-1}$.

After membrane production, mechanical and electrochemically characterization was performed. Nonwoven membranes showed a TS of 3.7 ± 1.0 MPa, a Young's modulus of 42.1 ± 13.8 MPa and a strain of 14.3 ± 5.0 %, which are values quite similar to those found in soft materials, suggesting interesting mechanical properties for biomedical applications.

Additionally, the electrochemical behavior of CA membranes was determined by cyclic voltammetry under physiological conditions (0.9% (wt/v) of NaCl aqueous solution). When impregnated with the salt solution, the membranes revealed a current enhancement, from 10^{-9} A to 10^{-5} A, and redox reactions were detected in the voltammograms. The electrochemical reactions showed to be directly related with the high surface area of the electrospun matrix and, consequently, with the increase of sites found in polymer structure. Finally, it is suggested that the redox reactions are mainly associated with the free hydroxyl groups of cellulose acetate.

The CA electrospun membranes produced during this research have been successfully activated in the presence of physiological fluids, making it a good candidate to be used in the construction of electrochemical devices.

The next chapter covers the preparation of functional fibers with enhanced electrical characteristics in order to be used as electrode materials.

Chapter 4

Development of cellulose-based conductive fibers for bio-batteries

This chapter covers the research of processing functional conductive nanofibers by means of the electrospinning method. The functionalization of electrospun substrates with conductive polymers will be addressed in detailed for the preparation of functional fibers with enhanced electrical properties.

4.1 Background

Electrically conductive polymers (ECPs) have attracted great interest in the past 20 years because they simultaneously display the physical and chemical properties of organic polymers and interesting electrical characteristics. Progresses in the fabrication of nanostructures based on polyaniline (PANI) [106], [107], poly(p-phenylene vinylenes) (PPVs) [108], polypyrrole (PPy)[109] and polythiophenes (PThs) [110] have been recently reported (see chemical structures in Figure 4.1).

Among them, PPy and PANI are the most commonly investigated conductive polymers due to its easier synthesis and relatively high electrical conductivity. Both polymers can be synthesized either chemically or electrochemically. Chemical polymerization has the advantage to combine these polymers with various non-conducting substrates to form composites with interesting tailored properties, while the electrochemical polymerization

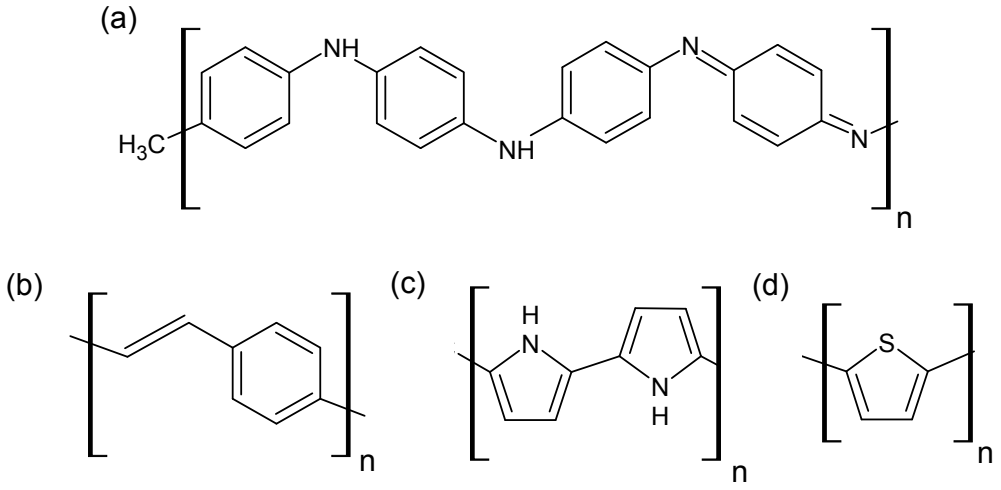

Figure 4.1: Structural units of (a) PANI, (b) PPVs, (c) PPy and (d)PThs.

can be carried out only on electrically conducting substrates.

The ability to customize the conductive nanostructures to meet the requirements of specific applications gives electrospinning an advantage over other production methods. Intrinsically conductive polymers have a fairly rigid backbone due to the high amount of aromatic groups and are usually available only in relatively low molecular weight forms, so the elasticity of its solutions is generally insufficient for it to be electrospun directly into fibers. Therefore, the electrospinning of continuous conductive fibers directly from conductive solutions seems to be a great challenge to overcome. Some authors propose the addition of a carrier polymer to facilitate the electrospinning process; others report on the combination of the electrospinning technique with a nanocoating procedure.

Deposition of PPy or PANI on fiber surface of fabrics and yarns have been widely investigated in the last few years due to its importance to the fabrication of new and functional devices, including gas sensors [111], sensors and biosensors [112] and scaffolds for tissue engineering [113].

4.1.1 Cellulose/ECPs composites

Huang [114] and his colleagues have described the first attempt to successfully achieve an homogeneous coating of natural cellulosic nanostructured substrates with PPy. PPy was

synthesized by *in situ* chemical oxidation of pyrrole using copper chloride ($CuCl_2.2H_2O$) as the oxidant agent followed by the slow precipitation of PPy. Then, the solution is filtered to remove the bulk PPy and the clear filtrate is used to coat the filter paper. A homogeneous PPy layer was adhered onto the cellulose fiber and its thickness (20−25 nm) was precisely controlled by changing the adsorption time.

A novel conducting polypyrrole-based composite material was reported by Mihranyan [115] and his research team. They described the chemical oxidation of pyrrole with iron (III) chloride ($FeCl_3$) on a cellulose substrate derived from *Cladophora sp. algae*. The high surface area and porosity of the Cladophora cellulose fibers was preserved upon the chemical polymerization of a 50 nm thin layer of polypyrrole onto the cellulose fibers creating a conducting paper sheet. Later, the same research group applied a similar procedure to coat wood-based microfibrillated cellulose with PPy [116]. Conductivity measurements on composite sheets indicated an average electrical conductivity of 1.5 $S.cm^{-1}$, which is somewhat higher than that for the algae-cellulose-based composites.

Recently, Huanhuan Wang [117] have reported the preparation of a core−sheath structured conductive nanocomposites by covering a homogenous layer of PPy around bacterial cellulose (BC) nanofibers via *in situ* polymerization of self-assembled pyrrole. Outstanding electrical conductivity of 77 $S.cm^{-1}$ was achieved under optimized reaction conditions (HCl doping, reaction temperature of 0°C and reaction time of 6h).

Similar studies have been found for cellulose/PANI composites. Weili Hu [118] has described the fabrication of PANI/BC conductive nanocomposite membranes by oxidative polymerization of aniline using ammonium persulfate as the oxidant and BC as the template. The study concluded that higher conductivity can be obtained when PANI is doped by stronger protonic acids, such as HCl (10^{-2} $S.cm^{-1}$), since it successfully improves the accessibility and reactivity of the hydroxyl groups of BC.

Also Zhijun Shi [119] and his research team report the *in situ* nano-assembly of BC nanofibers and PANI. PANI was prepared by the oxidation of aniline with ammonium persulfate as the oxidant in an acidic aqueous medium (HCl) and deposited as an adhering layer on the surface of the BC hydrogel. Later, the BC/PANI hybrid sheets were

obtained by pressing the hydrogel composite at 120°C and 1−2 MPa. The electrical conductivity of composites reached up to 10^{-1} S.cm^{-1} depending of the doping state.

4.1.2 Applications of ECPs in medicine

Due to their easier synthesis pathway, biocompatibility [120] [121] and good conductivity, polymers such as PPy and PANI have been extensively studied for medical applications.

4.1.2.1 Tissue engineering

Electrically conductive polymers are attractive materials for the construction of nerve guidance channels. The use of conductive polymers allows local electrical stimulation with precise external control over the level and duration of stimulation, providing a useful physical template for cell growth and tissue repair. Conductive polymeric composites can be used to host the growth of cells, so that electrical stimulation can be applied directly to the cells through the composite, proving to form a valuable scaffold for regenerative medicine, including neural and cardiac tissue engineering.

Jae Young Lee [122] has fabricated electroconducting scaffolds by depositing PPy on electrospun PLGA fibers. *In vitro* cell culture using rat pheochromocytoma 12 (PC12) cells and embryonic hippocampal neurons have demonstrated that compatible cellular interactions on the fabricated PPy-PLGA meshes are appropriate for neuronal applications and present topographies for modulating cellular interactions. Also, electrical stimulation of PC12 cells on the conducting nanofiber scaffolds have shown to improved neurite outgrowth.

Electrical stimulation of nerve stem cells on conducting polymeric scaffolds has been reported by Prabhakaran and his research team [123]. They have shown that the electrical stimulation of nerve stem cells on electrospun PLLA/PANI fibers can stimulate the differentiation or neurite elongation, highlighting the relevant application of electrical impulses as target signals for nerve tissue regeneration.

4.1.2.2 Controlled drug release

ECPs have been also explored for externally controlled polymeric drug-delivery system allowing the tailoring of release profiles to match physiologic processes.

A CNTs/PPy nanoreservior has been developed by the research team of Xiliang Luo [124]. Pretreated hydrophilic CNTs were filled with an anti-inflammatory drug solution (dexamethasone, Dex). Then, to keep the loaded Dex inside the CNTs, an electropolymerized PPy film was used to seal the tubes. The PPy release mechanism is well known and it is mainly attributed to the de-doping process during negative charge that electrochemically reduces the positively charged polymer backbone to a neutral state, causing the release of negatively charged drug from the film. Considering the CNTs/PPy composite, the actuation effect of PPy film upon electrical stimulation may cause the expansion or contraction of the polymer, and thus temporarily open the seal on each end of the nanotubes and accelerate the drug release. Therefore, release from the CNTs/PPy film can be more sustainable due to the extra drug stored inside the CNT capsules demonstrating to have a suitable release profile than that of a conventional PPy film.

Recently, Esrafilzadeh and co-workers [125] have presented the fabrication of a coaxial conducting polymer fibers loaded with an antibiotic drug that can then be subsequently released (or sustained) in response to electrical stimulation. The method involves wet-spinning of poly(3,4-ethylenedioxythiophene) poly(styrenesulfonate) (PEDOT:PSS) fiber, which served as the inner core to the electropolymerised outer shell layer of PPy/Ciprofloxacin hydrochloride (Cipro). Cipro was selected as the model drug and as the dopant in the PPy synthesis. When the core-shell fiber is electrically stimulated so that the outer layer (PPy/Cipro) is in the oxidized state, the amount of Cipro release has decreased when compared to the passive profile. Conversely, when a reducing potential is applied, longer term sustained release up to 72 h is observed with approximately 2 times higher concentration of released drug compared to the passive mode. These results have demonstrated that the release profile can be controlled by switching the redox state of PPy/Cipro layer. Additionally, *in vitro* cytotoxic testing using neural B35 cell line confirmed the cytocompatibility of the drug loaded composite fibers.

Since the rate of drug release can be modulated from an external source, drug releasing systems based on intrinsically conductive polymers can be a valuable solution for chronic disease where the release of anti-inflammatory drugs or neurotrofic factors is not constant.

4.1.2.3 Electrodes for implantable batteries

The interest for bio-batteries to supply implantable medical devices has been increasing. Bio-batteries can be implantable in the body and rely on oxygen in the internal body fluid to produce a voltage between the anode and the cathode. Recently, the research group of Dr. Gordon Wallace has made great achievements in this area. In 2012, his research team proposed the use of PPy as an active component within a bioelectric battery [126]. They have developed a cathode made of PPy doped with a biological polyelectrolyte (dextran sulfate, DS) using a bioresorbable Mg alloy as the anode. PPy-DS cathode can be used as a catalyst for oxygen reduction process; on the other hand the reduced or undoped PPy produced during the discharge process can be re-oxidized by oxygen contained in the electrolyte and retained its electroactivity. Actually, the battery mechanism is quite similar to that of a typical metal-air battery. This battery exhibited an energy density of 790 $W.h.kg^{-1}$ with commonly used biological media as electrolyte, which should be sufficient to drive some implantable devices requiring low power densities.
More recently, in 2013, they have proposed the development of a novel biocompatible battery (or bio-battery) activated by simulated body fluids [71]. PPy/CNTs composites were chemically synthetized and used as cathode with a cellulose paper as the substrate and separator. For battery characterization, a zinc foil was used as the anode material and protein free simulated body fluid as the electrolyte. In this system, zinc is the unlimited sacrificial electrode, while the PPy/CNTs composite acts as the catalyst for the oxygen reduction process. The cathode developed has shown a good stability and a high discharge capacity under simulated body fluids.

As previously stated in this chapter, electrically conductive polymers, such PPy and PANI, have shown to be biocompatible and an ideal material for implantable biomedical

applications. Innovative bioelectronic devices are being developed in this area making these materials ideal for the processing of lightweight, flexible and conductive components. The research work presented in this thesis has started in 2010 and is focused on the development of bio-batteries made of electrospun fibers for medical applications taking advantage of the ionic content of the biological fluids. For that reason, electrically conductive materials have shown to be a valuable material for the development of biocompatible cellulose-based composite electrodes.

4.2 Methodology

4.2.1 Preparation of CA/PPy fibers by *in situ* vapor-phase polymerization

For the preparation of CA/PPy composites, the CA membrane was produced by electrospinning (as described in the Methodology section from Chapter 3) and a thin coating of PPy was deposited by *in situ* vapor-phase polymerization onto the surface of the electrospun fibers. The experimental procedure for vapor-phase polymerization was adapted from literature [127].

The nonwoven membranes were cut into samples of dimensions 3 cm × 2 cm and were immersed in an oxidant-containing aqueous solution (Ox), $FeCl_3.6H_2O$ (Sigma-Aldrich), for 24 hours under gentle stirring. After this period, the $FeCl_3$-impregnated membranes were dried and then placed in a closed chamber over pyrrole (Py) monomer liquid (Sigma-Aldrich) being the nonwoven membrane fully exposed to the vapors of the monomer (Mon) at room temperature, as illustrated in Figure 4.2. During pyrrole oxidative polymerization, the membranes turned from white to black, which indicated the formation of PPy. The coated membranes were taken out of the chamber and washed with abundant water and ethanol to remove unreacted oxidants, pyrrole monomer and by-products. Finally, the samples were dried in air. The exposure time (t_{pol}) of membrane to monomer vapors was evaluated during 30 and 60 min. A summary of the polymerizations conditions is provided in Table 4.1.

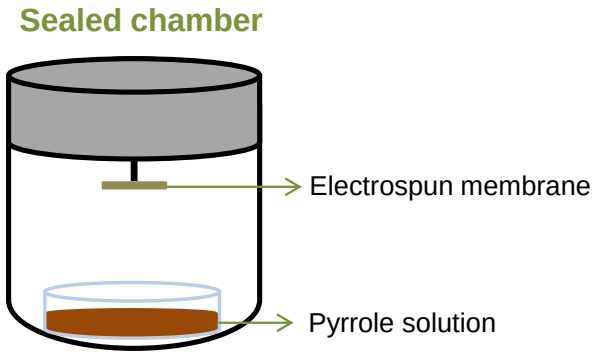

Figure 4.2: Illustration of the setup carried out for the *in situ* vapor-phase polymerization of PPy.

Table 4.1: Summary of the conditions used for *in situ* vapor-phase polymerization of PPy.

Method	**Monomer**	**Oxidant**	$\mathbf{t_{pol}}$ **(min)**
Vapor-phase polimerization	Py (6.77g Mon, 7ml water)	$FeCl_3$ (0.8g Ox, 10ml water)	30; 60

4.2.2 Preparation of CA/PPy composite fibers by *in situ* chemical oxidation

Dried CA electrospun membranes with approximately 3 cm × 2 cm of dimensions were coated with PPy through *in situ* oxidative polymerization.

The CA membranes were immersed in an aqueous solution of pyrrole with concentrations varying from 0.025 to 0.075 mol.L^1 for 10 min under magnetic stirring. The polymerization was carried out at room temperature by gently adding an aqueous solution of $FeCl_3.6H_2O$, as the oxidant agent. The first study has evaluated the better Mon/Ox mass ratio (Table 4.2). Later, different monomer concentrations and reaction times have been studied (Table 4.3).

During pyrrole oxidative polymerization, the CA membranes turned from white to black within a few minutes, which confirmed the formation of PPy. After polymerization, the CA/PPy composites were thoroughly washed with distilled water and ethanol in order to extract the by-products and residues of the reaction and dried in air.

Table 4.2: Monomer/oxidant mass ratios in Py polymerization by chemical oxidation.

[Mon] mol.L^{-1}	t_{pol} (min)	Ox/Mon
0.025	60	1
		2
		3
		4

Table 4.3: Evaluation of the monomer concentration and reaction time in PPy polymerization by chemical oxidation.

[Mon] mol.L^{-1}	Ox/Mon	t_{pol} (min)
0.025	2	30
		45
		60
		90
		1440
0.05	2	15
		30
		45
		60
		90
		1440
0.075	2	15
		30
		45

4.2.3 Preparation of CA/PANI fibers by *in situ* chemical oxidation

Dried CA electrospun membranes with approximately 3 cm × 2 cm of dimensions were coated with PANI through *in situ* oxidative polymerization. PANI is frequently prepared by the oxidation of aniline with ammonium persulfate, $(NH_4)_2S_2O_8$, as the oxidant in an acidic aqueous medium [118].

The CA membranes were immersed in 10 ml of an aqueous acid solution, HCl (1M), containing aniline monomer under magnetic stirring and ice bath. The oxidant-containing solution was prepared by adding ammonium persulfate to 10 ml of an acid solution of HCl (1M). After an impregnating period of 60 min, the oxidant solution was added drop-wise to the monomer-containing solution. The mixture was stirred in an ice bath for 30, 45 and 60 min, respectively. Different monomer concentrations and Ox/Mon molar ratios have been evaluated for each reaction time. All the synthesis conditions studied are presented in Table 4.4.

During aniline polymerization, the CA membranes turned from white to dark green color, which indicates the formation of PANI. At the end of each experiment, the obtained fibers were thoroughly washed with distilled water and ethanol in order to extract the by-products and residues of the reaction and dried in air at room temperature.

4.2.4 Morphological characterization

The surface morphology of the electrospun composites was evaluated by using SEM-FIB Zeiss (Auriga) and SEM Zeiss (DSM-962). Double-sided conductive carbon tape was used to attach the samples to the samples support. The samples were sputtered with gold to avoid electrons charging. Transmission Electron Microscopy (TEM, model H-8100 II from Hitachi), was carried out to estimate the thickness of PPy coating. Measurements on TEM images were made using an image processing software (ImageJ, NIST).

Table 4.4: Summary of the conditions used for PANI polymerization.

[Mon] mol.L^{-1}	Ox/Mon	t_{pol} (min)
4	0.5	30
		45
		60
	0.25	30
		45
		60
	0.125	30
		45
		60
2	0.5	30
		45
		60
	0.25	30
		45
		60
	0.125	30
		45
		60

4.2.5 Electrical characterization

The electrical conductivity was measured along the fiber and, for that purpose, the fibers were placed in a rigid substrate and two electrical contacts were placed on the fibers with silver past separated about 1 mm apart as illustrated in Figure 4.3.

The in-plane electrical conductivity was calculated from the linear I–V plot obtained by a Cascade Microtech/Alessi REL-4500 probing platform connected to a HP 4145B Semiconductor Parameter Analyzer at room temperature. The electrical conductivity was calculated using Equation 4.1:

$$\sigma = \frac{l}{AR} \Leftrightarrow \sigma = \frac{l}{A} \times \frac{I}{V} \Leftrightarrow I = \sigma \times \frac{A}{l} \times V \tag{4.1}$$

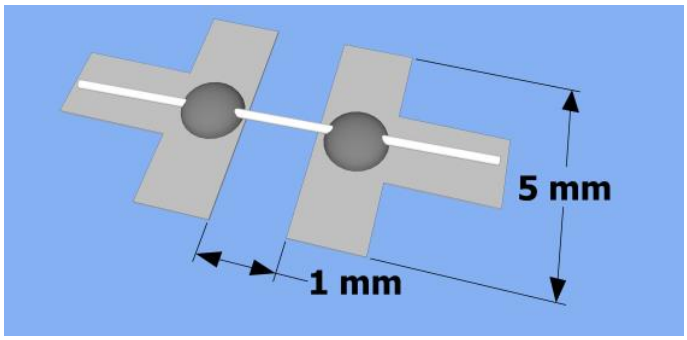

Figure 4.3: Illustration of the setup carried out for preparation of electrospun fibers for electrical characterization.

where σ is the electrical conductivity (S.cm^{-1}), R is the resistence (Ω), A the area of the membrane (cm^2), l the distance between electrodes (cm), V the applied voltage (V) and I the current (A).

The temperature dependence of conductivity can be fitted by Arrhenius equation:

$$\sigma = \sigma_0 \times e^{-\frac{E_a}{k_B T}} \Leftrightarrow \ln(\sigma) = \ln(\sigma_0) - \frac{E_a}{k_B} \times \frac{1}{T} \tag{4.2}$$

where E_a is the activation energy (eV), k_B the Boltzmann constant (eV.K^{-1}), T the absolute temperature (K) and σ_0 the pre-exponential factor (S.cm^{-1}).

In order to determine if the fibers are thermally activated, the sample was heated up from 303 to 377 K in a vacuum chamber (10^{-2} mbar) and then cooled down using a computer controlled cryostat. The current passing through the fibers was measured using a Keithley 618 ammeter during the cooling of the sample with temperature intervals of 8 K and applying a voltage of 1V.

Each measurement was repeated three times to minimize errors.

4.2.6 Mechanical characterization

Mechanical characterization of composite membranes was carried out as described in the Methodology section of Chapter 3. Ten samples were analyzed to obtain mean values for tensile strength, Young's modulus and strain. The applied deformation rate was 1 mm.min^{-1} and the temperature was kept constant at 25°C.

4.2.7 *In vitro* cytotoxic testing

The cellular response induced by the CA fibers and CA/PPy composite fibers was investigated using a cell toxicity indirect standard procedure [128].

Vero cells were seeded for 24 h at 2×10^4 cells per well in a 48-well plate at 37°C. At the same time, composite fibers were sterilized by UV exposure for 2 h and added to the culture medium (Figure 4.4) for 24 h at 37°C.

Following incubation, the culture medium from the cell monolayers was replaced by the extract of the experimental and control samples. After 24 h of incubation, resazurin indicator solution was added. Resazurin is a redox-sensitive dye that is reduced by viable cells into a fluorescent compound, Resorufin [129]. There is a direct correlation between the reduction of resazurin in the growth media and the quantity/proliferation of living organisms.

The plate was placed into a spectrophotometric plate reader set to read the absorbance at 570 and 600 nm, which directly correlates to the number of living cells in the culture. The experiments were performed in triplicate for CA fibers, CA/PPy composite fibers, medium control and cells control.

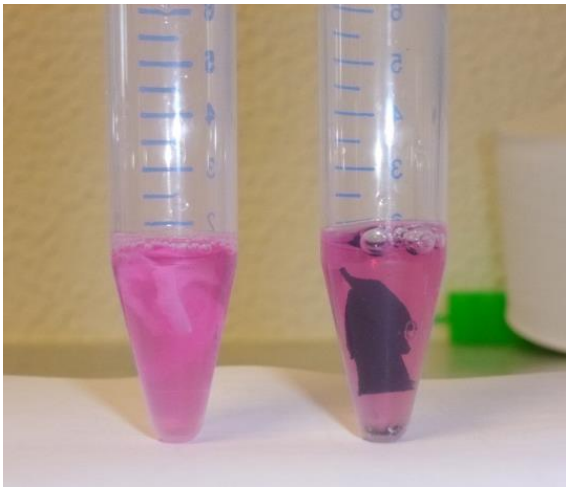

Figure 4.4: Photograph of the CA membrane (on the left side) and the CA/PPy composite membrane (on the right side) in the culture medium.

4.2.8 Electrochemical characterization

The electrochemical performance of cellulose-based bio-batteries was characterized by cyclic voltammetry. For that purpose, three different bio-batteries structures were evaluated, as illustrated in Figure 4.5.

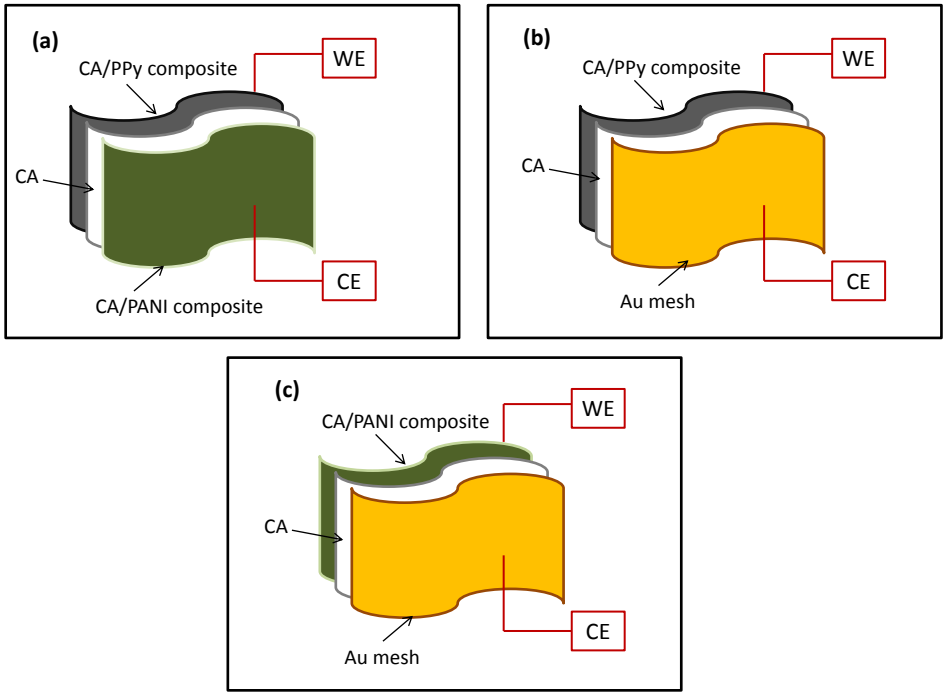

Figure 4.5: Illustration of the three structures used for battery testing: (a) PPy/cellulose acetate membrane/PANI, (b) PPy/cellulose acetate/Au mesh and (c) PANI/cellulose acetate/Au mesh. In each structure, the working and the counter electrodes are identified.

The electrochemical experiments were carried out using a potentiostat Gamry Instruments-Reference 3000 and the batteries were tested in a home made Teflon cell (Figure 4.6 (a)). Figure 4.6 (b) displays the photograph of the setup carried out for the battery testing. The bio-battery cell was constructed using two identical pieces (0.5 cm $\times$ 0.5 cm) of the conductive materials separated by a CA electrospun membrane with a thickness of 120 μm, approximately. Additionally, two flexible carbon meshes were used as the collectors. The electrochemical cell has a reservoir, as observed in Figure 4.6 (c) in order to easily inject the electrolyte. Similar to what was previously described in Chapter 3, NaCl 0.9% (w/v) was used to simulate the ionic content of body fluids.

Besides testing the PPy and PANI composite membranes as electrode materials, a com-

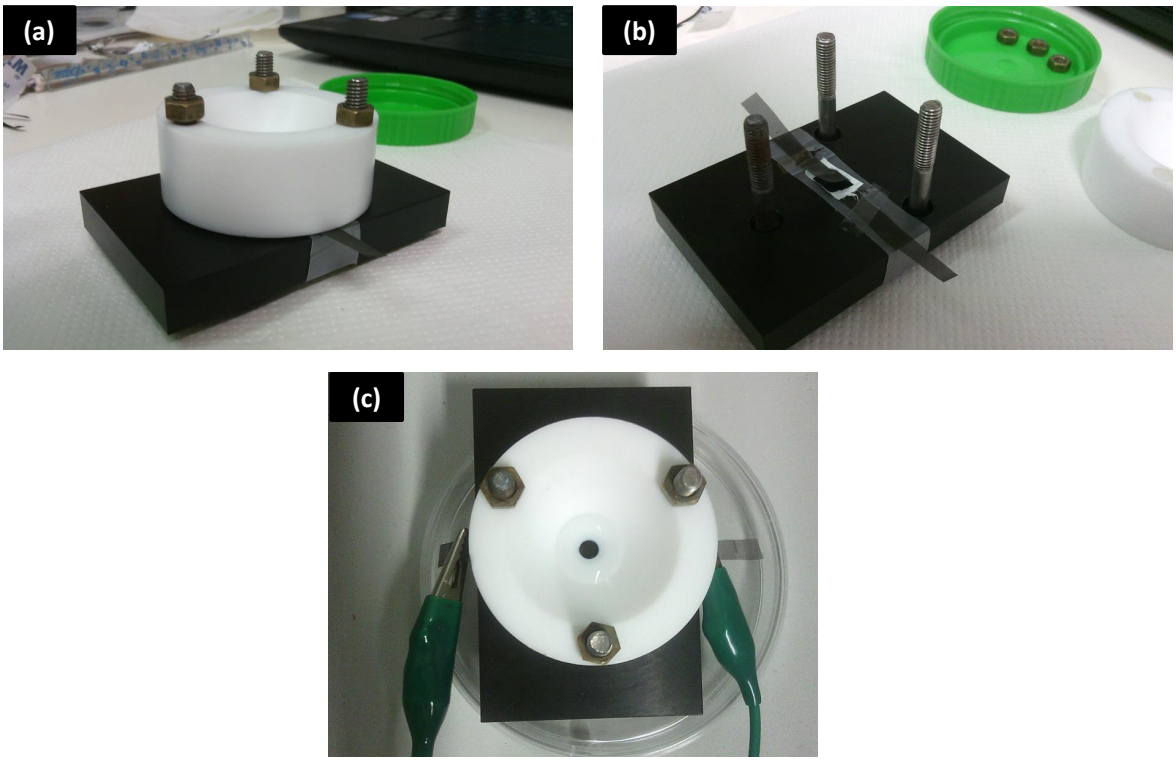

Figure 4.6: Photograph of the electrochemical cell setup used for battery testing (a) general view, (b) bio-battery assembly with two carbon mesh contacts and (c) top view of the cell during electrochemical measurements with NaCl solution in the reservoir.

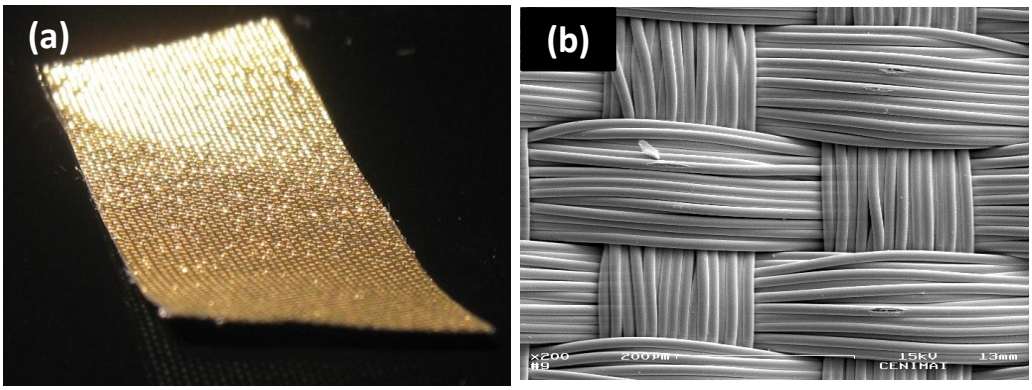

Figure 4.7: Conductive fabric composed of gold-based fibers used as counter electrode for bio-battery testing (a) photograph and (b) SEM image.

mercial conductive fabric composed of gold-based fibers purchased from A-Jinelectron Company (Metaline) was also considered during electrochemical characterization (Figure 4.7).

During electrochemical characterization, a two-electrode configuration was considered for cyclic voltammetry and discharge testing. The reference electrode (RE) and the counter

electrode (CE) were merged into one electrode resulting in a two-electrode system. For cyclic voltammetry measurements, the potential was scanned in both directions between -1 and 1 V for 10 consecutive cycles with a scan rate of 80 $mV.s^{-1}$ under atmospheric conditions.

4.3 Results and discussion

This section presents and discusses the main results achieved in the development of functional fibers with electrical conductivity. The preparation of nonwoven membranes of CA/PPy and CA/PANI has been intensively investigated due to their high surface area, biocompatibility and flexibility. These interesting cellulose-based composites are ideal electrodes for the development of the proposed bio-batteries.

4.3.1 CA/PPy composite fibers by *in situ* vapor-phase polymerization

Due to their large surface area, flexibility and biocompatibility, CA electrospun membranes are favorable templates for the development of conductive polymer composites. To produce cellulose-based composite fibers the *in situ* vapor-phase polymerization of PPy onto the surface of CA fibers has been considered (Figure 4.8).

Since pyrrole monomer has relatively high vapor pressure, the polymerization of pyrrole on the oxidant-impregnated CA membrane could be readily initiated by exposing the fibers directly to pyrrole vapor.

The oxidant was applied to the electrospun membrane by soaking it in an aqueous solution of the $FeCl_3$. Iron (III) chloride has been found to be the best chemical oxidant for the polymerization of PPy with respect to desirable conductivity characteristics. Beneventi and his co-workers have reported about the importance of the impregnation step in the success of Py polymerization [130]. A small amount of $FeCl_3$ deposited on fibers could be insufficient to initiate the polymerization and poorer electrical conductivities are estimated for the composite. Thus, it is also expected that the generation of a homogeneously

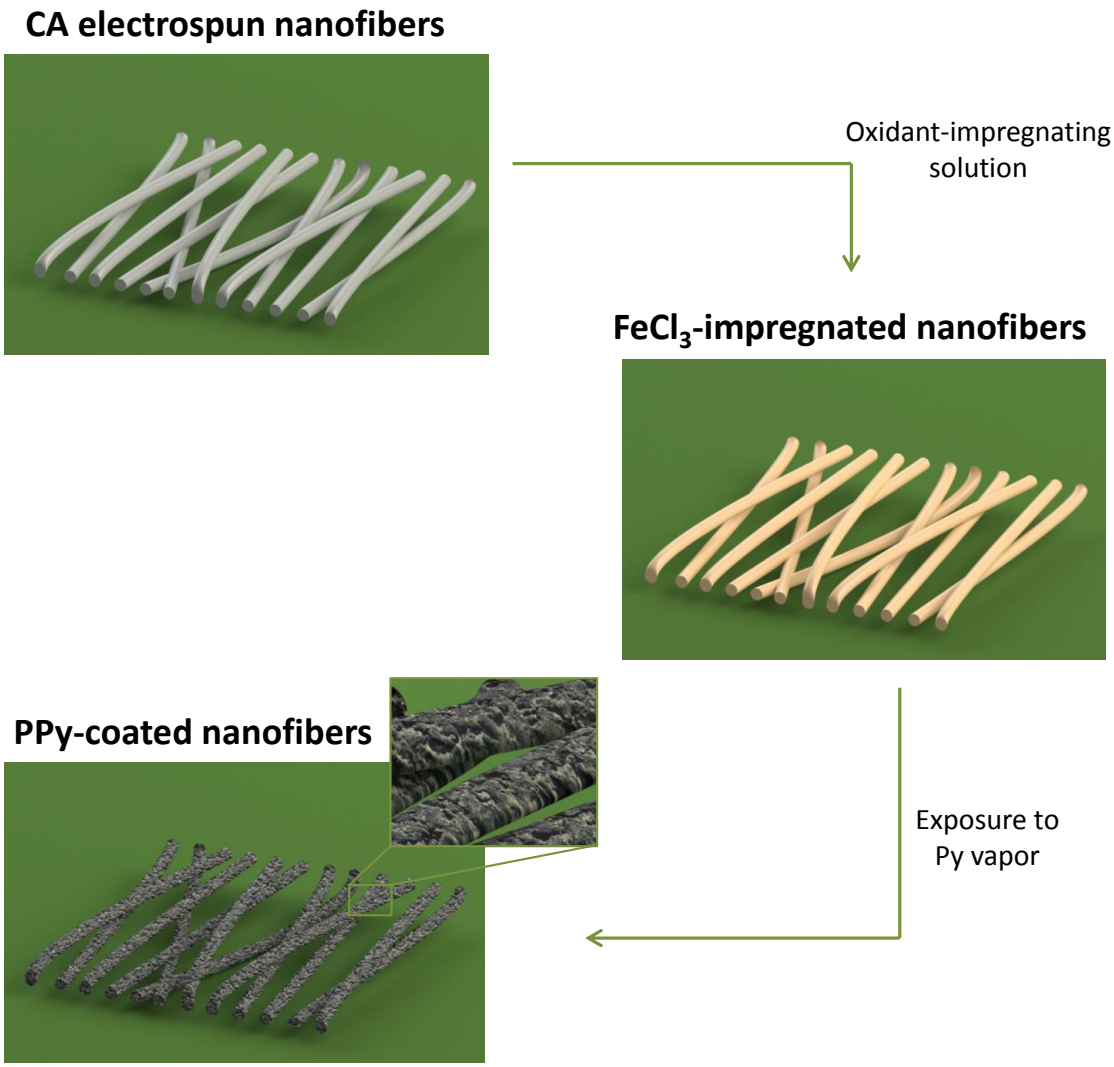

Figure 4.8: Illustration of the fiber template methodology for the preparation of composite fibers of CA and PPy by *in situ* vapor-phase polimerization.

dispersed PPy clusters on the fiber surface can be directly related with the concentration of $FeCl_3$ in the impregnating solution.

When the $FeCl_3$-impregnated membranes were exposed to pyrrole vapor the color changed gradually to black. The black color clearly indicated the formation of PPy. Figure 4.9 shows the SEM images of uncoated CA electrospun fibers and composite fibers obtained through *in situ* vapor-phase polymerization of Py.

The CA membrane consist of a network structure of nonwoven nanofibers with high aspect ratio and mean diameter of 243 $\pm$ 58 nm (Figure 4.9 (a)). As shown in Figure 4.9

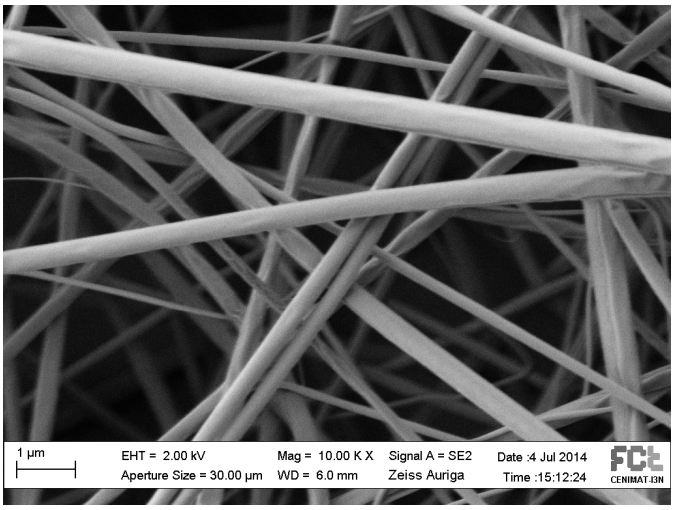

(a)

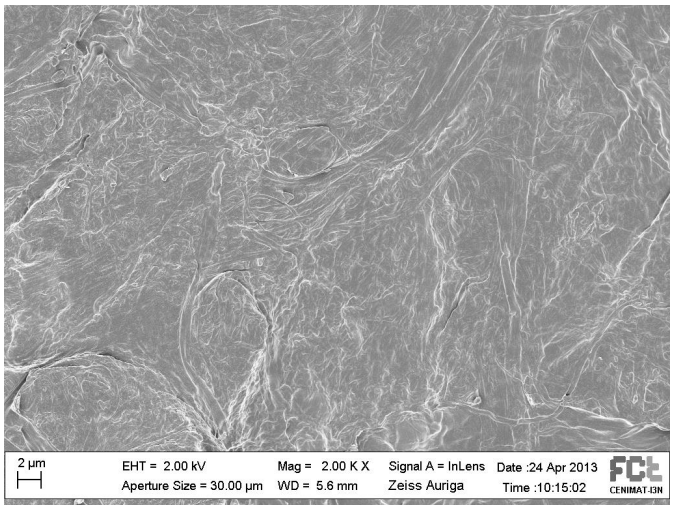

(b)

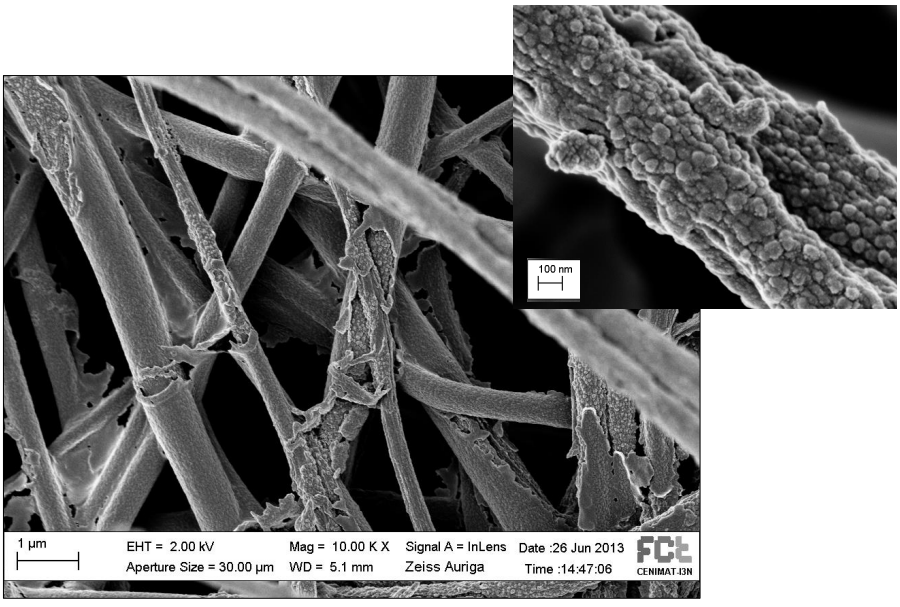

(c)

Figure 4.9: SEM images of CA electrospun fibers: (a) uncoated, (b) coated with PPy after 60 min and (c) 30 min of polymerization.

(b), a continuous layer of PPy is formed on the surface of CA membrane after 1 hour of polymerization. Besides losing its original fibrous structure, and thus porosity, the membrane has revealed to be extremely brittle making difficult the preparation of samples for electric measurements. According to some authors, cellulose can be subjected to some degradation process under prolonged polymerization reaction or under aggressive reaction conditions which can explain the fragility of the membrane [130].

Consequently, decreasing exposure time to pyrrole vapors has been considered. Figure 4.9 (c) reveals that for 30 min of polymerization the CA membrane has preserved its natural fibrous structure. However, a rough surface and an irregular coating of PPy aggregates has been observed.

The electrical conductivity of the nanofibers was highly improved with the formation of PPy, around eight orders of magnitude (Table 4.5).

Table 4.5: Summary of the electrical conductivity and morphology of uncoated CA electrospun fibers and CA/PPy composites.

Sample	**t_{pol} (min)**	**Conductivity ($S.cm^{-1}$)**	**Morphology**
CA fibers	0	$(7.1 \pm 0.8)x10^{-11}$	Flexible and highly porous
CA/PPy fibers	60	n.m[a]	Nonporous membrane; Extremely fragile
CA/PPy fibers	30	$(5.1 \pm 0.4)x10^{-3}$	Not uniform coating; Fragile

[a] Not measured. The electrical conductivity was not measured due to the fragility of the membrane

The conductivity of conjugated polymers, such as PPy, involves charge transport along the polymer chains, as well as hopping of carriers. Conjugated polymers are formed by a main backbone containing alternating single and double chemical bonds. Whereas a single bond (or sigma bond, σ) is strong and contains strongly localized electrons under a sp^3 orbital symmetry, a double bond (or pi bond, π) is weaker and electrons are less localized following a sp^2 orbital symmetry. This means that π electrons may exhibit higher mobility when compared to σ electrons and can move along the backbone since the conjugation leads to the formation of extended delocalized orbitals [131].

Nevertheless, these composite fibers are more brittle than the pristine CA ones. Thus, for the application as electrodes for medical batteries, this characteristic is undesirable and, consequently, a different fiber coating methodology has been considered.

4.3.2 CA/PPy composite fibers by *in situ* chemical oxidation

Cellulose acetate/PPy composite fibers were prepared through the *in situ* pyrrole oxidative polymerization by using $FeCl_3$ as oxidant.

Electrospun CA fibers were immersed in a monomer solution in which the pyrrole impregnates through the inner network of CA. The large amounts of hydroxyl groups presented in CA structure can easily interact with the amine groups of pyrrole ensuring a uniform distribution of the monomer through the surface of nanofibers. After oxidant addition, the pyrrole monomer polymerizes covering the nanofibers. Comparing with CA nanofibers, the composite fibers showed a black color which indicated the successful incorporation of PPy in the electrospun membrane. In addition, composite membranes were still flexible enough to be stretched and bended (Figure 4.10).

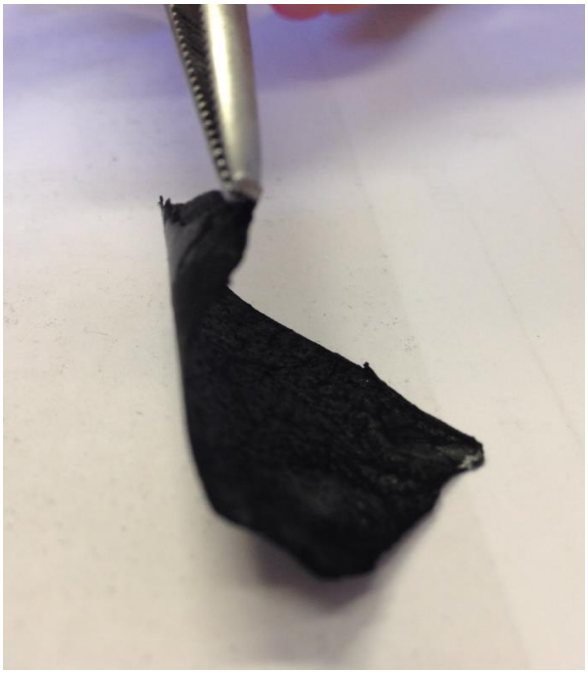

Figure 4.10: Photograph of CA/PPy composite membrane prepared by *in situ* chemical oxidation.

The effects of chemical synthesis conditions, such as monomer concentration, the mass ratio oxidant/monomer and reaction time were investigated in detail. The influence of the oxidant/monomer mass ratio on the electrical conductivity of CA/PPy fibers after 1 hour of polymerization using a pyrrole concentration of 0.025 mol.L^{-1} is shown in Figure 4.11. The electrical conductivity increased as the $FeCl_3$/Py mass ratio increases reaching values of 10^{-3} S.cm^{-1} for ratios up to 2.

Due to its extreme toxicity, small amounts of $FeCl_3$ should be considered for the optimization of this chemical synthesis. On the other hand, the oxidant amount should be adequate to attain a good electrical conductivity. Considering both evidences, the Ox/Mon ratio of 2 was selected for Py polymerization.

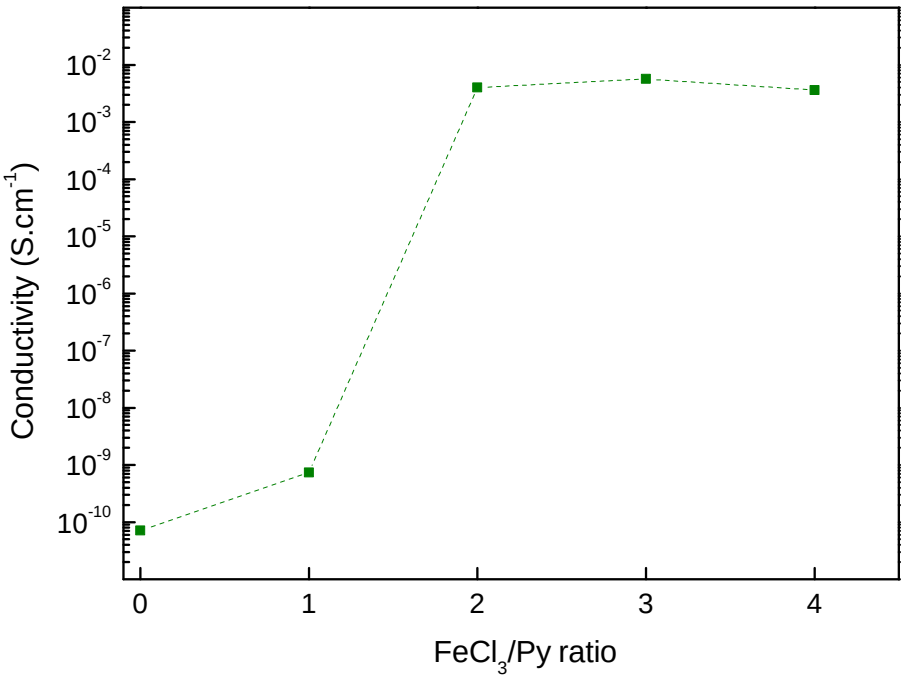

Figure 4.11: Influence of oxidant/monomer ratios on electrical conductivity of CA/PPy fibers prepared by *in situ* chemical oxidation. Electrical conductivity values are presented in Appendix B, Table B.1.

In order to reach CA/PPy composite fibers with higher electrical conductivity at low $FeCl_3$/Py ratio and prevent CA degradation, the influence of the monomer concentration and the reaction time on the electrical conductivity was investigated (Figure 4.12).

The polymerization time plays a crucial role on the electrical conductivity of fibers. A sharp increase in the electrical conductivity is observed after 15 min of polymerization. The electrical conductivity reached values of 10^{-2} S.cm^{-1} after 15 and 30 minutes with

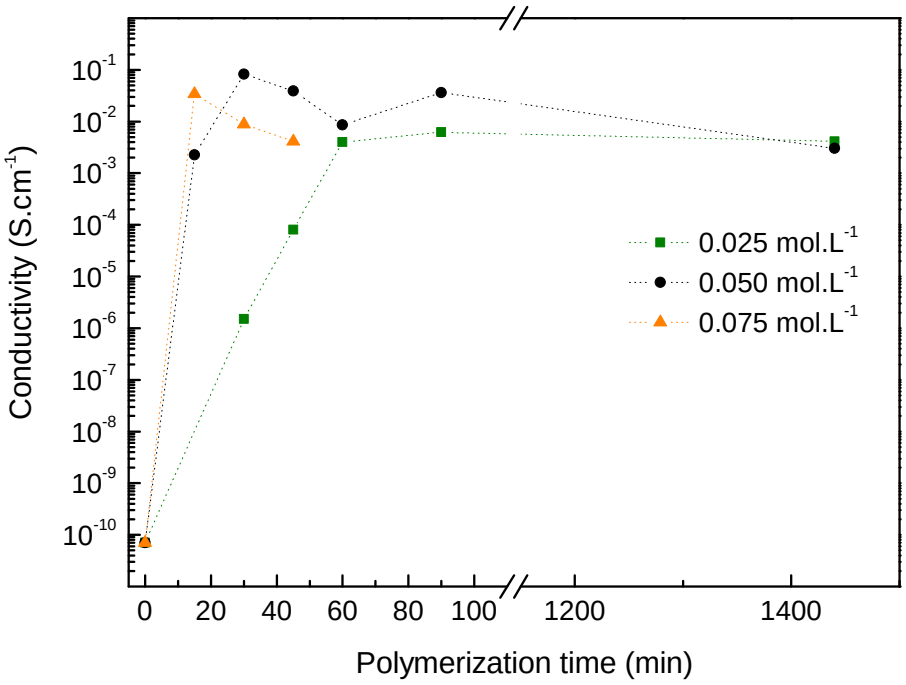

Figure 4.12: Influence of the monomer concentration and the reaction time on the electrical conductivity of CA/PPy nanofibers prepared by *in situ* chemical oxidation. Electrical conductivity values are presented in Appendix B, Table B.2.

monomer concentrations of 0.075 and 0.05 mol.L^{-1}, respectively. This behavior can be probably attributed to the high PPy yield achieved at that time allowing the formation of a continuous layer on CA nanofibers surface. Lower monomer concentrations needed more than 90 min to reach close to 10^{-2} S.cm^{-1}.

The morphology of CA/PPy composite fibers for the different synthesis conditions was evaluated through SEM images. Figure 4.13 shows the SEM images of the composite fibers using 0.025 mol.L^{-1} (Figure 4.13 (a)), 0.05 mol.L^{-1} (Figure 4.13 (b)) and 0.075 mol.L^{-1} (Figure 4.13 (c)) of pyrrole for a reaction time of 45 min.

The CA/PPy fibers obtained with a pyrrole concentration of 0.025 mol.L^{-1} are not continuously coated with PPy, which may explain the lower electrical conductivity. The increase of monomer concentration led to the formation of a continuous PPy layer on the surface of CA nanofibers. However, for higher concentrations, such as 0.075 mol.L^{-1}, it is observed the formation of PPy aggregates that might be responsible for the slight decrease of the electrical properties. The morphology of CA/PPy fibers after 24 hours (1440 min) using a monomer concentration of 0.05 mol.L^{-1} is also presented in Figure 4.14

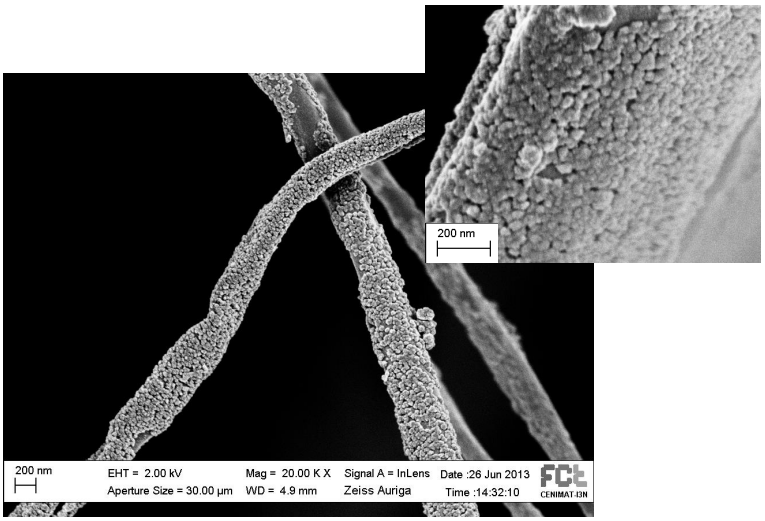

(a)

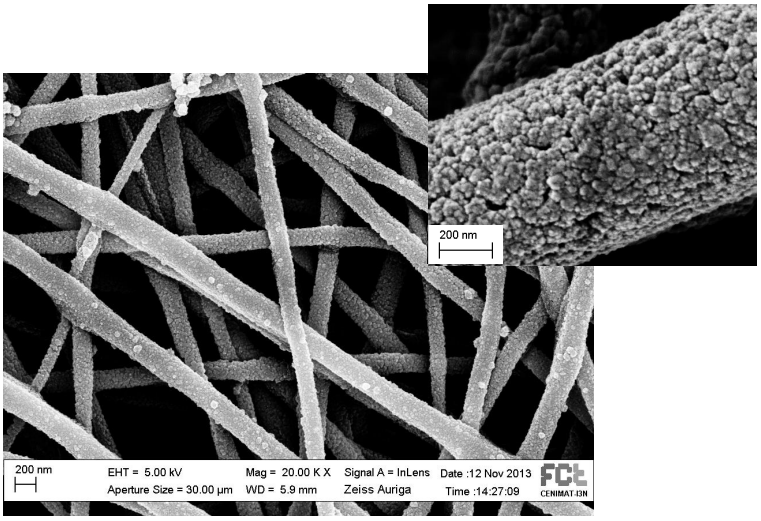

(b)

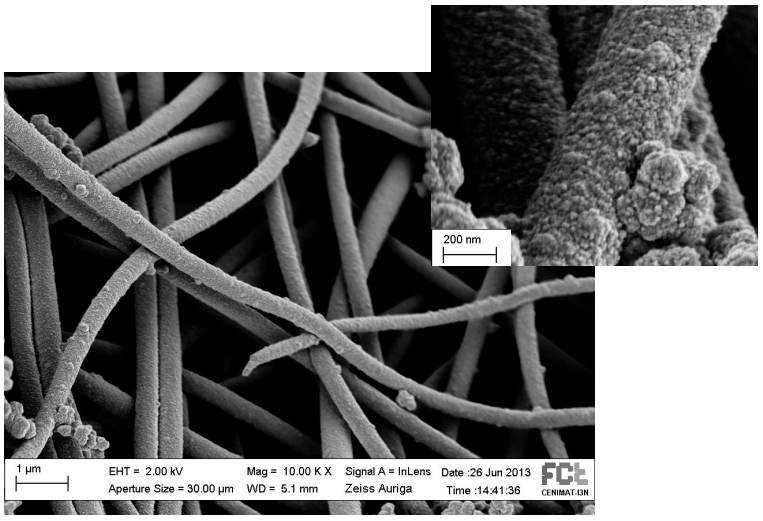

(c)

Figure 4.13: SEM images of the CA/PPy fibers prepared by *in situ* chemical oxidation using (a) 0.025 mol.L^{-1}, (b) 0.05 mol.L^{-1} and (c) 0.075 mol.L^{-1} of pyrrole and a time reaction of 45 min.

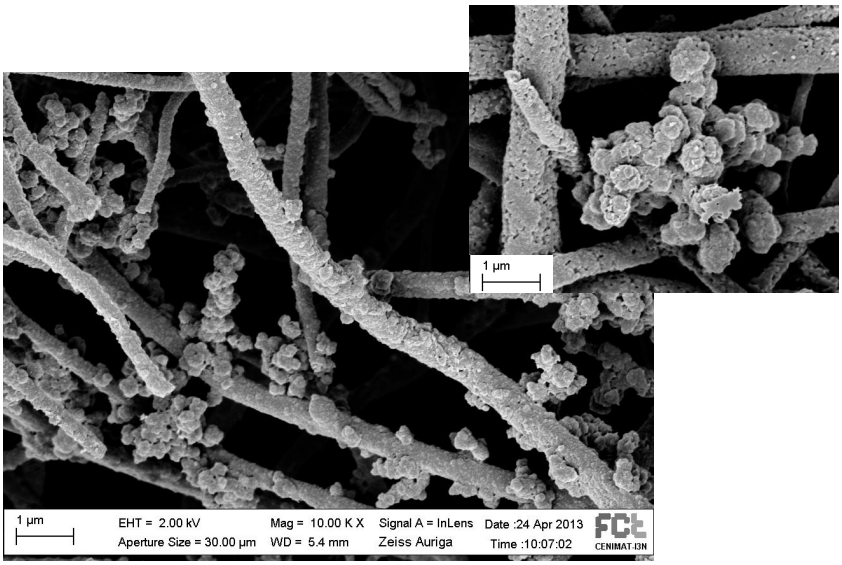

Figure 4.14: SEM images of the CA/PPy fibers prepared by *in situ* chemical oxidation using a pyrrole concentration of 0.05 mol.L^{-1} and a time reaction of 24 hours.

where the formation of large aggregates of PPy on the surface of the fibers is observed. The average diameter of CA/PPy composite fibers was estimated with the increase of monomer concentration and reaction time (Figure 4.15). The increase of both parameters led to an increase of PPy polymerization and a thicker layer of PPy was formed on CA fibers' surface.

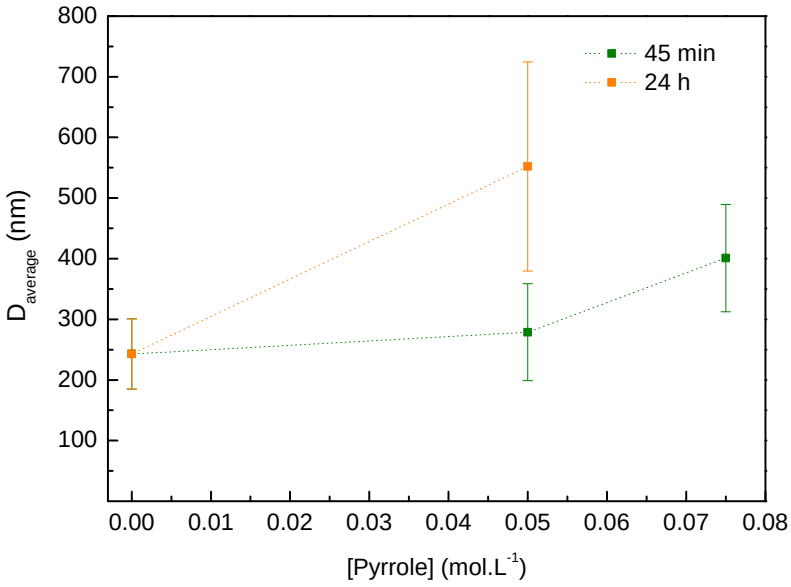

Figure 4.15: Influence of monomer concentration and time reaction on the diameter of CA/PPy nanofibers prepared by *in situ* chemical oxidation.

Considering both electrical and morphological analysis, the adequate conditions for the

preparation of uniform PPy-coated CA fibers with higher electrical conductivity are: 0.05 mol.L^{-1} of Py, an Ox/Mon ratio of 2 and a reaction time of 30 min.

Figure 4.16 shows the TEM images of PPy coated CA nanofibers using the previous synthesis conditions (Figure 4.16). Nonwoven composite fibers with a uniform and continuous PPy coating and an average diameter of 290 ± 69 nm are observed in Figure 4.16 (a). Figure 4.16 (b) shows a PPy nanocoating of, approximately, 40 nm on the surface of CA electrospun fibers.

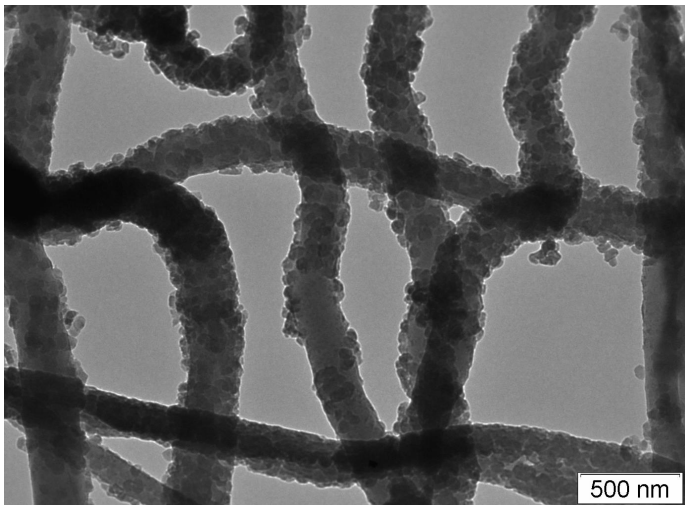

(a)

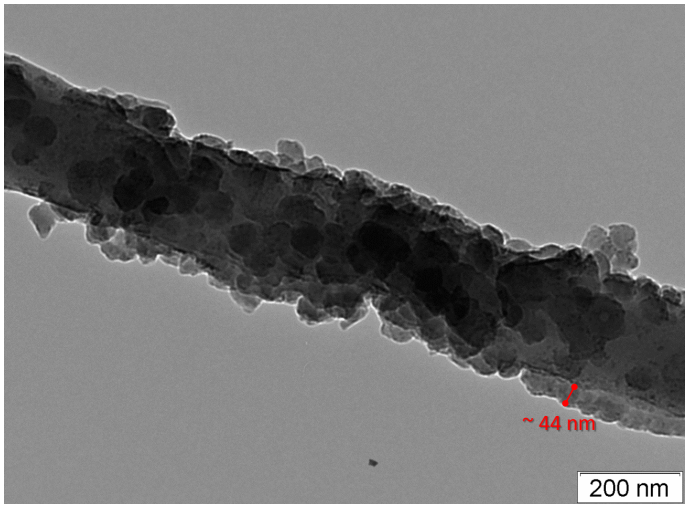

(b)

Figure 4.16: TEM images of CA/PPy composite fibers prepared by in situ chemical oxidation using 0.05 mol.L^{-1} of pyrrole concentration and 30 min of reaction time.

The rise of conductivity upon increasing the temperature is a common response for semiconductor materials, which can be explained by the increase of the mobility of charge

carriers in the composite fibers. The lack of ordering in amorphous conducting polymers is expected to produce localized electronic states. An electron initially in a localized state can be thermally activated, hopping to another localized state where it has higher mobility and then the conduction can occur through variable range hopping of electrons between these localized states [132].

Figure 4.17 shows an Arrhenius-type plot of ln(σ) vs 1/T over a temperature range from 303 to 377 K. The linear dependence may indicate a standard behavior of a semicondutor, where an energy gap separates the conduction band from a valance band, and the carriers can be activated thermally, increasing the conductivity with the increase of temperature. The slope enables the determination of the activation energy for the CA/PPy fibers (E_a = 0.024 eV). In this CA/PPy composite, Arrhenius-type temperature dependence of conductivity is likely that of a thermally activated charge transport within the segment of PPy. As reported by Migahed and co-workers, the activation energy can decrease as the PPy content (see Table 4.6) or the conductivity increases, suggesting the formation of more polarons, which are responsible for electrical conduction in PPy [133]. The formation of the nanosized PPy particles on surface of the CA electrospun fibers and their controlled dispersion on them are expected to contribute to the improvement of the mechanical properties of fibers.

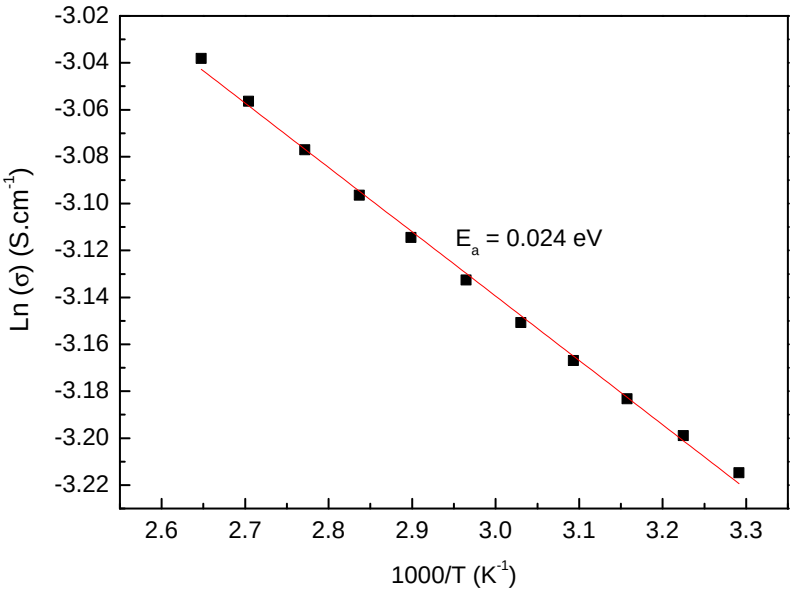

Figure 4.17: Arrhenius plot of ln (σ) vs 1000/T obtained for CA/PPy composite fibers.

Table 4.6: Activation energy for PPy/ethylene-vinylalcohol copolymer composite films as a function of PPy concentration [133].

PPy concentration (wt %)	7.6	8.5	9.3	10.4
$\mathbf{E_a}$	0.610	0.053	0.045	0.033

Tensile tests were conducted to measure the mechanical properties of the composite fibers, such as the Young's modulus, the tensile strength and strain. An example of a typical stress-strain curve obtained for the CA/PPy composite fibers are shown in Figure 4.18.

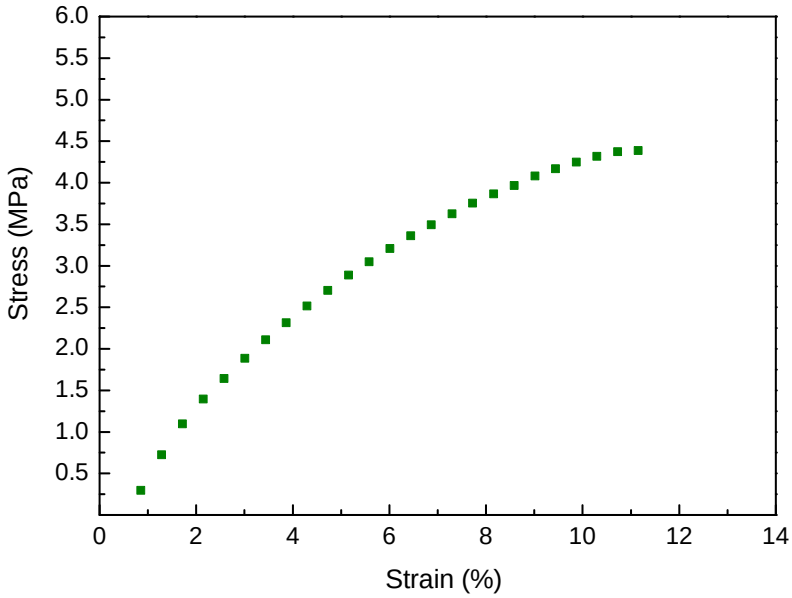

Figure 4.18: Typical stress-strain curve obtained for the CA/PPy composite membrane in uniaxial strain.

The mechanical properties obtained for the composite membrane are presented in Table 4.7 along with the ones found for pristine CA nonwoven membranes, previously discussed in Chapter 3. The slight increase of the Young's modulus together with the increase of the tensile strength of composite fibers can be attributed to a greater fiber entanglement. The nodular morphology caused by the formation of nanosized PPy particles on the surface of fibers in opposition to the smooth and regular surface found for pristine CA fibers can be the most evident cause for such observation.

Finally, testing for toxicity is the first step towards ensuring the biocompatibility of the material to be used in the medical field.

Although some authors have suggested that PPy can generally be regarded as a bio-

Table 4.7: Comparison of the mechanical properties of CA/PPy composite membranes with those obtained of pristine CA nonwoven membranes.

Sample	**Young's modulus (MPa)**	**TS (MPa)**	**Strain (%)**
CA/PPy composite membrane	59.0±12.5	4.5±0.7	12.3±2.3
CA nonwoven membrane	42.1±13.8	3.7±1.0	14.3±5.0

compatible synthetic polymer, it is very important to understand if the processing and morphology of PPy-containing composites affect the toxicity of the material [134], [135]. In standard cytotoxicity test methods (ISO-10993 [128]), cell monolayers are grown to near confluence in flasks and are then exposed to test or control samples directly or indirectly by means of fluid extracts.

In this particular case, the cellular response induced by CA and CA/PPy fibrous membranes was investigated using a cell toxicity indirect test in which cells were exposed to extract solutions of the studied materials. In the indirect test method, extracts are obtained by placing the test and control materials in separate cell culture media under standard conditions. Each fluid extract obtained is then applied to a cultured-cell monolayer, replacing the medium that had nourished the cells to that point. In this way, test cells are supplied with a fresh nutrient medium containing extractables derived from the test samples or control.

An indicator of toxicity is cell viability that can be measured by using Resazurin reduction test. Resazurin, or Alamar Blue, is a redox sensitive dye that is reduced by viable cells. The oxidized form of Alamar Blue is characterized by the nonfluorescent blue color and when reduced by cell activity in the medium turns to a pink fluorescent dye. Thus, the change in fluorescence correlates approximately with the cell proliferation in the sample. Figure 4.19 shows a microscope image of viable cells on well after 24h in CA/PPy composite extract medium. Few round-shaped cells (dead cells) were found on the culture plate in composite sample extract medium.

After 4 h of Resazurin addition, the absorbance was read on the plate reader at 570 and

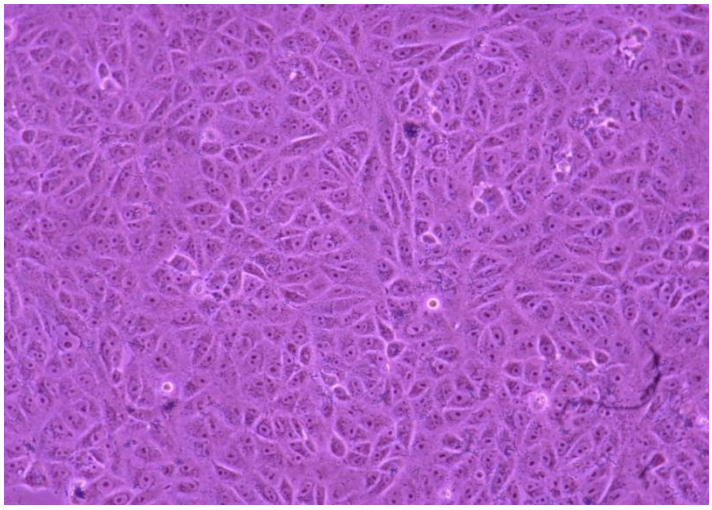

Figure 4.19: Representative light microscopy images of Vero cells on well after 24h in CA/PPy composite extract medium.

600 nm and the results were presented as percentage of cell proliferation of the negative control (cells control). Cell proliferation in CA electrospun membrane was found to be 103% of the negative control and for the PPy-containing composite it was 97%. Both mean values are above the toxicity limits of 70% defined by the ISO standard indicating that the materials tested are free of harmful extractables or have an insufficient quantity of them to cause acute effects under exaggerated conditions with isolated cells.

4.3.3 CA/PANI composite fibers by *in situ* chemical oxidation

Besides studying the development of CA/PPy composite fibers, this work has also considered the preparation of CA/PANI fibers using a similar methodology as the one previously described for PPy. PANI was synthesized onto the surface of CA electrospun fibers template by *in situ* chemical oxidation (Figure 4.20).

The electrical conductivity of polyaniline can change from 10^{-9} (an insulator) to 100 $S.cm^{-1}$ (a conductor) depending of its oxidation state and degree of protonation. Moreover, the electrical conductivity of PANI-based composites is influenced by the type of dopant used. Higher conductivity could be reached by using stronger protonic acids, such as HCl, as dopant agent.

In this study, the synthesis of PANI was investigated considering different synthesis conditions using ammonium persulfate ($(NH_4)_2S_2O_8$) as the oxidant agent with the purpose

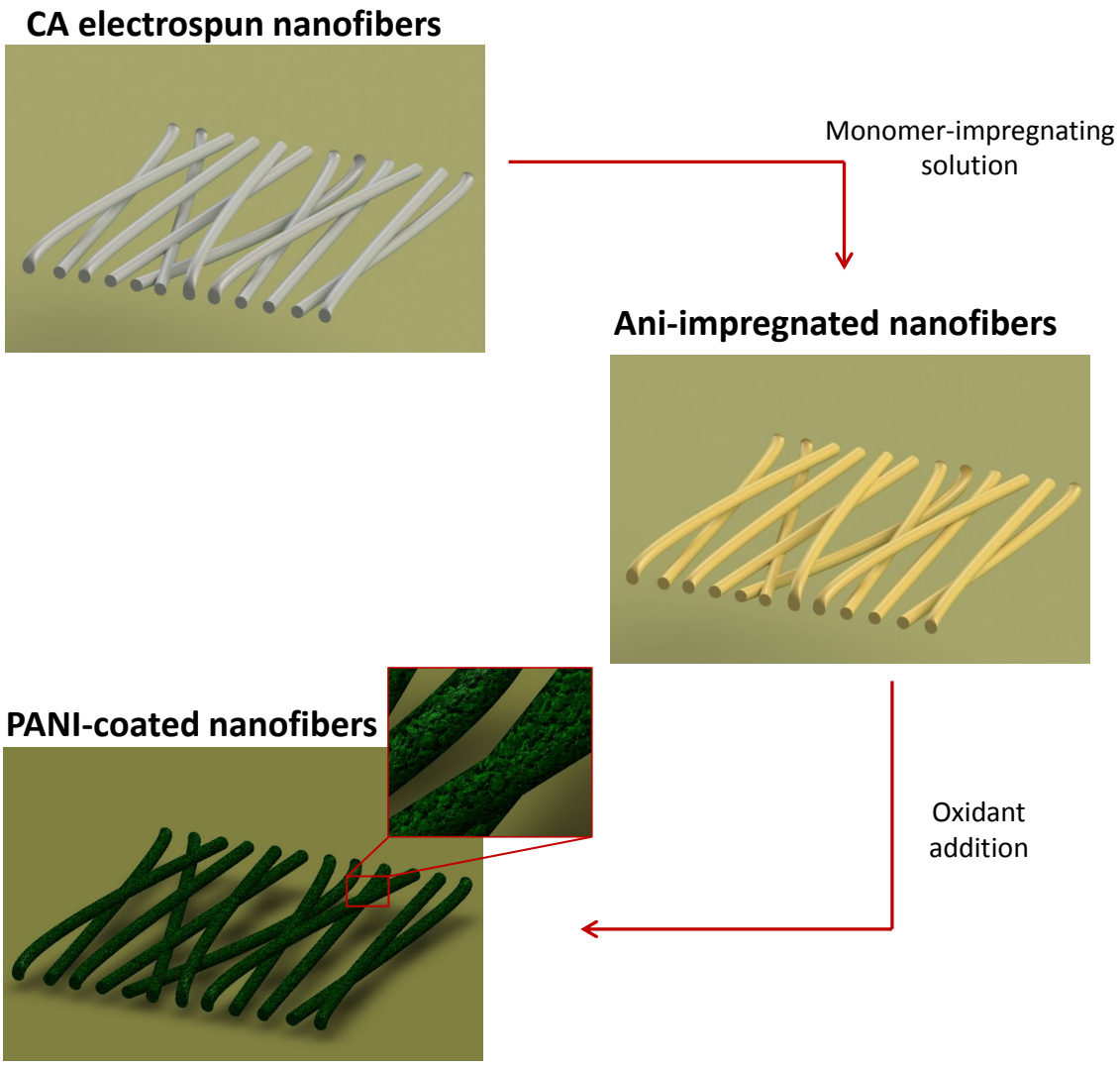

Figure 4.20: Illustration of the fiber template methodology for the preparation of composite fibers of CA and PANI by *in situ* vapor-phase polymerization.

of achieving highly conductive composite fibers.

The CA electrospun membranes with approximately 60 μm of thickness were used to synthesize composite membranes. These were soaked in an aqueous acid aniline-containing solution for 60 min and, after this period, an appropriate amount of ammonium persulfate was added to the medium and the polymerization of aniline took place, preferentially, on fiber's surface forming a continuous conducting coating that fully encapsulates the fibers. Some reports found in literature explain such coating with a probable interaction between the protonated nitrogen of PANI (in acid medium) with the hydroxyl groups of cellulose

through the formation of hydrogen bonds [119]. The final composite membranes showed a typical dark green color, indicating the successful incorporation of PANI layer in the CA network.

The influence of monomer concentration, Oxi/Mon molar ratio and reaction time on the electrical conductivity of CA/PANI composites was also evaluated.

As observed in Figure 4.21, the increase of the polymerization time of aniline leads to an increase of electrical conductivities. The pristine CA electrospun fibers are an insulator with electrical conductivity of $(7.1 \pm 0.8) \times 10^{-11}$ S.cm^{-1}. During aniline polymerization, PANI nanoparticles gradually grow into a continuous nanosheath on the CA template fibers and an increase in the conductivity is obtained. Higher conductivities are mainly displayed for PANI-based composites synthesized with greater amounts of oxidant agent when considering a monomer concentration of 4M (Ox/Mon molar ratio of 0.25 and 0.5).

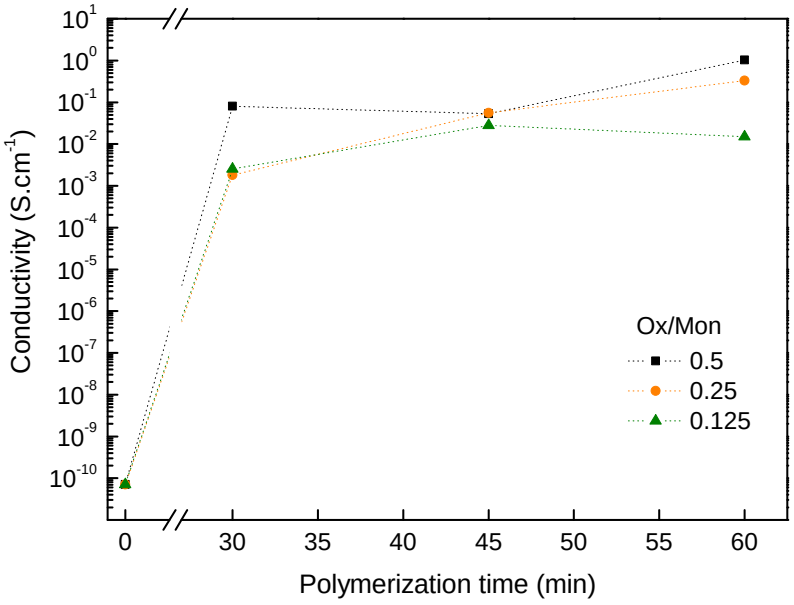

Figure 4.21: Influence of polymerization time on the electrical conductivity of CA/PANI composite fibers using an aniline concentration of 4mol.L^{-1} and Ox/Mon molar ratios of 0.125, 0.25 and 0.5, respectively. Electrical conductivity values are presented in Appendix B, Table B.3.

Regarding the morphologies obtained for an Ox/Mon molar ratio of 0.5 along the reaction time, the SEM images have confirmed the presence of a non-uniform PANI coating for 30 min (Figure 4.22 (a)) and an increase of PANI aggregates onto the fiber's surface with the

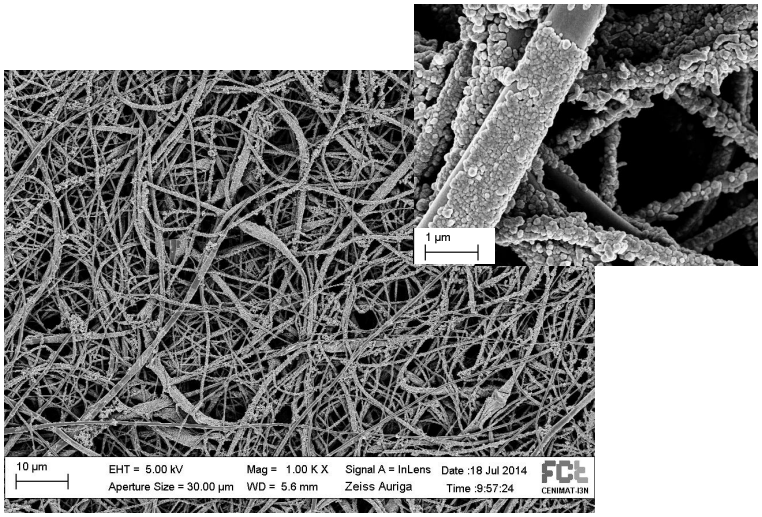

(a)

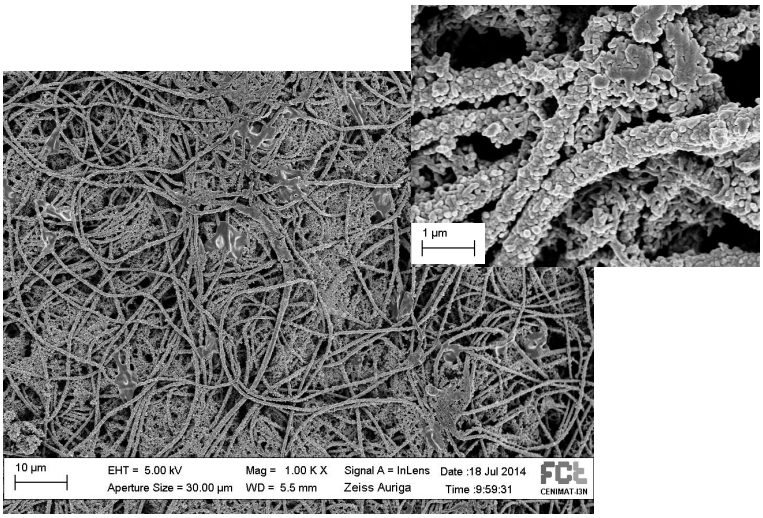

(b)

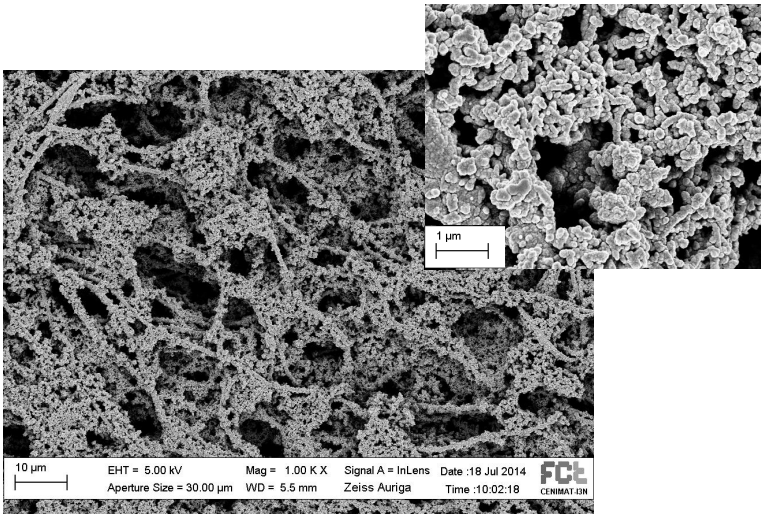

(c)

Figure 4.22: SEM images of CA/PANI composite fibers obtained after (a) 30 min, (b) 45 min and (c) 60 min of polymerization. A monomer concentration of 4 mol.L^{-1} and an Ox/Mon molar ratio of 0.5 have been considered for all synthesis.

increase of polymerization time from 45 (Figure 4.22 (b)) to 60 min (Figure 4.22 (c)). It is clearly observed that the original fibrous structure of CA membrane is not preserved for longer polymerization periods due to the tendency of PANI particle aggregation. Thus, longer polymerization time leads to a decrease of conductivity values.

As observed, the agglomeration of PANI particles was formed on the surface of CA fibers and thus it was necessary to study the influence of lower monomer concentration. A decrease on conductivity values is observed in Figure 4.23. This reveals that for the Ox/Mon ratio of 0.25, the amount of monomer used is not enough to have fibers completly covered by PANI even for prolonged polymerization time. Considering an Ox/Mon ratio of 0.5, the produced composites showed electrical conductivity values of 10^{-1} S.cm^{-1} for reaction times of 45 and 60 min.

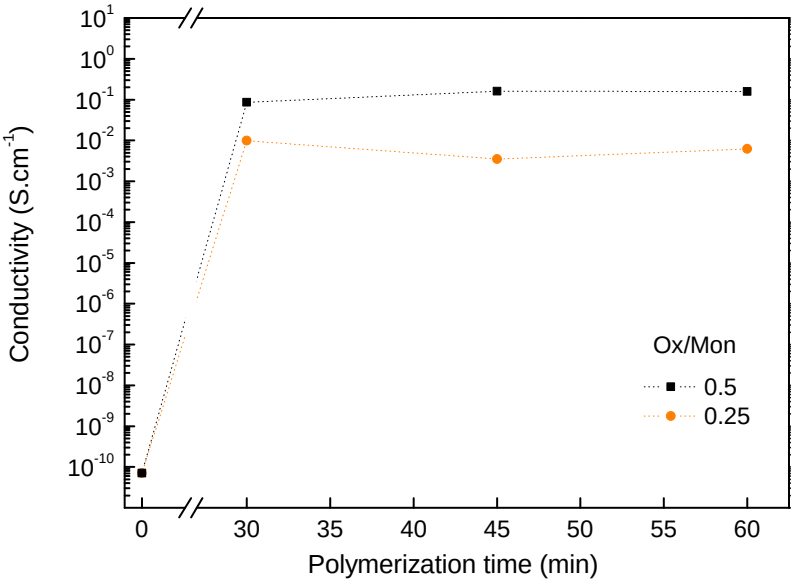

Figure 4.23: Influence of polymerization time on the electrical conductivity of CA/PANI composite fibers using an aniline concentration of 2 mol.L^{-1} and Ox/Mon molar ratios of 0.25 and 0.5, respectively. Electrical conductivity values are presented in Appendix B, Table B.3.

The SEM image of CA/PANI composite fibers obtained for both polymerization times are shown in Figure 4.24. As anticipated, less agglomeration of PANI particles can be observed on the surface of CA fibers for both polymerization periods.

The average diameter of CA/PANI composite fibers was also estimated with the increase of monomer concentration and reaction time as shown in Figure 4.25. The average diam-

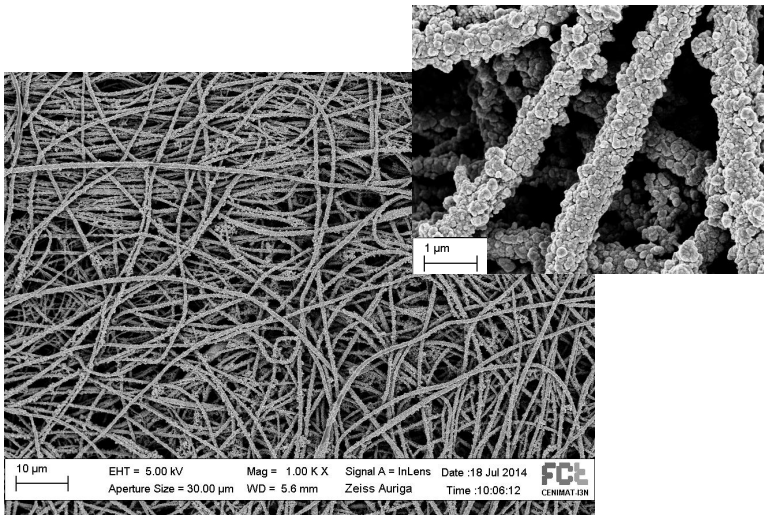

(a)

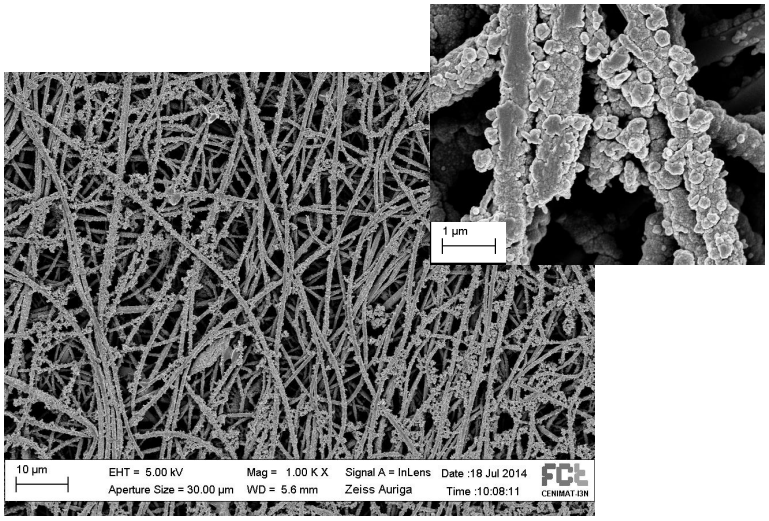

(b)

Figure 4.24: SEM images of CA/PANI composite fibers obtained after (a) 45 min and (b) 60 min of polymerization. A monomer concentration of 2 mol.L^{-1} and an Ox/Mon molar ratio of 0.5 have been considered for all synthesis.

eter of pristine CA electrospun fibers is 243 ± 58 nm, but it gradually increases with the formation of PANI particles on their surface. A direct correlation between fiber diameter and polymerization time it is, thus, obtained. For the monomer concentration, such correlation is not evident. However, for longer polymerization periods, it is observed a greater increase of fibers diameter related to the increase of PANI particles agglomeration on the surface of CA fibers.

Overall, the suitable conditions to obtain a continuous and uniform PANI coating on CA fibers and high electrical conductivity are: 2 mol.L^{-1} of Aniline, an Ox/Mon ratio of 0.5

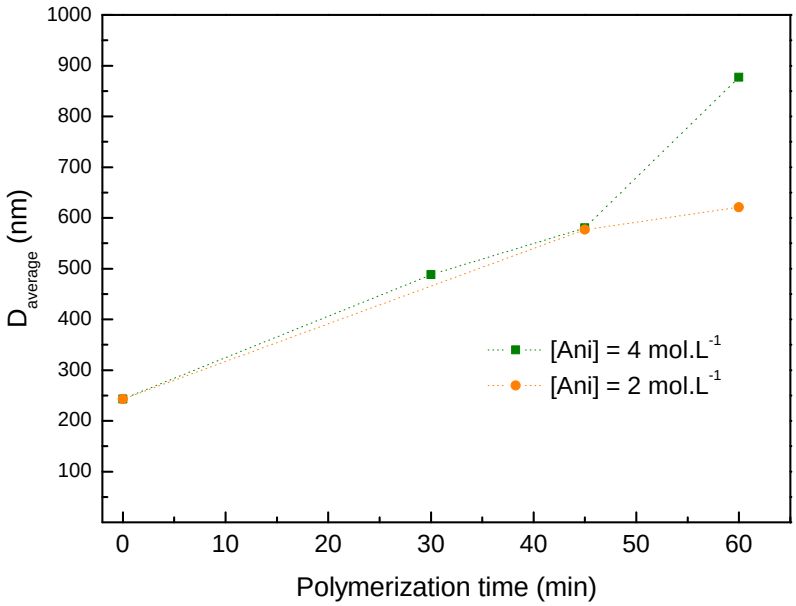

Figure 4.25: Influence of monomer concentration and time reaction on the diameter of the CA/PANI fibers prepared by *in situ* chemical oxidation.

and a reaction time of 45 min. Using these polymerization conditions, CA/PANI composite fibers with diameters of 577 ± 59 nm were obtained suggesting the formation of a PANI layer of 334 nm, approximately – Figure 4.26.

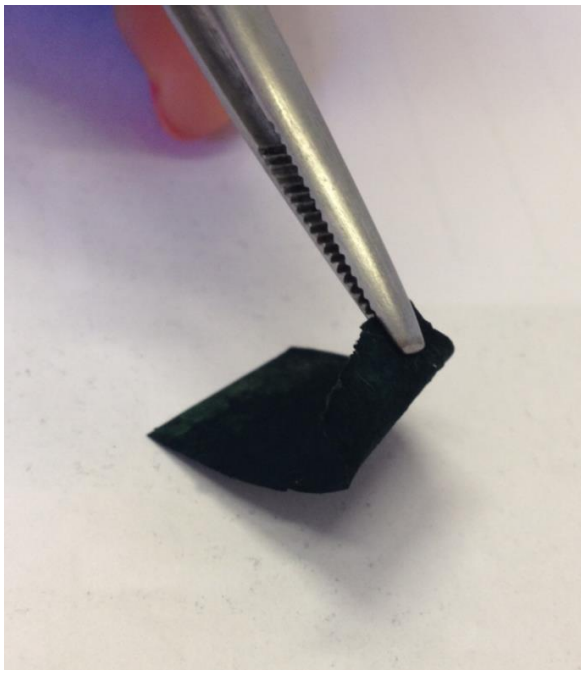

Figure 4.26: Photograph of CA/PANI composite membrane prepared by *in situ* chemical oxidation.

To investigate the mechanical characteristics of CA/PANI composite fibers, tensile tests were performed. An example of a typical stress-strain curve obtained for the CA/PANI composite fibers is shown in Figure 4.27. The values of Young's modulus, tensile strength and strain were determined and are presented in Table 4.8 along with the ones found for pristine CA nonwoven membranes and CA/PPy composite fibers, previously discussed in section 4.3.2.

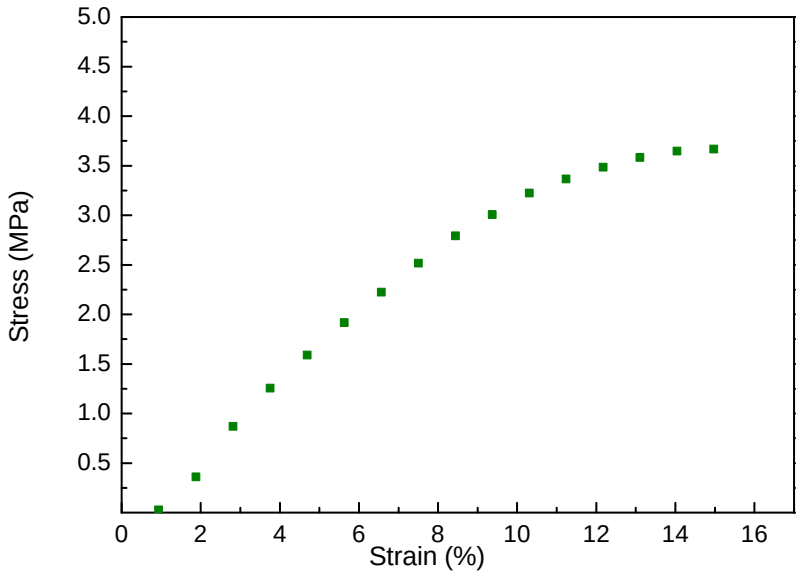

Figure 4.27: Typical stress-strain curve obtained for the CA/PANI composite membrane CA/PANI composite membrane in uniaxial strain.

Table 4.8: Comparison of the mechanical properties of CA/PPy composite membranes with those obtained from pristine CA nonwoven membranes.

Sample	**Young's modulus (MPa)**	**TS (MPa)**	**Strain (%)**
CA/PANI composite membrane	33.5±6.9	3.2±0.9	13.1±3.0
CA/PPy composite membrane	59.0±12.5	4.5±0.7	12.3±2.3
CA nonwoven membrane	42.1±13.8	3.7±1.0	14.3±5.0

The values of Young's modulus and tensile strength determined for CA/PANI nonwoven membrane are lower than those observed either for CA/PPy composite fibers or CA fibers. This decrease might be explained with the weakening of the CA structure associated with the acidic synthesis route of PANI.

4.3.4 Bio-battery electrochemical characterization

To evaluate the composite materials described above as an electrode material for energy harvesting, CA/PPy and CA/PANI were assembled in the construction of a bio-battery. Additionally, a conductive textile made of Au fibers, with a thickness of 100 μm, was also used as electrode for bio-battery testing. Three bio-batteries were evaluated using different combinations of electrodes separated by a CA membrane:

1. PPy composite | CA membrane | PANI composite
2. PPy composite | CA membrane | Au mesh
3. PANI composite | CA membrane | Au mesh

Gold plays an important role in medical implants due to its biocompatibility and high level of resistance to bacterial colonization making it the material of choice for implants where there is a high risk of infection. Gold implants are used in various medical procedures, including reconstructive surgery of the middle ear and drug delivery microchips, among others [136]. Such advantages led to the use of a commercial Au mesh for bio-batteries testing. Two carbon meshes were also used as current collectors.

The electrochemical behavior of the bio-batteries structures was recorded by cyclic voltammograms using a scan rate of 80 $mV.s^{-1}$ during 10 consecutive cycles (Figures 4.28, 4.29 and 4.30). The voltammograms of both PPy and PANI composites showed reversible oxidation and reduction peaks due to Faradaic process occurring during the anodic and cathodic scans.

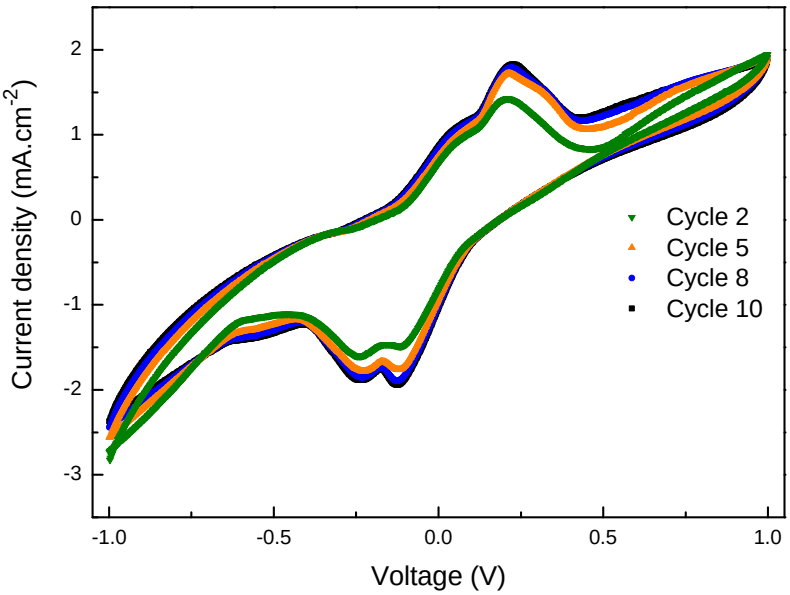

Figure 4.28: Cyclic voltammograms obtained for the PPy/CA/PANI structure during 10 consecutive cycles in the presence of NaCl solution. The structure has a thickness of 240 ± 64 μm and the measurement was carried out at a voltage scan rate of 80 mV.s^{-1}.

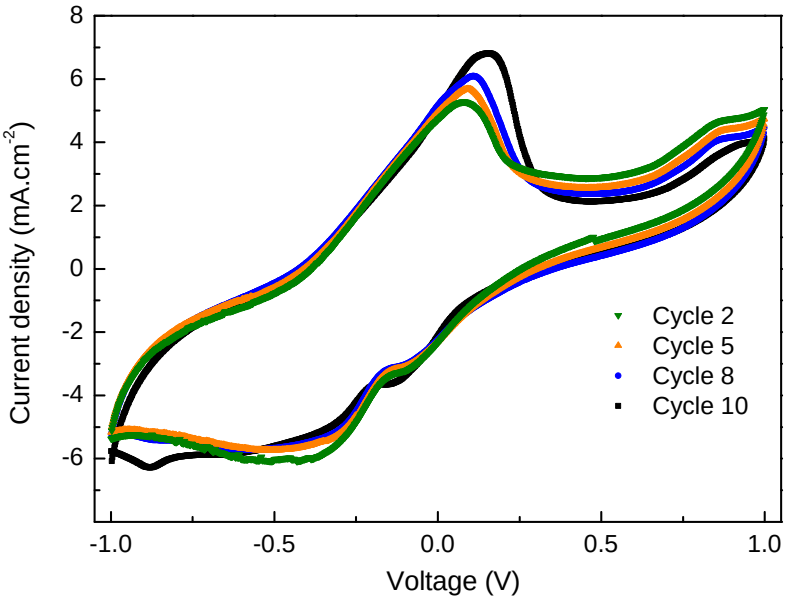

Figure 4.29: Cyclic voltammograms obtained for PPy/CA/Au mesh structure during 10 consecutive cycles in the presence of NaCl solution. The structure has a thickness of 280 ± 33 μm and the measurement was carried out at a voltage scan rate of 80 mV.s^{-1}

In the context of a metal-air battery, the cathode reactions are mainly due to oxygen reduction. Molecular oxygen (from the electrolyte) can be absorbed by the carbon atoms of the PPy chain forming an "oxygen-conductive polymer" complex. It can be subsequently reduced to release oxygen intermediates, which eventually form hydroxyl groups [137]. The cathode reactions for the PPy/CA/ PANI and PPy/CA/ Au mesh battery

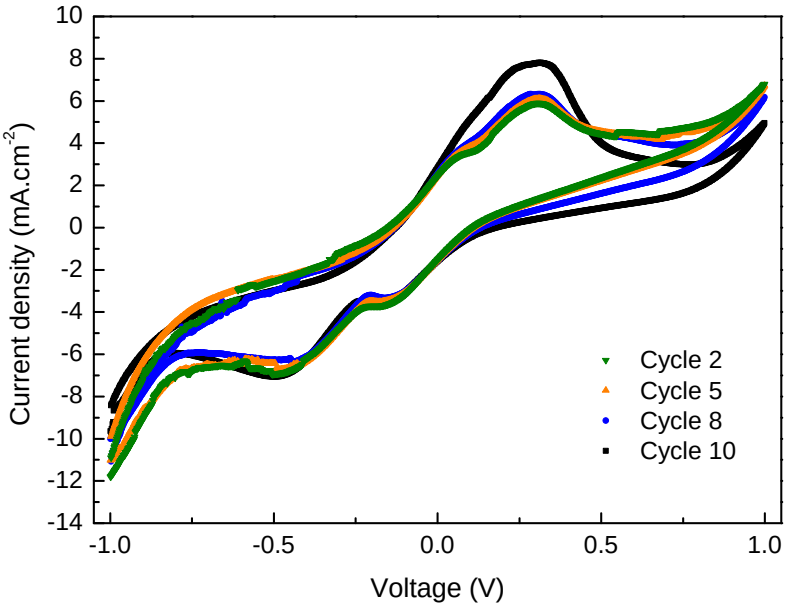

Figure 4.30: Cyclic voltammograms obtained for PANI/CA/Au mesh bio-battery structure during 10 consecutive cycles in the presence of NaCl solution. The structure has a thickness of 287 ± 21 μm and the measurement was carried out at a voltage scan rate of 80 mV.s^{-1}.

structures can be described by the following electrochemical equations:

$$PPy^{+} + e^{-} \rightleftharpoons PPy^{0} \tag{4.3}$$

$$O_2 + 4e^{-} + 2H_2O \rightarrow 4OH^{-} \tag{4.4}$$

Similarly, for the PANI/CA/Au structure the cathode reaction should be:

$$PANI^{+} + e^{-} \rightleftharpoons PANI^{0} \tag{4.5}$$

$$O_2 + 4e^{-} + 2H_2O \rightarrow 4OH^{-} \tag{4.6}$$

The electrochemical equations expected to occur in the anode are mainly associated with the oxidation of the conductive polymer (PPy or PANI) and could be as follow:

$$PPy^{0} \rightarrow PPy^{+} + e^{-} \tag{4.7}$$

$$PPy^{+} \rightarrow PPy^{2+} + e^{-} \tag{4.8}$$

for the PPy/CA/Au mesh biobattery structure or

$$PANI^0 \rightarrow PANI^+ + e^- \tag{4.9}$$

$$PANI^+ \rightarrow PANI^{2+} + e^- \tag{4.10}$$

for PPy/CA/PANI and PANI/CA/Au mesh structures.

From the I-V curves obtained from cyclic voltammetry, the maximum power density – P_{max} – of the bio-batteries was determined. The obtained values are shown in Table 4.9.

Table 4.9: Power values and main characteristics of bio-batteries evaluated.

Structure	**Area (cm^2)**	**Volume (cm^3)**	**Mass (g)**	**Voc (mV)**	P_{max} **($\mu W.cm^{-2}$)**	P_{max} **($\mu W.g^{-1}$)**
PPy/CA/PANI	0.25	0.006	0.0029	-2.1	20[a]	1724
PPy/CA/Au	0.25	0.007	0.014	64.2	450[b]	8036
PANI/CA/Au	0.25	0.007	0.014	56.1	80[c]	1429

[a] Determined from J = 357 $\mu A.cm^{-2}$, V = 56 mV.
[b] Determined from J = 2345 $\mu A.cm^{-2}$, V = 191 mV.
[c] Determined from J = 1174 $\mu A.cm^{-2}$, V = 68 mV.

The fully polymeric bio-battery showed a maximum power density of 1.7 $mW.g^{-1}$ which is a promising power value since a typical pacemaker requires less than 10 μW to operate. Besides being flexible, lightweight and ultra-thin (< 300 μm of thickness), this bio-battery has the advantage to have an economic production process making it a likely alternative to the current power sources used in implantable medical devices. In particular, the PPy/CA/Au mesh structure has showed a higher power density value which could be explained by the greater potential difference between the materials.

4.4 Summary

In this chapter, cellulose acetate electrospun membranes were evaluated as a polymer platform to produce fibrous conducting composites with high surface area. To produce cellulose-based composite fibers, the *in situ* polymerization of Py and Ani on the surface of CA electrospun fibers was investigated.

Composites of CA/PPy were prepared by *in situ* vapor-phase polymerization of pyrrole. Since pyrrole monomer has relatively high vapor pressure, the polymerization of pyrrole on the oxidant-impregnated CA membrane is initiated by exposing the fibers directly to pyrrole vapor. As expected, the electrical conductivity of the nanofibers was remarkably improved from 7.08×10^{-11} to 5.11×10^{-3} S.cm^{-1} with the formation of PPy on the fibers' surface. However, brittle composite fibers were obtained using this methodology.

As an alternative, CA/PPy composite fibers were prepared through the *in situ* pyrrole oxidative polymerization by using $FeCl_3$ as oxidant. During this study, the effects of chemical synthesis conditions, such as monomer concentration, the mass ratio oxidant/monomer and reaction time were investigated in detail. Considering both electrical and morphological analysis, uniform PPy-coated CA fibers with high electrical conductivity, 8.19×10^{-2} S.cm^{-1}, were prepared using the following synthesis conditions: 0.05 mol.L^{-1} of Py, an Ox/Mon ratio of 2 and a reaction time of 30 min. Further analysis has indicated composite fibers with an average diameter of 290 $\pm$ 69 nm and the PPy nanocoating was estimated to be, approximately, 40 nm.

Temperature dependence of conductivity was observed for CA/PPy fibers which is typical of a thermally activated charge transport and the activation energy was determined to be about 0.024 eV.

The mechanical properties of CA/PPy composite fibers were also investigated. A slight increase of the Young's modulus together with tensile strength of composite fibers was observed when comparing with those of a pristine CA nonwoven membrane. This enhancement may be attributed to the nodular morphology caused by the formation of nanosized PPy particles on the surface of fibers.

Finally, toxicity tests were performed for CA pristine membranes and CA/PPy composite fibers. The cell proliferation in CA electrospun membrane was found to be 103% of the negative control and for the PPy-containing composite it was 97%. Both mean values are above the toxicity limits of 70% defined by the ISO standard indicating that the materials tested are free of harmful extractables or have an insufficient quantity of them to cause acute effects under exaggerated conditions with isolated cells.

The preparation of CA/PANI fibers using a similar methodology as the one considered for the preparation of CA/PPy composites was also investigated. PANI was synthesized onto the surface of CA electrospun fibers template by *in situ* chemical oxidation. The suitable synthesis conditions to achieve a continuous and uniform PANI coating on CA fibers with an electrical conductivity of 1.60×10^{-1} S.cm^{-1} were: 2 mol.L^{-1} of Aniline, an Ox/Mon ratio of 0.5 and a time reaction of 45 min. Using these polymerization conditions, CA/PANI composite fibers with diameters of 577 $\pm$ 59 nm were obtained suggesting the formation of a PANI layer of 334 nm, approximately.

The electrochemical performance of cellulose-based bio-batteries was characterized by cyclic voltammetry. The composite materials, CA/PPy and CA/PANI, were used as electrodes (cathode and anode respectively) for the construction of the bio-battery. Such fully polymeric bio-battery showed a maximum power density of 1.7 mW.g^{-1}, which is a promising power value since a typical pacemaker requires less than 10 μW to operate. Additional structures were also evaluated using polymer composite materials as the anode and an Au-based mesh as the cathode. Power densities of 8.0 mW.g^{-1} and 1.4 mW.g^{-1} were obtained for PPy/CA/Au mesh and PANI/CA/Au mesh structures, respectively.

In conclusion, conductive CA/PPy and CA/PANI composite fibers have been successfully obtained with the advantage of preserving the main properties of electrospun membranes, such as the flexibility, porosity and large surface area, making them interesting electrodes for the bio-batteries proposed. The biocompatibility of PPy and PANI-based materials is well reported in literature [120], [121] being a fundamental requirement for biomedical applications. A fully polymeric bio-battery was constructed showing a promising power density under physiological conditions. Such objective was positively accomplished and validated demonstrating innovative and promising results for the supplying of low-power consumption medical devices.

The next chapter explores additional functionalities of electrospun membranes. Photoluminescent electrospun membranes were investigated as innovative functional materials which can enlarge the field of potential applications for the bio-batteries.

Chapter 5

Exploring functional electrospun fibers for other applications

This chapter explores additional functionalization of electrospun fibers. The investigation of functional electrospun fibers has enabled the development of innovative photoluminescent electrospun fibers in optoelectronic devices and phototherapy. These accomplishments can enlarge the field of applications of bio-batteries.

5.1 Background

The demand for 1D nanostructures with suitable optoelectronic properties to applications such as sub-wavelength light generation, detection or guiding [138] has grown considerably in the recent years. The most common technologies to produce them are template-based methods, scanning probe lithography, self-assembly and electrospinning. For organic optoelectronics, the electrospinning provides a valuable compromise concerning throughput and the control of size and shape that can be tuned by proper control of electrostatic forces.

Recently, photoluminescence in electrospun fibers has been studied by our research team [139]. Poly[(9,9-dioctylfluorenyl-2,7-diyl)-co-bithiophene] (F8T2) fibers were successfully produced by electrospinning without a carrier polymer. The obtained fibers showed a high photosensitivity and photoluminescence, in the cyan, yellow, and red if excited with

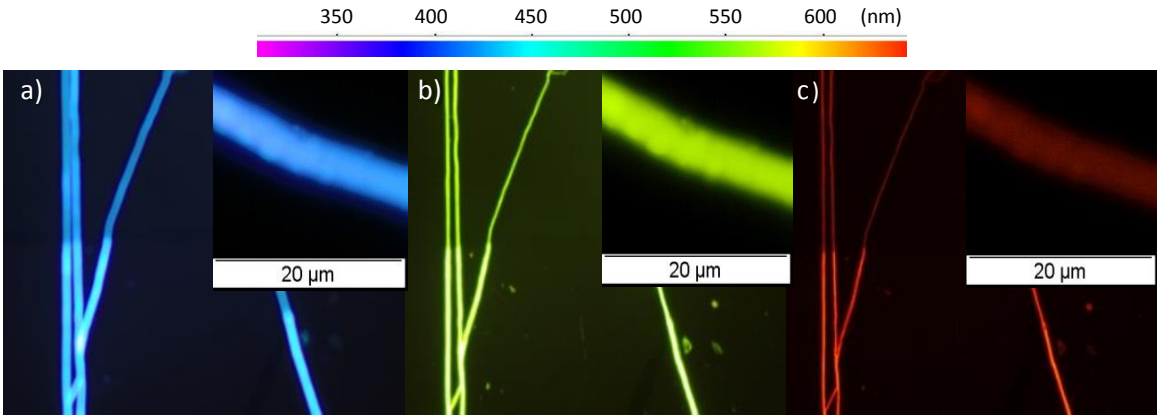

Figure 5.1: Optical microscopy fluorescence images of F8T2 fibers excited with: (a) UV; (b) blue; and (c) green light. The inset is the magnification of the fiber in the respective image.

UV, blue, and green wavelengths, respectively (Figure 5.1).

5.1.1 Electrospun composites incorporating inorganic nanoparticles

Fluorescence is conventionally applied to fibers using fluorescent dyes and coatings. These dyes have the potential to leak in certain environments, and to lose their strength during exposure to certain wavelengths of light. Therefore, it is recommended to use a more contained method if longer-term fluorescence is desired.

Embedding semiconducting nanoparticles into polymer matrices allow the combination of the diversity and processability of organic materials with the high electronic and optical performances of inorganic crystals.

Recently, the intrinsic photoluminescence (PL) of metallic nanoparticles has received considerable attention. Noble metal nanostructures such as silver and gold have attracted attention because of their superior electrical, optical, mechanical, and catalytic properties. At nanometer dimensions electrons can oscillate on the particle's surface and absorb electromagnetic radiation at a particular energy [140]. This resonance known as surface plasmon resonance or plasmon absorbance of nanoparticles is a consequence of their small size but it can be influenced by numerous factors, such as solvent and surface functionalization. The size and shape of metal nanoparticles determine the spectral position of

plasmon band absorption as well as its width. Nanosize gold and silver particles show size dependent optical properties [141].

Photoluminescence has been reported in electrospun fibers embedding active components (NPs or molecular species). Camposeo [142] describes the PL studies of poly(methyl methacrylate) (PMMA) electrospun fibers incorporated with chromophores such as Coumarin 334, Rhodamine 6G (R6G) and Nile Blue A perchlorate. Composite fibers of poly(acrylic acid) (PAA) with CdSe/ZnS nanoparticles were successfully electrospun and optically characterized by Atchison and her colleagues [143]. Up conversion photoluminescence was observed in PMMA nanofibers containing lanthanide-doped NPs [144], and down conversion photoluminescence in CdSe/CdS/ZnS quantum dots-embedded poly(9-vinylcarbazole) (PVK) [145].

However, photoluminescence studies of electrospun nanofibers incorporating metallic nanoparticles are still lacking in literature. For that reason, Au and Ag nanoparticles have been considered in this work to develop luminescent electrospun fibers.

5.1.2 Applications in regenerative medicine

Luminescent electrospun membranes can be attractive for organic optoelectronic applications, fluorescent clothing or security labels (as counterfeiting labels). Still, their use in regenerative medicine can be foreseen as innovative and promising.

The ultimate aim of regenerative medicine is to provide safe and efficient therapies for a large number of clinical conditions. The idea that light may be used in medicine is not new, however, since it has been recognized as a potential source of healing. The use of laser (Light Amplification by the Stimulated Emission of Radiation) as a non-surgical medical treatment modality for assisting the normal processes of healing has increased over the last few years. Therapeutic lasers use monochromatic light in the 630 to 905 nm range, and are athermic with no appreciable heat transfer so the photonic energy is transferred directly to the target cells avoiding thermal damage [146]. Phototherapy induces the increase of Ca^{2+} concentration in the cell cytoplasm by a couple of molecular biological reactions, which results in an increase in cell proliferation.

Since human skin is the outer covering of the body and it is under frequent exposure to sunlight, which spectrum lies in the visible short-wave region of the electromagnetic spectrum, the use of photosensitive materials on tissue repairs can be a valuable approach. Recently, Dr. Seeram Ramakrishna's research group has focused on the application of photosensitive materials, such as Poly(3-hexylthiophene-2,5-diyl) (P3HT), in skin regeneration. Jin and his co-workers [147] have reported the development of a functional photosensitive P3HT-containing PCL electrospun scaffold remarking a good fibroblast proliferation after light stimulation. They suggested that when P3HT absorbs light (sunlight) photo-induced current is further generated in the fibers, while the electromagnetic field is created. When cells are stimulated by the electromagnetic field, Ca^{2+} ions translocate through the cell membrane voltage-gated calcium channel and this leads to an increase in cytosolic Ca^{2+}. The cytosolic Ca^{2+} can complex with Calmodulin, a low molecular weight protein, which then activates several key intracellular processes leading to cell division. Activated calmodulin is known to promote nucleotide synthesis and cellular proliferation. However, the optimal amount of P3HT incorporated in PCL scaffold is still being investigated in order to be non-toxic to the cells and support the proliferation of cells after light stimulation.

The previous work has demonstrated the potential use of photosensitive electrospun membranes on photocurrent therapy for skin tissue engineering, which introduced an unexplored field of investigation.

5.2 Methodology

5.2.1 Electrospun CA/Au NPs membranes

For the preparation of the CA/Au NPs composite, the CA membrane was produced by electrospinning as described in the Methodology section from Chapter 3.

The electrospun membrane ($\approx$ 0.02 mg) was firstly sonicated in water (5 ml) for 20 min using an ice bath to overcome possible water heating. Then, 0.5 ml of poly(ethyleneimine) (PEI - 1 $g.L^{-1}$) purchased from Sigma-Aldrich was added to the aqueous solution contain-

ing the CA membrane. After stirring for 30 min at room temperature, 0.25 ml of $HAuCl_4$ (20 mM) (purchased from Sigma-Aldrich) was added. Then, the suspension was kept at 60°C, under static conditions, for 1 h, leading to the formation of CA/Au NPs composite characterized by its dark purple color. The fibers were washed by centrifugation with distilled water until the supernatant became colorless.

The fluorescence of the composite fibers was characterized by optical microscopy using an Olympus BX51 microscope with X-Cite series 120Q fluorescence excitation of ultraviolet, blue and green light. Morphological characterization was carried out by SEM.

5.2.2 Electrospun PVP/Ag NPs membranes

The silver nanoparticles were prepared by *in situ* chemical reduction of silver nitrate ($AgNO_3$) [148]. 1 g of polyvinylpyrrolidone (PVP) (MW 10,000, supplied by Sigma-Aldrich) was dissolved in 20 ml of ethanol followed by the addition of 50 mg of $AgNO_3$ ((purchased from Riedel-de Han) under continuous stirring. The yellow color of the colloidal solution indicated the presence of Ag NPs.

The stability of nanoparticles suspensions was assessed by Ultra-Violet/Visible (UV/Visible) spectrophotometry (T90+ from PG Instruments) and they were characterized by TEM (model H-8100 II from Hitachi).

An 18% (w/v) solution of PVP (MW 1,300,000, from Sigma-Aldrich) was prepared by dissolving the polymer directly in the Ag NPs colloidal solution. Then, the prepared solution was loaded into a syringe with a nozzle with an internal diameter of 23G (0.41 mm). A high-voltage supply was used to generate an electric field of 15 kV between the nozzle and an aluminum foil used as a collector, kept at 15 cm of distance. The process was performed at a relative humidity of 70% and a temperature of 20°C.

PVP/Ag NPs electrospun membranes were characterized either by TEM and SEM. The fiber diameters were obtained from SEM images using the ImageJTM software.

Electrical characterization was carried out at room temperature as described in the Methodology section of Chapter 4. Fluorescence micrographs were obtained using an

Olympus BX51 microscope with X-Cite series 120Q fluorescence excitation of ultraviolet, blue and green light. The photoluminescence (PL) was measured at room temperature in the visible region using a Spex 1704 monochromator fitted with a cooled Hamamatsu R928 photomultiplier. The excitation sources used were Kimmon HeCd laser operating at 325 nm and Laser Quantum Ventus working at 532 nm, with a power of 25mW and 125mW, respectively.

The antibacterial activity of the membranes prepared was studied by Agar diffusion method against Gram-negative bacteria *Escherichia coli K-12* and Gram-positive bacteria *Bacillus subtilis 168*. Media-culture plates containing *E. coli* or *B. subtilis* were prepared using the Kirby Bauer technique [149]. *E. coli* and *B. subtilis* bacteria have grown overnight (37°C, with aeration) in liquid Luria-Bertani (LB) medium [150]. The resulting culture was diluted to 10^{-1} of the initial optical density and plated on LB medium solidified with 1.6% (w/v) Agar (LabM); the membranes were placed on top of it. Before placing the membranes on the Agar plates the samples were irradiated with UV light for 2 h (at 40 W), to crosslink PVP and avoid contaminations. Inhibition halos were measured after 24 h of incubation at 37°Cand are an indication for the antibacterial activity. All tests were repeated in triplicate.

Cytotoxic assays were carried out as described in Methodology section of Chapter 4.

5.3 Results and discussion

In this section is discussed and presented the main achievements regarding the development of functional fibers with enhanced luminescence envisaging novel applications in optoelectronics and medicine.

5.3.1 Development of luminescent CA/Au NPs electrospun membranes

The development of electrospun nanofibers incorporating metallic nanoparticles with luminescence and electrical conductivity has been considered during the first part of this

thesis. Electrospun nanofibers can easily incorporate functional molecules by using the electrospun membrane as a template for NPs attachment; or by direct electrospinning of a blended NPs-polymer colloidal solution.

The template-based method usually requires surface treatment of the electrospun fibers to prepare NPs electrospun composites. It consists in immersing the surface-treated electrospun fibers into the colloidal solution, through which the prepared NPs could be adsorbed on the surface of the fibers by electrostatic force, hydrogen bonding or by interactions among functional groups.

The first attempt has considered the attachment of Au NPs onto the surface of the electrospun CA membrane. The Au NPs synthesis was carried out by controlled reduction of an aqueous $HAuCl_4$ solution using PEI as a reducing agent and a linking molecule.

PEI is an amine-rich cationic polyelectrolyte that acted both as a linker between metal ions and cellulose and as the reducing agent for *in situ* reduction of $HAuCl_4$ to Au NPs. In order to evaluate the luminescence, the composite produced was observed in an optical microscope under different light excitation, which is shown in Figure 5.2: (a) white, (b) UV, (c) blue, and (d) green.

The luminescence of singular fibers in the CA/Au NPs composite indicated that the amount of Au NPs attached to the surface of the CA electrospun membrane was too low to form a uniform coating. This explanation is also supported by the SEM image (Figure 5.3) where the attachment of NPs to the surface of the fibers was observed but did not seem to be uniform. As a consequence, no electrical conductivity was observed. Alternative methods such as layer-by-layer deposition and electrochemical deposition was also evaluated during this work. However, in both cases, uniform distribution of Au NPs throughout the fibers was not obtained.

The electrospinning of blended NPs-polymer solution was studied but it was required the use of a suitable solvent in which the NPs can be uniformly dispersed and a polymer that can be dissolved in the same solvent. One of the major limitations of Au NPs synthesis methods used is the restriction of using aqueous solvents, which difficults the dispersion of the NPs in the cellulose acetate solution.

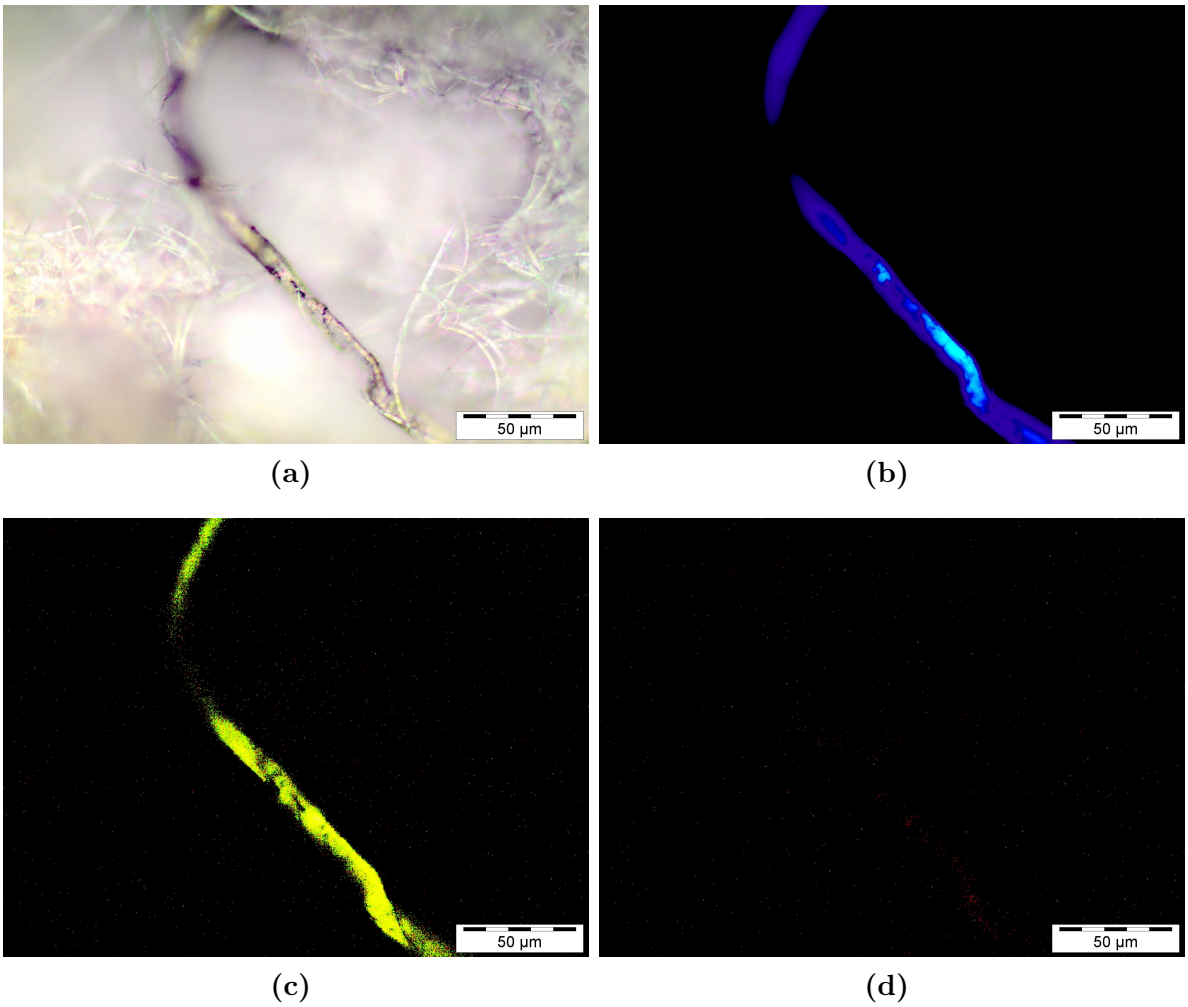

Figure 5.2: Optical microscopic images of CA/Au NPs composites under different light excitation: (a) white, (b) UV, (c) blue, and (d) green.

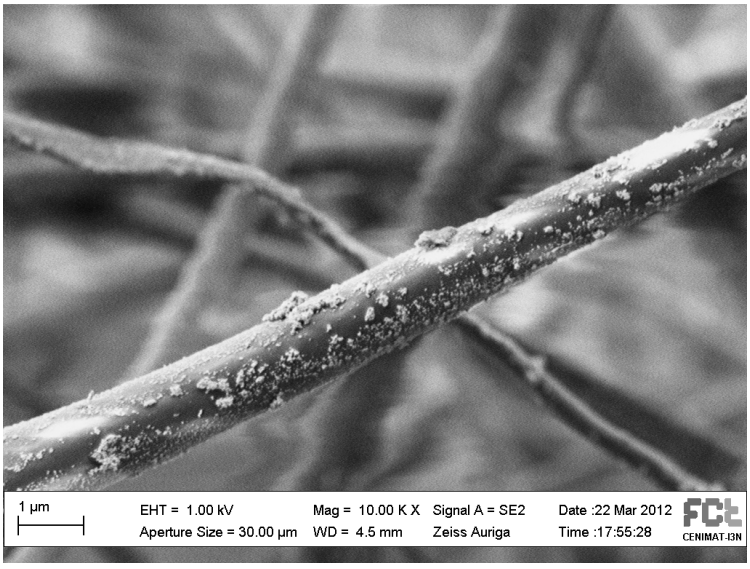

Figure 5.3: SEM image of CA/Au NPs composites.

5.3.2 Development of luminescent PVP/Ag NPs electrospun membranes

The development of a composite of electrospun PVP fibers incorporating Ag NPs has been explored by blend electrospinning. Primarily, the Ag NPs colloidal solution has been prepared by *in situ* chemical reduction of $AgNO_3$ using a solution of PVP in ethanol as a reducer and stabilizer agent at room temperature. The TEM image of the colloidal solution presented in Figure 5.4 (a) shows that Ag NPs are well dispersed having a spherical shape with an average diameter of 3.4 ± 1.2 nm (see diameter distribution in Figure 5.4 (b)).

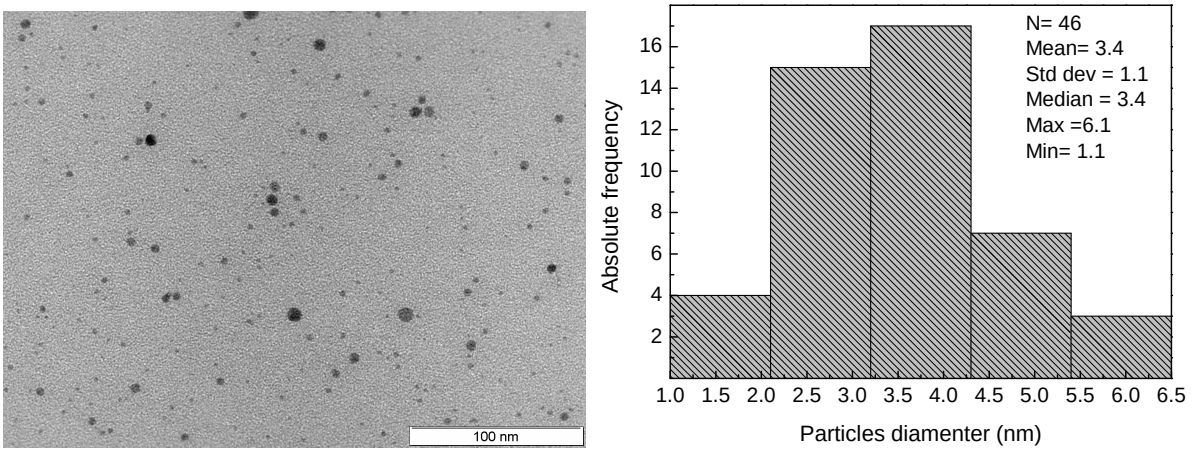

Figure 5.4: (a) TEM image and (b) diameter distribution of the synthesized Ag NPs.

With the introduction of PVP of low molecular weight, silver ions coordinate with N or O in PVP and a covered layer is generated on the surface of the particles. This layer inhibits the agglomeration of the nanoparticles, as reported by several authors [148], [151].

In order to validate the efficiency of PVP as a stabilizer, the aggregation of Ag NPs along time was evaluated. The absorption spectra of the Ag NPs colloidal solution with PVP after 4 and 21 days of preparation is indicated in Figure 5.5. The absorption peak detected at 424 nm is clearly characteristic of spherical silver nanoparticles with small diameters [148]. Moreover, both spectra have a similar behavior indicating the high stability of the prepared NPs suspension.

The prevention of NPs aggregation and their possible sedimentation is therefore a very

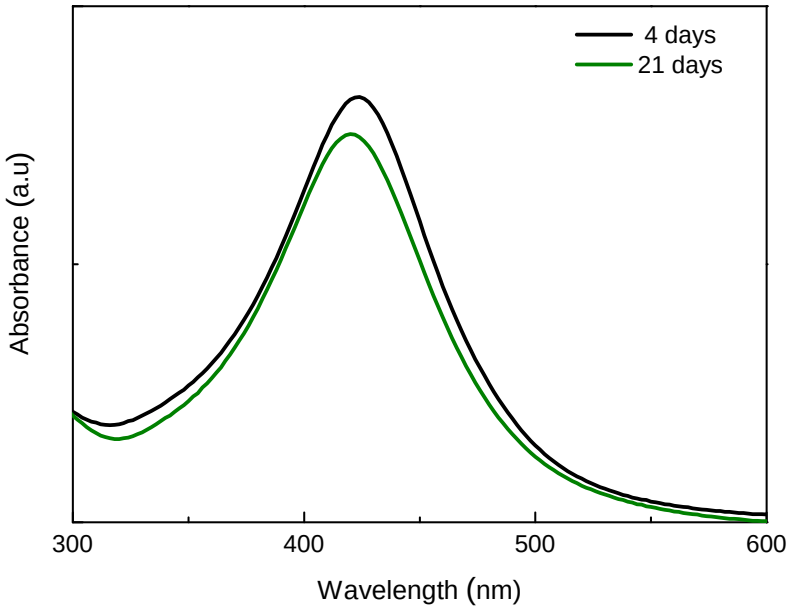

Figure 5.5: Absorption spectra of Ag NPs colloidal solution using PVP as stabilizer after 4 and 21 days of preparation.

important issue that should be considered during NPs synthesis. The preparation of stable NPs suspensions enabled storing and allowed the preparation of electrospun fibers incorporating well dispersed NPs.

Then, PVP of high molecular weight was added to the colloidal solution of Ag NPs in order to perform the electrospinning of a nonwoven membrane.

The obtained membrane is formed by a mesh of fibers randomly distributed (Figure 5.6 (a)) whose diameters are within 0.07-1.80 μm range (Figure 5.6 (b)). The wide distribution of diameters is probably due to partial fusion of fibers probably caused by incomplete evaporation of ethanol during the ES process. The magnification of fibers shown in Figure 5.6 (a) reveals a smooth surface where the perceptible dots are Ag NPs. Finally, Figure 5.6 (c) confirms the presence of well dispersed Ag NPs within electrospun fibers.

The luminescence of the electrospun composite was investigated by optical microscopy under excitation with different wavelengths, namely, UV ($\approx$ 375 nm), blue ($\approx$ 490 nm) and green ($\approx$ 550 nm) excitations. Therefore, the uniform emission seen in the membranes (Figure 5.7) reflected the emission of their fibers, with and without NPs. Without NPs the PVP electrospun membrane exhibited luminescence that depended on the excitation wavelength. Nevertheless, with the inclusion of NPs, the membrane showed a color change

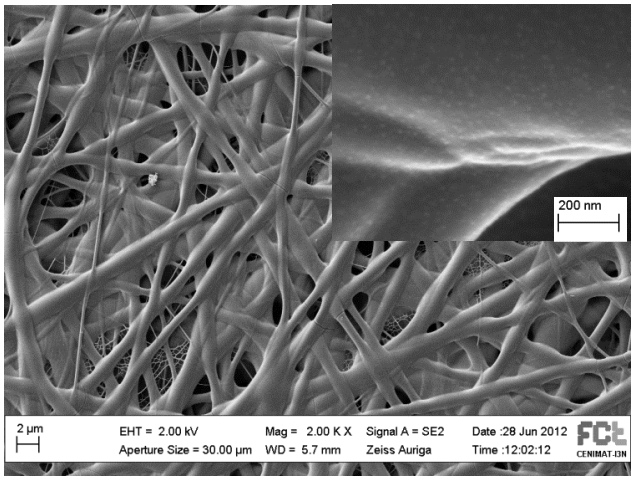

(a)

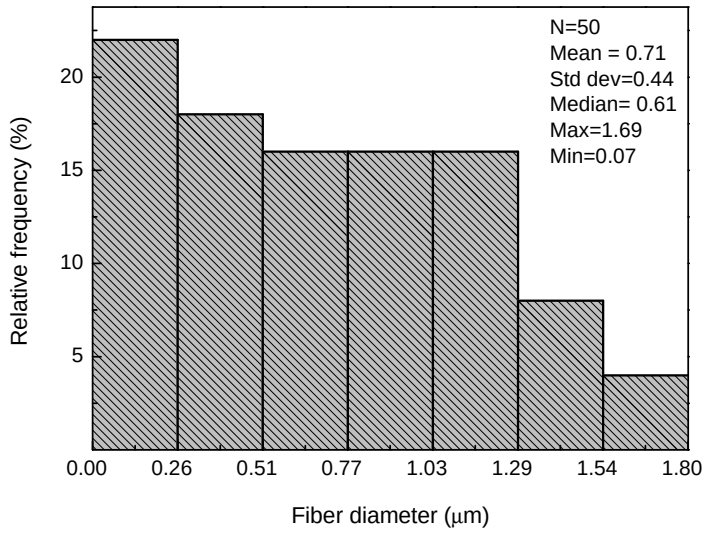

(b)

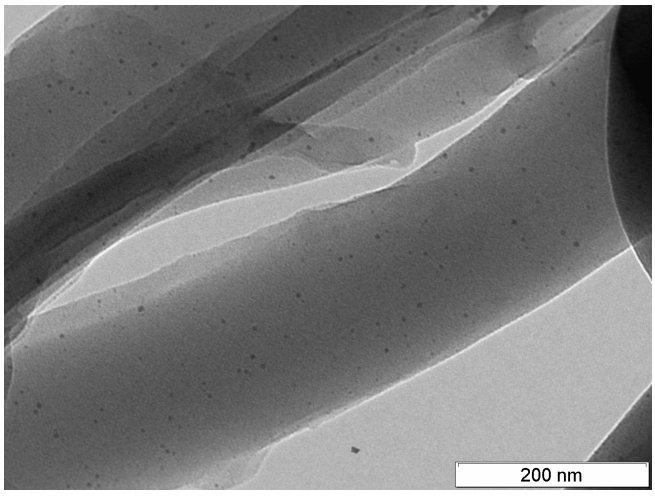

(c)

Figure 5.6: Electrospun PVP/Ag NPs fibers: (a) SEM image of the membrane and surface morphology of a single fiber (inset figure), (b) diameter distribution and (c) TEM image of a fiber.

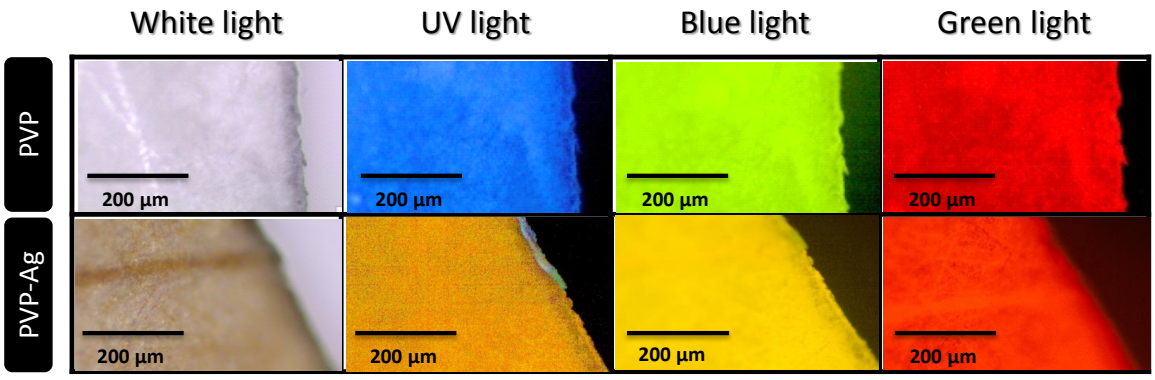

Figure 5.7: Microscopy images of a PVP electrospun membrane, with and without Ag-NPs, under white light, UV, blue and green excitations.

of emission when the excitation energy was modified.

In order to confirm the light emission observed under the microscope, the photoluminescence of a PVP electrospun membrane, with and without Ag NPs, was measured at room temperature under wavelength excitation of 325 nm (see Figure 5.8 (a)). The PVP membrane without NPs shows a low intensity emission in the wavelength range of 500-700nm which is in agreement with the observed images under UV radiation in Figure 5.7, as the luminescence emission is blue. For the PVP/Ag NPs membrane, a broad band with peaks at 575 and 620 nm is observed overlaying the previous one. These results are also in accordance with Figure 5.7 since an orange emission is observed under UV excitation.

Some authors also raised the possibility that a local field associated with surface plasmons could enhance the PL from the NPs [152] . The orange PL in PVP/Ag-NPs might due to the presence of Ag that serves as an intermediate level probably caused by the formation of Schottky barrier at metal/semiconductor (Ag-NPs/PVP), leading to photoluminescence with a wavelength that only depends of the barrier height in the range of 1.8 to 2.13 eV. Similar behavior was observed by Reisfeld and co-workers [153] in the fluorescence of europium/ethylenediamine tetraacetic acid (EuEDTA) complex in PVP films by adding Ag NPs. The fluorescence of PVP doped by the EuEDTA was explained by the interaction of the complex with silver plasmons. Fluorescence was also reported by Ricca [154] on PVP hydrogels due to the presence of hydrophobic compartments in the PVP network that occlude 1-anilino-8-naphthalene sulphonate (ANS) from water quenching.

An important issue in a real optoelectronic application of the nanofibers is their photo-

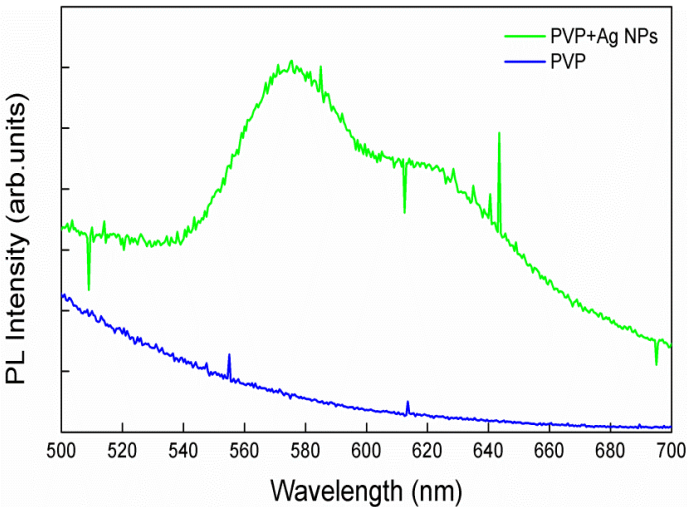

(a)

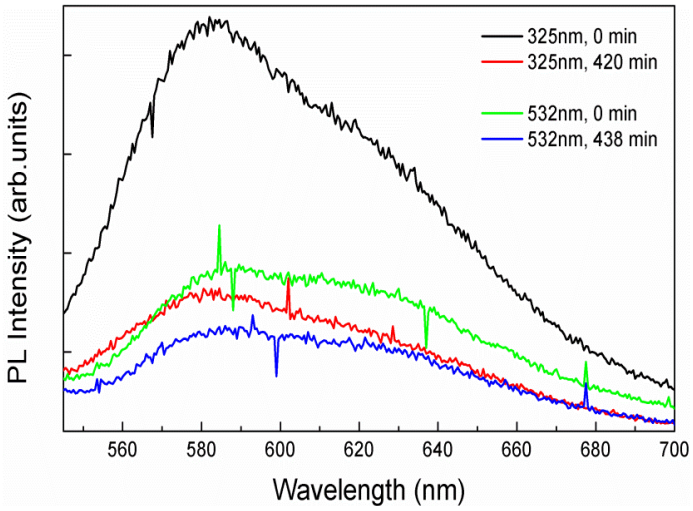

(b)

Figure 5.8: PL spectra of a PVP electrospun membrane, with and without Ag NPs (a) with excitation at 325nm and b) the time dependence of the laser incidence for wavelengths of 325 and 532nm.

stability under prolonged excitation. The quenching of the fluorescence in polymers after being stored at air condition was reported and related to the interaction of the polymer with oxygen [155] but also stable luminescence was mentioned for fibers after being stored in dark during several months. However, little is known concerning the PL stability under prolonged excitation. Figure 5.8 (b) shows PL spectra of PVP-Ag NPs membranes before and after a continuous incidence of the laser spot over more than 7 hours for two excitation wavelengths: 325nm (UV); and 532nm (green). Clearly, the PL intensity decreases after excitation for a long period of time, being more noticeable for ultraviolet excitation. Even so, it is still observed a PL signal with high intensity. This decay of photoluminescence

can be due to several causes, being the degradation of PVP the most probable one. The heating caused by the prolonged exposition to the radiation can contribute for the breaking of polymer chains and their subsequent oxidation and, for that reason, recombination of charges can be enhanced.

Electrical conductivity of the electrospun PVP and PVP/Ag NP membranes was also evaluated. Table 5.1 presents the mean conductivity achieved for the electrospun membranes under no light excitation and UV excitation. The electrical conductivity of the PVP fibers was improved with the addition of Ag NPs which is in agreement with literature reports [156]. However, conductivity does not seem to be affected by light excitation.

Table 5.1: Conductivity achieved for the electrospun membranes under no light excitation and UV excitation.

Sample	**Conductivity with no light excitation ($\Omega.cm^{-1}$)**	**Conductivity with UV light excitation ($\Omega.cm^{-1}$)**
PVP fibers	$(9.3\pm0.1)x10^{-7}$	$(9.3\pm0.1)x10^{-7}$
PVP/Ag NPs fibers	$(6.3\pm0.1)x10^{-6}$	$(6.8\pm0.1)x10^{-6}$

Since silver acts as an effective antimicrobial agent showing a broad inhibitory biocide spectrum, antibacterial assays using the Kirby-Bauer method [149] were performed to evaluate the antimicrobial characteristics of the electrospun PVP-Ag nanocomposites.

Figures 5.9 (a) to (f) show the images of the antibacterial assays for two bacteria: *E.coli* and *B. subtilis*. After incubation at 37°C for 24 h, no inhibition halos were observed in the PVP fibers' sample - Figure 5.9 (b) and (e)) - confirming that no antibacterial activity was detected for the two model bacteria studied. Therefore, PVP membranes have no influence in the growth of bacteria. Conversely, the PVP-Ag fibers exhibit antibacterial activity as proven by the appearance of inhibition halos shown in Figure 5.9 (c) and (f). The E. coli bacteria model showed the typical inhibition halo indicating the release of Ag NPs from the membrane and the restraining of bacteria growth. The antibacterial effect was less evident for the *B. subtilis* bacteria suggesting that antimicrobial effects depended on the characteristics of bacterial species [157]. The peptidoglycan layer of gram-negative bacteria (i.e. *E. coli*) is thinner than that of gram-positive bacteria (i.e. *B. subtilis*). So,

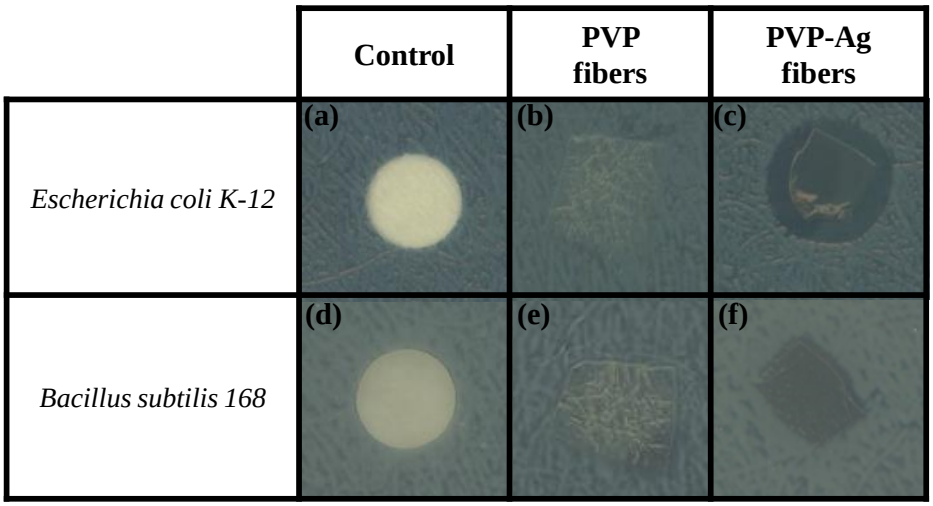

Figure 5.9: Photographs of the antibacterial assays: incubated E.coli with (a) control, (b) PVP electrospun fibers and (c) PVP-Ag electrospun fibers; and incubated B. subtilis with (d) control, (e) PVP electrospun fibers and (f) PVP-Ag electrospun fibers.

probably the Ag NPs can penetrate into the cell membrane of E. coli more easily and inhibit its growth more efficiently.

These results demonstrated that PVP-Ag composites had antibacterial activity. However, cytotoxic assays also proved the toxicity of Ag NPs. Ongoing studies are considering different ratios of $AgNO_3$/PVP in order to achieve biocompatible luminescent fibers.

Nevertheless, the composites developed exhibit good properties for optoelectronics, in particular for smart textiles applications.

5.4 Summary

The influence of Ag NPs on the luminescence of electrospun membranes made of PVP was studied during this thesis. The PVP fibers incorporating 2.3–4.6 nm size Ag NPs showed a significant photoluminescence (PL) band between 580 and 640 nm under 325 nm laser excitation. The down conversion luminescence emission was presented even after several hours of laser excitation, which denoted the durability and stability of fibers to consecutive excitations. As so, these one-dimensional photonic fibers made using cheap methods are of great importance for organic optoelectronic applications.

Chapter 6

Conclusions and perspectives

This last chapter presents the main findings of this thesis, comparing the key results against the state-of-the-art. In addition, future work arising from this research is proposed and discussed.

6.1 Thesis findings

To recapitulate, the present PhD thesis proposed the development of an ultra-low power source made of cellulose-based electrospun fibers that can take advantage of the ionic content of body fluids to generate electrical energy to supply low-power consumption implantable medical devices. Three main research goals were initially defined to accomplish this task, as referred in Chapter 1:

- Production and characterization of cellulose-based electrospun membranes;
- Development of functional electrospun fibers with enhanced electrical properties;
- Development of bio-batteries activated by body fluids.

The following sections summarize the results obtained to meet each of the previous three objectives and, in addition, the innovative findings that resulted from the exploration of functional fibers for optoelectronic applications are also recapitulated.

6.1.1 Production and characterization of cellulose-based electrospun membranes

The bio-battery proposed is mainly composed of cellulose acetate fibers produced using the electrospinning technique. During electrospinning, a number of process parameters can influence the morphology of the fibers obtained. For that reason, the effects of polymer concentration and process conditions on the membranes morphology were evaluated to produce defect-free fibers with controlled diameters. Smooth fibers with an average diameter of 243 ± 58 nm were obtained using a solution of CA 12% (wt) in acetone/ DMAc (2:1) for a ES voltage of 20kV, a scan rate of 0.2ml.h^{-1} and distance between the needle and the collector of 15 cm.

The electrochemical characterization of CA electrospun membranes carried out under physiological conditions revealed the presence of redox reactions, which can be attributed mainly to the free hydroxyl groups present in the cellulose acetates chemical structure. The membrane produced is, therefore, a good candidate as substrate for the development of biocompatible and flexible electrochemical devices.

6.1.2 Development of functional electrospun fibers with enhanced electrical properties

Cellulose-based composite electrodes for the bio-battery construction were also successfully developed. Cellulose acetate electrospun membranes were selected as a good polymer platform to produce fibrous conductive composites with high surface area and flexibility. In order to obtain highly conductive fibers, the *in situ* polymerization of Py and Ani was carried out on the surface of CA electrospun fibers.

CA/PPy composite fibers were prepared through the *in situ* pyrrole oxidative polymerization using $FeCl_3$ as oxidant. The effects of chemical synthesis conditions, such as monomer concentration, the mass ratio oxidant/monomer and reaction time were investigated in detail. Considering both electrical and morphological characteristics, uniform PPy-coated CA fibers with high electrical conductivity – 8.2×10^{-2} S.cm^{-1} – were obtained

using a monomer concentration of 0.05 mol.L^{-1}, an Ox/Mon ratio of 2 and a reaction time of 30 min. These composite fibers presented an average diameter of 290 ± 69 nm and a PPy coating of approximately 40 nm. Finally, the toxicity of CA/PPy composite membranes was evaluated. Testing for cytotoxicity is a first step towards ensuring the biocompatibility of a material envisaging a medical application. The results indicated that the composite was free of harmful extractables or had an insufficient quantity to cause acute effects under exaggerated conditions with isolated cells.

Additionally, CA/PANI fibers were obtained using a similar methodology. A continuous and uniform PANI coating on CA fibers was achieved and an electrical conductivity of 1.60x10^{-1} S.cm^{-1} was obtained for a monomer concentration of 2 mol.L^{-1}, an Ox/Mon ratio of 0.5 and a reaction time of 45 min. Using these conditions, CA/PANI composite fibers with an average diameter of 577 ± 59 nm were obtained and with a PANI coating thickness of 334 nm, approximately.

The cellulose-based composites produced are innovative highly conductive materials, with the additional advantages of lightweight, flexibility and high porosity and surface area. The cellulose-based composites developed during this thesis emerge as competitive materials when comparing to similar composites already reported Table 6.1. Using a similar methodology, the CA/PPy composite fibers proposed in this thesis showed a competitive electrical conductivity for thinner PPy coating and lower process time.

Considering reported literature, the CA/PANI composite fibers here presented are highly conductive concerning the time of the production process and the preservation of its fibrous morphology.

These scientific and technical achievements make the cellulose-based composite fibers produced a promising solution for flexible and stretchable electronics.

6.1.3 Development of bio-batteries activated by body fluids

A fully polymeric bio-battery was constructed by assembling the CA/PPy and CA/PANI composite membranes separated by a CA electrospun membrane. Such structure presented a stable electrochemical behavior with a maximum power density of 1.7 mW.g^{-1}.

Table 6.1: Summary of the main characteristics of PPy and PANI-based composites found in literature and comparison with the ones developed during this thesis.

Composite	**Year**	**Process time/ coating thickness**	**Fiber diameter (nm)**	**Conductivity ($S.cm^{-1}$)**	**Methodology**
PPy/CA [this thesis]	2014	<1h / ≈40 nm	290	8.19×10^{-2}	Fiber template/ Chemical polymerization in aqueous solution
PANI/CA [this thesis]	2014	<2h / ≈335 nm	577	1.60×10^{-1}	Fiber template/ Chemical polymerization in acidic aqueous solution
BC-PPy [117]	2013	>6h / ≈100 nm	200	77	Fiber template/ Chemical polymerization in acidic aqueous solution
PMMA/PANI [158]	2012	n.a.[a]	1600	2.3×10^{-2}	Electrospinning with a carrier polymer
PEO/PANI [158]	2012	n.a.	2300	8.1	Electrospinning with a carrier polymer
BC/PANI [119]	2012	>48h / ≈60 nm	180	3.8×10^{-2}	Fiber template/ Chemical polymerization in acidic aqueous solution
BC/PANI [118]	2011	<3h / ≈160 nm	200	5.0×10^{-2}	Fiber template/ Chemical polymerization in acidic aqueous solution
PVDF/PPy [109]	2010	n.a. / ≈100 nm	320	4.0×10^{-2}	Fiber template/ Vapor-phase polymerization
PEO/PPy [159]	2005	>48h / n.a.	96	1.0×10^{-3}	Fiber template/ Vapor-phase polymerization

[a] Not available.

Additional structures were also evaluated using polymer composite materials as the anode and an Au-based mesh as the cathode. Power densities of 8.0 $mW.g^{-1}$ and 1.4 $mW.g^{-1}$ were obtained for the PPy/CA/Au mesh and PANI/CA/Au mesh structures, respectively. These bio-batteries are an interesting alternative to power portable microwatt electronic devices. Due to its inherent biocompatibility, the fully polymeric bio-battery is a particularly interesting solution to power ultra-low implantable medical devices. Comparing the main properties of the bio-batteries developed during this thesis against other ultra-low power sources found in literature (Table 6.2), it is possible to conclude that their power densities per volume are extremely competitive. The fully polymeric bio-battery has achieved a power density 8 times higher than the first structure with this concept [15] and using only biocompatible materials.

Table 6.2: Summary of the main characteristics of the ultra-low power sources found in literature and comparison with the ones developed during this thesis.

Electrodes	**Year**	**Source of energy**	**Voc (mV)**	**Power density ($mW.cm^{-3}$)**
CA/PPy and CA/PANI [This work]	2014	Simulated biological fluids	2.1	0.8
CA/PPy and Au mesh [This work]	2014	Simulated biological fluids	64	16.1
CA/PANI and Au mesh [This work]	2014	Simulated biological fluids	56	2.7
Bi_2Te_3 and Sb_2Te_3 [59]	2013	Body heat	2.9	0.014
Al/CA and Ag/CA [15]	2011	Simulated biological fluids	280	0.1
Mg and Cu [67]	2005	Urine	n.a.[a]	1.7

[a] Not available.

Considering the structure constructed in 2011 [15], which used thin films coating to form the electrodes of the bio-battery, one of the major challenges found was the poor adhesion of the thin metallic layers to the surface of CA fibers. When the bio-battery is in an

aqueous medium, those layers have the tendency to detach themselves from the fibers surface. This is an undesirable characteristic envisaging implantable medical applications that needed to be overcome.

The development of conductive polymer composites of CA/PPy and CA/PANI is a viable solution to achieve completely biocompatible and flexible electrodes for the bio-batteries proposed.

In conclusion, taking into account these results, it can be stated that the bio-battery concept has been largely improved throughout the course of this scientific research.

6.1.4 Exploring functional electrospun fibers

As an additional result to functionalization of fibers for flexible electronics, the final chapter explored also the development of electrospun fibers with enhanced photoluminescence. A composite of PVP fibers incorporating Ag NPs was explored by blend electrospinning. The in situ chemical reduction of AgNO3 using a solution of PVP in ethanol as a reducer and stabilizer agent at room temperature was used to obtain Ag NPs with an average diameter of 3.4 nm and spherical shape. The electrospinning technique was used to produce nonwoven membranes of PVP/Ag NPs fibers exhibiting a strong and durable room temperature down conversion luminescence. Furthermore, the electrospun membrane showed strong antibacterial properties.

This one-dimensional nanostructured composite can be attractive for organic optoelectronics and, in particular, for application in smart textiles. Additional applications in regenerative medicine are foreseen for these luminescent fibers membranes that open an important and unexplored field of scientific and technological investigation.

6.2 Future work

Based on the findings from this thesis and considering the scientific accomplishments recently found in literature reports, some recommendations for future work on the devel-

opment of ultra-low power sources are presented and discussed in this section. Additional research paths are also suggested to explore the potential use of functional electrospun fibers in controlled drug delivery systems and smart textiles, taking advantage of the main results achieved during this thesis work.

6.2.1 Ultra-low power-sources

Several challenges remain for the development of innovative cellulose-based bio-batteries. The concept was successfully demonstrated during this thesis, but additional studies need to be made:

(i) **Electrochemical performance of cellulose-based electrodes.**

The specific capacitance and energy density of both CA/PPy and CA/PANI electrodes needs to be evaluated under different discharge conditions.

(ii) **Integration of bio-batteries.**

Bio-batteries need also to be tested by integrating several cells in serie or parallel. The performance of bio-batteries can be enhanced with such integration and their electrochemical behavior investigated. Along with the electrochemical characterization, discharge measurements need to be carried out for different periods of time to evaluate the bio-batteries performance for long term-term applications. The validation of the integrated bio-batteries is also an important step to demonstrate its potential for powering low energy consumption electronics.

(iii) **Biocompatibility and degradability.**

Fundamental studies need to ensure the biocompatibility and stability of the materials used in bio-batteries. Investigations to confirm the preservation of the morphology and electrical properties of the materials that composes the bio-battery are required to demonstrate its stability when operating for long periods of time in the presence of simulated body fluids.

(iv) **Alternative electrodes.**

In addition, alternative organic and biocompatible electrodes could be evaluated for

bio-batteries. Considering short-term applications, the development of biologically derived electrodes can be a challenging and attractive approach for biodegradable electronic medical devices. A few studies can be found in literature reporting the use of natural melanin pigments as anodes to be used in the next generation of biocompatible energy storage systems to power transient biomedical electronics, such as camera pills, sensors, drug delivery systems or tissue-stimulating devices [160]. The key advantage of such biodegradable device is their potential use in edible electronics when compared with alternative exotic synthetic electrodes materials which carry unknowing risks.

6.2.2 Functional electrospun fibers

With the growth of nanoscience and nanotechnology over the last decades, progresses have been made in the preparation of functional nanomaterials. Structures made of nanofibers show distinct characteristics such as an extremely high specific surface area and porosity. In addition, polymers themselves impart nanofibers with many desirable properties for advanced applications.

In this context, looking for sophisticated structures made from nanofibers assemblies is still a great topic of investigation targeting their use in multiples innovative applications. Based on the history and current developments of the electrospinning technique, electrospun nanofibers are expected to play an important role in emerging areas, such as in controlled drug delivery systems and smart textiles.

- **Controlled drug release systems**

Recently, ECPs have been explored for externally controlled polymeric drug-delivery systems allowing the tailoring of release profiles to match physiological processes. The use of PPy in such systems has been reported by different research teams [124], [125]. Taking advantage of the results obtained with conductive composites, an additional exploratory study has been carried out in order to evaluate the possibility of using CA/PPy electrospun fibers in controlled drug release.

As it was described in Chapter 1, the electrospinning technique can be used to incorporate

therapeutic compounds into the electrospun fibers. Considering this possibility, a model drug Ibuprofen (Ibu) - was incorporated into CA solution and the electrospinning was performed forming a nonwoven membrane. Then, in situ polymerization of Py was carried out covering the fibers incorporating the drug. The release profile of Ibu was investigated by UV/Visible spectrophotometry when an electrical stimulus was applied to a membrane partially immersed in a simulated body fluid solution. The drug can be easily identified in solution by the presence of a well-defined peak at 220 nm, approximately. Electrical stimulus of + 1V were applied for 1 minute followed by a resting period for monitoring the release profile. The absorbance values of the solution were collected during 15 cycles (each cycle corresponding to 1 minute of stimulation) and compared with the ones obtained for a similar sample where no stimulus was applied (diffusional release behavior), as shown in Figure 6.1.

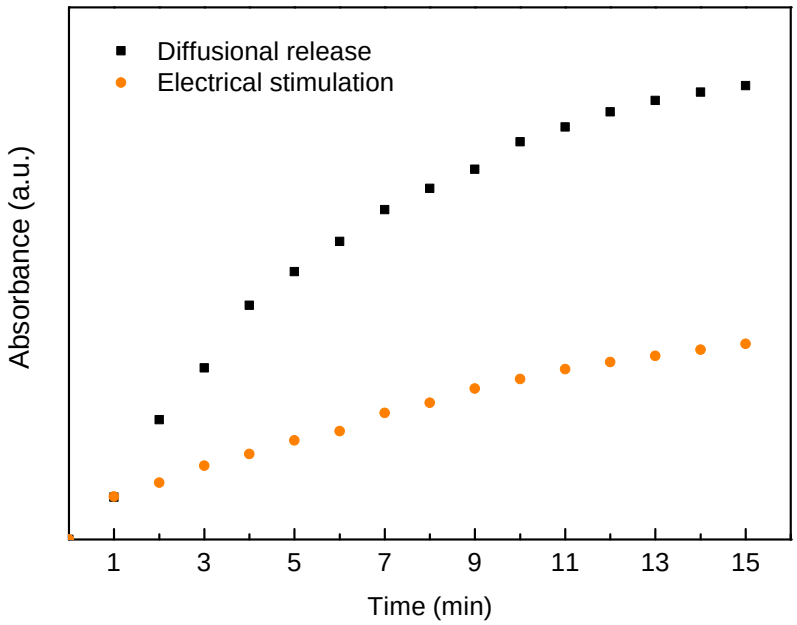

Figure 6.1: Ibuprofen release profile from CA/PPy electrospun membrane with and without electrical stimulation.

From this study, it was confirmed that when electrical stimulation is used, the drug is released in smaller quantities for a longer period of time (more than two hours to reach the same release amount obtained for 15 min of diffusion). However, additional studies need to be carried out to understand the release mechanisms. These preliminary results demonstrated the potential use of CA/PPy electrospun membrane in controlled drug re-

lease systems thus enlarging the applicability of these cellulose-based composites. These systems can potentially be integrated with bio-batteries which provide the electrical stimulations.

- **Wearable textiles**

Smart textiles is a recent topic of investigation that covers different research disciplines such as materials science, chemistry, physics and textile technology. The investigation of wearable textiles is a consequence of the recent achievements in the development of conductive materials and electronic miniaturization which allows the integration of electronics into fabric structures. Wearable fabrics are an actual interest for both academy and a diversity of industrial sectors. A report from Grand View Research (2014) evaluated the global smart textile market in 2012 in approximately USD 289.5 million and estimated a market growth to USD 1.5 billion by 2020. Protection and military clothing has been the dominant sector, although sport and health applications are predicted to see the fastest growth. The powering of wearable electronics remains the major challenge since the main components of a battery should be functional during unusual mechanical motions.

Recently, a new family of fibers able to integrate multiple functional components into one single fiber or assembly structures composed by multiple fibers has emerged and allowed the development of sophisticated multifunctional fabrics. The electrospinning of functional polymer-based fibers with controlled morphologies and properties can be foreseen as a scientific challenge.

Taking advantage of the knowledge and experience gained throughout this thesis work, the functionalization of electrospun fibers with multifunctional properties for wearable applications can be a promising topic of investigation with potential impact in the wearable electronics market.

6.3 Summary

Organic electronics represents an attractive and emerging paradigm in medical devices. The research developed during this thesis is aligned with a modern and growing topic of investigation resultant from the synergy of medicine, electronic and nanotechnology. Polymer-based electronic represents an attractive technology providing innovative and economical solutions for the development of flexible, ultra-thin and biocompatible miniaturized devices. As summarized in the previous sections, important findings were obtained during this thesis regarding the development of functional fibers for application in organic electronics envisaging medical applications.

Bibliography

[1] The Fredonia Group. Implantable medical devices. `http://www.qmed.com/mpmn/medtechpulse/report-us-demand-implantable-medical-devices-reach-52b-2015`, 2012. [Online; accessed 30-August-2014].

[2] A. P. Chandrakasan, N. Verma, and D. C. Daly. Ultralow-power electronics for biomedical applications. *Annu. Rev. Biomed. Eng.*, 10:247–274, 2008.

[3] L. Wong, S. Hossain, A. Ta, J. Edvinsson, D. Rivas, and H. Naas. A very low-power CMOS mixed-signal IC for implantable pacemaker applications. *IEEE J. Solid-State Circuits*, 39(12):2446–2456, 2004.

[4] S. Kim, N. Cho, S-J. Song, D. Kim, and H-J. Yoo. A 0.9V 96μW digital hearing aid chip with heterogeneous S-D DAC. *Proc. IEEE Symp VLSI Circuits*, pages 55–56, 2006.

[5] H. Neuteboom, B.M.J. Kup, and M. Janssens. A DSP based hearing instrument. *IEEE J. Solid-State Circuits*, 32(11):1790–806, 1997.

[6] J. Georgiou and C. Toumazou. A 126μW cochlear chip for a totally implantable system. *IEEE J. Solid-State Circuits*, 40(2):430–43, 2005.

[7] R. Sarpeshkar, C. Salthouse, J-J. Sit, M.W. Baker, and S.M. Zhak. An ultra-low-power programmable analog bionic ear processor. *IEEE Trans. Biomed. Eng.*, 52(4):711–27, 2005.

[8] K.D. Wise, D.J. Anderson, J.F. Hetke, D.R. Kipke, and K. Naja. Wireless im-

plantable microsystems: high-density electronic interfaces to the nervous system. *Proc. IEEE*, 92(1):76–97, 2004.

[9] S. ODriscoll, T. Meng, K. Shenoy, and C. Kemere. Neurons to silicon: implantable prosthesis processor. *IEEE Int. Solid-State Circuits Conf. Dig. Tech. Pap.*, pages 552–53, 2006.

[10] J. D. Weiland, W. Liu, and M. S. Humayun. Retinal prosthesis. *Annu. Rev. Biomed. Eng.*, 7:361401, 2005.

[11] W. Liu and M.S. Hurnayun. Retinal prosthesis. *IEEE Int. Solid-State Circuits Conf. Dig. Tech. Pap.*, 1:21819, 2004.

[12] V. S. Mallela, V. Ilankumaran, and N. S. Rao. Trends in cardiac pacemaker batteries. *Indian Pacing Electrophysiol*, 4(4):201–212, 2004.

[13] Medtronic. The pacemaker evolution. `http://www.medtronic.com/innovation/smarter-miniaturization.html`, 2013. [Online; accessed 30-August-2014].

[14] 21st Century Tech. New leadless heart pacemaker making debut in europe. `http://www.21stcentech.com/headlines-leadless-heart-pacemaker-making-debut-europe/`, 2013. [Online; accessed 30-August-2014].

[15] A. C. Baptista, J. I. Martins, E. Fortunato, R. Martins, J. P. Borges, and I. Ferreira. Thin and flexible bio-batteries made of electrospun cellulose-based membranes. *Biosens Bioelectron*, 26(5):2742–5, 2011.

[16] S. A. Harfenist, S. D. Cambron, E. W. Nelson, S. M. Berry, A. W. Isham, M. M. Crain, K. M. Walsh, R. S. Keynton, and R. W. Cohn. Direct drawing of suspended filamentary micro- and nanostructures from liquid polymers. *Nano Lett*, 4(10):1931–1937, 2004.

[17] Y. Zhang, C. T. Lim, S. Ramakrishna, and Z. M. Huang. Recent development of polymer nanofibers for biomedical and biotechnological applications. *J Mater Sci-Mater M*, 16:933 946, 2005.

[18] G Che, B B Lakshmi, C R Martin, and E R Fisher. Chemical vapor deposition based synthesis of carbon nanotubes and nanofibers using a template method. *Chem. Mater.*, 10:260–267, 1998.

[19] W. Hwang, B. H. Kim, R. Dandu, J. Cappello, H. Ghandehari, and J. Seog. Surface induced nanofiber growth by self-assembly of a silk-elastin-like protein polymer. *Langmuir*, 25(21):12682–6, 2009.

[20] S. Ramakrishna, K. Fujihara, W. E. Teo, T. Yong, Z. Ma, and R. Ramaseshan. Electrospun nanofibers: solving global issues. *Mater Today*, 9(3):40–50, 2006.

[21] F. Yang, R. Murugan, S. Wang, and S. Ramakrishna. Electrospinning of nano/micro scale poly(L-lactic acid) aligned fibers and their potential in neural tissue engineering. *Biomaterials*, 26(15):2603–10, 2005.

[22] H. Zhuo, J. Hu, S. Chen, and L. Yeung. Preparation of polyurethane nanofibers by electrospinning. *J of Appl Polym Sci*, 109(1):406–411, 2008.

[23] B. M. Min, G. Lee, S. H. Kim, Y. S. Nam, T. S. Lee, and W. H. Park. Electrospinning of silk fibroin nanofibers and its effect on the adhesion and spreading of normal human keratinocytes and fibroblasts in vitro. *Biomaterials*, 25(7-8):1289–1297, 2004.

[24] L. Buttafoco, N. G. Kolkman, P. Engbers-Buijtenhuijs, A. A. Poot, P. J. Dijkstra, I. Vermes, and J. Feijen. Electrospinning of collagen and elastin for tissue engineering applications. *Biomaterials*, 27(5):724–34, 2006.

[25] J. P. Canejo, J. P. Borges, M. H. Godinho, P. Brogueira, P. I. C. Teixeira, and E. M. Terentjev. Helical twisting of electrospun liquid crystalline cellulose micro- and nanofibers. *Adv Mater*, 20(24):4821–4825, 2008.

[26] C. W. Kim, D. S. Kim, S. Y. Kang, M. Marquez, and Y. L. Joo. Structural studies of electrospun cellulose nanofibers. *Polymer*, 47(14):5097–5107, 2006.

[27] C. M. Vaz, S. van Tuijl, C. V. Bouten, and F. P. Baaijens. Design of scaffolds for blood vessel tissue engineering using a multi-layering electrospinning technique. *Acta Biomater*, 1(5):575–82, 2005.

[28] P. Q. Franco, C. F. C. João, J. C. Silva, and J. P. Borges. Electrospun hydroxyapatite fibers from a simple sol-gel system. *Mater Lett*, 67(1):233–236, 2012.

[29] S. J. Lee, R. Tatavarty, and M. B. Gu. Electrospun polystyrene-poly(styrene-co-maleic anhydride) nanofiber as a new aptasensor platform. *Biosens Bioelectron*, 38(1):302–7, 2012.

[30] J. Miao, R. C. Pangule, E. E. Paskaleva, E. E. Hwang, R. S. Kane, R. J. Linhardt, and J. S. Dordick. Lysostaphin-functionalized cellulose fibers with antistaphylococcal activity for wound healing applications. *Biomaterials*, 32(36):9557–67, 2011.

[31] W. Ji, Y. Sun, F. Yang, J. J. van den Beucken, M. Fan, Z. Chen, and J. A. Jansen. Bioactive electrospun scaffolds delivering growth factors and genes for tissue engineering applications. *Pharm Res*, 28(6):1259–72, 2011.

[32] H. R. Pant, B. Pant, P. Pokharel, H. J. Kim, L. D. Tijing, C. H. Park, D. S. Lee, H. Y. Kim, and C. S. Kim. Photocatalytic TiO_2-RGO/Nylon-6 spider-wave-like nano-nets via electrospinning and hydrothermal treatment. *J Membrane Sci*, 429:225–234, 2013.

[33] X. Li, C. Gao, J. Wang, B. Lu, W. Chen, J. Song, S. Zhang, Z. Zhang, X. Pan, and E. Xie. TiO_2 films with rich bulk oxygen vacancies prepared by electrospinning for dye-sensitized solar cells. *J Power Sources*, 214:244–250, 2012.

[34] A. C. Baptista, Isabel Ferreira, and João Borges Borges. Electrospun fibers in composite materials for medical applications. *Journal of Composites and Biodegradable Polymers*, 1:56–65, 2013.

[35] S. Sarkar, T. Schmitz-Rixen, G. Hamilton, and A. M. Seifalian. Achieving the ideal properties for vascular bypass grafts using a tissue engineered approach: a review. *Med Biol Eng Comput*, 45(4):327–36, 2007.

[36] S. A. Sell, M. J. McClure, K. Garg, P. S. Wolfe, and G. L. Bowlin. Electrospinning of collagen/biopolymers for regenerative medicine and cardiovascular tissue engineering. *Adv Drug Deliv Rev*, 61(12):1007–19, 2009.

[37] S. J. Lee, J. Liu, S. H. Oh, S. Soker, A. Atala, and J. J. Yoo. Development of a composite vascular scaffolding system that withstands physiological vascular conditions. *Biomaterials*, 29(19):2891–8, 2008.

[38] A. H. Dorafshar, N. Angle, M. Bryer-Ash, D. Huang, M. M. Farooq, H. A. Gelabert, and J. A. Freischlag. Vascular endothelial growth factor inhibits mitogen-induced vascular smooth muscle cell proliferation. *J Surg Res*, 114(2):179–186, 2003.

[39] Y. Yoshikawa and S. O. Abrahamsson. Dose-related cellular effects of platelet-derived growth factor-bb differ in various types of rabbit tendons in vitro. *Acta Orthop Scand*, 72(3):287292, 2001.

[40] H. Zhang, X. Jia, F. Han, J. Zhao, Y. Zhao, Y. Fan, and X. Yuan. Dual-delivery of VEGF and PDGF by double-layered electrospun membranes for blood vessel regeneration. *Biomaterials*, 34(9):2202–12, 2013.

[41] M. P. Prabhakaran, J. Venugopal, and S. Ramakrishna. Electrospun nanostructured scaffolds for bone tissue engineering. *Acta Biomater*, 5(8):2884–93, 2009.

[42] W. Ji, F. Yang, J. Ma, M. J. Bouma, O. C. Boerman, Z. Chen, J. J. van den Beucken, and J. A. Jansen. Incorporation of stromal cell-derived factor-1alpha in PCL/gelatin electrospun membranes for guided bone regeneration. *Biomaterials*, 34(3):735–45, 2013.

[43] P. Gentile, V. Chiono, C. Tonda-Turo, A. M. Ferreira, and G. Ciardelli. Polymeric membranes for guided bone regeneration. *Biotechnol J*, 6(10):1187–97, 2011.

[44] E. L. Fong, C. K. Chan, and S. B. Goodman. Stem cell homing in musculoskeletal injury. *Biomaterials*, 32(2):395–409, 2011.

[45] Z. J. Liu, Y. Zhuge, and O. C. Velazquez. Trafficking and differentiation of mesenchymal stem cells. *J Cell Biochem*, 106(6):984–91, 2009.

[46] J. S. Choi, S. J. Lee, G. J. Christ, A. Atala, and J. J. Yoo. The influence of electrospun aligned poly(caprolactone)/collagen nanofiber meshes on the formation of self-aligned skeletal muscle myotubes. *Biomaterials*, 29(19):2899–906, 2008.

[47] P. J. Yang and J. S. Temenoff. Engineering orthopedic tissue interfaces. *Tissue Eng PT B*, 15(2):127–141, 2009.

[48] M. R. Ladd, S. J. Lee, J. D. Stitzel, A. Atala, and J. J. Yoo. Co-electrospun dual scaffolding system with potential for muscle-tendon junction tissue engineering. *Biomaterials*, 32(6):1549–1559, 2011.

[49] D. G. Yu. Electrospun nanofiber-based drug delivery systems. *Health*, 01(02):67–75, 2009.

[50] J. S. Choi, K. W. Leong, and H. S. Yoo. In vivo wound healing of diabetic ulcers using electrospun nanofibers immobilized with human epidermal growth factor (EGF). *Biomaterials*, 29(5):587–96, 2008.

[51] H. Peng, S. Zhou, T. Guo, Y. Li, X. Li, J. Wang, and J. Weng. In vitro degradation and release profiles for electrospun polymeric fibers containing paracetanol. *Colloids Surface B*, 66(2):206–12, 2008.

[52] X. Xu, X. Zhuang, X. Chen, X. Wang, and X. Yang, L.and Jing. Preparation of core-sheath composite nanofibers by emulsion electrospinning. *Macromol Rapid Comm*, 27(19):1637–1642, 2006.

[53] K. Wei, Y. Li, H. Mugishima, A. Teramoto, and K. Abe. Fabrication of core-sheath structured fibers for model drug release and tissue engineering by emulsion electrospinning. *Biotechnol J*, 7(5):677–85, 2012.

[54] H. Tang, F. Yan, Q. Tai, and H. L. Chan. The improvement of glucose bioelectrocatalytic properties of platinum electrodes modified with electrospun TiO_2 nanofibers. *Biosens Bioelectron*, 25(7):1646–51, 2010.

[55] M. Zhao, J. Huang, Y. Zhou, Q. Chen, X. Pan, H. He, and Z. Ye. A single mesoporous ZnO/Chitosan hybrid nanostructure for a novel free nanoprobe type biosensor. *Biosens Bioelectron*, 43:226–30, 2013.

[56] D. C Bock, A. C. Marschilok, K. J. Takeuch, and E. S. Takeuch. Batteries used to power implantable biomaedical devices. *Electrochimica acta*, 84:155–164, 2012.

[57] Y. Yang, X.J. Wei, and J. Liu. Suitability of a thermoelectric power generator for implantable medical electronic devices. *J Phys D*, 40:57905800, 2007.

[58] Y. Yang, G.D. Xu, and J. Liu. A prototype of an implantable thermoelectric generator for permanent power supply to body inside a medical device. *J. Med. Devices*, 8(1):014507–014513, 2013.

[59] S. J. Kim, J. H. We, and B. J. Cho. Wearable thermoelectric generator fabricated on glass fabric. *Energ Environ Sci*, 00:1–3, 2013.

[60] R. Yang, Y. Qin, C. Li, G. Zhu, and Z.L. Wang. Converting biomechanical energy into electricity by a muscle-movement-driven nanogenerator. *Nano Lett*, 9(3):1201–1205, 2009.

[61] C. Dagdeviren, B. D. Yang, Y. Su, P. L. Tran, P. Joe, E. Anderson, J. Xia, V. Doraiswamy, B. Dehdashti, X. Feng, B. Lu, R. Poston, Z. Khalpey, R. Ghaffari, Y. Huang, M.J. Slepian, and J.A. Rogers. Conformal piezoelectric energy harvesting and storage from motions of the heart, lung, and diaphragm. *Proceedings of the National Academy of Sciences*, 111(5):1927–1932, 2014.

[62] R. Martins, I. Ferreira, and E. Fortunato. Electronics with and on paper. *Phys. Status Solidi RRL*, 5(9):332–335, 2011.

[63] R. Martins, P. Barquinha, L. Pereira, N. Correia, G. Gonalves, I. Ferreira, and E. Fortunato. Selective floating gate non-volatile paper memory transistor. *Phys. Status Solidi RRL*, 3(9):308–310, 2009.

[64] L. Hu, J. W. Choi, Y. Yang, S. Jeong, F. La Mantia, L. F. Cui, and Y. Cui. Highly conductive paper for energy-storage devices. *PNAS*, 106(51):21490–4, 2009.

[65] I. Ferreira, B. Brás, N. Correia, P. Barquinha, E. Fortunato, and R. Martins. Self-rechargeable paper thin-film batteries: Performance and applications. *J. Display Technol.*, 6:332–335, 2010.

[66] D. Tobjörk and R. Österbacka. Paper electronics. *Adv Mater*, 23(17):1935–61, 2011.

[67] Ki Bang Lee. Urine-activated paper batteries for biosystems. *J Micromech and Microeng*, 15(9):S210–S214, 2005.

[68] V. L. Pushparaj, M. M. Shaijumon, A. Kumar, S. Murugesan, L. Ci, R. Vajtai, R. J. Linhardt, O. Nalamasu, and P. M. Ajayan. Flexible energy storage devices based on nanocomposite paper. *Proc Natl Acad Sci U S A*, 104(34):13574–7, 2007.

[69] G. Nystrom, A. Razaq, M. Strømme, L. Nyholm, and A. Mihranyan. Ultrafast all-polymer paper-based batteries. *Nano Lett.*, 9(10):3635–3639, 2009.

[70] I. Ferreira, B. Brás, J. I. Martins, N. Correia, P. Barquinha, E. Fortunato, and R. Martins. Solid-state paper batteries for controlling paper transistors. *Electrochim Acta*, 56(3):1099 – 1105, 2011.

[71] S. Li, Z.P. Guo, C.Y. Wang, G.G. Wallace, and H.K. Lui. Flexible cellulose based polypyrrole/multiwalled carbon nanotube films for bio-compatible zinc battery activated by simulated body fluid. *J. Mater. Chem A*, 1:14300–14305, 2013.

[72] A. Baptista, I. Ferreira, and J. P. Borges. *Cellulose-based bioelectronic devices*, chapter 4. InTech, 2013.

[73] L. Yang and S. Shijie Liu. Kinetic model for kraft pulping process. *Ind Eng Chem Res*, 44:7078–7085, 2005.

[74] X. Wang, H. Li, Y. Cao, and Q. Tang. Cellulose extraction from wood chip in an ionic liquid 1-allyl-3-methylimidazolium chloride (AmimCl). *Bioresource Technol*, 102:7959–7965, 2011.

[75] A. Dufresne, J-Y. Cavaille, and M. R. Vignon. Mechanical behavior of sheets prepared from sugar beet cellulose microbrils. *J Poly Sc*, 64(6):1185–1194, 1997.

[76] R. Zuluaga, J. L. Putaux, A. Restrepo, I. Mondragon, and P. Ganan. Cellulose microfibrils from banana farming residues: isolation and characterization. *Cellulose*, 14(6):585–592, 2007.

[77] I. Tsekos. The sites of cellulose synthesis in algae: diversity and evolution of cellulose synthesizing enzyme complexes. *J Phycol*, 35:635–655, 1999.

[78] M. Szymanska-Chargot, J. Cybulska, and A. Zdunek. Sensing the structural differences in cellulose from apple and bacterial cell wall materials by raman and ft-ir spectroscopy. *Sensors (Basel)*, 11(6):5543–60, 2011.

[79] T. Kondo. *Hydrogen bonds in cellulose and cellulose derivatives*. Marcel Dekker, Inc., 1998.

[80] R. J. Moon, A. Martini, J. Nairn, J. Simonsen, and J. Youngblood. Cellulose nanomaterials review: structure, properties and nanocomposites. *Chem. Soc. Rev*, 40:3941–3994, 2011.

[81] M. H. Godinho, D. Filip, I. Costa, A. L. Carvalho, J. L. Figueirinhas, and E. M. Terentjev. Liquid crystalline cellulose derivative elastomer films under uniaxial strain. *Cellulose*, 16:199–205, 2009.

[82] M. M. Giraud-Guille, E. Balamie, G. Mosser, C. Helary, F. Gobeaux, and S. Vegier. Liquid crystalline properties of type i collagen: Perspectives in tissue morphogenesis. *C. R. Chimie*, 11:245–252, 2008.

[83] D. Li and Y. Xia. Electrospinning of nanofibers: Reinventing the wheel. *Adv Mater*, 16(14):1153–1170, 2004.

[84] Z. M. Huang, Y. Z. Zhang, M. Kotaki, and S. Ramakrishna. A review on polymer nanofibers by electrospinning and their applications in nanocomposites. *Compos Sci Technol*, 63(15):2223–2253, 2003.

[85] K. Y. Lee, L. Jeong, Y. O. Kang, S. J. Lee, and W. H. Park. Electrospinning of polysaccharides for regenerative medicine. *Adv Drug Deliv Rev*, 61(12):1020–32, 2009.

[86] T. J. Sill and H. A. von Recum. Electrospinning: applications in drug delivery and tissue engineering. *Biomaterials*, 29(13):1989–2006, 2008.

[87] H. Penchev, D. Paneva, N. Manolova, and I. Rashkov. Degradation and healing characteristics of small-diameter poly(caprolactone) vascular grafts in the rat systemic arterial circulation. *Carbohyd Res*, 345(16):2374–2380, 2010.

[88] J. Li, S. Vadahanambi, C. D. Kee, and I. K. Oh. Electrospun fullerenol-cellulose biocompatible actuators. *Biomacromolecules*, 12(6):2048–54, 2011.

[89] L. Shuiping, T. Lianjiang, H. Weili, L. Xiaoqiang, and C. Yanmo. Cellulose acetate nanofibers with photochromic property: Fabrication and characterization. *Mater Lett*, 64(22):2427–2430, 2010.

[90] R. B. Rakhi, Wei Chen, Dongkyu Cha, and H. N. Alshareef. High performance supercapacitors using metal oxide anchored graphene nanosheet electrodes. *J. Mater. Chem*, 21:16197–16204, 2011.

[91] A. I. Gopalan, K. M. Manesh, and P. Santhosh. Poly(vinylidene fluoride)polydiphenylamine composite electrospun membrane as high-performance polymer electrolyte for lithium batteries. *J Memb Sc*, 318:422–428, 2008.

[92] A. I. Gopalan, P. Santhosh, K. M. Manesh, J. Nho, S. Kim, C. Hwang, and K. Lee. Development of electrospun PVDF/PAN membrane-based polymer electrolytes for lithium batteries. *J Memb Sc*, 325(2):683–690, 2008.

[93] T. Kokubo and H. Takadama. How useful is sbf in predicting in vivo bone bioactivity? *Biomaterials*, 27(15):2907–2915, 2006.

[94] R. M. Morgan, M. J. Patterson, and M. A. Nimmo. Acute effects of dehydration on sweat composition in men during prolonged exercise in the heat. *Acta Physiol Scand*, 182(1):37–43, 2004.

[95] L. Müller and F. A. Müller. Preparation of sbf with different HCO_3 content and its inuence on the composition of biomimetic apatites. *Acta Biomater*, 2:181–189, 2006.

[96] S. Tungprapa, T. Puangparn, M. Weerasombut, I. Jangchud, P. Fakum, S. Semongkhol, C. Meechaisue, and P. Supaphol. Electrospun cellulose acetate fibers: effect of solvent system on morphology and fiber diameter. *Cellulose*, 14(6):563–575, 2007.

[97] R. Konwarh, N. Karak, and M. Misra. Electrospun cellulose acetate nanofibers: the present status and gamut of biotechnological applications. *Biotechnol Adv*, 31:421–437, 2013.

[98] J.M. Deitzel, J. Kleinmeyer, D. Harris, and N.C. Beck Tan. The effect of processing variables on the morphology of electrospun nanofibers and textiles. *Polymer*, 42:261–272, 2001.

[99] C. Mit-uppatham, M. Nithitanakul, and P. Supaphol. Ultrafine electrospun polyamide-6 fibers: effect of solution conditions on morphology and average fiber diameter. *Macromol Chem Phys*, 205:2327–2328, 2004.

[100] P. Heikkilä and A. Harlin. Parameter study of electrospinning of polyamide-6. *Eur Polym J*, 44:3067–3079, 2008.

[101] R. Balamurugan, S. Sundarrajan, and S. Ramakrishna. Recent trends in nanofibrous membranes and their suitability for air and water filtrations. *Membranes*, 1(3):232–248, 2011.

[102] C. Edwards and R. Marks. Evaluation of biomechanical properties of human skin. *Clinics in Dermatology*, 13:375–380, 1995.

[103] G. A. Holzapfel. *Biomechanics of Soft Tissue*, chapter 10.11. Academic Press, 2001.

[104] P. Choi, N. H. Jalani, and R. Datta. Thermodynamics and proton transport in nafion. *J Electrochem Soc*, 152(3):E123, 2005.

[105] Agmon N. The grotthuss mechanism. *Chem Phys Lett*, 244(5):456–462, 1995.

[106] N. J. Pinto, A. T. Johnson, A. G. MacDiarmid, C. H. Mueller, N. Theofylaktos, D. C. Robinson, and F. A. Miranda. Electrospun polyaniline/polyethylene oxide nanofiber field-effect transistor. *Appl Phys Lett*, 83:4244, 2003.

[107] J. H. Jun, K. Cho, J. Yun, K.S. Suh, T.Y Kim, and S. Kim. Enhancement of electrical characteristics of electrospun polyaniline nanofibers by embedding the nanofibers with ga-doped zno nanoparticles. *Org Electron*, 9:445–451, 2008.

[108] Y. Xin, Z. H. Huang, L. Peng, and D. J. Wang. Photoelectric performance of poly(p-phenylene vinylene)/Fe_3O_4 nanofiber array. *J Appl Phys*, 105:086106, 2009.

[109] K. Ketpang and J. S. Park. Electrospinning PVDF/PPy/MWCNTs conducting composites. *Synthetic Met*, 160:1603–1608, 2010.

[110] A. Laforgue. All-textile flexible supercapacitors using electrospun poly(3,4-ethylenedioxythiophene) nanofibers. *J Power Sources*, 196:559–564, 2011.

[111] Y. Chen, Y. Li, H. Wang, and M. Yang. Gas sensitivity of a composite of multi-walled carbon nanotubes and polypyrrole prepared by vapor phase polymerization. *Carbon*, 45(2):357–363, 2007.

[112] H. Yoon. Current trends in sensors based on conducting polymer nanomaterials. *Nanomater*, 3:524–549, 2013.

[113] L. G. Mobarakeh, M. P. Prabhakaran, M. Morshed, M. H. N. Esfahani, Hossein Baharvand, Sahar Kiani, S. A. Deyab, and S. Ramakrishna. Application of conductive

polymers, scaffolds and electrical stimulation for nerve tissue engineering. *J Tissue Eng. Regen Med*, 5:e17–e35, 2011.

[114] J. Huang, I. Ichinose, and T. Kunitake. Nanocoating of natural cellulose fibers with conjugated polymer: hierarchical polypyrrole composite materials. *Chem Commun (Camb)*, 13:1717–1719, 2005.

[115] A. Mihranyan, L. Nyholm, A. E. G. Bennett, and M. Strømme. A novel high specific surface area conducting paper material composed of polypyrrole and cladophora cellulose. *J. Phys. Chem. B*, 112:1224912255, 2008.

[116] G. Nystrom, A. Mihranyan, A. Razaq, T. Lindstro, and M. Strømme. A nanocellulose polypyrrole composite based on microfibrillated cellulose from wood. *J. Phys. Chem. B*, 114:41784182, 2010.

[117] H. Wang, L. Bian, P. Zhou, J. Tang, and W. Tang. Coresheath structured bacterial cellulose/polypyrrole nanocomposites with excellent conductivity as supercapacitors. *J Mater Chem A*, 1:578–584, 2013.

[118] W. Hu, S. Chen, Z. Yang, L. Liu, and H. Wang. Flexible electrically conductive nanocomposite membrane based on bacterial cellulose and polyaniline. *J Phys Chem B*, 115(26):8453–7, 2011.

[119] Z. Shi, S. Zang, F. Jiang, and L. Huang. In situ nano-assembly of bacterial cellulosepolyaniline composites. *RSC Adv*, 2:1040–1046, 2012.

[120] X. Wang, X. Gu, C. Yuan, S. Chen, P. Zhang, T. Zhang, J. Yao, F. Chen, and G. Chen. Evaluation of biocompatibility of polypyrrole in vitro and in vivo. *J Biomed Mater Res A*, 68A(3):411–422, 2004.

[121] M. F. Shie, W. T. Li, C. F. Dai, and J.M. Yeh. *In vitro Biocompatibility of Electrospinning Polyaniline Fibers*, volume 25/10. Springer Berlin Heidelberg, 2010.

[122] J. Y. Lee, C. A. Bashur, A. S. Goldstein, and C. E. Schmidt. Polypyrrole-coated electrospun plga nanofibers for neural tissue applications. *Biomaterials*, 30(26):4325–35, 2009.

[123] M. P. Prabhakaran, L. Ghasemi-Mobarakeh, G. Jin, and S. Ramakrishna. Electrospun conducting polymer nanofibers and electrical stimulation of nerve stem cells. *J Biosci Bioeng*, 112(5):501–507, 2011.

[124] L. Luo, C. Matranga, S. Tan, N. Alba, and X. T. Cui. Carbon nanotube nanoreservior for controlled release of anti-inflammatory dexamethasone. *Biomaterials*, 32:6316 – 6323, 2011.

[125] D. Esrafilzadeh, J. M. Razal, S. M. Moulton, E. M. Stewart, and G. G Wallace. Multifunctional conducting bres with electrically controlled release of ciprooxacin. *J control release*, 169:313–320, 2013.

[126] Y. Kong, C. Wang, C. O. Yang, Y.and Too, and G. G. Wallace. A battery composed of a polypyrrole cathode and a magnesium alloy anode-toward a bioelectric battery. *Synthetic Met*, 162(7/8):584–589, 2012.

[127] Y. Srivastava, M. Marquez, and T. Thorsen. Multijet electrospinning of conducting nanobers from microuidic manifolds. *J App Polym Sci*, 106:3171–3178, 2011.

[128] ISO. Biological evaluation of medical devices – part 5:tests for in vitro cytotoxity. ISO ISO10993-5, International Organization for Standardization, Geneva, Switzerland, 2009.

[129] J. OBrien, I. Wilson, T. Orton, and F. Pognan. Investigation of the alamar blue (resazurin) fluorescent dye for the assessment of mammalian cell cytotoxicity. *Eur. J. Biochem*, 267:5421–5426, 2000.

[130] D. Beneventi, S. Alila, S. Boufi, D. Chaussy, and P. Nortier. Polymerization of pyrrole on cellulose fibres using a $FeCl_3$ impregnation- pyrrole polymerization sequence. *Cellulose*, 13:725–734, 2006.

[131] P. H. S. Picciani, E. S. Medeiros, W. J. Orts, and H. C. Mattoso. *Advances in electroactive electrospun nanofibers*, chapter 5. InTech, 2011.

[132] P. S. Abthagir and R. Saraswath. Thermal stability of polypyrrole prepared from a ternary eutectic melt. *Mater Chem Phys*, 92:21–26, 2005.

[133] M. D. Migahed, T. Fahmy, M. Ishra, and A. Barakat. Preparation, characterization, and electrical conductivity of polypyrrole composite films. *Polymer Testing*, 23:361–365, 2004.

[134] N. Ferraz, M. Strmme, B. Fellstrom, S. Pradhan, and Mihranyan. A. Nyholm, L. In vitro and in vivo toxicity of rinsed and aged nanocellulosepolypyrrole composites. *J Biomed Mater Res A*, 100A(8):2128–2138, 2012.

[135] P. M. George, A. W. Lyckman, D. A. LaVan, A. Hegde, Y. Leung, R. Avasare, C. Testa, P. M. Alexander, R. Langer, and M. Sur. Fabrication and biocompatibility of polypyrrole implants suitable for neural prosthetics. *Biomaterials*, 26:3511–3519, 2005.

[136] E.T.K. Demann. Gold as an implant in medicine and dentistry. *J Long Term Eff Med Implants*, 15(6):687–698, 2005.

[137] S. Li, K. Shu, C. Zhao, C. Wang, Z. Guo, G. Wallace, and H. K. Liu. One-step synthesis of graphene/polypyrrole nanofiber composites as cathode material for a biocompatible zinc/polymer battery. *ACS Appl Mater Interfaces*, 6(19):16679–16686, 2014.

[138] F. Gu, H. Yu, P. Wang, Z. Yang, and L. Tong. Light-emitting polymer single nanofibers via waveguiding excitation. *ACS Nano*, 4(9):5332–5338, 2010.

[139] I. Ferreira, A. C. Baptista, J. P. Leitão, J. Soares, E. Fortunato, R. Martins, and J. P. Borges. Strongly photosensitive and fluorescent F8T2 electrospun fibers. *Macromol Mater Eng*, 298(2):174–180, 2013.

[140] N. A. M. Barakat, K. D. Woo, M. A. Kanjwal, K. E. Choi, M. S. Khil, and H. Y. Kim. Surface plasmon resonances, optical properties, and electrical conductivity thermal hystersis of silver nanofibers produced by the electrospinning technique. *Langmuir*, 24:11982–11987, 2008.

[141] S. D. Solomon, M. Bahadory, A. V. Jeyarajasingam, S. A. Rutkowsky, and C. Boritz. Synthesis and study of silver nanoparticles. *J Chem Educ*, 84(322-325), 2007.

[142] A. Camposeo, F. Di Benedetto, R. Stabile, A. A. Neves, R. Cingolani, and D. Pisignano. Laser emission from electrospun polymer nanofibers. *Small*, 5(5):562–6, 2009.

[143] J. S. Atchison and C. L. Schauer. Fabrication and characterization of electrospun pristine and fluorescent composite poly(acrylic acid) ultra-fine fibers. *J Eng Fibers Fabr*, special issue:50–57, 2012.

[144] Y. Bao, Q. A. Luu, Y. Zhao, H. Fong, P. S. May, and C. Jiang. Upconversion polymeric nanofibers containing lanthanide-doped nanoparticles via electrospinning. *Nanoscale*, 4(23):7369–75, 2012.

[145] S. Y. Min, J. Bang, J. Park, C. L. Lee, S. Lee, J. J. Park, U. Jeong, S. Kim, and T. W. Lee. Electrospun polymer/quantum dot composite fibers as down conversion phosphor layers for white light-emitting diodes. *RSC Adv.*, 4(23):11585–11589, 2014.

[146] D Hawkins and H. Abrahamse. Phototherapy a treatment modality for wound healing and pain relief. *Afr J Biom Res*, 10:99–109, 2007.

[147] G. Jin, M. P. Prabhakaran, D. Kai, M. Kotaki, and S. Ramakrishna. Electrospun photosensitive nanobers: potential for photocurrent therapy in skin regeneration. *Photochem Photobiol Sci*, 12:124–134, 2013.

[148] R. P. Chahal, S. Mahendia, A.K. Tomar, and S. Kumar. Effect of ultraviolet irradiation on the optical ans structural characteristics of in-situ prepared PVP-Ag nanocomposites. *Dig J Nanomater Bios*, 5(3):569–575, 2010.

[149] A. W. Bauer, W. M. M. Kirby, J. C. Sherris, and M. Turck. Antibiotic susceptibility testing by a standardized single disk method. *Am J Clin Pathol*, 45:493–496, 1966.

[150] J. H Miller. *Experiments in molecular genetics*. Cold Spring Harbor Laboratory, N.Y., 3rd edition, 1971.

[151] H. Wang, X. Qiao, J. Chen, X. Wang, and S. Ding. Mechanisms of pvp in the preparation of silver nanoparticles. *Mater Chem Phys*, 94(2-3):449–453, 2005.

[152] G. Boyd, Z. Yu, and Y. Shen. Photoinduced luminescence from the noble metals and its enhancement on roughened surfaces. *Phys Rev B*, 33(12):7923–7936, 1986.

[153] R. Reisfeld, T. Saraidarov, G. Panzer, V. Levchenko, and M. Gaft. New optical material europium edta complex in polyvinyl pyrrolidone films with fluorescence enhanced by silver plasmons. *Opt Mater*, 34(2):351–354, 2011.

[154] M. Ricca, V. Fodera, D. Giacomazza, M. Leone, G. Spadaro, and C. Dispenza. Probing the internal environment of PVP networks generated by irradiation with different sources. *Colloid Polym Science*, 288(9):969–980, 2010.

[155] M. Yan, L. Rothberg, F. Papadimitrakopoulos, M. Galvin, and T. Miller. Defect quenching of conjugated polymer luminescence. *Phys Rev Lett*, 73(5):744–747, 1994.

[156] B. Zhao and Z. Nan. Enhancement of electric conductivity by incorporation of Ag into core/shell structure of Fe_3O_4/Ag/PPy NPs. *Mater Sci Eng C*, 32:804–810, 2012.

[157] C. Quadros, V. W. Faria, M. P. Klein, P. F. Hertz, and C. W. Scheeren. Chitosan/carboxymethylcellulose/ionic liquid/ag(0) nanoparticles form a membrane with antimicrobial activity. *J Nanotechnology*, 2013:1–9, 2013.

[158] Y. Zhang and G. C. Rutledge. Electrical conductivity of electrospun polyaniline and polyaniline-blend fibers and mats. *Macromolecules*, 45(10):4238–4246, 2012.

[159] S. Nair, S. Natarajan, and S. H. Kim. Fabrication of electrically conducting polypyrrole-poly(ethylene oxide) composite nanofibers. *Macromol Rapid Comm*, 26(20):1599–1603, 2005.

[160] Y. J. Kim, W. Wu, S. Chun, J. F. Whitacre, and C. J. Bettinger. Biologically derived melanin electrodes in aqueous sodium-ion energy storage devices. *PNAS*, 110(52):20912–20917, 2013.

Appendix A

Morphology of the electrospun fibers

The APPENDIX A provides complementary information about the morphology of the produced CA electrospun fibers with different ES conditions (Chapter 3). Table A.1 summarizes the electrospun membranes that were analyzed indicating the corresponding fiber average diameter. This appendix also includes the SEM images and histograms obtained for all the CA electrospun membranes evaluated during the study of the best ES conditions (Figures from A.1 to A.21).

Table A.1: Summary of the produced samples with the indication of their fiber average diameter. The corresponding polymer concentration and ES condition are indicated for each sample.

Sample No.	**AC (%wt)**	**ES parameters**	**D_{av} (nm)**
22	8	20 kV/15 cm/0.1ml.h^{-1}	149 ± 45
23	8	20 kV/15 cm/0.2ml.h^{-1}	96 ± 23
24	8	20 kV/15 cm/0.4ml.h^{-1}	87 ± 29
34	10	20 kV/15 cm/0.1ml.h^{-1}	118 ± 44
35	10	20 kV/15 cm/0.2ml.h^{-1}	130 ± 55
36	10	20 kV/15 cm/0.4ml.h^{-1}	193 ± 57
37	12	15 kV/10 cm/0.1ml.h^{-1}	196 ± 68
38	12	15 kV/10 cm/0.2ml.h^{-1}	340 ± 92
39	12	15 kV/10 cm/0.4ml.h^{-1}	357 ± 128
40	12	20 kV/10 cm/0.1ml.h^{-1}	385 ± 162
41	12	20 kV/10 cm/0.2ml.h^{-1}	265 ± 118
42	12	20 kV/10 cm/0.4ml.h^{-1}	300 ± 139
43	12	15 kV/15 cm/0.1ml.h^{-1}	220 ± 100
44	12	15 kV/15 cm/0.2ml.h^{-1}	243 ± 99
45	12	15 kV/15 cm/0.4ml.h^{-1}	282 ± 88
46	12	20 kV/15 cm/0.1ml.h^{-1}	268 ± 90
47	12	20 kV/15 cm/0.2ml.h^{-1}	243 ± 58
48	12	20 kV/15 cm/0.4ml.h^{-1}	257 ± 76
58	14	20 kV/15 cm/0.1ml.h^{-1}	468 ± 158
59	14	20 kV/15 cm/0.2ml.h^{-1}	487 ± 199
60	14	20 kV/15 cm/0.4ml.h^{-1}	422 ± 115

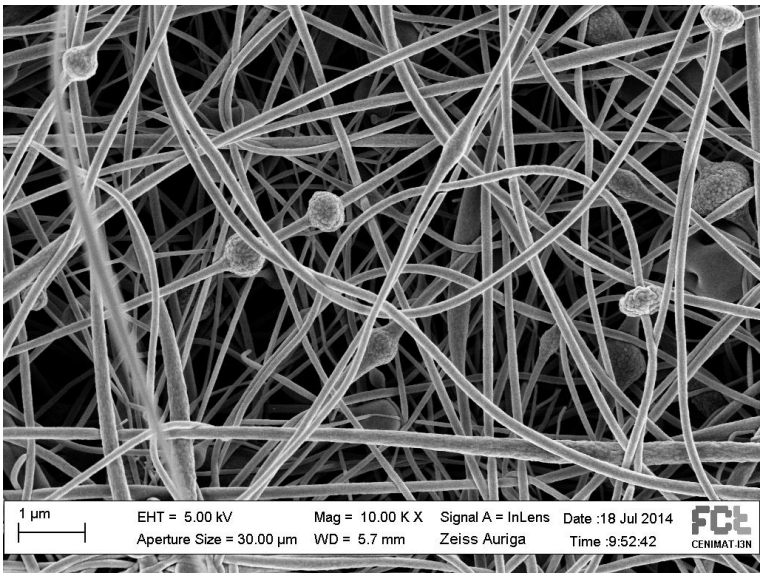

(a)

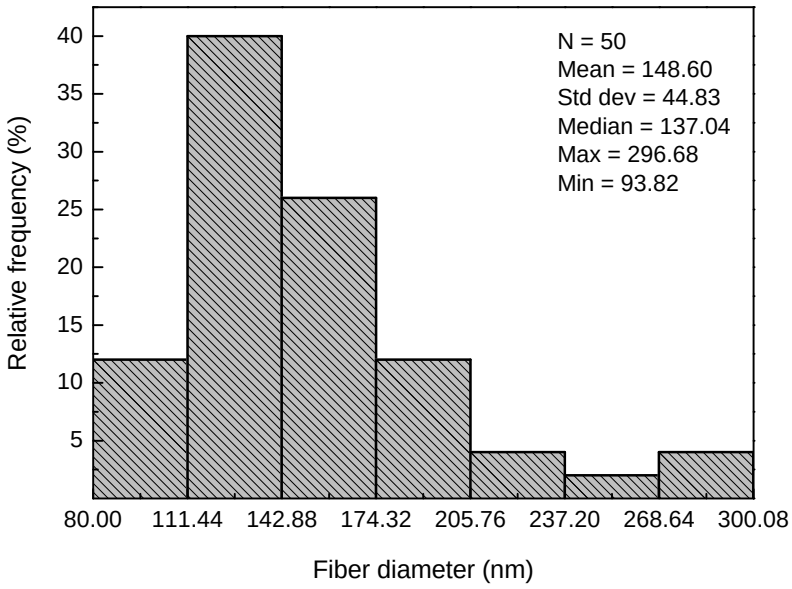

(b)

Figure A.1: Evaluation of SAMPLE No. 22 (a) SEM image and (b) histogram

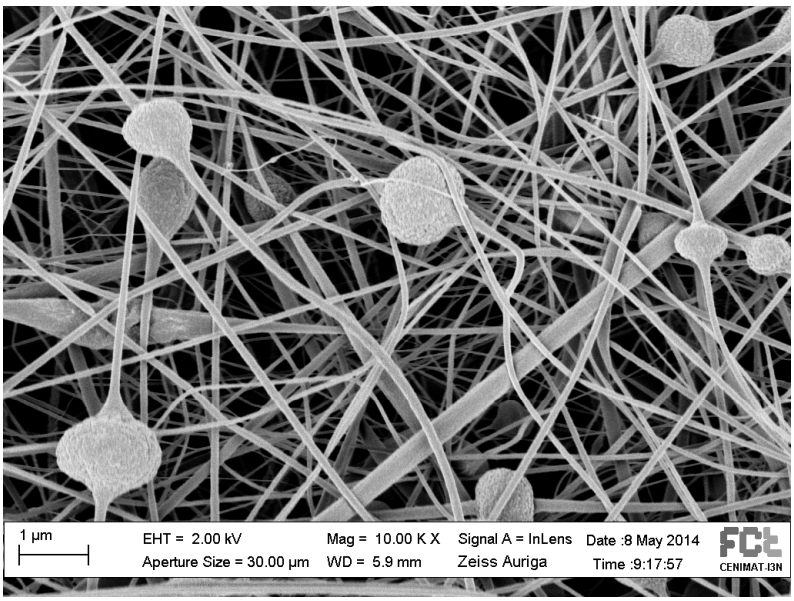

(a)

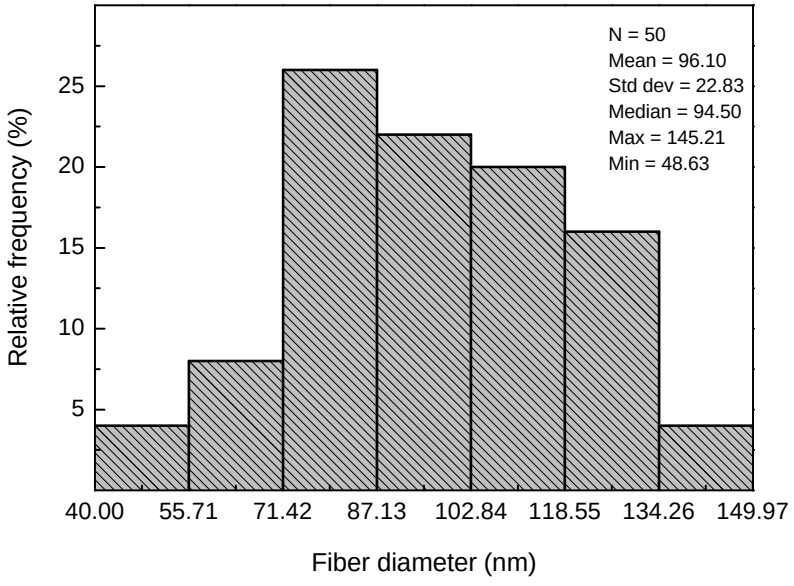

(b)

Figure A.2: Evaluation of SAMPLE No. 23 (a) SEM image and (b) histogram

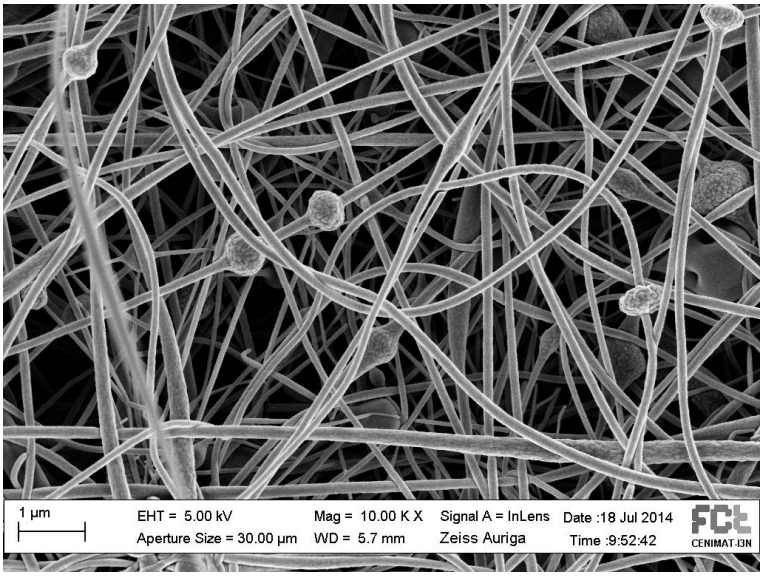

(a)

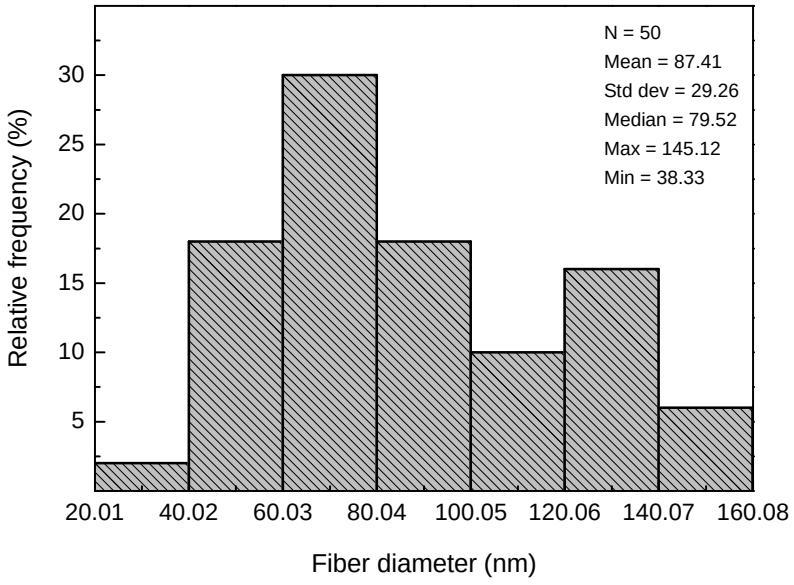

(b)

Figure A.3: Evaluation of SAMPLE No. 24 (a) SEM image and (b) histogram

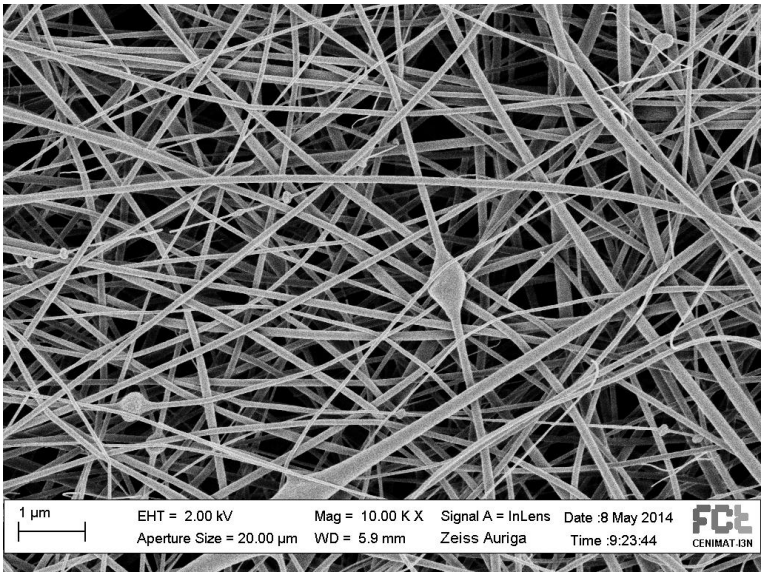

(a)

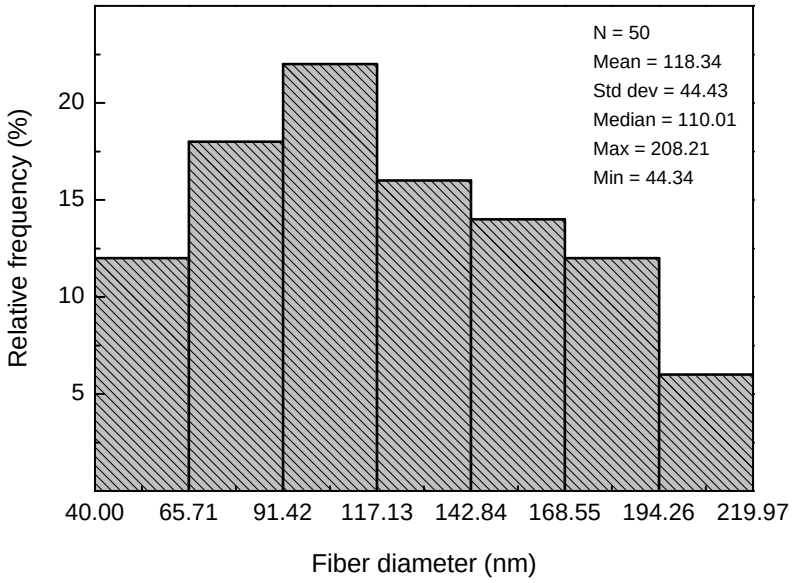

(b)

Figure A.4: Evaluation of SAMPLE No. 34 (a) SEM image and (b) histogram

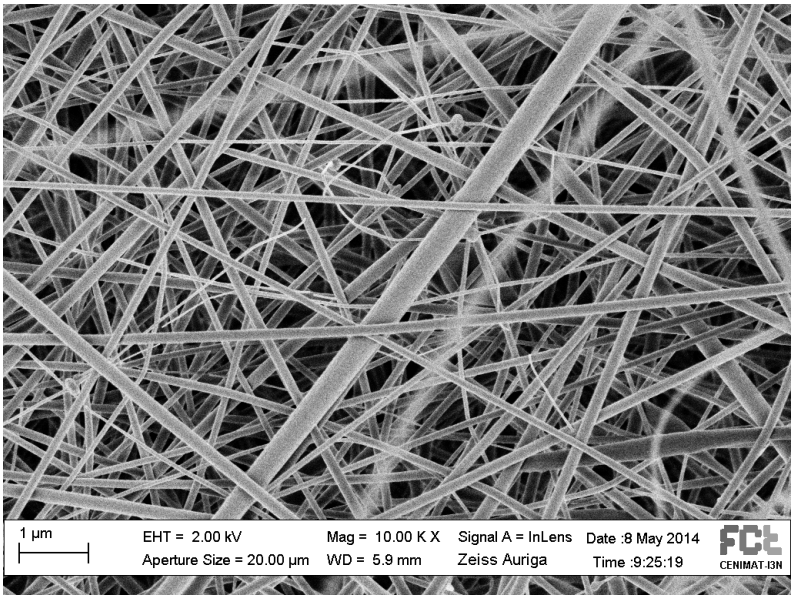

(a)

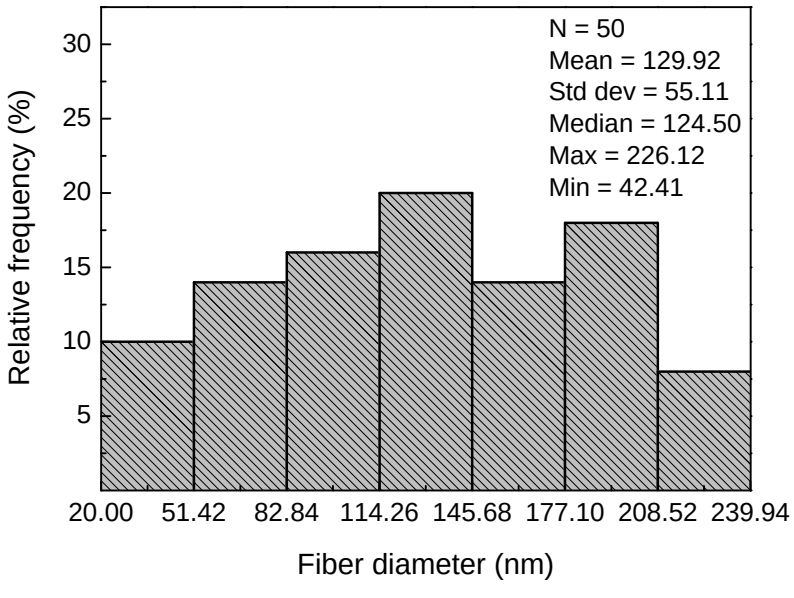

(b)

Figure A.5: Evaluation of SAMPLE No. 35 (a) SEM image and (b) histogram

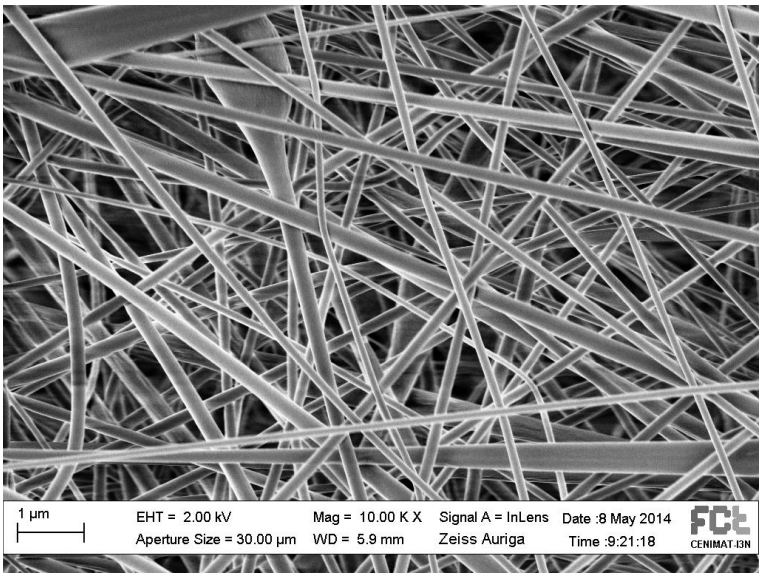

(a)

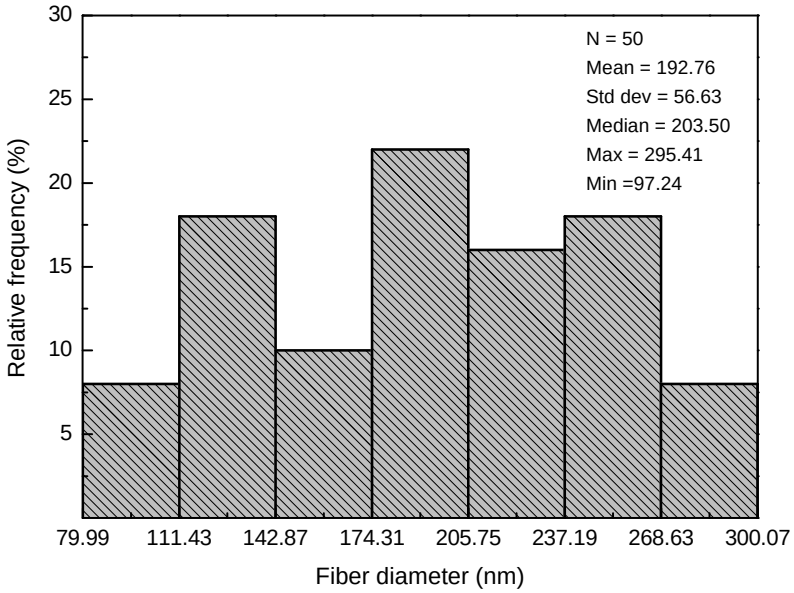

(b)

Figure A.6: Evaluation of SAMPLE No. 36 (a) SEM image and (b) histogram

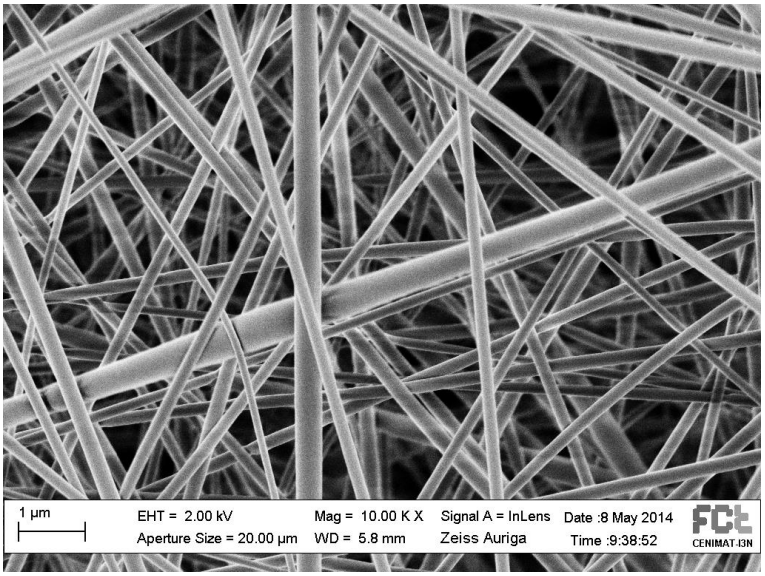

(a)

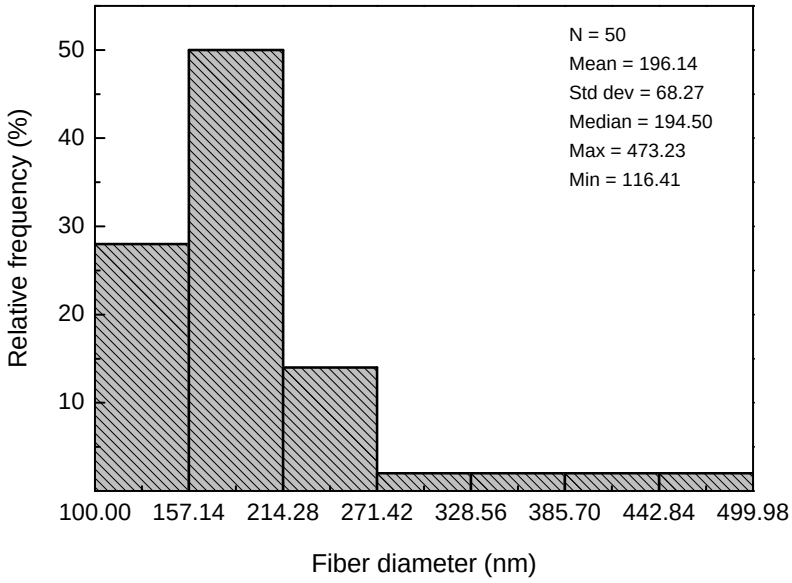

(b)

Figure A.7: Evaluation of SAMPLE No. 37 (a) SEM image and (b) histogram

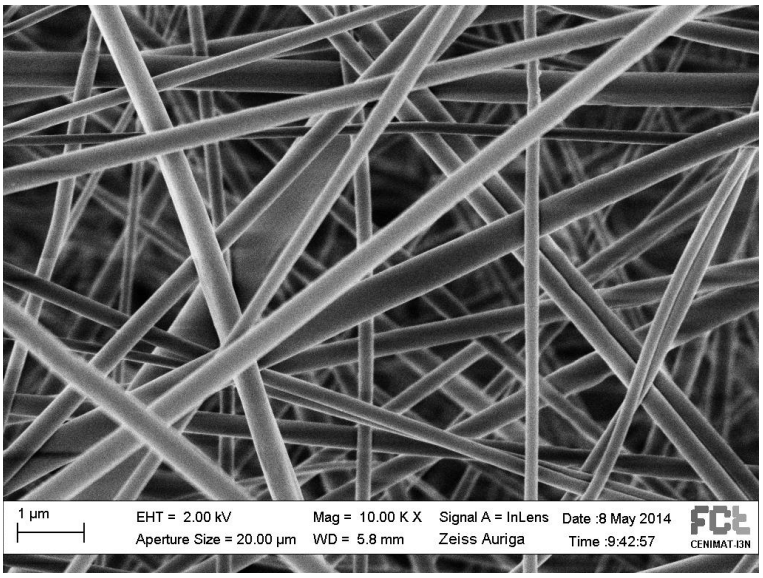

(a)

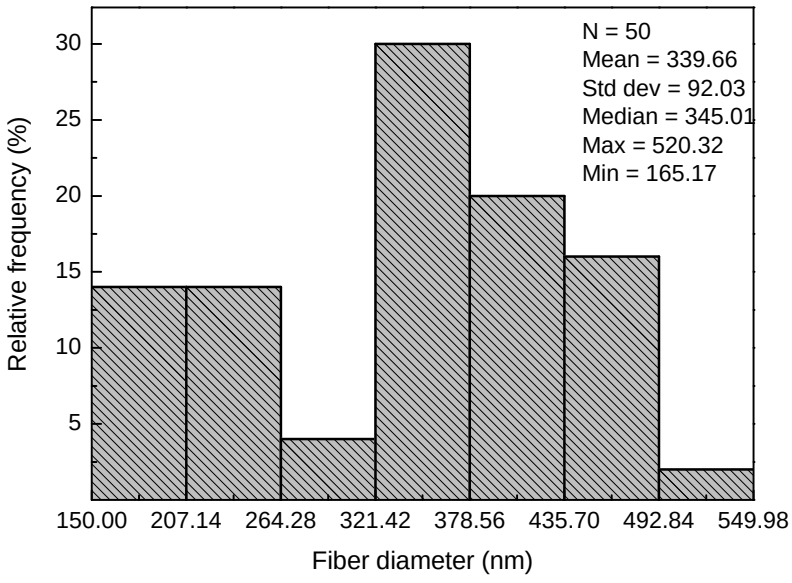

(b)

Figure A.8: Evaluation of SAMPLE No. 38 (a) SEM image and (b) histogram

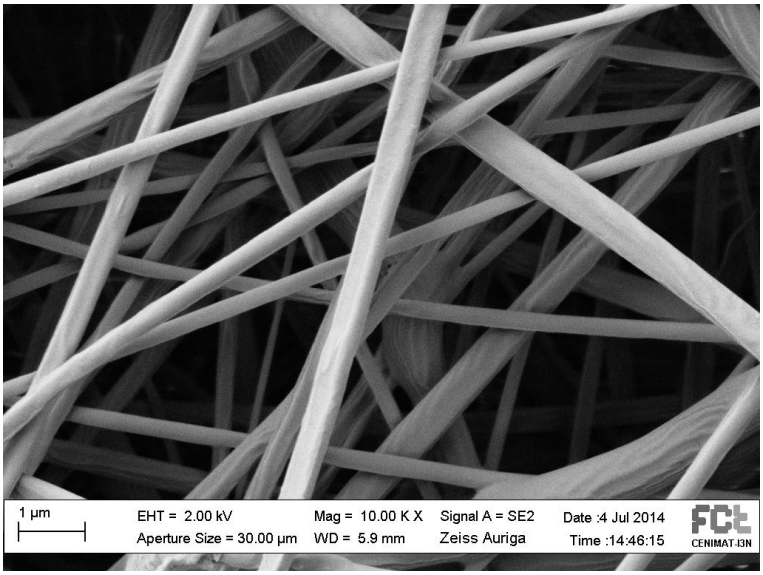

(a)

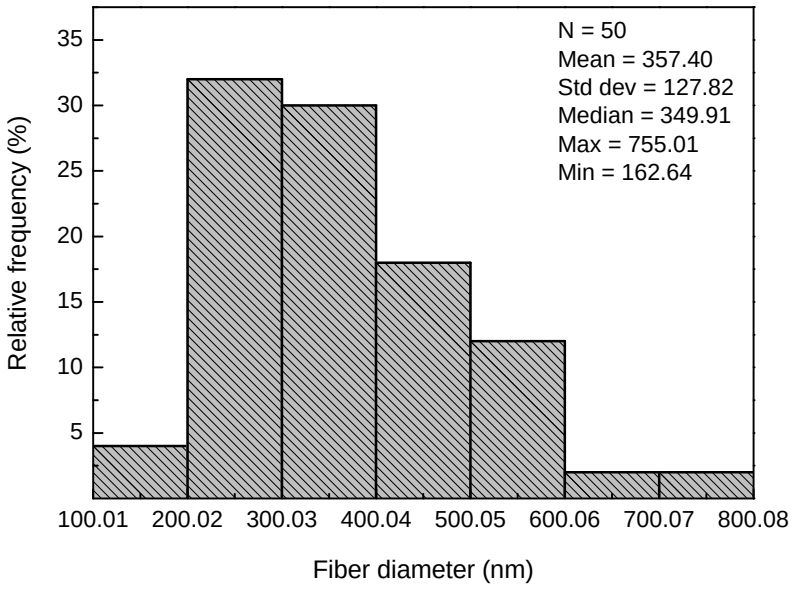

(b)

Figure A.9: Evaluation of SAMPLE No. 39 (a) SEM image and (b) histogram

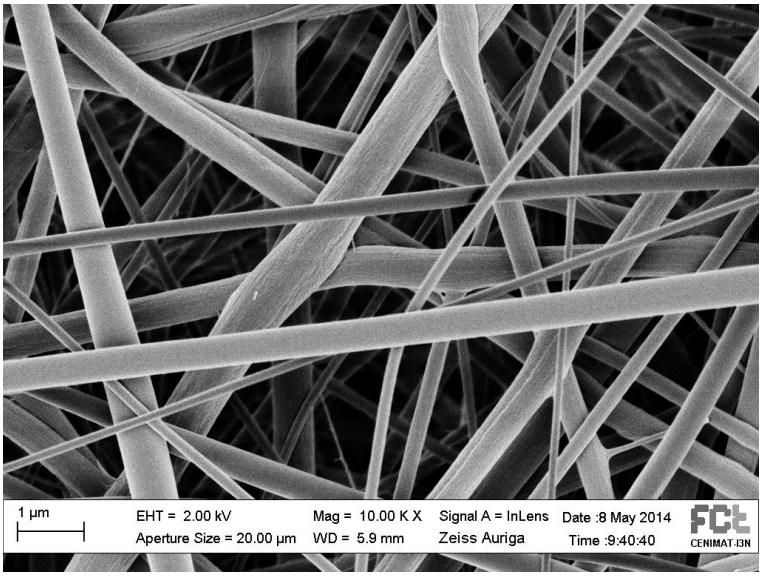

(a)

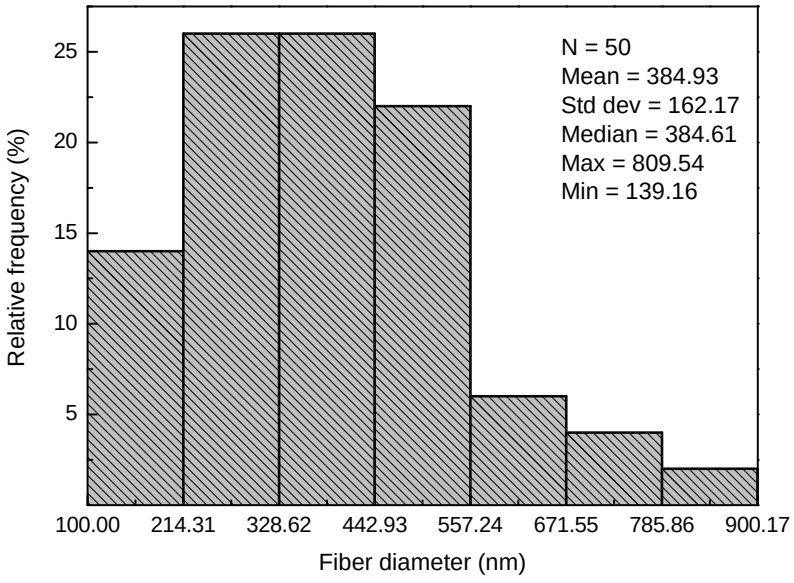

(b)

Figure A.10: Evaluation of SAMPLE No. 40 (a) SEM image and (b) histogram

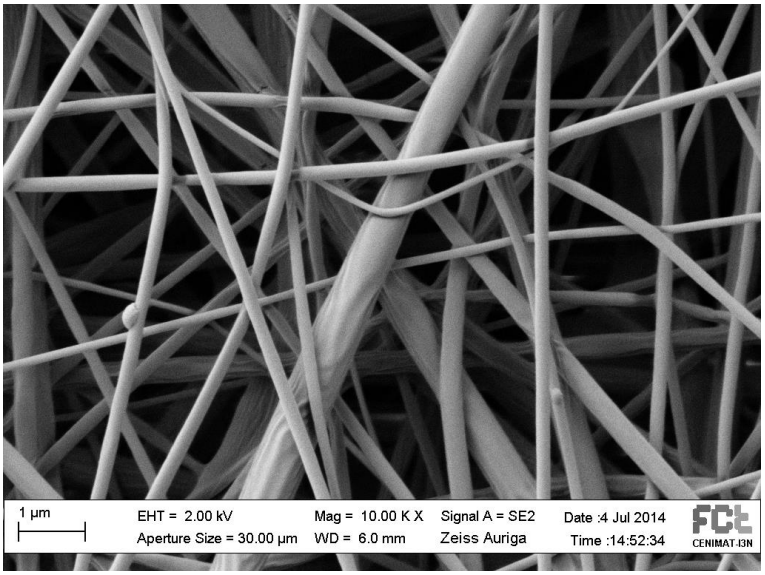

(a)

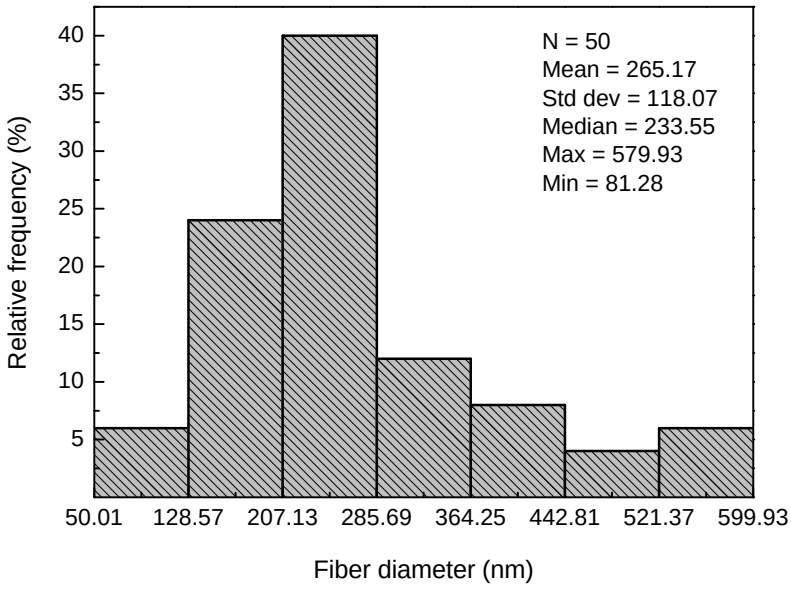

(b)

Figure A.11: Evaluation of SAMPLE No. 41 (a) SEM image and (b) histogram

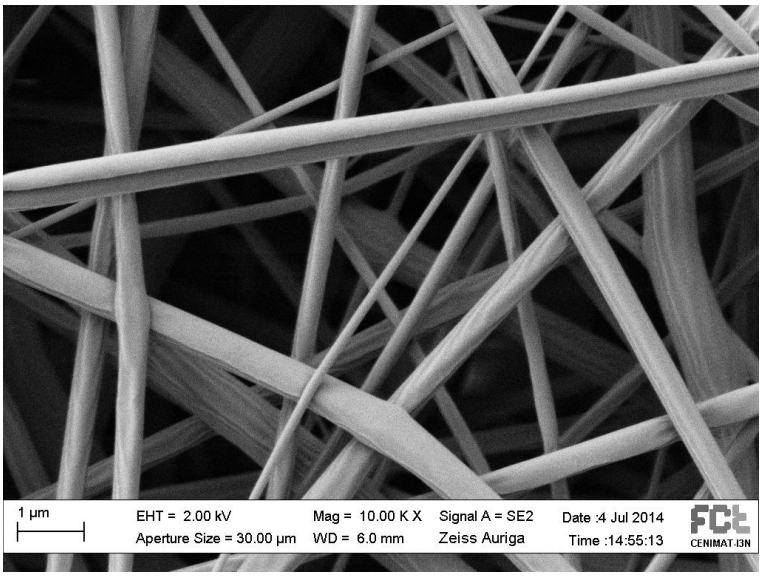

(a)

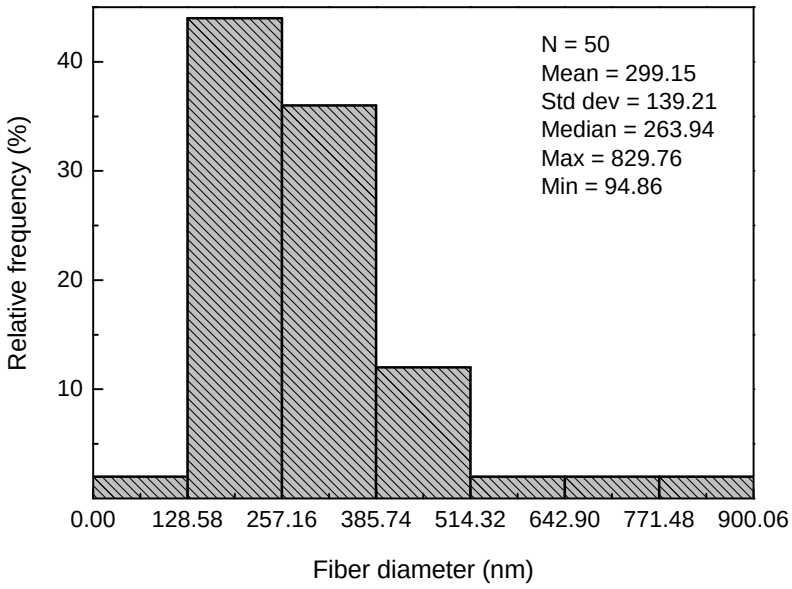

(b)

Figure A.12: Evaluation of SAMPLE No. 42 (a) SEM image and (b) histogram

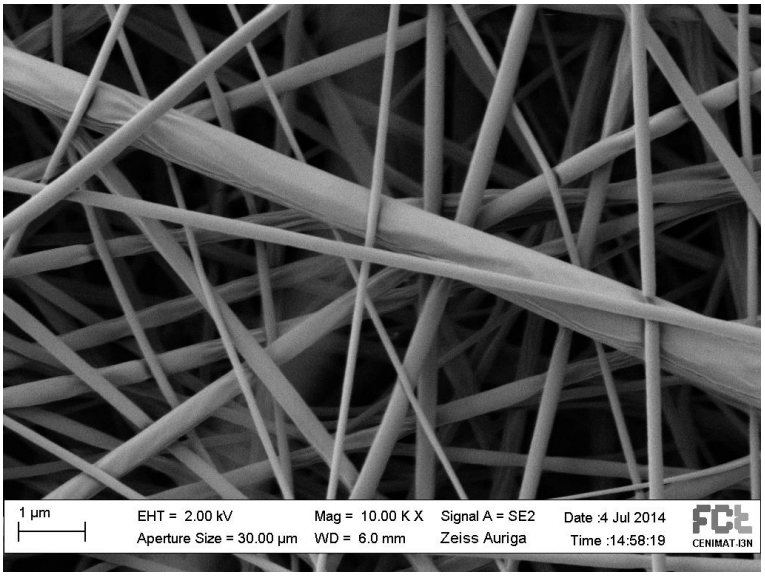

(a)

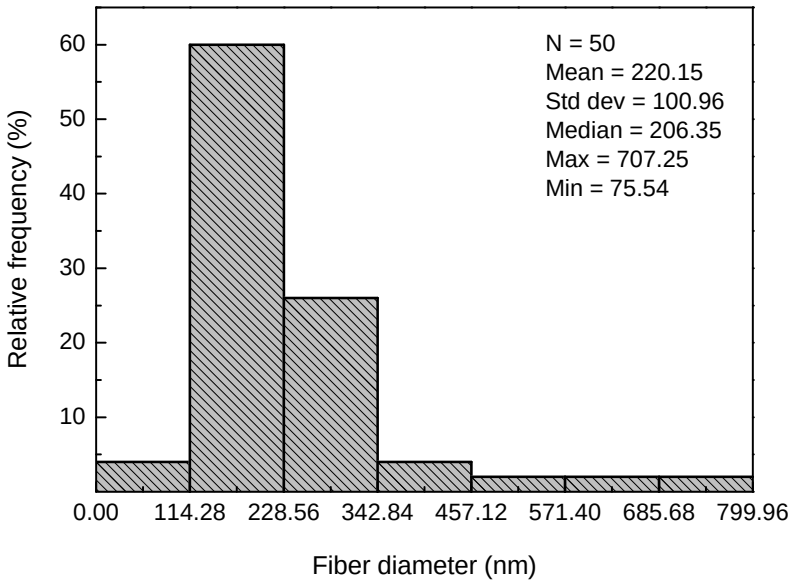

(b)

Figure A.13: Evaluation of SAMPLE No. 43 (a) SEM image and (b) histogram

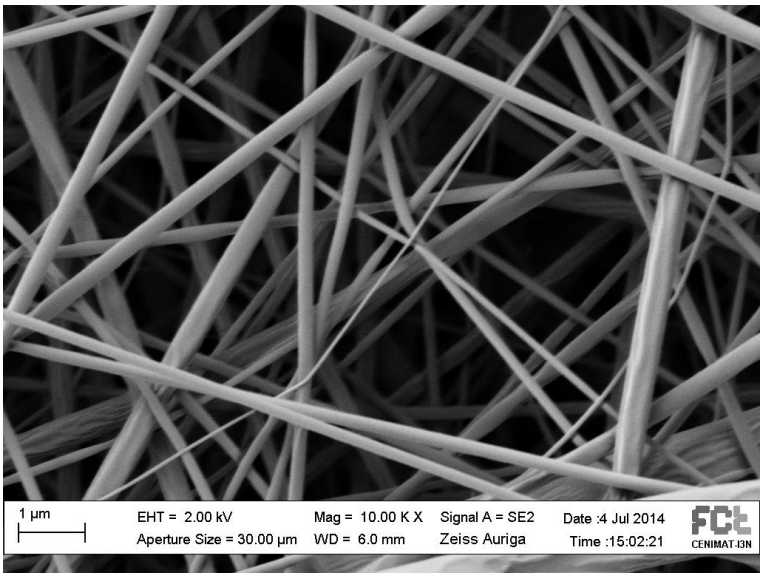

(a)

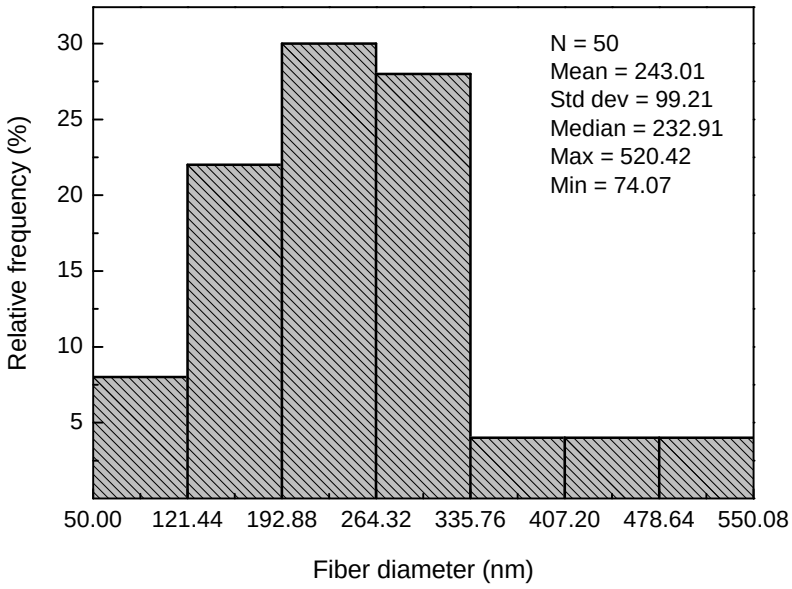

(b)

Figure A.14: Evaluation of SAMPLE No. 44 (a) SEM image and (b) histogram

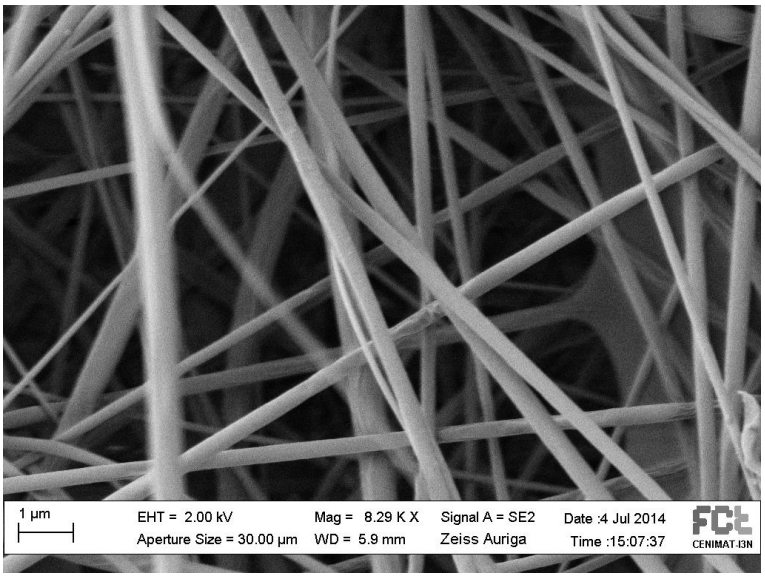

(a)

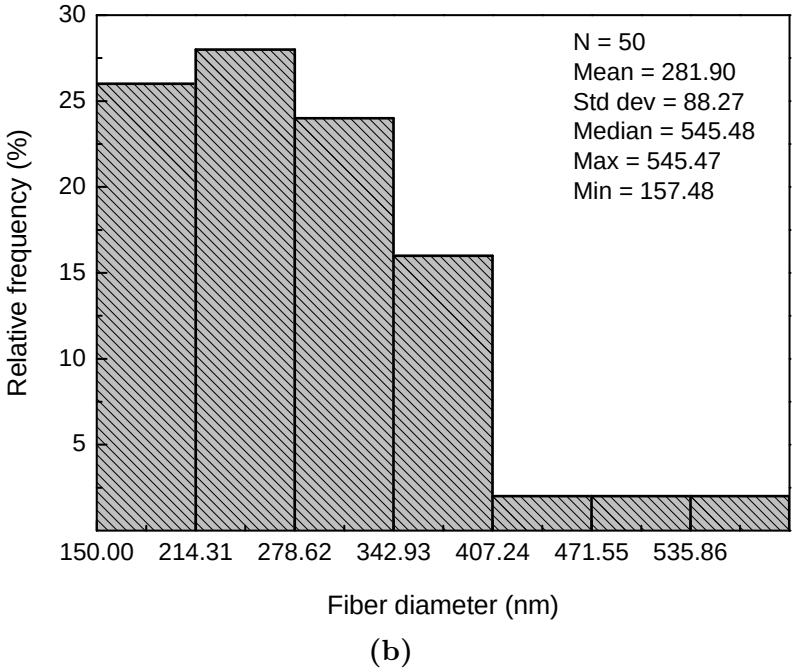

(b)

Figure A.15: Evaluation of SAMPLE No. 45 (a) SEM image and (b) histogram

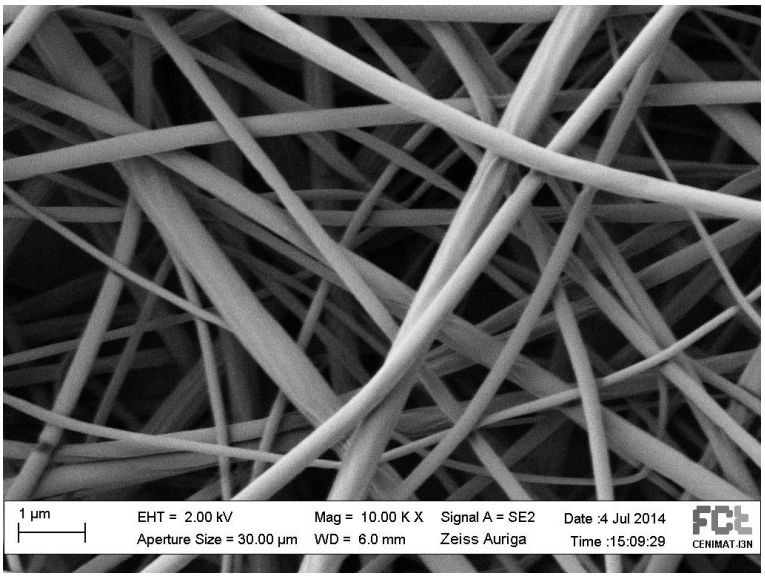

(a)

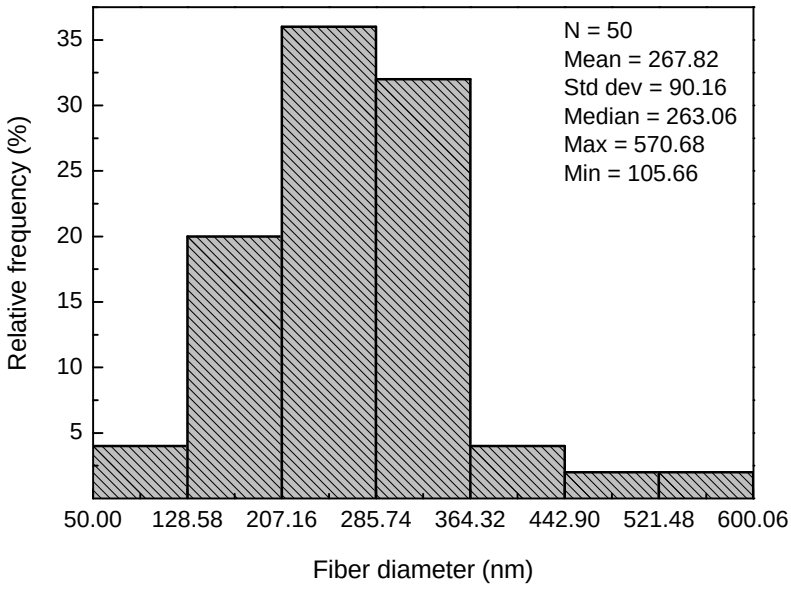

(b)

Figure A.16: Evaluation of SAMPLE No. 46 (a) SEM image and (b) histogram

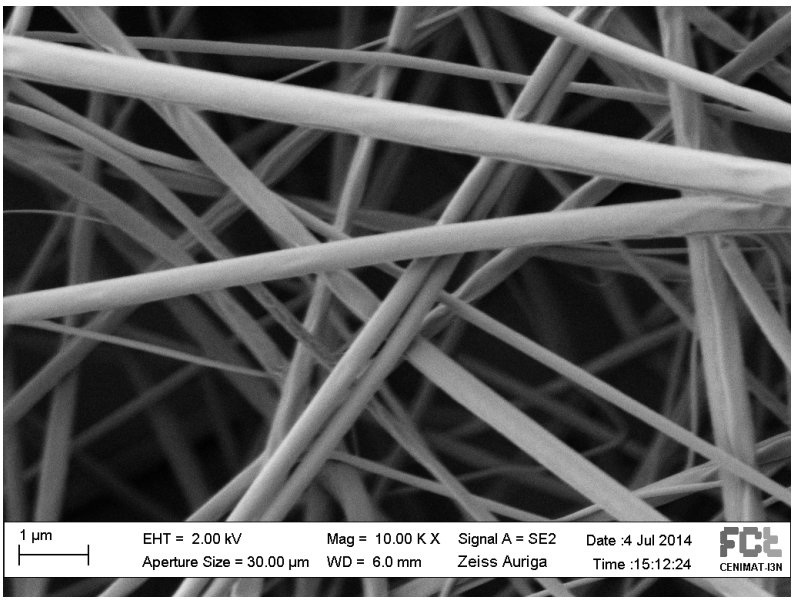

(a)

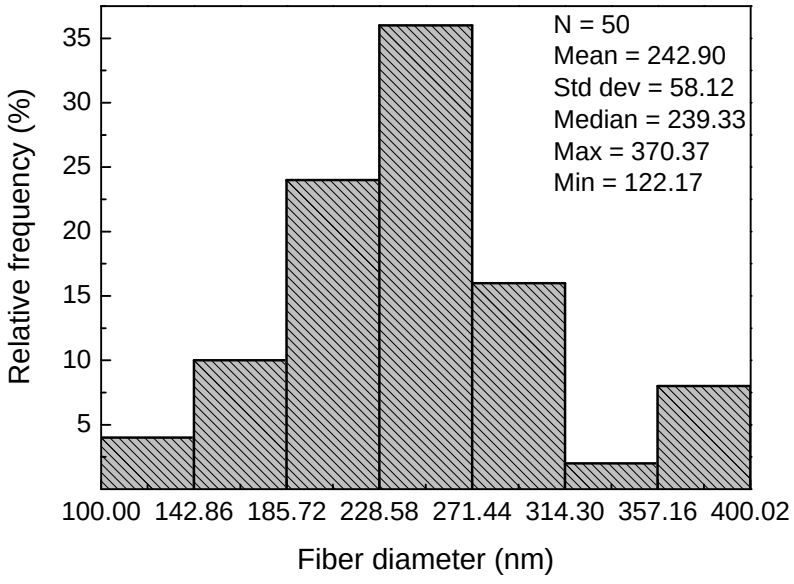

(b)

Figure A.17: Evaluation of SAMPLE No. 47 (a) SEM image and (b) histogram

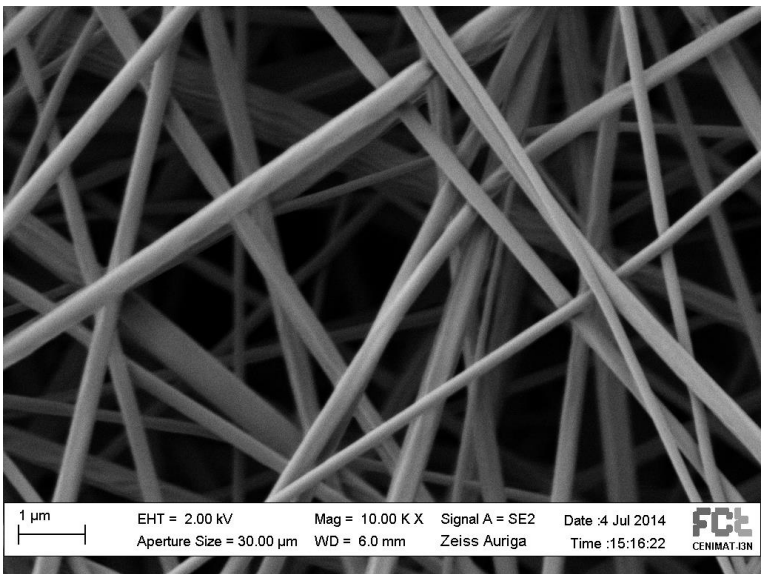

(a)

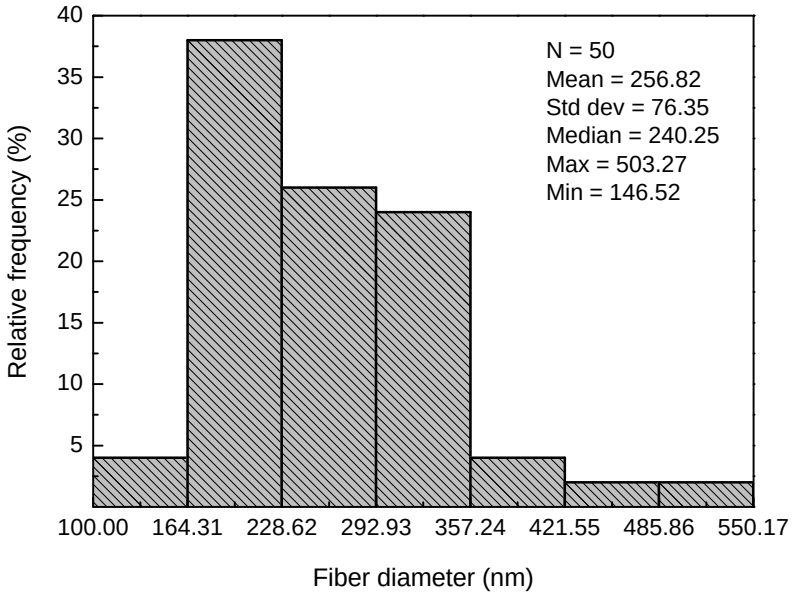

(b)

Figure A.18: Evaluation of SAMPLE No. 48 (a) SEM image and (b) histogram

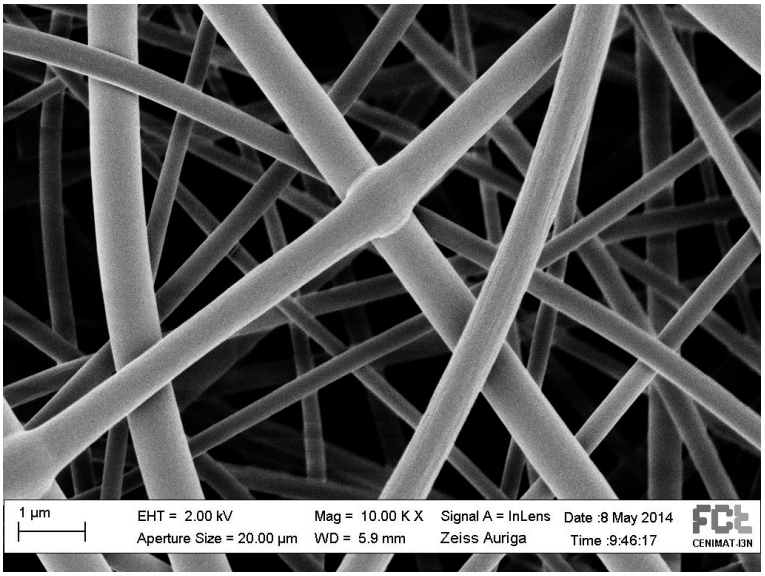

(a)

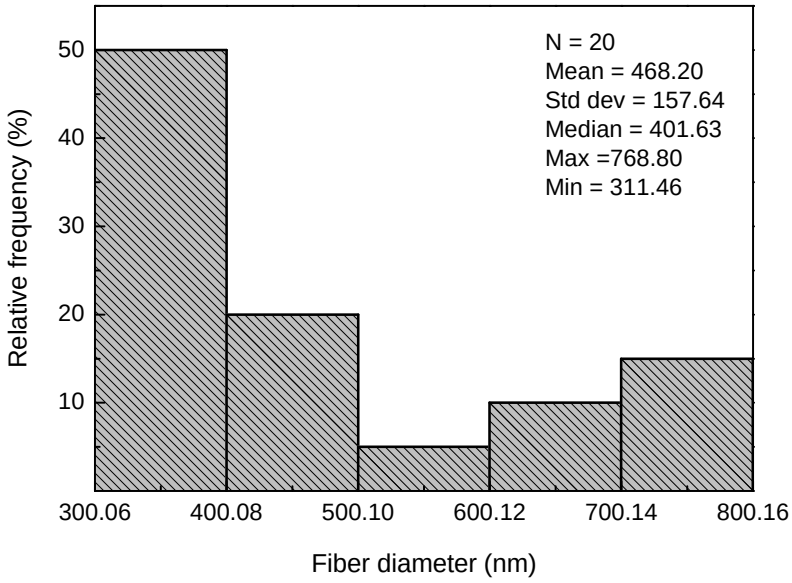

(b)

Figure A.19: Evaluation of SAMPLE No. 58 (a) SEM image and (b) histogram

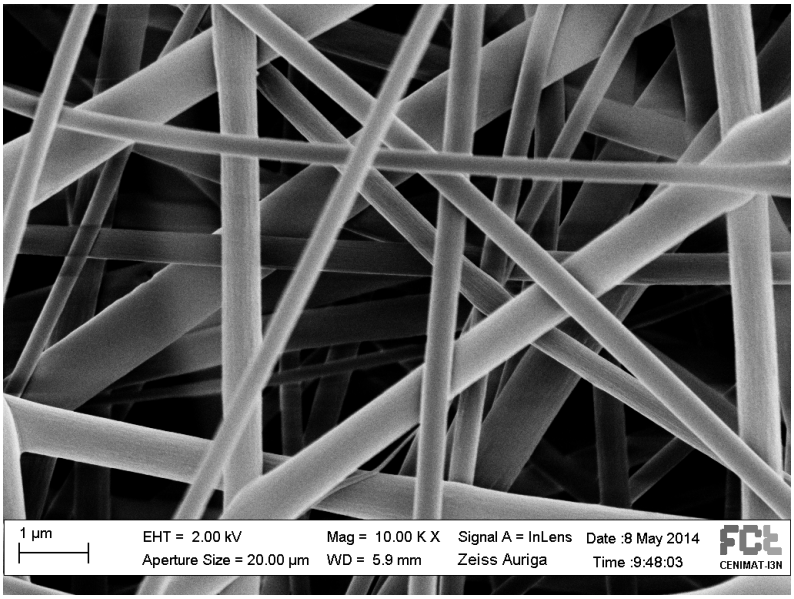

(a)

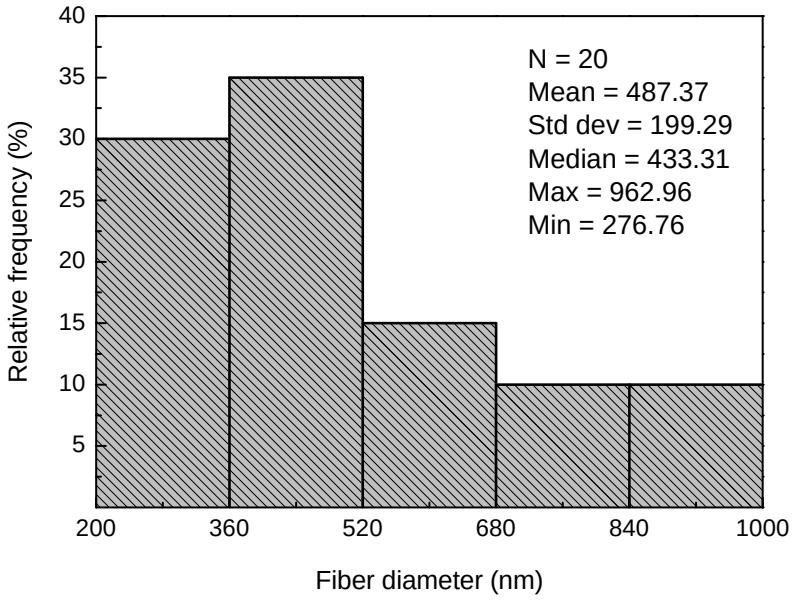

(b)

Figure A.20: Evaluation of SAMPLE No. 59 (a) SEM image and (b) histogram

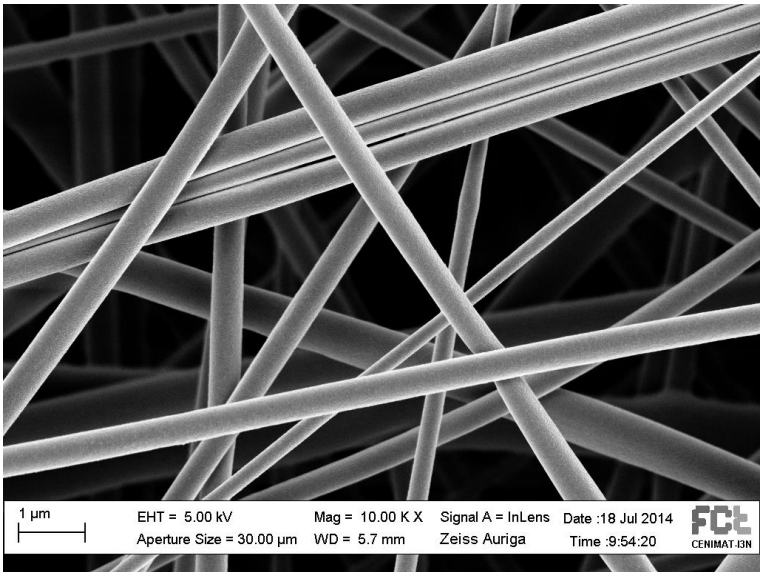

(a)

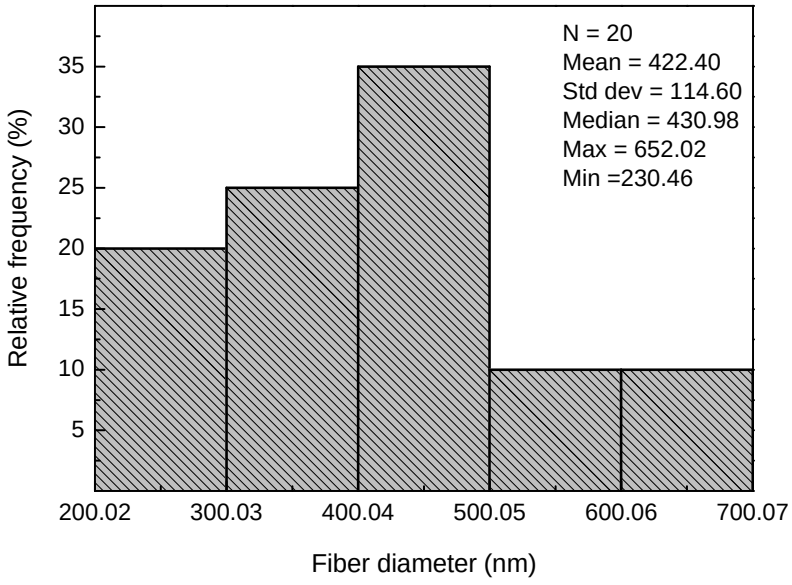

(b)

Figure A.21: Evaluation of SAMPLE No. 60 (a) SEM image and (b) histogram

Appendix B

Electrical characterization

This appendix complements the results presented in Chapter 4 through the presentation of the electrical conductivity values obtained for the CA/PPy and CA/PANI fibers.

Table B.1 shows the electrical conductivity values obtained for different oxidant/monomer mass ratios during *in-situ* chemical polymerization of Py for 60 minutes. This Table complements the results presented in Figure 4.11.

Table B.1: Electrical conductivities of CA/PPy fibers prepared by *in situ* chemical oxidation using different oxidant/monomer ratios.

[Mon] mol.L^{-1}	**t_{pol} (min)**	**Ox/Mon**	**Conductivity (S.cm^{-1})**
0.025	60	1	$(7.3 \pm 0.4) \times 10^{-10}$
		2	$(4.0 \pm 0.2) \times 10^{-3}$
		3	$(5.7 \pm 0.1) \times 10^{-3}$
		4	$(3.6 \pm 0.5) \times 10^{-3}$

In addition, Table B.2 shows the electrical conductivity values obtained for Py chemical polymerization using an oxidant/monomer mass ratio of 2, different monomer concentrations and different reaction times. This Table complements the results presented in Figure 4.12. Table B.3 shows the electrical conductivity values obtained for CA/PANI composite fibers prepared by *in situ* chemical oxidation. This Table complements the results presented in Figures 4.21 and 4.23.

Table B.2: Electrical conductivity of CA/PPy nanofibers prepared by *in situ* chemical oxidation using different monomer concentrations and reaction times.

[Mon] mol.L^{-1}	**Ox/Mon**	**t_{pol} (min)**	**Conductivity (S.cm^{-1})**
0.025	2	30	$(1.5 \pm 0.1) \times 10^{-6}$
		45	$(8.1 \pm 0.2) \times 10^{-5}$
		60	$(4.0 \pm 0.1) \times 10^{-3}$
		90	$(6.2 \pm 0.1) \times 10^{-3}$
		1440	$(4.1 \pm 0.4) \times 10^{-3}$
0.05	2	15	$(2.3 \pm 0.1) \times 10^{-3}$
		30	$(8.2 \pm 0.7) \times 10^{-2}$
		45	$(3.9 \pm 0.3) \times 10^{-2}$
		60	$(8.6 \pm 0.1) \times 10^{-3}$
		90	$(3.6 \pm 0.7) \times 10^{-2}$
		1440	$(3.0 \pm 0.3) \times 10^{-3}$
0.075	2	15	$(3.4 \pm 0.2) \times 10^{-2}$
		30	$(8.8 \pm 0.1) \times 10^{-3}$
		45	$(4.1 \pm 0.4) \times 10^{-3}$

Table B.3: The influence of monomer concentration, Oxi/Mon molar ratio and reaction time on the electrical conductivity of CA/PANI composite fibers prepared by in situ chemical oxidation.

[Mon] mol.L^{-1}	**Ox/Mon**	**t_{pol} (min)**	**Conductivity (S.cm^{-1})**
4	0.5	30	$(8.11 \pm 0.10) \times 10^{-2}$
		45	$(5.34 \pm 0.04) \times 10^{-2}$
		60	$(1.03 \pm 0.01) \times 10^{0}$
	0.25	30	$(1.81 \pm 0.14) \times 10^{-3}$
		45	$(5.53 \pm 0.20) \times 10^{-2}$
		60	$(3.28 \pm 0.01) \times 10^{-1}$
	0.125	30	$(2.53 \pm 0.04) \times 10^{-3}$
		45	$(2.78 \pm 0.06) \times 10^{-2}$
		60	$(1.49 \pm 0.02) \times 10^{-2}$
2	0.5	30	$(8.63 \pm 0.14) \times 10^{-2}$
		45	$(1.60 \pm 0.08) \times 10^{-1}$
		60	$(1.58 \pm 0.01) \times 10^{-1}$
	0.25	30	$(9.88 \pm 0.56) \times 10^{-3}$
		45	$(3.51 \pm 0.04) \times 10^{-3}$
		60	$(6.20 \pm 0.14) \times 10^{-3}$